Wave transformation at select locations along the Indian coast through measurements, modelling and remote sensing

Thesis submitted for the Degree of

Doctor of Philosophy

in

Marine Sciences

to the

Goa University

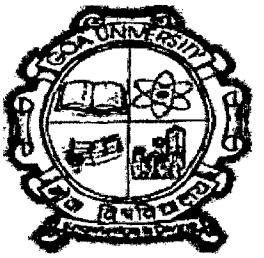

by

Aboobacker V.M.

National Institute of Oceanography (CSIR)
Dona Paula, Goa – 403004, India.

November 2010

Dedicated to...

my "Uppa" and "Umma"

Statement

As required under the University Ordinance 0.19.8 (vi), I state that the present thesis entitled "**Wave transformation at select locations along the Indian coast through measurements, modelling and remote sensing**" is my original research work carried out at the National Institute of Oceanography, Goa and that no part thereof has been submitted for any other degree or diploma in any University or Institution.

The literature related to the problem investigated has been cited. Due acknowledgements have been made wherever facilities and suggestions have been availed of.

Aboobacker V.M.

National Institute of Oceanography
Dona Paula, Goa - 403 004

November 2010

Certificate

This is to certify that the thesis entitled "**Wave transformation at select locations along the Indian coast through measurements, modelling and remote sensing**" submitted by **Aboobacker V.M.** for the award of the degree of Doctor of Philosophy in the Department of Marine Sciences is based on his original studies carried out by him under my supervision. The thesis or any part thereof has not been previously submitted for any degree or diploma in any University or Institution.

Dr. P. Vethamony

National Institute of Oceanography
Dona Paula, Goa - 403004

All the corrections suggested by the examiners have been incorporated.

19.2.2011
P. Vethamony

19.2.11
(M.C. Deo)

Acknowledgments

It was a perfect decision, which I made during my visit to the National Institute of Oceanography (NIO) in December 2003 to meet Dr. P. Vethamony. In him, I found a 'Guide' and a person of good behaviour and positive approach. Since I joined in NIO as a Junior Research Fellow (JRF) during January 2004 under his supervision, he provided me a good platform to grow up in academic and personal level. He guided me with constant support and encouragement. He spent his valuable time with me for scientific discussions, which helped me to improve my understanding of ocean waves. It gives me great pleasure to thank him on this occasion, as I wind up the interpretations and discussions in the form of 'thesis'.

I am very grateful to the Council of Scientific and Industrial Research (CSIR), India for offering me research fellowships (JRF and SRF) to carry out research work of my interest.

I express my sincere gratitude to Dr. S.R. Shetye, Director, NIO, Goa, for providing me necessary facilities to carry out my work at NIO.

I thank Prof. H.B. Menon, Head, Department of Marine Sciences, Goa University for his valuable advice on several occasions, both scientific and administrative. I am thankful to the VC's nominee, Dr. S. Prasannakumar, Scientist, NIO, Goa, for providing critical comments and reviews on progress report.

I extend my sincere gratitude to Mr. K. Sudheesh, who helped me in learning modelling tools. Support from Mrs. Rashmi Vasuki in wave spectra analysis is greatly appreciated. Special thanks to Mr. Seemanth M., and Mrs. Dhanya Roshin for their help in setting up MM5 model. I acknowledge with gratitude, all those who participated in the field data collection, especially Mr. P.S. Pednekar and Mr. Ashok Kumar, K.

I thank Dr. Luigi Cavaleri, Former Director, Institute of Marine Science (ISMAR), Italy, for useful discussions on wave modelling, which helped me to improve the quality of the thesis. I thank Dr. M.T. Babu, Mr. S. Jayakumar, Dr. V. Sanil Kumar, Mr. D. Illangovan and Mr. R. Mani Murali for their support and encouragement during various stages of my research career.

My dearest friends, Grinson George, Vineesh, Divya Tenson, Sindhu Krishnakumar, Ricky, Ajay, Nisha Kurian, Deepthi Jagadeesh, Sini Anoop and Syam Sankar, who

always supported and encouraged me throughout my career. Their presence made me happier than ever. Thanks to all of them for their good words and deeds!

The pleasant ambience and nice work atmosphere in our lab is due to my dearest lab mates: Saheed, Renjith, Samiksha, Betty, Manu, Jyoti, Vinod, Suneel, Ratnamala and Mr. Krishnama Charyulu, who were very helpful and enthusiastic! I express my sincere gratitude to all of them.

It would be a difficult task to list all of my friends who supported directly or indirectly throughout my career! I extend my thanks to all those who helped me in various occasions. My special thanks to Mr. Simon, Mr. Vijayan, Dr. Yatheesh, Manoj Nambiar, Feby, Traicy, Prachi, Ratheesh, Smitha, Rupali, Siddharth, Vidya, Haris, Vijay, Laju, Ramya, Rajani, Nuncio, Ramesh, Sijin, Suprit and Manoj N.T for their support and encouragement.

All the success in my life is due to the everlasting support, love and prayers of my parents! May Allah bless them with good health, happiness and prosperity! I extend my thanks to my parents, all my family members and friends from my native, who were ever supportive and very kind in every situation in my life. At last, but not the least, love and regards to my (niece) sweet Hifa mol .

Aboobacker V.M.

National Institute of Oceanography, Goa
November 2010

Abstract

Wind generated wave is the dominant forcing parameter for most of the nearshore processes. Accurate and fine resolution (both spatial and temporal resolutions) wave information is very essential for navigation, design of coastal/offshore structures and other marine activities. When waves generated by storms leave the zone of generation, they couple with locally generated waves, and create complex characteristics in the nearshore region. In the past, the source of wave information was mainly from ship observations. Advanced technologies led to the development of directional wave rider buoys and moored buoys which measure directional wave energy spectra at fixed point locations. Remote sensing sensors such as altimeter and scatterometer provide wind speed & wave height and wind speed & direction, respectively covering a large space. At times, in situ point measurements as well as satellite observations may not be adequate for site specific studies such as coastal development and beach stability. In this context, numerical modelling provides an opportunity to obtain the required wave information in fine resolution. Wave modelling results are also crucial to support forecasts and warnings to reduce risk of accidents and improve the efficiency of marine operations.

Wave characteristics along the Indian coast have been studied by earlier researchers based on ship observations, buoy measurements and remote sensing data. Most of these studies are restricted to specific locations or periods. However, a complete description of sea states for all seasons and extreme events is still in demand. Further, interaction between multi-directional and multi-frequency waves (both swells and wind seas) is still recognized as a complex phenomenon in the coastal region, as the local wind seas play a major role in controlling the wave generation and propagation mechanisms in this region. Influence of sea breeze on wind sea generation along the west coast of India is dominant during pre-monsoon season. The superimposition of these wind seas with pre-existing swells results in complex sea states, which makes the sea-faring more difficult than a single wave system. Generation and propagation of the multi-directional swells in the Arabian Sea, especially during pre-monsoon and NE monsoon seasons, their interaction with local wind seas along the west coast of India and their transformation at nearshore regions are a few scientific problems which find applications in the areas mentioned elsewhere. In this background, objectives of the present study are framed as follows:

i) understanding the wave generation and propagation processes in the select nearshore regions along the Indian coast through measured data

ii) validation of wave modelling results of deep and shallow waters using measurements and remote sensing data

iii) to study the interaction between pre-existing swells and wind seas generated by coastal winds

iv) prediction of wave transformation along the select Indian coasts using high resolution winds such as MM5

Chapter 1: Introduction, describes wind waves in general, regional wave scenarios, objectives, area of study and literature review.

Chapter 2: Data and methodology, describes the data used (wind, wave and pressure) and the methodologies applied. Wave measurements carried out at several deep and shallow waters locations in the north Indian Ocean using moored data buoys, directional wave rider buoys and non-directional wave recorders have been used in the present study along with satellite data (Jason-1). Winds measured using Autonomous Weather Station (AWS) and moored data buoys, QuikSCAT winds, re-analysed winds from various sources such as NCEP (National Centers for Environmental Prediction, USA), IFREREMER (French Research Institute for Exploitation of the Sea) and NCMRWF (National Centre for Medium Range Weather Forecasting, India), and MM5 (Mesoscale Model) were analysed and used in the wave model. Cyclone track data obtained from JTWC (Joint Typhoon Warning Centre, U.S.A.) and pressure data obtained from IDWR were also analysed. Wave spectra were separated into wind sea and swell energies and the corresponding wave parameters were calculated using the methodology provided by Gilhousen and Hervey (2001). The wind sea and swell parameters were further analysed to study their characteristics during different seasons. The dominance (in percentage) of swells and wind seas has been computed and anaysed for studying the monthly, seasonal and annual variations. Validation of MM5 winds and details of numerical models used are also described in Chapter 2.

Chapter 3: Numerical simulations - model set up and validation, it explains the setting up of numerical model for the Indian Ocean, model calibration and validation of model results with in situ and remote sensing data. Regional and local model domains were setup for the Indian Ocean (65° S to 30° N and 20° E to 130° E) and select coastal regions (Dwarka, Ratnagiri, Goa, Paradip and Dhamra). Bathymetry is set for rectangular grids and flexible

mesh. Moreover, a model with varying resolutions at deep water (coarse mesh) and coastal regions (fine mesh) has been setup to study the nearshore wave transformation along the Indian coast. Wind data from various sources have been applied as input parameter to simulate waves in the Indian Ocean. Sensitivity to various wind fields has been tested. Wind seas off Goa have been simulated using MM5 winds, and validated with calculated (separated from measured spectra) wind sea parameters.

Chapter 4: Seasonal response of coastal waves along the Indian coast: spectral approach. This chapter describes wave characteristics during monsoons and extreme events, dominance of swells along the west coast of India, potential swell generation regions, "Shamal" swells in the Arabian Sea and superimposition of coastal wind seas on pre-existing swells. The wave energy spectra off typical east coast (off Paradip) and west coast (off Goa) of India show the response of coastal waves to the seasons. It has been found that the spectra during extreme events are primarily single-peaked, and multi-peaked spectra of other seasons indicate the presence of multi-directional wave systems. The analysis of dominance of swells and wind seas show that the swells are dominated along the Indian coast during major part of the years and wind seas are dominated along the west coast of India during the pre-monsoon season. Potential swell regions were identified from measurements and modelling results and their propagation towards the west coast of India has been analysed. The presence of "Shamal" swells has been identified from the measured waves along the west coast of India during winter season. Typical mean periods of the Shamal swells are between 6 and 8 s and significant wave heights are between 1.0 and 2.0 m along the west coast of India. The generation and propagation of these "Shamal" swells and their influence along the west coast of India have been studied using numerical simulations. The results are discussed in detail.

The wind and wave data off Goa during pre-monsoon season (May 2005) reveals a distinct and systematic diurnal variation in wind speed, wave height and wave period, especially increase in wave height and decrease in wave period with increase in the intensity of coastal winds due to sea breeze system. Measured wave spectra distinctly bring out salient features of deep water swell and wind seas generated by the local sea breeze. Numerical simulations reproduced the characteristics of this daily cycle. The characteristic features observed in the wave parameters are due to the superimposition of wind seas with pre-existing swells. This phenomenon has been subject to detailed analysis, and the results are discussed in Chapter 4.

Chapter 5: Wave transformation along open coasts and semi-enclosed regions. This study illustrates the nature of wave transformation that can occur along the Indian coast. Wave patterns along the west coast of India are nearly the same, but wave heights are in the increasing order of magnitude from south to north. Wave heights along the east coast of India are in the increasing order during pre-monsoon and SW monsoon seasons, and in the decreasing order during NE monsoon season, from south to north, and the reduction among various depths are relatively less as compared to those along the west coast of India. Towards application of wave modelling, a case study has been carried out for the Mormugao Port region (Goa) to demarcate the inland vessels' limit (IVL) based the distribution of significant wave heights. Results are discussed in detail.

Chapter 6: Summary and conclusions. It describes the summary of the entire work and the main conclusions of the present study. Scope is provided for future work.

Contents

List of Tables

List of Figures

Chapter 1

Introduction

Chapter 1

Introduction

1.1. Ocean surface waves

Ocean surface waves are generated due to various forces acting on the ocean. The characteristics of the waves depend on controlling forces such as wind stress, earthquakes, gravity, Coriolis force and surface tension. Tidal waves are generated by the response to gravity of the moon and the sun, and are rather large-scale waves. Capillary waves, at the other end of the scale, are generated by surface tension in the water. For gravity waves, the major determining factors are earth's gravity and buoyancy of water (WMO, 1998). Based on period, the time taken by successive wave crests to pass a fixed point, the waves are classified into different categories. Figure 1- 1 shows their classifications by wave period (Munk, 1951). Waves with period less than 0.1 s are called capillary waves, between 0.1 and 1 s are gravity-capillary waves and between 1 and 30 s are ordinary gravity waves. The long-period waves such as storm surges and tsunamis have a range of period between 5 min. and 12 h, whereas the tidal waves range between 12 h and 24 h. Gravity waves generated by winds are present on the sea surface.

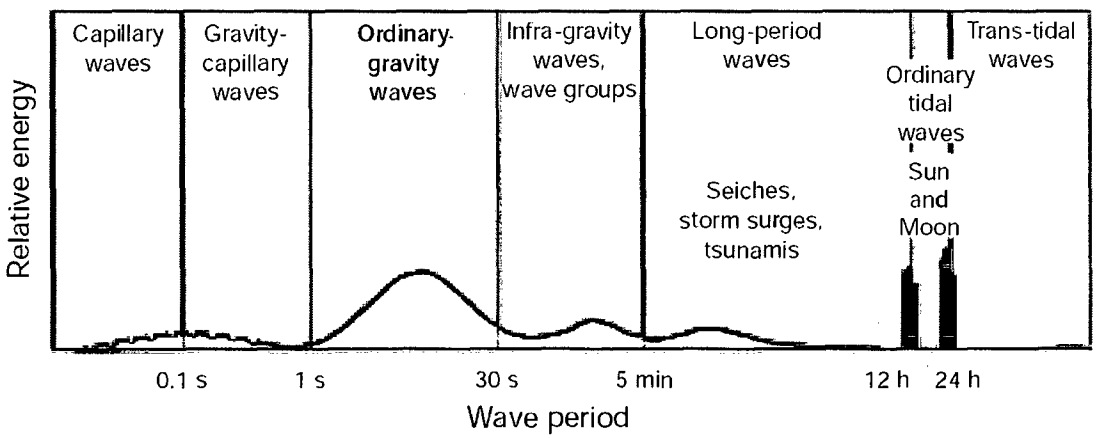

Figure 1- 1. Classification of ocean waves by wave period (Munk, 1951).

1.1.1. Definitions and relations

The simple wave motion is represented by a sinusoidal, long-crested and progressive wave (Figure 1- 2). The horizontal distance between two successive crests or troughs is called the

wavelength represented by λ, the time interval between the passage of successive crests or troughs passed a fixed point is called the *wave period* represented by T. The magnitude of the maximum displacement from mean sea-level is called the *wave amplitude* represented by a and the difference in surface elevation between the wave crest and the previous wave trough is called the *wave height* represented by H. For a simple sinusoidal wave $H = 2a$. The *frequency, f*, is the number of crests which pass a fixed point in 1 s; unit is Hertz and is same as $1/T$. The *phase speed, c*, is the speed at which the wave profile travels, i.e. the speed at which the crest and trough of the wave advance. The *wave steepness* is the ratio of wave height to wave length (H/λ).

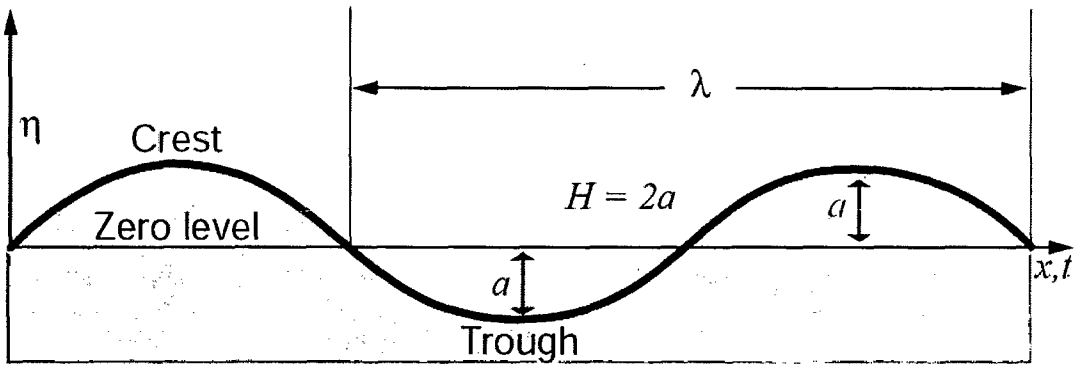

Figure 1- 2. A simple sinusoidal wave (WMO, 1998).

The wave profile has the form of a sinusoidal wave:

$$\eta(x,t) = a\,sin(kx - \omega t) \qquad (1.1)$$

where, η is the surface elevation, $k = 2\pi/\lambda$ is the *wavenumber* and $\omega = 2\pi/T$, the *angular frequency*. Wavenumber is a cyclic measure of the number of crests per unit distance and angular frequency is the number of radians per second. The variation of wave speed with wavelength is called *dispersion,* and the functional relationship is called the *dispersion relation*. The dispersion relation follows from the equations of motion for finite water depth can be expressed in terms of frequency, wavelength and water depth as follows:

$$\omega^2 = gk\,tanh\,(kh) \qquad (1.2)$$

where, g is gravitational acceleration and h is the water depth. In deep water ($h > \lambda/4$), tanh kh approaches unity. Hence,

$$\omega^2 = gk \qquad (1.3)$$

Therefore, wave speed in deep water is:

$$c = {}^{\lambda}/_{T} = {}^{\omega}/_{k} = \sqrt{{}^{g}/_{k}} \qquad (1.4)$$

When the relative water depth becomes shallow ($h < \lambda/25$), *tanh* (*kh)* approximately equals *kh.* Hence, Equation 1.2 becomes,

$$\omega^2 = gk^2h \qquad (1.5)$$

Therefore, wave speed in shallow water is:

$$c = \sqrt{gh} \qquad (1.6)$$

Hence, the waves in the shallow water are non-dispersive as the wave speed is independent of k.

1.1.2. Wave generation, growth and decay

The main input of energy to the ocean surface comes from the wind. Transfer of energy to the wave field is achieved through the surface stress applied by the wind and this varies as the square of the wind speed. Wind wave generation and growth are mainly controlled by three factors; wind speed, duration and fetch. Fetch is the area where the wind blows continuously without change in direction. Strong winds with long duration over a wide fetch could generate larger waves with long periods. These waves can travel hundreds (or thousands) of kilometers without much dissipation until it feels the bottom. In deep waters, the particle motion associated with the waves is circular and it is negligible beyond a depth equals $\lambda/2$. In shallow waters, the particle motion is elliptical and this extends upto the bottom.

Two mechanisms associated with wind wave growth are Philips' resonance (Philips, 1957) and shear flow instability (Miles, 1957). The resonance theory explains that small pressure fluctuations associated with turbulence in the airflow above the water are sufficient to induce small perturbations on the sea surface and to support a subsequent linear growth as the wavelets move in resonance with the pressure fluctuations. The theory of shear flow instability explains that air flow sucking at the crests and pushing on the troughs enables the waves to grow and the growth is exponential.

The ocean surface is represented by a combination of irregular wave components with different wavelength, amplitude and direction. Its chaotic pattern is due to the sum of wave components present at the region. The superimposition of various wave components creates an irregular pattern, which is usually observed at the wave generating areas. The waves in the generating area are termed as 'wind seas'. The waves propagating out from the generating area attain near sinusoidal and orderly patterns, and are termed as 'swells'. Total energy associated with the waves is equally divided between kinetic energy and potential energy. The energy moves with the speed of group of waves rather than individual waves. The speed associated with each individual waves is called 'phase speed' and the velocity associated with the wave groups or the velocity with which the energy is propagated is called 'group velocity'. In deep water, the magnitude of the group velocity (c_g) is half the phase speed (c), and, in shallow water, the group velocity is same as the phase velocity. The general expression for group velocity (c_g) in finite water depth (h) is given by,

$$c_g = \frac{c}{2}\left(1 + \frac{2kh}{Sinh\ 2kh}\right) \qquad (1.7)$$

Wave energy dissipation occurs mainly due to three processes; whitecapping, wave-bottom interaction and surf breaking. As waves grow, the steepness increases until it reaches a critical point, where the waves break. Whitecapping is highly non-linear and it limits the wave growth. 'Shoaling' is the effect of sea bottom when waves propagate into shallow water without changing direction. Generally, this enhances wave height and is best demonstrated when wave crests are parallel to depth contours. When waves enter into transitional depths, if they are not travelling perpendicular to the depth contours, the part of the wave in deeper water moves faster than the part in shallower water, causing the crest to turn parallel to the bottom contours. This phenomenon is called 'refraction'. Refraction causes reduction in wave energy, which depends on the depth contours and bottom characteristics. Obstruction, such as breakwaters, causes the energy to be transformed along a wave crest at the lee of the obstruction. This is called 'diffraction' and it causes much reduction in the wave height. Surf breaking occurs at extremely shallow waters, where depth and wave height are of the same order of magnitude (Battjes and Janssen, 1978).

1.2. Regional wave scenarios

Waves generated by winds or storms become ocean swells when they leave their generation zone, and travel long distances across the globe. Empirical data supports the idea that wind seas and swells together account for more than half of the energy carried by all waves on the ocean surface, surpassing the contribution of tides, tsunamis, coastal surges, etc. (Kinsman, 1965). Investigations on the contribution of ocean swell to the wind wave climate are, therefore, of great importance in a wide range of oceanographic studies, coastal management activities and ocean engineering applications. Design of coastal structures to a large extent depends on waves than any other environmental factors. When swells couple with locally generated waves, create complex wave characteristics in the nearshore region. The coexistence of wind sea and swell can significantly affect sea-keeping safety, offshore structural design, small boat operations and ship passages over harbour entrance and surf forecasting (Earle 1984). It also affects the dynamics of near-surface processes such as air-sea momentum transfer (Dobson et al., 1994; Donelan et al., 1997; Hanson and Phillips, 1999; Mitsuyasu, 2002). A wide range of activities such as shipping, fishing, recreation, coastal and offshore industry, coastal management and pollution control are affected by the wind waves (WMO, 1998).

In the past, the only source of wave information was visual observations made from ships. Advance technologies led to the development of directional wave rider buoys and moored buoys which measure the directional wave energy spectra. In situ wave measurements are essential for deriving design wave parameters and validation of wave model results. Remote sensing technologies have made good progress in the collection of various ocean parameters, including waves - altimeters and SAR are the main sensors for acquiring wave information. One of the limitations of point measurements is that the acquired information is applicable to a small area, may not be adequate for a large domain. Accurate wave information on fine spatial and temporal resolutions is necessary for navigation, design of coastal/offshore structures, etc. Numerical modelling technique provides an opportunity to obtain the required information on a reasonable resolution both temporal and spatial. Wave information provided by numerical models is crucial to support forecasts and warnings to reduce the risk of accidents and improve the efficiency of marine operations. Therefore, wave prediction has to be done accurately, several days in advance, the full range of sea states from the highest waves in storms to low-amplitude, long-period swells which may have been generated several hundreds of kilometers away.

Wave characteristics along the west and east coast of India are influenced by the three different seasons: pre-monsoon (February – May), southwest monsoon (June – September) and northeast monsoon (October - January). Along the west coast of India, wave heights are usually higher during SW monsoon and low during NE monsoon and pre-monsoon seasons. However, wave heights along the east coast of India are generally high during SW and NE monsoon seasons, and low during pre-monsoon season. In addition to these, tropical storms/cyclones occurring in the Bay of Bengal and in the Arabian Sea will have considerable impact on the wave characteristics along the Indian coast. Storms occur frequently in the Bay of Bengal than in the Arabian Sea. Wave heights above 5 m are usually observed along the coastal regions during tropical cyclones.

During fair weather season, the local winds become dominant due to weakening of global wind systems. Sea breeze and land breeze systems are prevalent along the west coast of India during pre-monsoon season. Wind seas generated due to sea breeze can create a highly dynamic environment in the nearshore regions, and beaches may respond rapidly to the changing wind wave climate. Interaction of local wind seas with pre-existing swells generate complex cross-sea conditions, which makes sea-faring more difficult than a single wave system.

Studies on wave characteristics in the Indian Ocean and coastal regions are primarily based on point measurements of limited duration and satellite measurements. The local wind effects on wind sea generation, interaction of wind seas with pre-existing swells and wave transformation at nearshore and semi-enclosed regions are not studied for the Indian coastal region. In this context, a dedicated effort has been made to understand the above complex phenomena using measurements, modelling and remote sensing. Use of numerical models in wave prediction can significantly improve the understanding of sea states, which are influenced by local wind seas. Fine resolution wave data at the nearshore regions are obtained through numerical simulations using a third generation wave model, which are further utilised to study the wave transformation along open coasts and semi-enclosed areas.

In the present study, numerical models are utilized to predict waves in the Indian Ocean for deep as well as shallow waters. Measured wave parameters at various locations have been used for model validation and detailed analysis. Remotely sensed wave parameters have been used for deep water wave analysis and model comparisons. Wind data obtained from

various sources, namely, in situ, simulated/reanalyzed and remotely sensed (gridded), have been utilized as input to the wave model.

Modelling results have been further applied for operational use in the coastal region. A pilot study for the safety of inland vessels has been carried out for the Mormugao Port region, to demarcate inland vessel's limit (IVL) based on distribution of significant wave heights.

1.3. Objectives

The objectives of the present study are given below:

i) understanding the wave generation and propagation processes in the select nearshore regions along the Indian coast through measured data.

ii) validation of wave modelling results of deep and shallow waters using measurements and remote sensing data.

iii) to study the interaction between pre-existing swells and wind seas generated by coastal winds.

iv) prediction of wave transformation along the select Indian coasts using high resolution winds such as MM5.

1.4. Area of study

Select locations along the Indian coast have been considered in the present study to understand wave transformation and interaction between local wind seas and pre-existing swells. West and east coasts of India differ in their topographic and bathymetric features and prevailing weather conditions. The east coast of India is characterized by narrow continental shelf width compared to the west coast. The sudden decrease in water depth causes the waves to surge further during extreme events, creating severe coastal hazards (Sanil Kumar et al. 2004c). The Bay of Bengal experiences three different weather conditions—fair weather, southwest monsoon and northeast monsoon. During fair weather season, the sea surface is usually calm and the coastal region is dominated by swells and to a smaller extent by the locally generated waves. Extreme weather events are common during NE monsoon (October–December) season and rare during SW monsoon (June–September) season. The most influencing wind system in the Arabian Sea is SW monsoon,

which has considerable impact along the west coast. During pre-monsoon and NE monsoon seasons, the global winds are generally weak, and the local winds play the major role of controlling the dynamics along the west coast of India.

Figure 1- 3 show the Indian Ocean region and coastal regions considered for the present study. Five locations along the west coast (Dwarka, Mumbai, Ratnagiri, Goa and Kochi) and four locations along the east coast (Nagapattinam, Visakhapatnam, Paradip and Dhamra) have been selected. Mormugao Port region (Figure 1-4) and Dhamra Port region (Figure 1-5) were considered specifically to study wave transformation at semi-enclosed water bodies.

Mormugao Port is situated on the west coast of India. Mormugao bay lies between Mormugao Point (15° 25'N, 73° 47'E) and Cabo Point. The south of the Mormugao bay is mostly rocky rising upto the tableland of Mormugao Head. The port of Mormugao, protected by a breakwater, lies on the north of Mormugao head. The Cabo point is a prominent headland (55m high).

Dhamra is located on the east coast of India, north of the mouth of the river Dhamra (20° 47.5'N, 86° 57.6'E). The Port is naturally protected by the river delta (Kanika sands), Gahirmatha landforms and surrounding mangroves, and these morphological features/vegetations dissipate waves propagating from various directions.

Numerical model domains and bathymetry used for the simulations are described in Chapter 3.

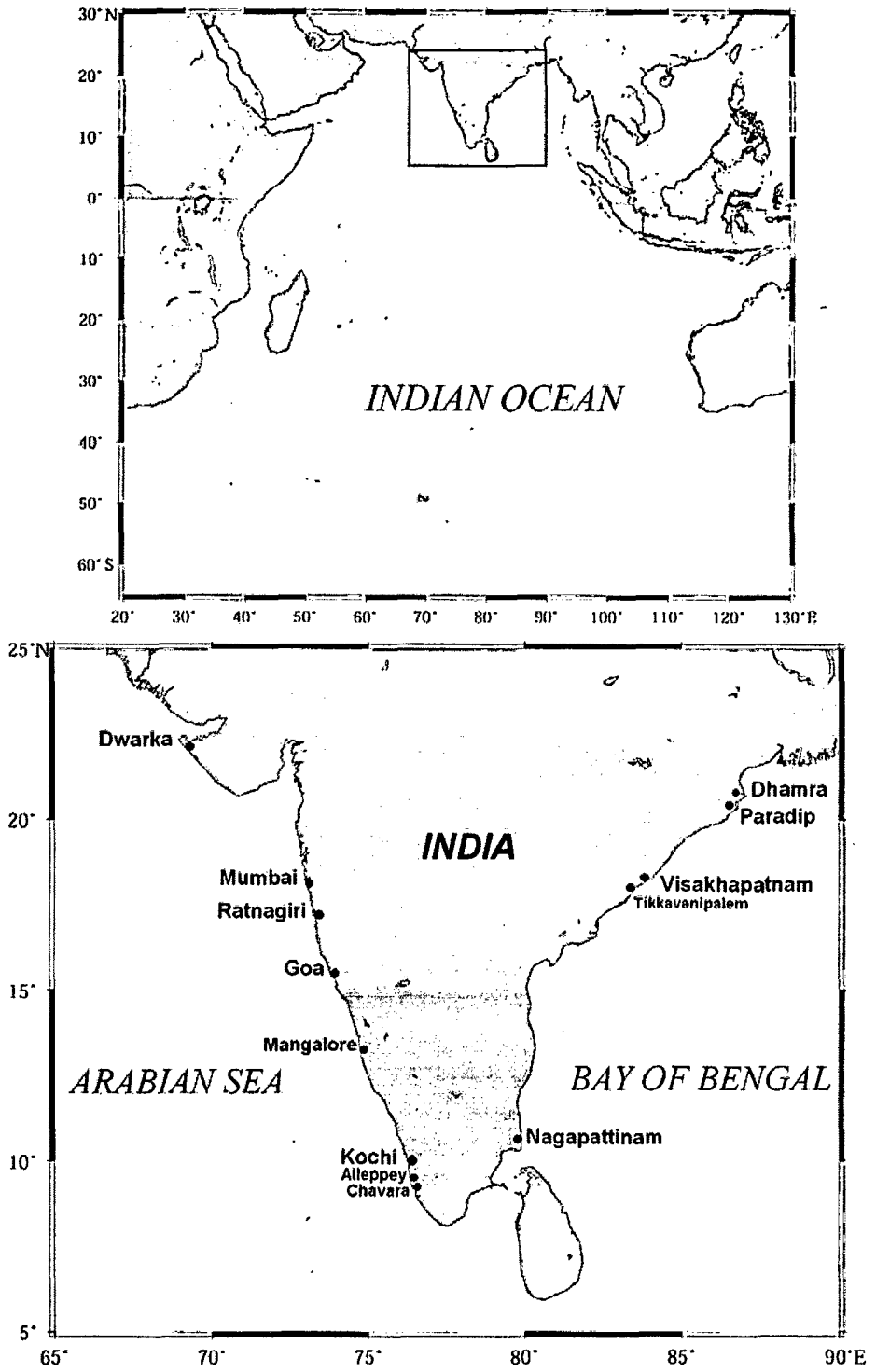

Figure 1- 3. Indian Ocean (top) and Indian coastal regions (bottom) considered for the study.

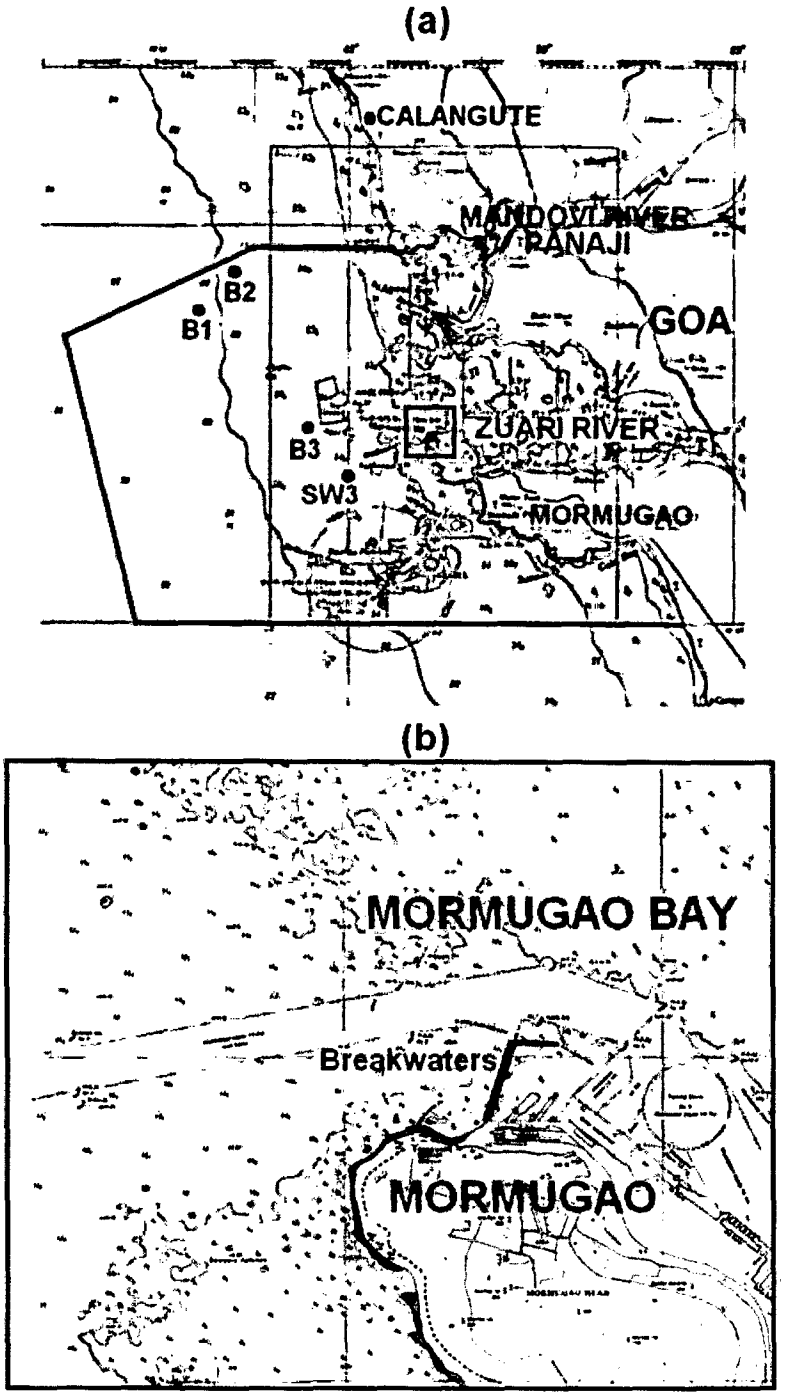

Figure 1-4. (a) Mormugao Port region including the locations of wave rider buoys and moored data buoy off Goa (Mormugao Port limit is marked inside with thick black line) and (b) breakwaters in the Mormugao Port. (taken from NHO Charts 2020 and 2078).

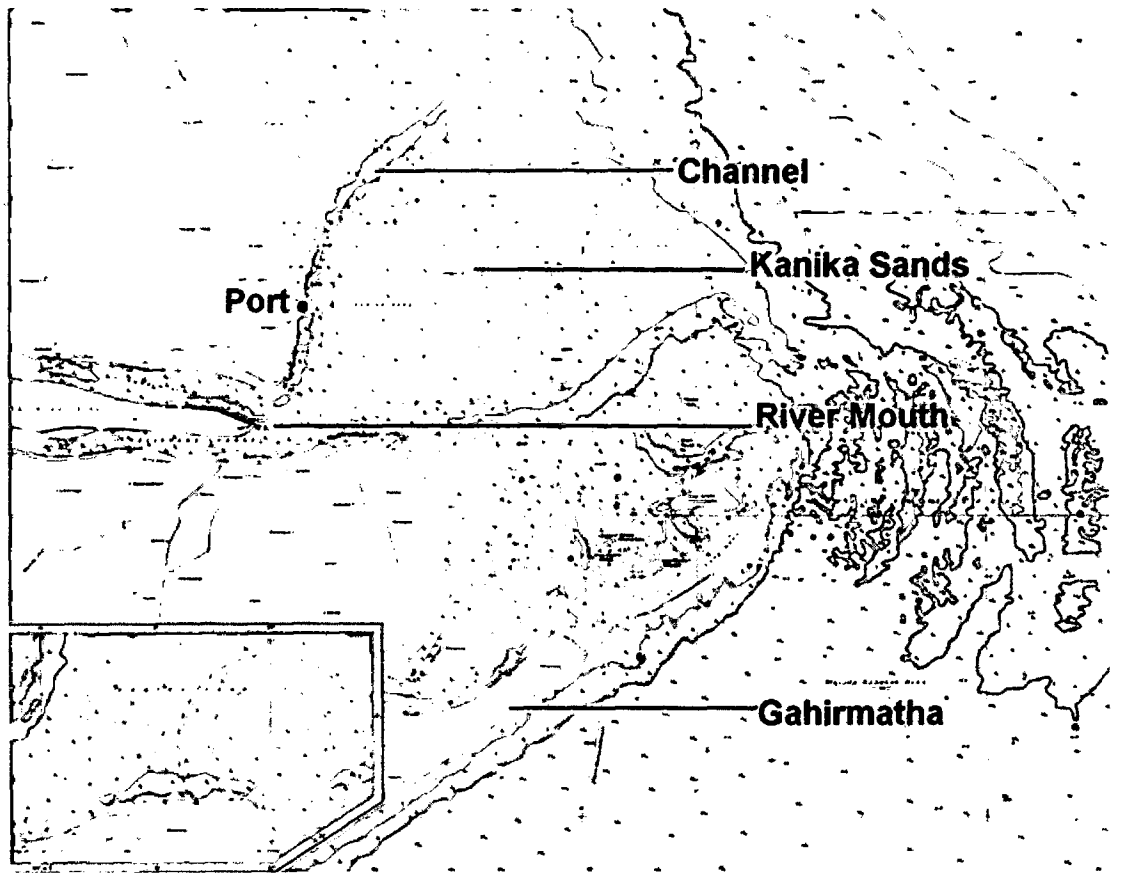

Figure 1-5. Dhamra Port and surrounding areas (taken from NHO Chart 3017).

1.5. Literature review

An extensive literature survey has been carried out to understand the dynamics of ocean waves, their interactions and transformations. As the subject is very vast, only relevant literature related to the specific work has been compiled and presented in the following sections.

1.5.1. Wave generation and growth – historical perspective

The study of ocean wave dynamics has a very long history. Lagrange, Airy, Stokes and Rayleigh, the 'nineteenth century pioneers of modern theoretical fluid dynamics' provided details about the properties of surface waves (Phillips, 1977). Jeffreys (1924, 1925) assumed that air flow over the waves causes 'sheltering' effect on the lee, so that work could be done by the wind as a result of the pressure difference across the moving wave.

Sverdrup and Munk (1947) postulated that the mechanical energy transferred from winds to water appeared as waves and not as currents. Barber and Ursell (1948) described a method for measuring ocean waves in shallow waters. Valuable contributions of Philips (1957) and Miles (1957) were added to the theory of wave generation by wind, and this led to rejection of Jeffreys' sheltering hypothesis. Both theories are based on wave generation by resonance: Phillips considered turbulent pressure fluctuations of surface waves, while Miles considered resonant interaction between the wave-induced pressure fluctuations and the free surface waves. Miles' mechanism looks more promising, because it implies exponential growth, and it is of the order of density ratio of air and water.

Miles' theory assumes that the air flow is inviscid, and turbulence does not play a role except in maintaining the shear flow (quasi-laminar approach). However, this approach oversimplifies the real problem. Early field experiments and laboratory studies by researchers (e.g., Dobson, 1971; Snyder, 1974; Snyder et al, 1981; Hasselmann and Bosenberg, 1991) show that the rates of energy transfer from wind to waves are larger than those predicted by Miles, especially for low-frequency waves. There are several limitations for the quasi-laminar approach; turbulence was not properly modelled and it ignored severe nonlinearities and wave-mean flow interaction. Wave-mean flow interaction is expected to be important at the height where the wind speed matches the phase speed of the surface waves (the so-called critical height). The advent of numerical modelling of the turbulent boundary layer flow over a moving sea surface resolved the issues associated with the turbulence for some extent. Further approaches (e.g., Al-Zanaidi and Hui, 1984; Jacobs, 1987 and Chalikov and Makin, 1991) considered the direct effects of small-scale turbulence on wave growth. Mixing length modelling or turbulent energy closure is then assumed to calculate the turbulent Reynolds stresses. However, the results are not very different from the one obtained in the quasi-laminar theory. Therefore, small-scale eddies and nonlinearities in wave steepness have only a small direct effect on wave growth. The efforts made by Fabrikant (1976) and Janssen (1982) on the theory of interaction of wind and waves indicates that at each particular time the wave growth follows Miles' theory and the results have been confirmed by observations. Combination of observations from field campaigns in the 1970's and the theoretical work on critical layer mechanism which started in the 1950's resulted in parameterizations of the wind-input source function. This provided good results in operational wave models.

Mixing length modelling assumes that the momentum transfer caused by turbulence is the fastest process in the fluid. This is not justified for low-frequency waves which interact with large eddy whose eddy-turnover time may become larger than the period of the waves. Nikolayeva and Tsimring (1986) considered the effect of gustiness on wave growth, and found a considerable enhancement of energy transfer due to large-scale turbulence, especially for long waves with a phase speed comparable to the wind speed at 10 m height. Belcher and Hunt (1993) have pointed out that mixing length modelling is even inadequate for slowly propagating waves. They argue that far away from the water surface turbulence is slow with respect to the waves so that again large eddies do not have sufficient time to transport momentum. This approach has been further developed by Mastenbroek (1996) in the context of a second-order closure model for air turbulence, confirming the ideas of rapid distortion. Following the rapid-distortion ideas, Janssen (2004) argued that the large eddies are too slow to transport a significant amount of momentum during one wave period.

The most direct evidence for the dependence of the air flow on the sea waves comes from the observed dependence of the drag coefficient on the so-called wave age (c_p/u_*, where c_p is the phase speed of the peak of the spectrum and u_* the friction velocity). Measurements by, for example, Donelan (1982), Maat et al (1991), Smith et al. (1992), Drennan et al. (1999) and Oost et al. (2002) indicate that the drag coefficient depends on the sea state through the wave age. For a fixed wind speed at 10 m height, the drag coefficient of air flow over young wind sea is 50% larger than the drag coefficient over old wind sea (Donelan, 1982). Including the effects of small scale turbulence, Jenkins (1992) observed similar results of the drag coefficient as obtained in the quasi-linear theory. Komen et al (1994) found that quasi-linear theory of wind wave generation gives a better description of momentum transfer than the usual theory of wave growth since quasi-linear theory gives a drag coefficient that describes the sea state dependence on the drag.

Parameterization of the roughness length in terms of wave-induced stress shows a fair agreement with observed roughness (Janssen, 1992). Short waves are the fastest growing waves; the wave-induced stress is to a large extent determined by the spectrum of the high-frequency waves (see, e.g. Janssen, 1989; Makin et al., 1995). Using wavelet analysis, Donelan et al. (1999) found that wavenumber spectrum of the short waves depends in a sensitive manner on wave age: 'young' wind sea shows much steeper short waves than 'old' wind sea. Sullivan et al. (2000) studied the growth of waves by wind in the context of

an eddy-resolving numerical model. He found a rapid fall-off of the wave-induced stress at the critical height, as expected from the Miles mechanism. The growing waves act as a rectifier, therefore gustiness may have a considerable impact on wave growth (Abdalla and Cavaleri, 2002). Furthermore, Hristov et al. (2003) identified direct evidence of the existence and relevance of the critical layer mechanism from in-situ observations obtained from FLIP (FLoating Instrument Platform). For long waves, a positive fluctuation in wind speed will result in enhanced wave growth but, a negative fluctuation will not give rise to reduced growth (WISE Group, 2007).

1.5.2. Wave energy spectrum

The concept of wave spectrum was first introduced to wind wave studies around 1950. Over the following decades, Fourier spectrum was the standard procedure used to analyse and predict wind waves. Notably, Barber and Ursell (1948) carried out the first measurement and analysis of wave spectra. Pierson and Marks (1952) introduced power spectrum analysis in wave data analysis. Later, the methods introduced by Pierson et al. (1955) led to the advancement of understanding wave dynamics. Wavelet analysis evolved as an effective alternative to the standard Fourier analysis (Combes et al., 1989). Further, with the development of Fast Fourier Transform (FFT), spectrum analysis becomes routine in time series wave data analysis (Liu, 2000).

The directional wave energy spectra provide a complete description of the wave energy distribution over spectral frequencies f and direction θ. The energy-density spectra can be written in the form of $E(f, \theta) = E(f)D(f, \theta)$, where, $E(f)$ represents the frequency spectrum which is assumed as a function of significant wave height (H_s) and the peak frequency (f_p), while $D(f, \theta)$ represents the directional spectrum which is assumed by the mean wave direction (θ) and directional spreading parameter (s).

As sea state consists of local wind-generated waves and swells of distant storms, the wave energy spectra often show two or more spectral peaks corresponding to different generation sources. Depending on sea states and measurement sites, the occurrence of double-peaked spectra could be even higher. Guedes Soares (1984) proposed the ratio of peak frequencies of the two components as spectral parameters to describe the relation of the two wave systems. Relatively close double peaks (looks as if single-peaked) indicate combination of sea state with two wave systems coming from the same or different directions (Guedes Soares,1991). According to Torsethaugen and Haver (2004), single-peakedness occurs

when spectral peak period (T_{pf}) for fully developed sea equals peak wave period (T_p). The sea dominance occurs when $T_p < T_{pf}$, where the spectral peak is in the high frequency region, and double or multiple peaks present during such conditions. The swell dominance occurs when $T_p > T_{pf}$, where the spectral peak is in the low-frequency region.

Separation of sea and swell parameters from the spectra is essential to understand the dynamics associated with each system. Identification and separation of the wave energies of wind sea and swell from the measured spectra allow us to have a more realistic description of the sea state, which is of great importance to offshore structural design, safety of marine operation and for the study of wind wave dynamics (Wang and Hwang, 2001). Algorithms are developed to separate wind sea and swell components from wave spectra. The partitioning methods primarily involve separating the wave spectra into two frequency bands: a low-frequency interval (swell component) and a high-frequency interval (wind sea component). Most methods for the automatic identification and separation of wave components of wind sea and swell rely on the determination of a separation frequency f_s for a given wave spectrum. Wang and Hwang (2001) used a separation frequency, f_s based on wave steepness to distinguish between wind seas and swells. Wave components with frequencies greater than f_s are generated by local winds and those with frequencies less than f_s are from distant swells. Earle (1984) proposes an empirical relation between the separation frequency and the local wind speed U based on the Pierson-Moskovitz (PM) spectral model (Pierson and Moskowitz, 1964). The algorithm introduced by Gerling (1992) takes into account identification and grouping of component wave systems from spatially and temporally distributed observations of directional wave spectra. Using wind and wave directional data, a directional spectra partitioning scheme has been developed for identifying wind sea and tracking storm sources (Gerling, 1992; Kline and Hanson, 1995; Hanson, 1996; Hanson and Phillips, 2001).

Violante-Carvalho et al. (2004) studied the wind sea and swell characteristics at Campos Basin, South Atlantic by calculating the sea-swell parameters from measured spectral data. Using an empirically determined width of the confidence intervals of the spectral data, a procedure is developed by Rodriguez and Guedes Soares (1999) to differentiate legitimate energy peaks of wind sea and swell from the spectral irregularities caused by the artifacts of random processes. Portilla et al. (2009) discussed various techniques and methods for partitioning and identifying wind sea and swell. Gilhousen and Hervey (2001) provided techniques to improve accuracy of the estimates of swell from moored buoys. This method

determines a separation frequency by assuming that wind seas are steeper than swells and that maximum steepness, or ratio of wave height to length, occurs in the wave spectrum near the peak of wind sea energy. This method has been used by National Data Buoy Centre (NDBC), NOAA, USA.

1.5.3. Remote sensing

Wind and wave data obtained from remotely sensed sources such as scatterometer and altimeter are widely used to understand wind and wave patterns around the globe. Remote sensing data are widely used in operational oceanography by assimilating them with third generation models.

Surface waves are measured by active microwave sensors by transmitting electromagnetic energy. Highly sophisticated signal analysis has made it possible to obtain information on the ocean waves by studying the reflected signal. The first ocean satellite SEASAT demonstrated in 1978 that wave heights could be accurately measured with a radar altimeter and that a SAR (Synthetic Aperture Radar) was capable of imaging ocean waves. Unfortunately, SEASAT failed after three months, and further satellite wave measurements were not made until the radar altimeter aboard GEOSAT was put into orbit in 1985. After the short parenthesis of GEOSAT operated till 1989, satellite data began flowing in 1991 with the launch of the first European Remote Sensing Satellite ERS-1, followed by Topex/Poseidon in 1992 and in 1995 by ERS-2. These satellites have onboard an altimeter (ERS 1 & 2 and Topex) and a scatterometer (ERS 1 & 2). The altimeter provides wind speed and wave height at 7 km intervals (once a second) along the ground track of the satellite. The scatterometer provides wind data, all along the width of the swath, a few hundreds of kilometers. ERS 1 and 2 have been following an orbit with a return period of 30 days; however, Topex has been following an orbit with 10 days period. Since 1999, wind data from QuikSCAT and since 2002, wave data from Jason-1 are available.

The SEASAT altimeter showed a good match when compared with buoy wave heights (Graber et al, 1996). Earlier studies for the ERS-1 altimeter (Goodberlet et al, 1992 and Gunther et al, 1993) also showed match for wave heights upto 4 m, although high waves tend to be underestimated by the altimeter relative to the buoy measurements. Mastenbroek et al (1994) reached a similar conclusion from a comparison of ERS-1 data with North Sea observations. The accuracy of altimeter wave height measurements is confirmed also by the global inter-comparison of ERS-1 altimeter and WAM model wave

heights for the month of July 1992 (Komen et al., 1994). The altimeters in Topex and ERS 1 & 2 provide accuracy of 2m/s in wind speed and 10% or 50 cm (whichever is better) in wave height (Duchossois, 1991; Fu et al., 1994). The wind speeds derived from the altimeter are not reliable at very low wind speeds, the threshold speed being 2 m/s. The retrieval algorithm also loses its reliability in the very high value range, above 20 m/s, due to physics involved in the sea surface processes.

The SeaWinds scatterometer onboard QuikSCAT gives instantaneous wind vectors along a wide swath (1800 km) with a spatial resolution of 25 km and two passes per day (ascending and descending) (Ebuchi et al., 2002). The accuracy of wind speed is 2 m/s between 3 and 20 m/s (approximately 10%) and that of wind direction is 20°. The gridded product of QuikSCAT winds were derived by IFREMER and it is available globally in every 0.5° x 0.5° (C2-MUT-W-03-IF, 2002). Gille et al. (2003) used QuikSCAT data to study the characteristics of sea breeze and land breeze systems present in most of the world's coastlines. Aparna et al. (2005) studied the seaward extension of the sea breeze along the southwest coast of India utilizing QuikSCAT winds. Satheesan et al. (2007) analysed the QuikSCAT winds by comparing with buoy winds in the Indian Ocean.

Jason-1 is relatively a small satellite developed by NASA and CNES for measuring oceanographic and meteorological parameters. It provides significant wave heights and wind speeds along the satellite ground tracks over 6-7 km with repeat cycle of 7 days. Gridded product of Jason-1 provides significant wave heights for every 1° x 1° resolution in alternate 3 and 4 days (Quilfen et al, 2004). The calibration of Jason-1 data (wind and wave) has been carried out by Bonnefond et al. (2003) and Chambers et al. (2003). Ardhuin et al. (2007) validated these data with buoy observations. Bhatt et al. (2005) used Jason-1 significant wave heights to assimilate in a third generation wave model.

The altimeter and scatterometer data may not be accurate close to the coast because of the interference with the land. Besides, when the satellite moves towards offshore, and entered in the marine area, it requires certain time to work properly again. This implies that reliable wind speeds are not available upto 25-30 km off the coasts (Cavaleri and Sclavo, 2006).

1.5.4. First, second and third generation models

Interest in wave prediction grew during the Second World War II because of the practical need for knowledge of the sea state during landing operations. At first, Sverdrup and Munk (1947) introduced a parametrical description of the sea state and empirical wind sea and

swell laws for the operational wave predictions. Gelci et al., (1957) introduced the concept of the spectral transport equation and he used a purely empirical expression for the net source function governing the rate of change of the wave spectrum. Based on the wave generation theories provided by Philips (1957) and Miles (1957), Hasselmann (1962) introduced the source functions for the nonlinear transfer. The general expression for the source function consists of three terms representing the input from the wind, the nonlinear transfer and the dissipation by white-capping or bottom friction.

A numerical spectral wave model calculates the evolution of the wave energy according to physical laws governing the change of wave energy. Several first and second generation numerical models were developed in the last few decades. Subsequently, third generation wave models were developed and at present, a few of them are widely used for the operational wave forecasting. Theoretical explanations about numerical wave modelling and a third generation wave model WAM are described in Komen et al. (1994).

1.5.4.1. First generation models

The first empirical wave model was developed by Sverdrup and Munk (1947) and introduced a parametric description of the sea state. Subsequently, PNJ-model was developed for estimating wave conditions created by distant storm (Pierson et al., 1955). Darbyshire (1961) made significant improvements in the PNJ-model and used it to predict waves over the North Atlantic. It was assumed that the sea state was fully developed after 12 hours and 200 nm of constant wind. However, the model proposed by Wilson (1955) was considered as ideal, and further used by several researchers (e.g., Bretshneider, 1963 and Barnet and Wilkerson, 1967). A directional de-coupled model was developed by Seymour (1977), in which a stationary homogeneous wind field is considered over a deep water basin with an arbitrary geometry of the coastline.

The first generation models accounted only wave energy growth and dissipation. At that time, very little was known about nonlinear interactions and energy loss due to whitecapping, and hence these were not taken into account in the first generation models. Later, it became clear that interactions between waves of different frequencies were important in determining the distribution of wave energy in the spectrum. These non-linear interactions are very difficult and expensive to compute explicitly, and parameterizations were developed to account for the effect.

1.5.4.2. Second generation models

Wave models using a parameterization of the non-linear interactions are known as 'second generation'. In second generation models, the sea surface is defined as the sum of a large number of individual wave components, each wave propagating with constant frequency according to the linear wave theory. The path of wave components is calculated by the conventional methods. After leaving the origin, the wave component interacts with the other wave components. Thus, the energy gained or released in the process can be evaluated till it reaches the forecast point at regular intervals.

Typically, there are two types of models in the second generation; coupled hybrid and coupled discrete. In coupled hybrid models the wind sea spectrum, which is strongly controlled by the nonlinear interactions, is assumed to adjust rapidly to a universal quasi-equilibrium form in which only a single scale parameter – normally the wind sea energy – or at the most a second frequency scale parameter need to be predicted as slowly varying parameters. The swell, which is not affected by nonlinear interactions, is then treated as a superposition of independent components in the same way as in a first generation model. Coupled discrete models retain the traditional discrete spectral representation, but have a parameterization of the nonlinear transfer with limited validity, so that the potential advantage of a more flexible representation of the wind sea spectrum and a uniform representation of the swell – wind sea transition regime cannot be properly exploited. Mandal (1985) used a deep water hybrid point model DOLPHIN developed by Holthuijsen and De Boer (1988), which is a combination of parametric wind-sea and spectrally treated swells. It is based on the directionally decoupled energy distribution of wind generated waves.

Results from many of the operational first and second generation models were inter-compared in the SWAMP (1985) study. Although the first and second generation wave models can be calibrated to give reasonable results in most wind situations, the inter-comparison study identified a number of shortcomings, particularly in extreme wind and wave situations for which reliable wave forecasts are most important. The differences between the models were most pronounced when the models were driven by identical wind fields from a hurricane. The models gave maximum significant wave heights in the range 8 to 25 m.

1.5.4.3. Third generation models

Further developments led to an approximation for the non-linear energy transfer, which consider the four most important interacting waves at each frequency out of the infinite number of interactions theoretically possible. This approximation is more expensive to compute than the parameterization of a second-generation model but, unlike a second-generation model, the wave spectrum is not forced to take a particular form for growing wind-sea, and is free to evolve according to the physical equations. Such a wave model is called 'third generation'. The major limitations of the first and second generation models are:

- first generation models do not have an explicit S_{nl} term. Non-linear energy transfers are implicitly expressed through the S_{in} and S_{ds} terms, where S_{nl}, S_{in} and S_{ds} are the source terms representing energy transfer due to non-linear interactions, energy input from wind and energy loss due to dissipation, respectively.
- second generation models handle the S_{nl} term by parametric methods: for example, by applying a reference spectrum (say, JONSWAP or Pierson-Moskowitz spectrum) to reorganize the energy (after wave growth and dissipation) over the frequencies.

As a consequence of the variable results from the SWAMP study, and with the advent of more powerful computers, scientists began to develop new, third generation wave models which explicitly calculate each mechanism identified in wave evolution. The main difference between the second and third generation wave models is that in the latter case, the wave energy-balance equation is solved without constraints on the shape of the wave spectrum. This is achieved by accurately calculating the S_{nl} term. Resio et al. (1991) derived a new method for the exact computation of this term. Hasselmann and Hasselmann (1985) introduced Discrete Interaction Approximation (DIA) in wave modelling. The efficient computation of the non-linear source term together with more powerful computers made it possible to develop third generation spectral wave prediction models (WAMDI Group, 1988). The operational wave models, such as WAM (WAMDI Group, 1988 and Komen et al., 1994), SWAN (Booij et al., 1999) and WAVEWATCH III (Tolman, 1999) are third generation models.

Third generation wave models are similar in structure, representing the state-of-the-art knowledge of the physics of the wave evolution. For the WAM model, the wind input term, S_{in}, for the initial formulation was adopted from Snyder et al. (1981) with a u_* (friction

velocity) scaling instead of U_5 (wind speed at 5 m). This has been superseded by new quasi-linear formulations by Janssen (1992) and Komen et al. (1994), which include the effect of growing waves on the mean flow. The dissipation source function, S_{ds}, corresponds to the form proposed by Komen et al. (1984), in which the dissipation has been tuned to reproduce the observed fetch-limited wave growth and to eventually generate the fully developed Pierson-Moskowitz spectrum. The non-linear wave interactions, S_{nl}, are calculated using the discrete interaction approximation of Hasselmann et al. (1985). The model can be used both as deep water and shallow water model (WAMDI Group, 1988). A comprehensive description of the model, its physical basis, and formulation and various applications are given in Komen et al. (1994). Other models may differ in the propagation schemes used, in the method for calculating the nonlinear source term, S_{nl}, and in the manner in which they deal with shallow water effects and the influence of ocean currents on wave evolution. In general, the governing equation (so called energy balance equation) applied in the third generation model is,

$$\frac{\partial F}{\partial t} + c_g \,.\, \nabla F = S_{in} + S_{nl} + S_{dis} \qquad (1.8)$$

where, the left hand side terms represent the time derivative and the kinematics of the field, and the right hand ones the physical processes at work for its evolution. $\partial/\partial t$ is the derivative with respect to time, $\mathbf{c_g}$ is the group speed and $\nabla \mathbf{F}$ represents the spatial gradient of the field.

Vledder (2001) improved the parameterization of nonlinear quadruplet wave-wave interactions for application in operational wave prediction models. Further improvements have been carried out to obtain a fast and accurate method for computing the nonlinear quadruplet wave-wave interactions in deep and shallow water. For reaching closer values of non-linear transfer, Tolman et al. (2005) developed a neural network parameterization called Neural Network Integration Approximation (NINA), which estimates nonlinear interactions as a function of frequency and direction from the corresponding spectrum in deep water. It is implemented in WAVEWATCH III model. Neural networks can be incorporated in numerical wave modelling for solving complex nonlinear functions in an efficient way (Mandal and Prabaharan, 2010).

The third generation models are widely used for operational wave forecasting. European Centre for Medium-Range Weather Forecasts (ECMWF) extensively use WAM model for

operational wave forecasting. Prasad Kumar and Stone (2007) used the third generation model, WAM to simulate the generation and propagation of typhoon waves in Korean seas. Kurian et al. (2009), Vethamony et al (2009) used third generation wave model, MIKE 21 SW, developed by Danish Hydraulic Institute (DHI), Denmark to simulate waves around the Indian Ocean and west coast of India. Aboobacker et al., (2009) used this model to simulate waves off Paradip, east coast of India.

1.5.5. Impact of sea breeze on nearshore waves

The sea breeze circulation system - a common mesoscale meteorological phenomenon - has a profound effect on the meteorology and oceanography of coastal areas (Simpson, 1994). It flows perpendicular to the coastline and drives a density current that moves cool moist marine air over the land. The sea breeze is at its maximum in the late afternoon. Relatively low speed land breeze starts blowing towards the sea in the night.

A few studies have been carried out on wave characteristics due to sea breeze. For example, the coastal region of Sydney, Australia, was studied by Linacre and Hobbs (1977), Short and Trenaman (1992) and Masselink and Pattiaratchi (1998). They observed that the sea breeze is most prevalent between 12 and 21 h (local time) during the summer season (October – April), and typically produces a wave with 1 – 1.5 m height and periods ranging between 6 and 9 s. Masselink and Pattiaratchi (1998) pointed out that, following the onset of the sea breeze, the addition of locally generated wind waves to background swell resulted in an increase in wave height and a decrease in wave period. Verhagen and Savov (1999) studied wave growth due to sea breeze in Cartagena (Colombia) region, and estimated the duration of wave action based on that of the sea breeze.

Sea breeze induces changes to the incident wave field that may significantly affect beach morphology and processes. Sonu et al. (1973) observed increase in nearshore wave height, decrease in wave period and change in wave angle depending on the direction of the sea breeze after the onset of the sea breeze, typically late morning or early afternoon. As a consequence, wave energy, current velocities, suspended sediment concentrations and sediment transport rates increase dramatically following the commencement of sea breeze (Pattiaratchi et al., 1997).

1.5.6. Wave transformation

Wind-generated waves are identified as the major driving force for near-shore circulation and sediment transport in the surf zone and inner continental shelf (Wright *et al.,* 1991). When the waves approach the shallow depths, the group velocity starts to reduce. This generally leads to turning of the wave direction (refraction) and shortening of wavelength (shoaling), which may result in increase or decrease in wave height. The most important physical processes, which affect the waves in shallow waters are dissipation due to bottom friction (e.g. Shemdin et al., 1980), bottom induced wave breaking (e.g. Battjes and Janssen, 1978) and triad wave-wave interactions (e.g. Madsen and Sorensen, 1993).

As waves shoal in coastal waters, wave energy spectra evolve due to refraction, nonlinear energy transfers to higher and lower frequencies (Freilich and Guza 1984; Freilich et al., 1990), and energy dissipation caused by wave breaking and bottom friction (Thornton and Guza, 1983; Sheremet and Stone, 2003). Smith and Vincent (2002) found that in the inner surf zone, wave spectra evolve to a similar, single-peaked shape, regardless of the complexity of shape outside the surf zone. It is postulated that spectral shape evolves from the strong nonlinear interactions in the surf zone.

Extensive observations in the Joint North Sea Wave Project (JONSWAP) revealed that swell attenuates in shallow water by bottom friction and the relative reduction in wave height is more pronounced for increasing near-bottom velocities (Hasselmann et al., 1973). Ardhuin et al. (2003) studied attenuation and directional transformation of waves in swell dominated conditions across North Carolina continental shelf during the 1999 Shoaling Waves Experiment (SHOWEX). They observed strong attenuation of large swells across the wide and shallow shelf, with typical wave height reductions of factor 2, and relatively weak variations for small swells with Hs < 1.0 m offshore. Strong decay of energetic swell in the absence of local winds suggests that dissipation of wave energy by bottom friction is the primary attenuation mechanism. Among other possible swell dissipation mechanisms, percolation was estimated to be much smaller than bottom friction for fine to medium sand and significant only for coarser sediments, while bottom elasticity is only important over sediments composed of mud or decomposed organic matter (Shemdin et al. 1980). In addition to dissipative processes, backscattering of waves by the bottom topography may cause attenuation of waves toward the shore (Long 1973), but the estimated wave decay over actual bathymetry is extremely weak (Richter et al., 1976; Ardhuin and Herbers

2002). However, forward scattering of waves can cause significant broadening of wave directional spectra (Ardhuin and Herbers, 2002).

Models for the wave transformation are important to predict nearshore circulation and sediment transport. In addition to the well understood linear processes of shoaling and refraction, the wave transformation is affected by nonlinear interactions and wave breaking (Herbers et al., 2003). These interactions not only broaden the frequency spectrum in shallow water, but also phase couple the spectral components, causing characteristic steepening and pitching forward of near-breaking wave crests (e.g., Freilich and Guza, 1984; Elgar and Guza, 1985). This nonlinear evolution is described well by depth integrated Boussinesq equations for weakly nonlinear, weakly dispersive waves in varying depth (Peregrine, 1967). Most models for the breaking of random waves are based on the analogy of individual wave crests with turbulent bores (Battjes and Janssen, 1978; Thornton and Guza, 1983). Estimates of nonlinear energy transfers in the surf zone based on bi-spectral analysis of near-bottom pressure fluctuations confirm the dominant role of triad interactions in the spectral energy balance (Herbers et al., 2000).

1.6. Studies along the Indian Ocean region

Studies on ocean surface waves carried out in the Indian Ocean waters and briefly given below: Sundara Raman et al. (1974) studied the distribution of wave characteristics in the coastal waters off Mangalore, southwest coast of India. They found that the relative frequency of occurrence of long period waves increases from April to November. Baba et al. (1983) studied wave refraction in relation to beach erosion along the Kerala coast, southwest coast of India. Kurian et al. (1985) studied wave transformation off Alleppey, southwest coast of India using a refraction model developed by Dobson (1967) and, subsequently modified by Coleman and Wright (1971) to accommodate bottom frictional attenuation. Wave damping and attenuation due to mud banks along the Kerala coast have been well studied by Mac Pherson and Kurup (1981), Mathew et al. (1995) and Jiang and Mehta (1996). Kurian and Baba (1987) conducted a detailed study of wave attenuation due to bottom friction at select locations across the southwest Indian continental shelf. Chandramohan et al. (1991) used ship observed data to study wave statistics around the Indian coast. Swain et al. (1993) studied shallow water wave characteristics off Cochin during the southwest monsoon of 1986. Directional spreading of waves in shallow waters have been studied by Sanil Kumar et al. (1999). They found that in shallow water, wave

directional spreading is narrow at the peak frequency and wide towards lower and higher frequencies. Shahul Hameed et al. (2007) studied seasonal and annual variations in wave parameters off Chavara coast, southwest coast of India, based on continuous measurements of 2 years.

Harish and Baba (1986) and Rao and Baba (1996) studied spectral characteristics of waves along the southwest coast of India and observed that the spectra are generally multipeaked. Vethamony and Sastry (1986) studied the characteristics of multipeaked spectra of ocean surface waves. Baba et al. (1989) also analysed the wave spectra off Cochin, southwest coast of India and studied the swell characteristics. Rao and Baba (1996) studied the wind sea and swell characteristics along the southwest coast of India and identified that wind sea energy was dominant over swell energy during pre-monsoon period. Sanil Kumar et al. (2000) studied the wave characteristics along the west coast of India during southwest monsoon and observed that swells are predominant during southwest monsoon season. Sanil Kumar et al. (2001) separated seas and swells from directional wave data collected off Tikkavanipalem, east coast of India and estimated longshore currents and longshore sediment transport rate. Sanil Kumar et al. (2002) studied sea and swell characteristics off Nagapattinam coast, east coast of India based on one year continuous directional wave measurements. Sanil Kumar et al. (2003a) studied multipeakedness and groupiness of shallow water waves along the Indian coast. Sea and swell dominated double peaked spectra were present for different periods at various locations. Sanil Kumar and Anand (2004a) used first and second order Fourier coefficients to estimate variations in wave direction at four locations in the west and east coast of India. Considering directional distribution of waves at three locations along the Indian coast and 18 years of ship reported data, Sanil Kumar and Deo (2004b) estimated design wave parameters Sanil Kumar and Ashok Kumar (2008) analysed spectral characteristics of high shallow water waves (significant wave heights above 2 m) and derived an empirical equation relating the JONSWAP parameters with significant wave height, peak wave period and mean wave period. Aboobacker et al. (2005 and 2009) studied spectral characteristics off Paradip during monsoons and extreme events. Vethamony et al., (2009) analysed the spectra measured off Goa during pre-monsoon season.

Numerical simulations have been carried out in the Indian Ocean to study the wave characteristics during various seasons (e.g., Aboobacker et al., 2009; Vethamony et al., 2009; Rajkumar et al., 2009; Kurian et al., 2009). Abhijit Sarkar et al. (1997) simulated

waves in the north Indian Ocean and compared predicted wave heights with altimeter measurements. Sudheesh et al. (2004) assessed wave modelling results with deep water buoy measurements and altimeter data during southwest monsoon. Vethamony et al. (2006) simulated waves in the north Indian Ocean using MSMR (Multi-channel Scanning Microwave Radiometer) analysed winds.

Prasad Kumar et al. (2000) analysed extreme wave conditions over the Bay of Bengal during severe cyclone utilizing numerical simulations. They used a second generation wave model (Resio model) and a third generation wave model (WAM) to simulate state of the sea for an exceptionally severe cyclone which occurred over the Bay of Bengal during November 1977. Sanil Kumar et al. (2003b) studied the wind and wave characteristics during cyclones (1960 – 1996), which crossed Nagapattinam coast, by estimating the wind speeds and wave heights using various techniques. Based on measured wave energy spectra, Sanil Kumar et al. (2004c) demonstrated wave characteristics along the Visakhapatnam coast, east coast of India during an extreme event. They identified that the spectra were single-peaked during the storm event and percentage occurrence of double-peaked spectra were higher during low sea states.

The sea state of the Indian Ocean is significantly modified by swells, and it has considerable implications on the coastal regions of India (Raj Kumar et al., 2009). However, role of local winds on wind sea generation along the Indian coast is not well understood. Only a few studies has been carried out on this aspect. Neetu et al. (2006) studied the impact of sea breeze on the wind seas off Goa, west coast of India. They identified that large scale winds are weak during pre-monsoon periods and hence the sea breeze has an impact on the diurnal cycle of the sea state along the west coast of India. Vethamony et al. (2009) also studied the characteristics of the waves off Goa during pre-monsoon season, when the sea-breeze dominates over global winds. They found that the diurnal pattern is due to the co-existence of locally generated wind seas and pre-existing swells. An in depth study on the influence of sea breeze on the pre-existing swells from the Indian Ocean has been carried out as part of the present work, and the results are discussed in the following chapters.

Chapter 2

Data and methodology

Chapter 2

Data and methodology

2.1. Introduction

Winds, waves and bathymetry are the major oceanographic paramters required for wave modelling / wave research. These can be obtained from sources such as visual observations, wave arrays, wave buoys and remote sensing sensors. Nowadays, directional wave rider buoys and moored data buoys are the main sources of direct wave measurements. They provide spectral information at a pre-defined location. Significant wave height and wind speed are obtained from the satellite altimeters and wind vectors are obtained from scatterometers. Spectral wave data can also be obtained from the Synthetic Aperture Radar (SAR), with a prior request. Wind and sea state information can be extracted from the altimeter measurements directly without prior knowledge of the local sea state or wind field, whereas a reliable interpretation of scatterometer and SAR data requires first-guess wind data and wave spectra, respectively as input for inverse modelling techniques (Komen et al., 1994).

Locally, we can obtain reliable wind data from Autonomous Weather Station (AWS), which is a point source. On global scale, altimeters and scatterometers provide wind data with reasonable spatial resolutions. Since, temporal resolutions of such data are very coarse, it may not be adequate for a proper time series analysis. However, gridded products of scatterometer data such as QuickScat are useful to obtain relatively fine resolution wind vectors. The re-analysis winds avaialable at NCEP (National Centres for Envrionmental Prediciton, USA), ECMWF (European Centre for Medium-Range Weather Forecasts) and blended winds available at IFREMER (French Research Institute for Exploitation of the Sea) are widely used for global wind analysis and used as the input for numerical wave modelling.

In the present study, wave data obtained from directional wave rider buoys, moored data buoys and Jason-1 altimer and wind data obtained from AWS, Scatterometers, re-analysis and blended winds have been used for analysis. Cyclone track data obtained from JTWC (Joint Typhoon Warning Centre, USA) and pressure level data from IDWR (Indian Daily Weather Report) (IMD, 1996) have also been used for the extreme weather event analysis.

Numerical modelling has been carried out utilising the wind data obtained from the above sources.

2.2. Data used

Based on availability, accuracy and regional/seasonal interest, various wind data have been used for the analysis and in numerical wave simulations. Each wind data (re-analysed/remsote sensing/simulated) has its own merits and demerits in terms of accuracy and temporal/spatial resolutions. An intercomparison between various winds has been made and described in Sec. 2.2.12.

Wave simulations have been carried out using winds from different sources, and the accuracy of the predictions has been tested (Sec. 3.3.3). NCEP re-analysis winds are reliable and used in the present study for analysis and wave modelling, though there are limitations in the spatial resolutions (Sudheesh et al., 2004; Vethamony et al., 2006; Aboobacker et al., 2009 and Vethamony et al., 2009). QuickSCAT data are used for wave simulations in the Indian Ocean, however, the temporal resolution is very coarse (Raj Kumar et al., 2009; Bhowmick et al., 2009). QuikSCAT data is very useful to analyse sea breeze distribution along the west coast of India during pre-monsoon season (Aparna et al., 2005). IFREMER/CERSAT provides blended winds with relatively fine spatial resolution, which is adequate to analyse localised/regional characteristics of winds to some extent, and thus incorporated in the wave simulations. NCMRWF wind data was also used to simulate waves in the north Indian Ocean, and provided reasonably good results (Sudheesh et al., 2004). However, fine resoution wind data are required for the analysis and modelling of waves in coastal regions. Therefore, as a particular case study, coastal winds off Goa have been simulated using MM5 and used in the numerical wave model.

The following sections describe about the wind and wave data used in the present study.

2.2.1. Directional wave rider buoy

Directional wave rider buoy (Figure 2-1) developed by Datawell b.v., the Netherlands are used for wave measurements (Datawell BV, 2006). It consists of a spherical steel shell of 90 cm diameter, designed to float on the sea surface. It has three accelerometers housed inside it and these accelerometers measure the vertical, north and west accelerations of the buoy. All these accelerations are then digitally integrated twice to get displacements (elevations) and filtered to a high frequency cut-off at 0.6 Hz. The vertical accelerometer

yields the measurement of wave height. Wave direction is determined by measurement of the horizontal motion of the buoy and correlating this motion with the vertical motion of the buoy.

The directional wave rider buoy transmits buoy motion time history, reduced data as spectral density, wave direction etc. in cyclic messages to a shore based receiving/recording station, with the help of 2 m long antenna mounted on top of the buoy. The signals from the directional wave rider buoy are received onshore by Wave Direction Receiver (WAREC) and record the data on a Personal Computer. The processor in the receiver also checks for transmission errors. The personal computer interfaced with the WAREC communicates and controls the WAREC system. The wave rider buoys were calibrated in the laboratory by giving known wave heights and periods and recorded by using WAREC and PC. The buoy can function within -20 to +20 m of wave height with an accuracy of 3% within the wave period 1.6 - 30 s. The direction accuracy is within 0.5 - 2° depending on the latitude.

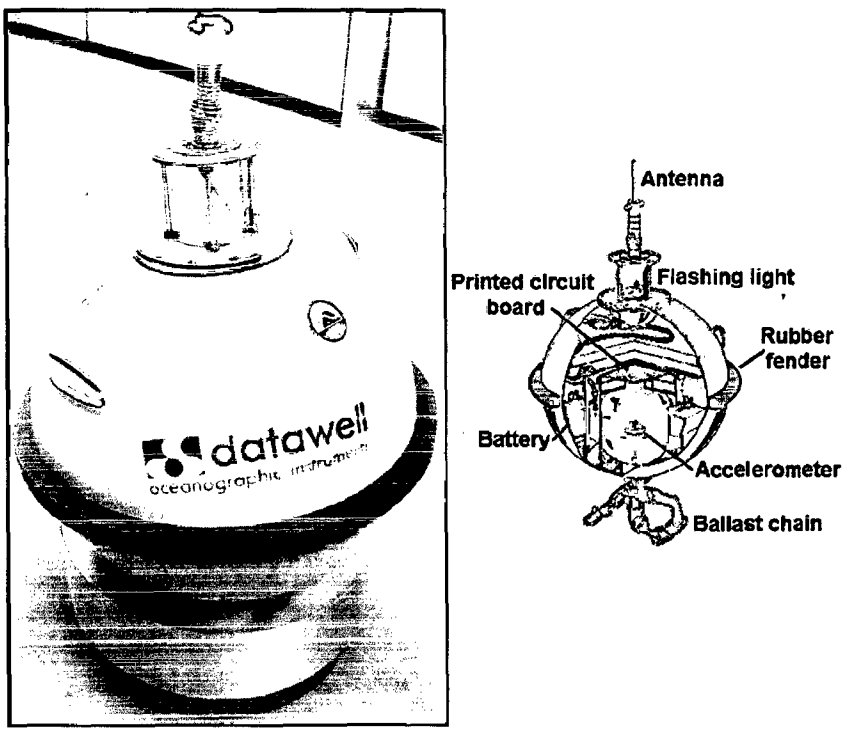

Figure 2-1. Datawell wave rider buoy and associated parts (www.datawell.nl).

Wave data collected using Datawell Directional Wave Rider Buoys (WRB) at different locations along the Indian coast during various periods have been analysed. The details of

the locations and measurement periods are listed in Table 2-1. Locations of wave measurements conducted by wave rider buoys (B1 to B10) are marked in Figure 2-2. The sampling duration is 20-minutes, and the spectra are calculated using Fast Fourier Transform (FFT) (Datawell, 2001).

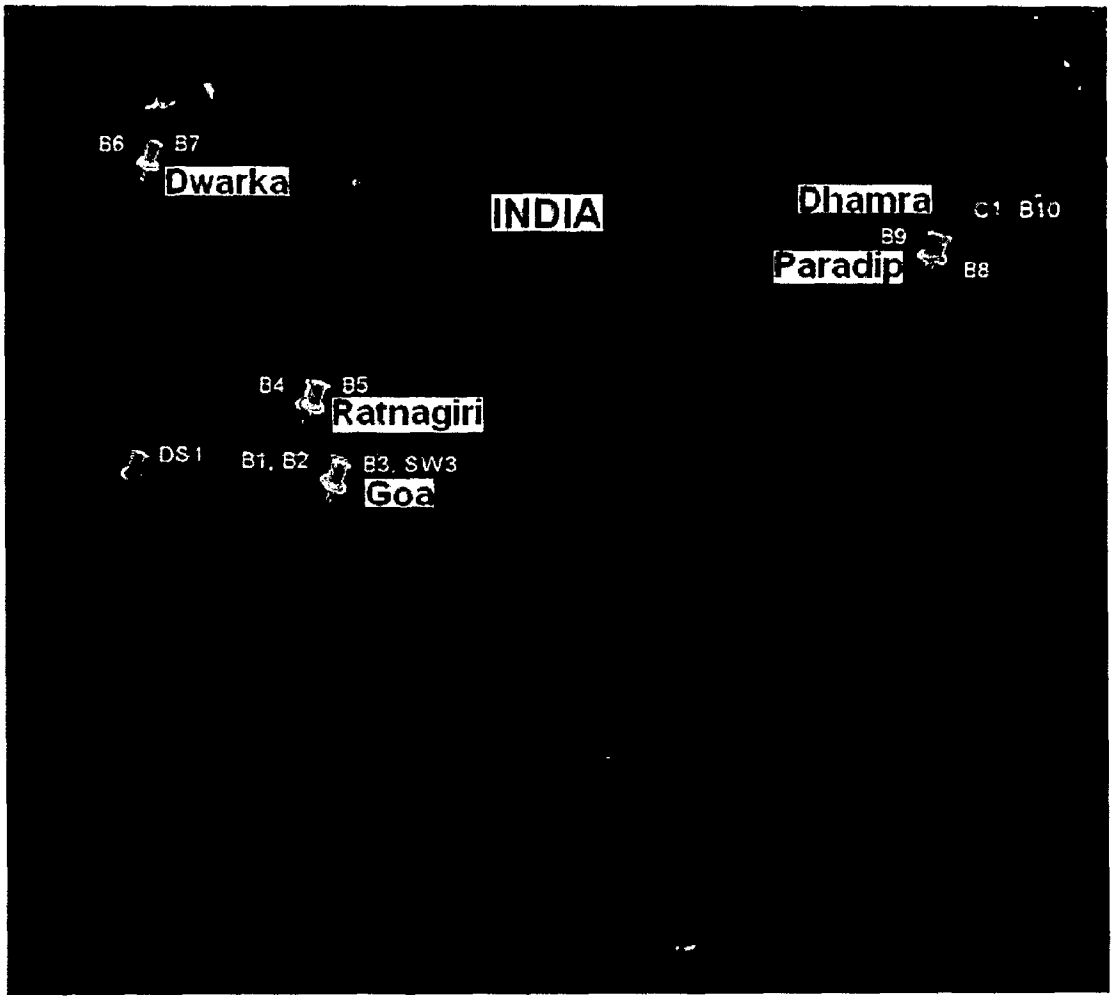

Figure 2-2. Wave measurement locations using wave rider buoys (B1 to B10), moored buoys (DS1 and SW3) and non-directional wave recorder (N1). Image courtesy: Google Earth.

Table 2-1. Details of wave measurement locations, water depth, measurement duration and data interval (directional wave rider buoys).

Region	Location	Water depth (m)	Duration	Data interval (h)
Goa	15.465° N 73.683° E (B1)	23	Feb 1996 - May 1997	3.0
	15.488° N 73.700° E (B2)	25	01 - 21 May 2005	1.0
	15.423° N 73.749° E (B3)	15	06 - 21 May 2005	0.5
Ratnagiri	17.004° N 73.120° E (B4)	35	24 Jan - 25 Feb 2008	0.5
	17.007° N 73.250 °E (B5)	15	24 Jan - 25 Feb 2008	0.5
Dwarka	22.088° N 69.040° E (B6)	30	05 Dec 2007 - 05 Jan 2008	0.5
	22.088° N 69.090° E (B7)	15	05 Dec 2007 - 05 Jan 2008	0.5
Paradip	20.143° N 86 .745° E (B8)	30	May 1996 - Jan 1997	3.0
	20.165° N 86.581° E (B9)	16	06 Sep - 05 Nov 2005	3.0
Dhamra	20.720° N 87.100° E (B10)	12	14 Jul - 14 Aug 2005	1.0

2.2.2. *Moored buoys*

The moored data buoys are floating platforms, which carry sensors to measure wind speed and direction, atmospheric pressure, air temperature, humidity, conductivity, sea surface temperature, current speed and direction and wave parameters. National Data Buoy Program (NDBP) of the National Institute of Ocean Technology (NIOT), Chennai, India deployed a number of such moored buoys at different locations around the Indian Ocean. The buoys are equipped with global positioning system, beacon light and satellite transceiver. These buoys are operable from 20m water depths to full ocean depth. It measures the full spectrum of the waves for 17 min. duration. It has an accuracy ±10 cm for wave height upto 20 m and ±5° for wave direction. The wind data measured at these buoys has an accuracy of ±1.5% for wind speed at the range 0 – 60 m/s and ±3.6° for wind direction.

In the present study, wave data measured at a deepwater location off Goa (DS1) during January – September 2001 has been used for validation of wave model results. The winds and waves at the deepwater location, DS1 during July - November 1999, May - July 2000, January 2001 and May - September 2001 and at shallow water location off Goa (SW3) during May - September 2001 and October 2004 - March 2005 are utilised for the case study described in Chapter 5. Apart from these, SW3 data during Feb – May 2004 is also used to analyse the nearshore wave characteristics off Goa during pre-monsoon season. The locations of DS1 and SW3 are marked in Figure 2-2. The details of deployment locations, water depth and data duration are listed in Table 2-2.

2.2.3. *Non-directional wave recorder*

The Non-directional Wave Recorder (Aanderaa WTR9) data collected 6 m at water depth off Dhamra Port is also used for the study of wave transformation. The data were sampled for every 30 min during 12 Jul – 14 Aug 2005. Table 2-3 describes the details on location, depth, duration and data intervals for the non-directional wave measurement. The location of wave measurement using non-directional wave recorder (C1) is marked in Figure 2-2.

The instrument records data internally in a removable and reusable solid state Data Storage Unit (DSU) 2990. It has a pressure sensor, which is based on a high precision quartz crystal oscillator. The pressure is measured every 0.5 s and 1024 samples are taken (512 s) and stored in an internal RAM for wave analysis. The parameters/ channels are transmitted as Aanderaa standard PDC-4 from the electronic control board to the removable DSU. The

instrument is housed in a pressure case that is closed by two C-clamps. By use of the Deck Unit 3127 interface, the output signals can be read by a PC via the same terminal and converted into engineering units. A mode switch, with a test and serial communication setting, a depth-setting switch and a recording interval switch is built into this board. The quartz pressure sensor is also attached to the board by a shock-absorbing bracket. A specially designed bottom mounting frame was used for installing the instrument on the seabed. The sensor is of quartz pressure type based on a pressure-controlled oscillator having frequency of 30 – 45 kHz. It has a range of 0-690 kPa, with an accuracy of 210 Pa and a resolution of 7 Pa.

Table 2-2. Details of wave measurement locations, water depth, measurement duration and data interval (NIOT moored buoys).

Region	Location	Depth (m)	Duration	Data interval (h)
off Goa Deep water (DS1)	15.500° N, 69.283° E	3700	July - Nov 1999	3
			May - Jul 2000	
			Jan - Sep 2001	
			May 2005	
off Goa Shallow water (SW3)	15.406° N, 73.755° E	20	May -September 2001	3
			October 2004 - March 2005	

Table 2-3. Details of wave measurement locations, water depth, measurement duration and data interval (non-directional wave recorder).

Region	Location	Depth (m)	Duration	Data interval (h)
Off Dhamra Port	86.970° E, 20.800° N (C1)	6	12 Jul - 14 Aug 2005	0.5

2.2.4. *Autonomous Weather Station (AWS)*

A state-of-art Autonomous Weather Station (AWS) has been designed for meteorological measurements on land and at sea by NIO, Goa. The weather station comprises of a suite of meteorological sensors such as wind speed and direction, air temperature, relative humidity and pressure, and has a flexibility to interface additional sensors. The accuracy in wind speed is 0.2 m/s for the range 0-60 m/s and the accuracy in wind direction is 3°.

The AWS was set at a height of 10 m at Dwarka and Ratnagiri coastal stations and at a height of 43.5 m at Dona Paula (Goa) coastal station. The details are listed in Table 2-4.

AWS winds at 43.5 m height were reduced to 10 m height using logarithmic wind profile (Roland, 1988) as follows:

$$U(z) = \frac{U_*}{\kappa} \ln (z/z_0) \quad \ldots\ldots\ldots\ldots \quad (2.1)$$

where, U(z)is the wind speed measured at a height, z (=43.5m), U_* the surface friction velocity, Z_0 (=0.22m) the aerodynamic roughness length and κ (=0.4) is the von Karman constant. As U(z), κ and z_0 are known at z=43.5m, the surface friction velocity U_* has been calculated using Eqn. 2.1. Further, wind speed at 10m height, U(z = 10) has been estimated. The reduced wind is used for further analysis.

Table 2-4. Details of AWS wind measurement locations, measurement height, measurement duration and data interval.

Region	Location	Height (m)	Duration	Data interval (min.)
Goa	73.800° E, 15.455° N	43.5	Feb 1996 - May 1997	10
Dwarka	68.970° E, 22.240° N	10.0	05 Dec 2007 - 05 Jan 2008	10
Ratnagiri	73.280° E, 16.890° N	10.0	24 Jan - 25 Feb 2008	10

2.2.5. *NCEP re-analysis winds*

NCEP provide reanalysis wind vectors (U and V components) globally on six-hourly interval for every 2.5° x 2.5° grid resolutions (Kalney et al., 1996). NCEP data are widely

used for applying in numerical models to generate waves on global scale. Tolman (1998) had validated NCEP re-analysed winds and used in offshore wave prediction models. Aboobacker et al. (2009) and Vethamony et al. (2009) used NCEP winds to simulate waves around the Indian Ocean.

NCEP reanalysis wind vectors in the Indian Ocean (65°S to 30° N and 20°E to 120°E) have been downloaded (http://www.esrl.noaa.gov/psd/data/reanalysis). The wind data from various locations during different seasons along the Indian coast has been analysed and used as the input parameter in wave modelling for the Indian Ocean. Following wind data has been used in the present study:

- Feb 1996 – May 1997
- May – Aug 2000
- May 2004 – Dec 2005
- Dec 2007 – Feb 2008

Wherever possible, NCEP winds were compared with measured wind data, as the accuracy of wave model results depends on the winds to a larger extent.

2.2.6. IFREMER/CERSAT Blended winds

To enhance the spatial and temporal resolutions of surface wind, the remotely sensed retrievals from QuikScat are blended to the operational ECMWF wind analyses over the global oceans by IFREMER/CERSAT (Bentamy et al., 2006 and Bentamy et al., 2009). The spatial resolution of the resulting wind fields is 0.25° in longitude and latitude and the data is available for every 6 hours. Ebuchi et al. (2002) analysed the quality of the blended winds by comparing with buoy winds and found a good correlation between them.

Since, the spatial resolution of blended winds is relatively fine, it can be used for the analysis of wind patterns near the coast. In the present study, blended winds during Jan. – Dec. 2005 and Dec. 2007 – Feb. 2008 have been utilised for the analysis of wind patterns around the Indian Ocean and Indian coastal regions. The accuracy of wave predictions using blended winds has been tested.

2.2.7. NCMRWF winds

NCMRWF (National Centre for Medium Range Weather Forecasting, India) wind data has been utilised to predict waves in the north Indian Ocean, as a part of the case study

described in Chapter 5. These winds are available in 1.5° x 1.5° grid size for every six hour interval in the form of U and V components. The data available during July - August 1999, May - July 2000 and May - September 2001 have been used in the present study. Vethamony et al. (2003) and Sudheesh et al. (2004) used NCMRWF winds to generate offshore waves in the north Indian Ocean using MIKE 21 Offshore Spectral Wave model (OSW).

2.2.8. QuikSCAT winds

QuikSCAT vector winds with 0.5^0 x 0.5^0 resolution available twice daily (Tang and Liu, 1996) have been downloaded for the Indian Ocean to study offshore as well as coastal wind variations. The QuikSCAT wind data during January – December 2005 and December 2007 – February 2008 have been used in this study.

To study the sea breeze characteristics during pre-monsoon season, QuikSCAT winds (u and v components) available for 06 h and 18 h (local time) were extracted along a section off Goa upto 200 km from the coast during May 2005.

2.2.9. MM5 winds

MM5, a Mesoscale Model developed by Pennsylvania State University / National Centre for Atmospheric Research (PSU/NCAR), is a three dimensional, limited area, non-hydrostatic model designed to simulate atmospheric circulation (Grell et al., 1994). Dhanya et al (2010) simulated the coastal winds along the central west coast of India using MM5 and studied the coastal atmospheric circulation over the region. In the present study, coastal winds off Goa, west coast of India have been simulated using MM5 during May 2005 to analyse the coastal wind patterns, especially sea breeze-land breeze systems. For this purpose, nested model domains were selected in the Arabian Sea covering Goa region with spatial resolutions of 27 km, 9 km and 3 km. The model simulates wind vectors for every 1 hour interval. These winds are further used to simulate wind seas off Goa during May 2005 (pre-monsoon season).

2.2.10. Jason-1 Altimeter

Gridded (1°x 1° resolution) significant wave heights from Jason-1, a mini-satellite developed by NASA and CNES designed for oceanographic and meteorological purposes are also utilized in the present study to explain the significant wave height distribution in the open ocean areas. The data is available in alternate 3 and 4 days time scale. These data

have also been used to validate the wave model results of deep waters, where the buoy measurements are not available. The significant wave heights off Goa in various grids during May 2005 have been downloaded and used in the present study.

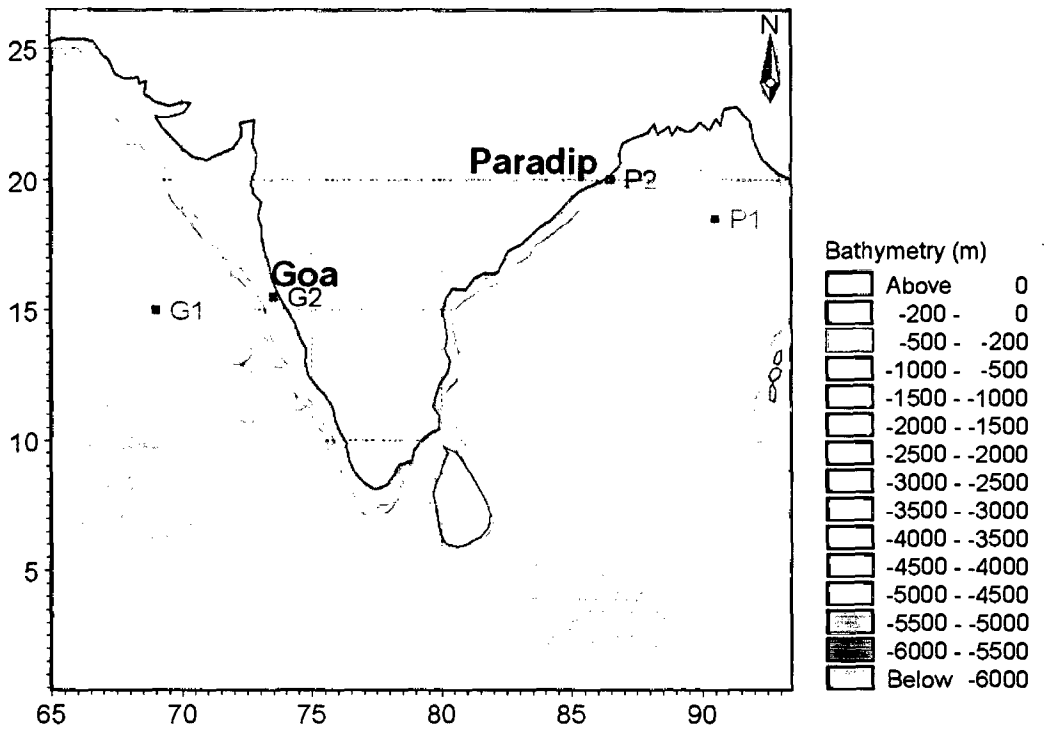

Figure 2-3. Jason-1 data extraction locations off Goa and Paradip.

2.2.11. JTWC and IDWR

A few cyclone track data obtained from JTWC (Joint Typhoon Warning Center, USA) were used to analyse characteristics of waves associated with these events in the Arabian Sea and Bay of Bengal. For example, the two tropical storms (15 -25 June 1996 and 14 Oct. – 2 Nov. 1996) occurred in the Arabian Sea and the two storms occurred in the Bay of Bengal during 11-18 June 1996 and 14 Oct – 2 Nov 1996. Cyclone tracks were obtained from Unisys Weather site (http://weather.unisys.com).

Indian Daily Weather Report (IMD, 1996) provides pressure level and wind speed of coastal stations twice daily. These data are useful to analyse atmospheric pressure fluctuations during extreme events. In the present study, the IDWR data has been used to identify the evolution of storms and depressions occurred during 1996 in the Paradip and

Goa regions. Pressure level data obtained from Cyclone Detection Radar Centre (CDRC) located at Paradip were also used.

2.2.12. Comparison of analysed winds with measured winds

Analysed winds (NCEP, Blended and QuikSCAT) are compared with measured buoy winds at location SW3 (Figure 2-1) during January – March 2005 (Figure 2-4). The wind speed and direction show good match for NCEP and Blended winds with buoy winds, however, the match is fair for QuikSCAT winds. Figure 2-5 shows the scatter between buoy wind speed and analysed (NCEP, Blended and QuikSCAT) wind speeds. Limitations in temporal and spatial resolution of analysed winds are reflected in the statistical parameters, correlation coefficient, bias, r.m.s. error and scatter index (Figure 2-5). The correlation is good for NCEP (0.49) and Blended (0.69) winds, and poor for QuikSCAT winds (0.39). Biases are minimum for NCEP (0.14 m/s) and Blended (-0.39 m/s) winds, and maximum for QuikSCAT winds (-1.58 m/s).

NCMRWF winds have been used specifically for the case study mentioned in Chapter 5. Accuracy of these winds has been tested earlier by Sudheesh et al. (2004). For instance, a comparison between buoy winds and NCMRWF winds during July 1999 at location DS1 (Figure 2-1) is shown in Figure 2-6. NCMRWF winds show very good match with buoy winds.

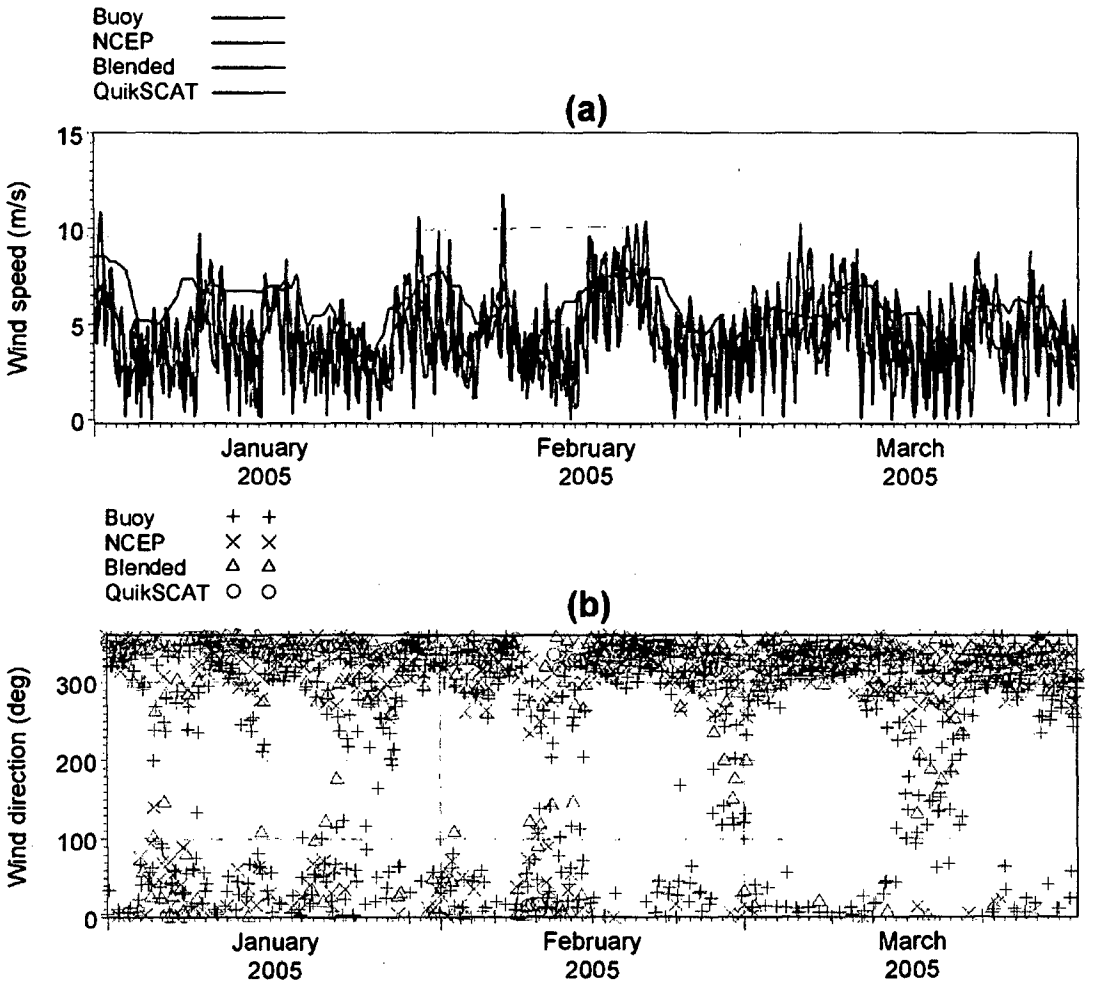

Figure 2-4. Comparison between measured (buoy) and analysed (NCEP, Blended and QuikSCAT) winds: (a) wind speed and (b) wind direction.

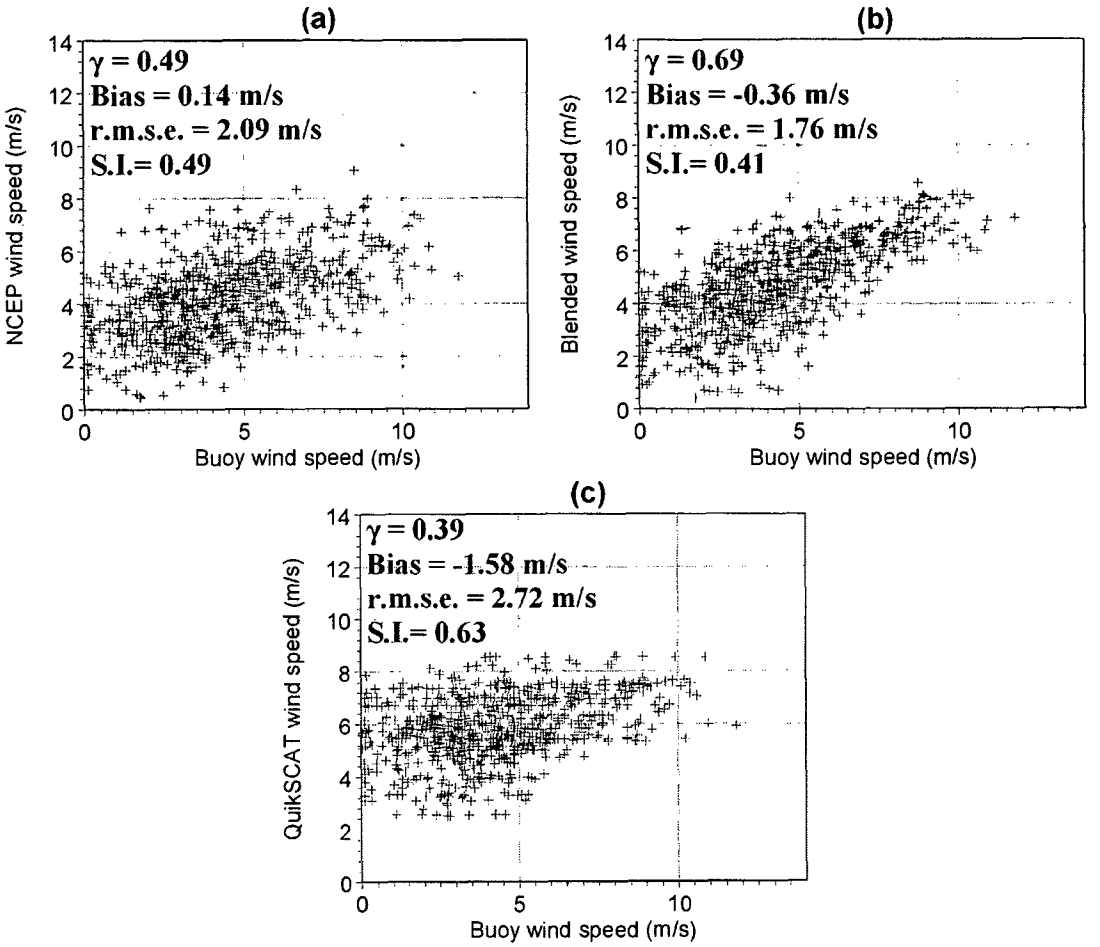

Figure 2-5. Scatter between measured wind speed and: (a) NCEP, (b) Blended and (c) QuikSCAT wind speeds.

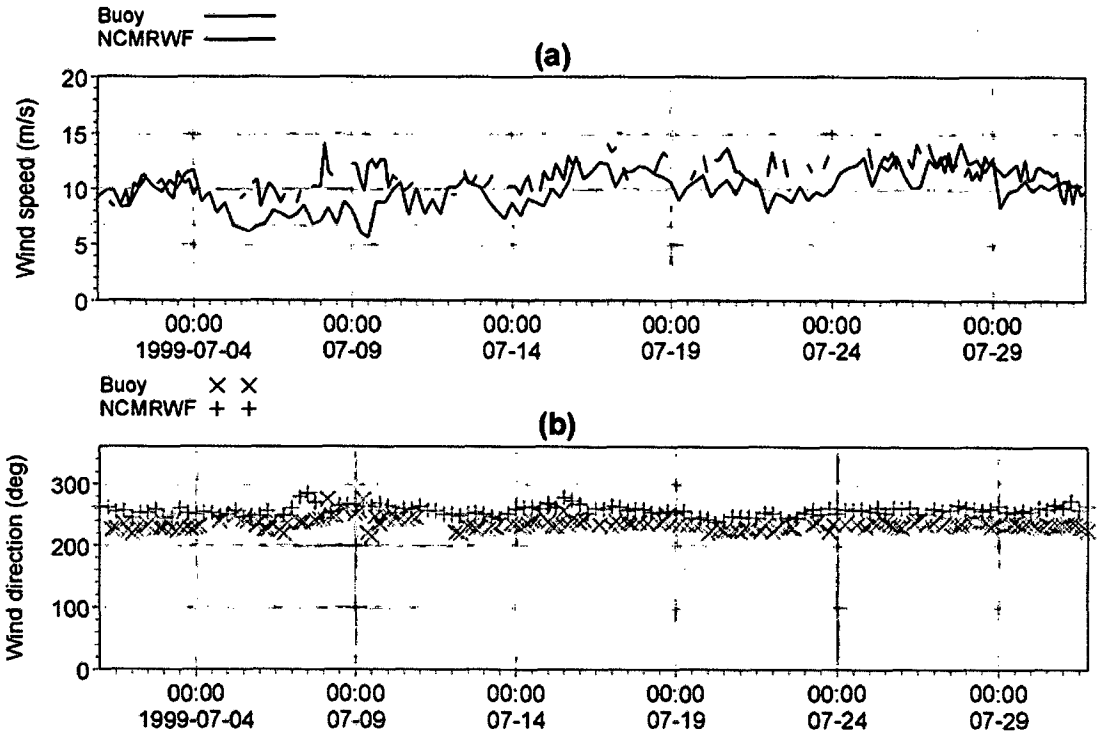

Figure 2-6. Comparison between measured and NCMRWF wind speed and direction.

2.3. Methodology

The methodologies used in the present study are described in the following sections. Sec. 2.3.1 describes the calculation of wind sea and swell parameters from the measured wave energy spectra. Sec. 2.3.2 introduces numerical modelling. Sec. 2.3.3 explains the analysis of extreme events and Sec. 2.3.4, the analysis of local effects on the wave characteristics along the Indian coasts. Sec. 2.3.5 describes the methodology of wave transformation.

2.3.1. Separation of wind sea and swell

Wind sea and swell parameters have been separated from the wave energy spectra utilizing the methodology provided by Gilhousen and Hervey (2001). The algorithm is based on wave steepness parameter from which the separation frequency has been derived.

The general definition of the steepness function is the ratio of wave height to wavelength. The wave steepness parameter, ξ, at all frequencies f, can be written as,

$$\xi(f) = \frac{2\pi H_s(f)}{gT_m^2(f)} \quad \text{..... (2.2)}$$

where, H_s (the significant wave height) and T_m (the mean wave period) are functions of a given frequency f. When wave spectrum components are expressed in terms of moments of the distribution, $\xi(f)$ for all frequencies f_l can be rewritten as,

$$\xi(f) = \frac{8\pi \int_{f_l}^{f_u} f^2 E(f) df}{g\sqrt{\int_{f_l}^{f_u} E(f) df}} \quad \text{..... (2.3)}$$

where, f_u (=0.58 hz) and f_l (= 0.03, 0.04,....0.58 hz) are the upper and lower frequency limits of measured wave spectra. Using Eqn.(2.3), $\xi(f)$ has been calculated for all frequencies from the measured data (f_u is fixed for all calculations and f_l varies in such a way that $f_l = f_1, f_2, \ldots, f_u$). The frequency f_x (peak frequency) corresponds to the maximum steepness parameter ($\xi(f)$) has been used to calculate the separation frequency f_s, as follows:

$$f_s = C\, f_x \quad \text{..... (2.4)}$$

where, $C = 0.75$, is an empirically determined constant (Gilhousen and Hervey, 2001).

The methodology proposed by Wang and Hwang (2001) has been applied to study the sensitivity of the results obtained from separation frequency method of Gilhousen and Hervey (2001). Figure 2-7 shows the comparison of separation frequencies obtained from both the methods, and there is an excellent agreement between them.

The wave spectra have been divided into two parts (swell region and wind sea region) after the separation using f_s. Each wind sea and swell spectrum has been used to calculate significant wave height (H_s), mean wave period (T_m) and mean wave direction (θ) separately for wind sea and swell. There are cases, where the multiple peaks are observed within the separated wind sea and swell spectra. Such cases were treated as a part of single wind sea or swell system. H_s and T_m are calculated as follows:

$$H_s = 4\sqrt{m_0} \quad \text{..... (2.5a)}, \quad T_m = \sqrt{\frac{m_0(f)}{m_2(f)}} \quad \text{..... (2.5b)}$$

where,

$$m_n = \int_{f_l}^{f_u} f^n E(f) df \quad \text{..... (2.6)}$$

f_l and f_u are the lower and upper frequencies, respectively for each wind sea and swell spectra. The directions correspond to the peak energy of the wind sea and swell spectra has been taken as the mean wave direction (θ) of wind sea and swell. Significant wave heights of wind sea, swell and resultant wave follow the relation given below:

$$H_s = \sqrt{H_{s\,swell}{}^2 + H_{s\,sea}{}^2} \quad \ldots\ldots\ldots\ldots\ldots \quad (2.7)$$

In general, resultant wave (or simply 'wave') is the combination of wind sea and swell energies, and from this energy the resultant wave parameters (such as wave height and wave period) are derived.

In the present study, wave data measured during February 1996 to May 1997 (16 months) at a nearshore location off Goa has been analysed to study the dominance of wind seas and swells during different seasons, including extreme events using the separation frequency method.

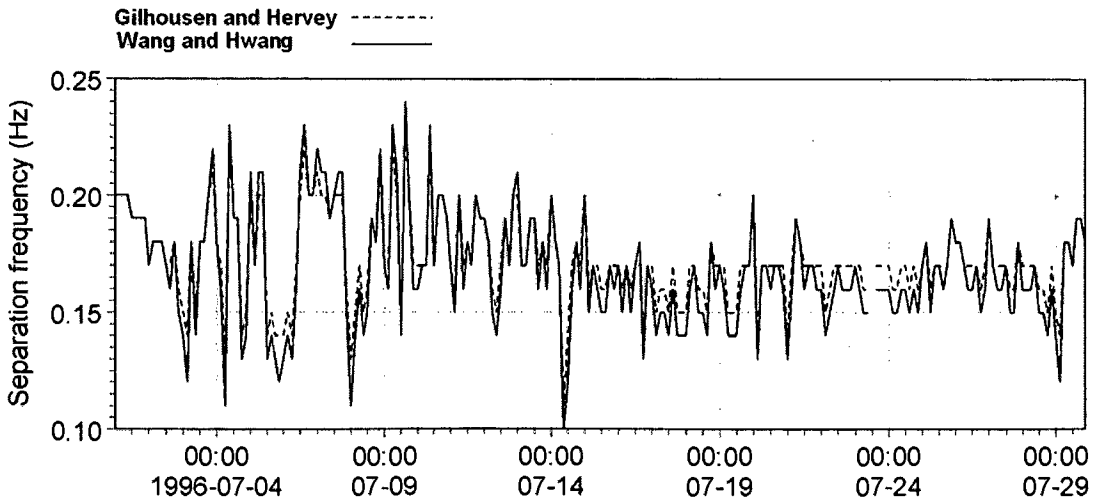

Figure 2-7. Comparison of separation frequencies obtained from 'Gilhousen and Harvey' and 'Wang and Hwang' methods.

2.3.2. Validation of MM5 winds

MM5 winds simulated during May 2005 have been validated to utilise in the numercial wave simulations. Winds measured using AWS at Dona Paula coastal station during May 2005 has been used for the validation purpose. Figure 2-8 shows the comparison between measured and modelled wind vectors (u and v components) at Dona Paula coastal station

during May 2005. There is good agreement between measured and simulated wind vectors Table 2-5. The correlation coefficient for the zonal component is 0.86, whereas it is 0.59 for the meridional component. Since the zonal component is due to sea breeze, a well predicted sea breeze distribution off Goa is obtained from the MM5 simulation results. The low correlation of meridional component is mainly due to irregular topographic features of the region. Recently, Dhanya et al. (2010) simulated the coastal winds along the central west coast of India and found a good match between measured and MM5 winds.

The MM5 winds have been further utilised to simulate wind seas off Goa during May 2005, and to study wind sea charactertisitics due to sea breeze along the west coast of India during pre-monsoon season.

Table 2-5. Correlation coefficient, bias and r.m.s. error between measured and simulated winds off Goa (May 2005).

Items	Correlation coefficient	Bias (m/s)	r.m.s. error (m/s)
u – component (zonal)	0.86	-0.56	0.76
v – component (meridional)	0.59	0.13	0.69

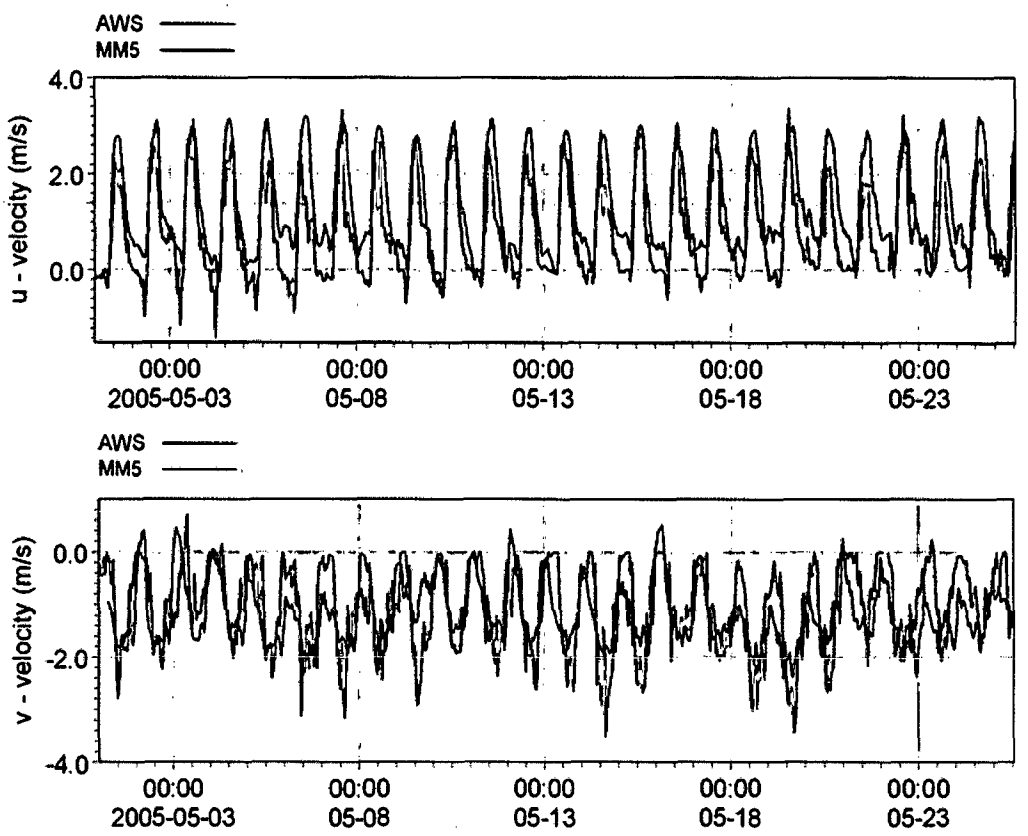

Figure 2-8. Comparison between measured and modelled wind vectors at Dona Paula coastal station (May 2005).

2.3.3. Wave modelling

State-of-the-art numerical models have been utilised to predict waves in the Indian Ocean and shallow waters along the coastal regions. The applied numerical models are MIKE 21 OSW (Offshore Spectral Wave), MIKE 21 NSW (Nearshore Spectral Wave) and MIKE 21 SW (Spectral Wave). Wave parameters and spectra obtained from the simulations are analysed to understand (i) seasonal wave characteristics, (ii) waves during extreme weather events and (iii) wave transformation at nearshore regions. A brief description of the above models is described in the following sections. Details of model setup, calibration and validation are described in Chapter 3.

2.3.3.1. MIKE 21 OSW

MIKE 21 OSW is a fully spectral wind-wave model developed by DHI Water & Environment, Denmark, which describes the propagation, growth, decay and

transformation of wind generated waves of short period and short crested waves in offshore as well as in coastal areas (DHI, 2001). It is a time dependent discrete spectral wind-wave model formulated in terms of the energy density spectrum with discrete resolution of frequencies and directions. The energy is calculated in discrete points of a rectangular grid for a number of discrete frequencies and directions. The model includes two different descriptions of physical processes governing the wind-wave generation and decay: state-of-the-art third generation formulation and second generation formulation. The third generation model is based on the internationally developed WAM Cycle 4 model originally developed for deep-water application on global and regional scales. The model is based on the numerical integration of the spectral energy (F) balance equation formulated in Cartesian co-ordinates.

$$\frac{DF}{Dt} = S_{wind} + S_{non-linear} + S_{bottom\ dissipation} + S_{whitecapping} + S_{wave\ breaking} \quad \ldots\ldots\ldots (2.8)$$

The left-hand side describes the wave propagation in time and space using linear wave theory. The right-hand side represents the superposition of source functions describing various physical phenomena. Wave-wave interaction, refraction and dissipation due to breaking are included in this model. The basic input parameters to the model are bathymetry and wind fields. The model domain is divided into different grids and input parameters are provided at each grid point. Time step corresponding to the Courant Number is chosen, keeping the minimum wave period present.

The output from the model consists of wave energy spectra and integral wave parameters including the significant wave height, peak wave period, average wave period, peak wave direction and mean wave direction. For detailed analysis of the wave climate in coastal and shallow waters, the MIKE 21 OSW model is used in combination with MIKE 21 NSW.

In the present study, MIKE 21 OSW is applied to simulate waves in the Indian Ocean during May – Dec 1996. Wave characteristics during monsoons and extreme events are discussed in Chapter 4. OSW is also applied to simulate waves during July – Aug 1999, May – July 2000, May – Sep 2001 and May 2004 – June 2005, and the results are discussed in Chapter 5.

2.3.3.2. MIKE 21 NSW

MIKE 21 NSW is a stationary and directionally de-coupled parametric wind-wave model, which describes the growth, decay and transformation of wind-generated waves and swells

in nearshore areas (DHI, 2001). The model takes into account the effects of refraction and shoaling due to varying depth, local wind generation and energy dissipation due to bottom friction and wave breaking and wave-current interaction. The basic equations are solved using an Eulerian finite difference technique. The zeroth and the first moment of the action spectrum are calculated on a rectangular grid for a number of discrete directions. A once-through marching procedure is applied in the predominant direction of wave propagation.

The high resolution nearshore model requires wave conditions along the offshore model boundary. Hence, the wave parameters at offshore boundaries are extracted from the OSW model results to use as the boundary conditions for the NSW model. The basic output from the NSW model is integral wave parameters such as significant wave height, mean wave period, mean wave direction, directional standard deviation and radiation stresses.

2.3.3.3. MIKE 21 SW

MIKE 21 SW is a spectral wind-wave model based on unstructured meshes, which simulates the growth, decay and transformation of wind generated waves and swell in offshore and in coastal areas. The spectral formulation is based on the wave action conservation equation as described in Komen et al. (1994) and Young (1999), where, the directional-frequency wave action spectrum is the dependent variable. The basic conservation equations are formulated in Cartesian polar spherical co-ordinates. The discretization of the governing equation in geographical and spectral space is performed using cell-centered finite volume method. In the geographical domain, an unstructured mesh technique is used. The time integration is performed using a fractional step approach, where a multi-sequence explicit method is applied for the propagation of wave action.

The energy source term, $S\ (=DF/Dt)$, represents the superposition of source functions as given in Eqn. 2.10. The model includes the following physical phenomena: (i) wave growth by action of wind, (ii) non-linear wave-wave interaction, (iii) dissipation due to white-capping, (iv) dissipation due to bottom friction, (v) dissipation due to depth-induce wave breaking, (vi) refraction and shoaling due to depth variations, (vii) diffraction, (viii) wave-current interaction and (ix) effect of time varying water depth.

Numerical simulations of waves in the deep waters as well as shallow waters have been carried out using MIKE 21 OSW, MIKE 21 NSW and MIKE 21 SW models.

Chapter 3

Numerical simulations: model setup and validation

Chapter 3

Numerical simulations: model setup and validation

3.1. Introduction

Numerical simulations have been carried out to study wave features prevailing along the Indian coast. Wave parameters obtained from the simulations are analysed to understand the phenomena associated with wave generation and dissipation in the Indian Ocean and coastal region. This chapter describes the model set up, calibration and validation using MIKE 21 model, and simulations using MM5 winds for the wind seas off Goa. Model set up consists: selection of model domain, generation of flexible mesh and gridded bathymetry, consideration of calibration parameters, initial/boundary conditions and wind input. Validation for model results was carried out wherever measurements are available within the selected domain. A sensitivity test with winds from various sources is also carried out to decide the accuracy of analysed winds used in the simulations.

3.2. Model setup

The model used to simulate waves over flexible mesh/gridded bathymetry is MIKE 21. The following sections describe the model set up in detail.

3.2.1. Model domain and bathymetry

In order to simulate waves in the Indian Ocean, a large domain, which ranges from 65° S to 30° N (latitude) and 20° E to 125° E (longitude) was selected. An unstructured triangulated mesh is generated with varying sizes of triangles (elements); 1.5° (south Indian Ocean), 0.75° (north Indian Ocean) and 0.25° (coastal regions). ETOPO5 bathymetry data obtained from NGDC (National Geophysical Data Center, Colorado, USA) is applied to deep water regions, whereas C-MAP data and improved bathymetry data sets of Sindhu et al. (2007) are applied to shallow water regions in the Indian Ocean, by interpolating them to each element in the flexible mesh bathymetry. The horizontal datum is referenced to World Geodetic System 1984 (WGS-84) and the vertical datum is referenced to Chart Datum (CD). Figure 3-1 shows the model domain, flexible mesh and bathymetry used for wave simulations in the Indian Ocean. The model used to simulate waves over flexible mesh bathymetry is MIKE 21 SW.

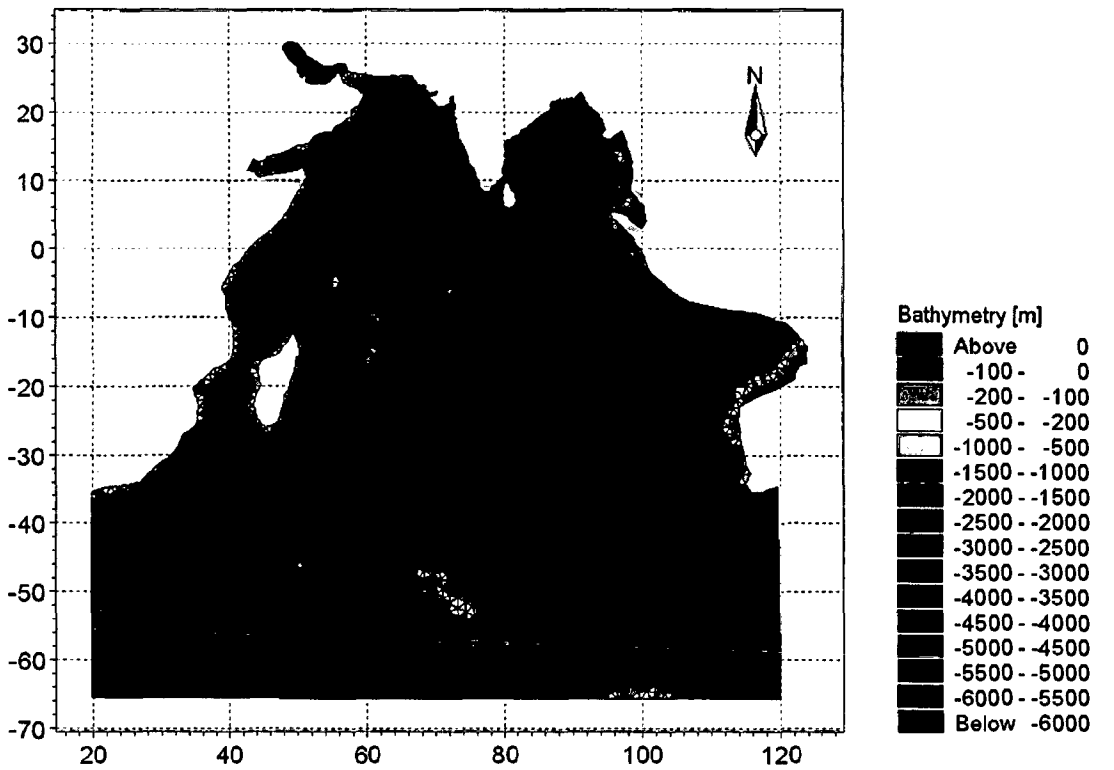

Figure 3-1. Model domain, bathymetry and flexible mesh used for wave simulations in the Indian Ocean.

Before switched over to MIKE 21 SW, the two-dimensional Offshore Spectral Wave model, MIKE OSW (DHI, 2001) was used to simulate the waves in the Indian Ocean over a rectangular grid bathymetry. Earlier, Vethamony et al (2006) used this model to simulate waves in the north Indian Ocean using MSMR (Multi-channel Scanning Microwave Radiometer) analysed winds. Since OSW has been replaced by SW, most of the offshore simulations in the present study have been carried out in SW, though some of the analysis was based on OSW results. Figure 3-2 shows the model domain and bathymetry used for OSW simulations in the Indian Ocean. The domain ranges from 5° S to 25° N and from 45° E to 100° E, and is divided into 40 x 74 grids in latitude and longitude, respectively with a grid spacing of 0.75° x 0.75°. The boundary along 5° S latitude was considered as open boundary, and all other boundaries were kept closed.

Local models were set up over fine resolution flexible mesh bathymetry at select nearshore regions along the east and west coasts of India. The select regions are Goa, Ratnagiri and Dwarka along the west coast, and Paradip and Dhamra along the east coast. Wave

measurements are available at these locations for validation. Figure 3-3 and Figure 3-4 show the model domain, bathymetry and triangulated mesh at locations along the west coast and east coast, respectively. Three open boundaries were made in all the model domains and utilized the boundary conditions obtained from the overall Indian Ocean model simulation results. The triangulated mesh sizes vary with respect to domains selected, and are listed below:

i. off Goa: 15 km, 5 km, 2 km, 500 m, 300 m and 50 m. The 50 m size is considered in and around the breakwater area at Mormugao Port.

ii. off Ratnagiri: 5 km, 1.5 km and 500 m.

iii. off Dwarka: 2.5 km, 1.5 km and 500 m.

iv. off Paradip: 2.5 km and 1.0 km.

v. off Dhamra: 5 km, 1.5 km and 300 m.

MIKE 21 NSW has been used to simulate nearshore waves off Goa to demarcate of inland vessel's limit (IVL) off Mormugao port region. However, it has been replaced with SW in further simulations, as the later performs well compared to NSW. The bathymetry and model domain used for NSW simulations off Goa is shown in Figure 3-5.

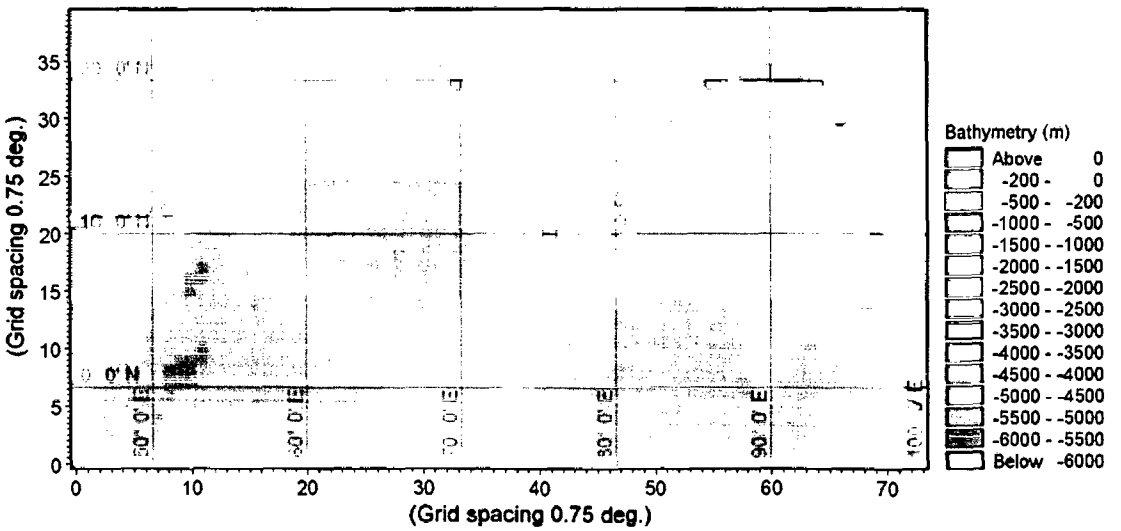

Figure 3-2. Model domain and bathymetry used for OSW simulations in the Indian Ocean.

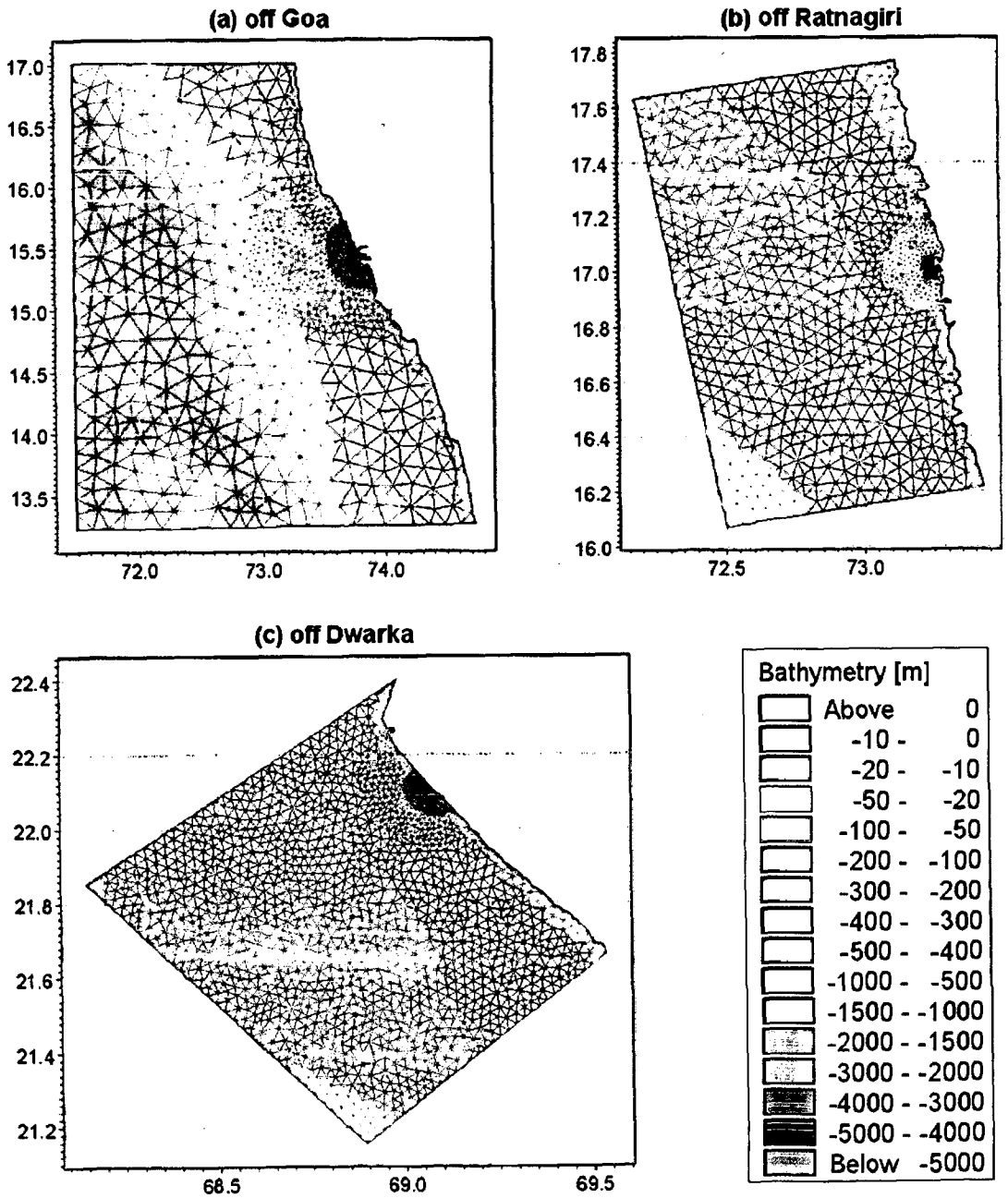

Figure 3-3. Domain, bathymetry and flexible mesh used for the local model (SW) simulations along the west coast of India: (a) off Goa, (b) off Ratnagiri and (c) off Dwarka.

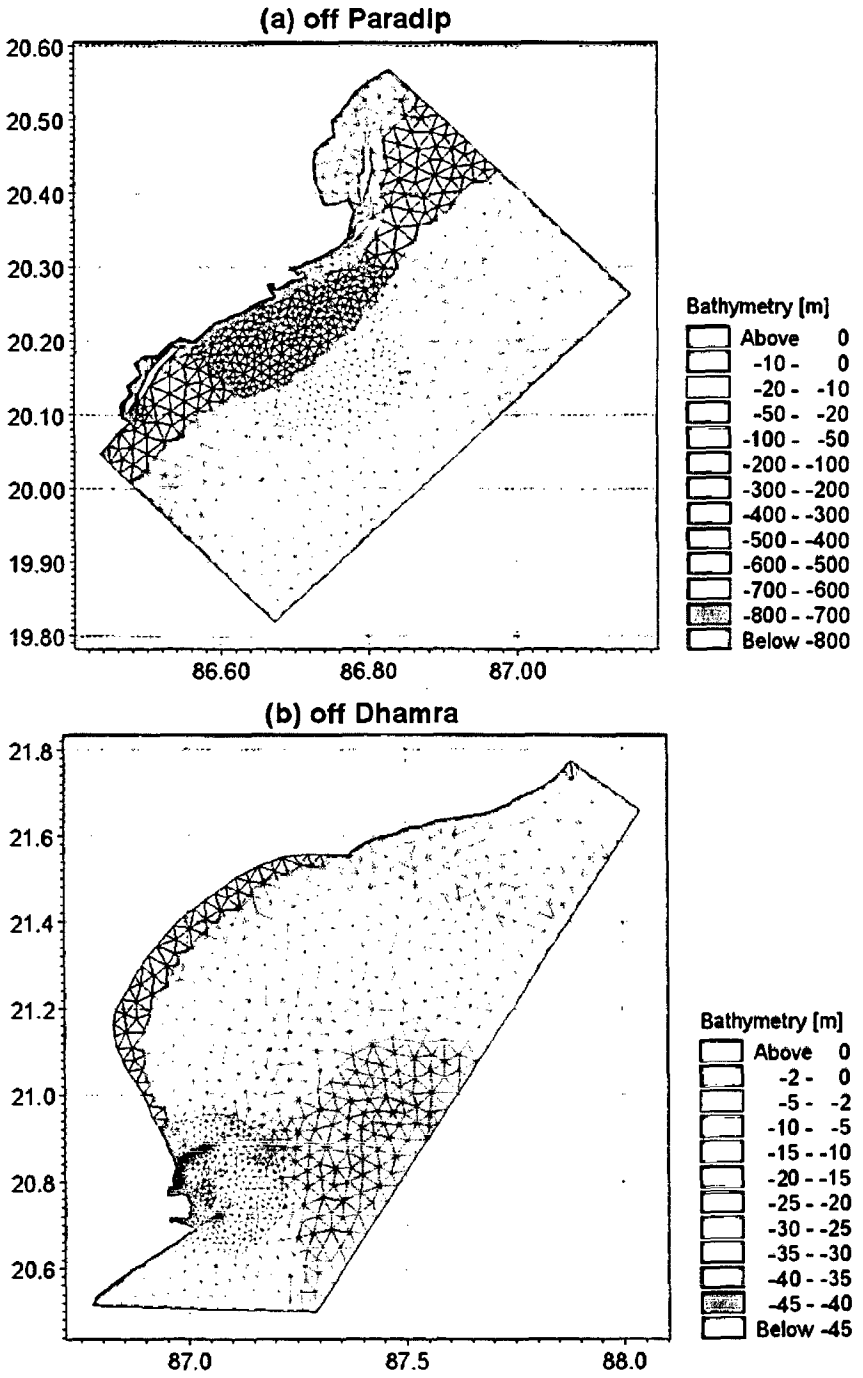

Figure 3-4. Domain, bathymetry and flexible mesh used for the local model (SW) simulations along the east coast of India: (a) off Paradip, (b) off Dhamra.

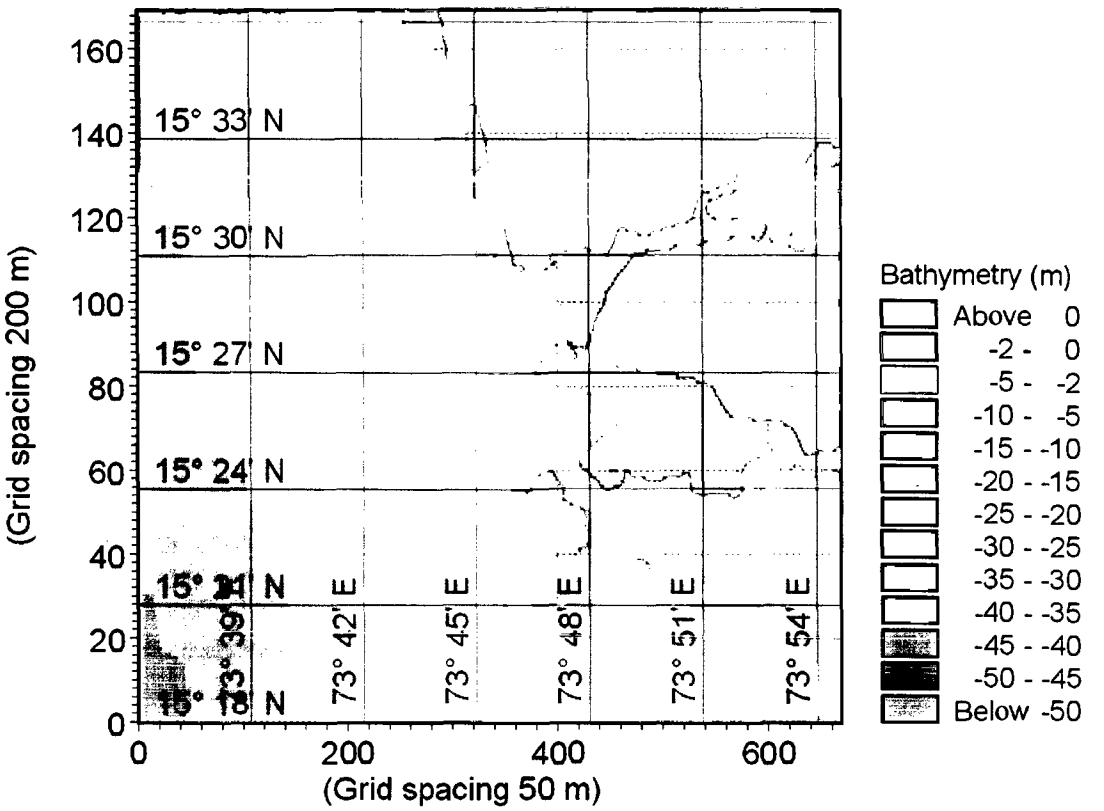

Figure 3-5. Domain and bathymetry used for the NSW simulations off Goa.

An overall wave transformation model was setup with fine resolution meshes in a single domain, specifically to study the wave transformation over a period of one year (Figure 3-6). Fine resolution meshes have been made for the regions Mumbai, Ratnagiri and Kochi along the west coast and Paradip, Visakapattinam and Nagappattinam along the east coast. The finest resolution considered is 500 m, and computational time is high.

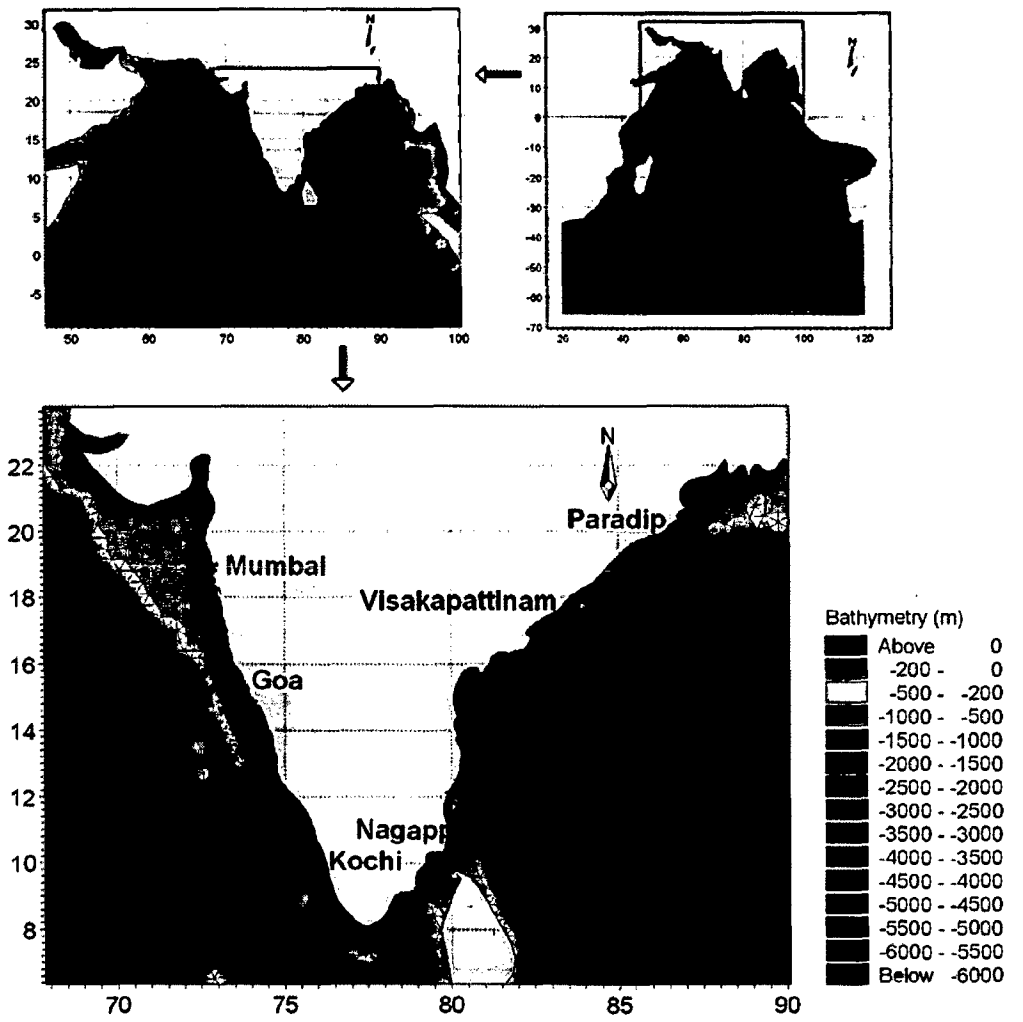

Figure 3-6. Bathymetry and flexible mesh used for SW simulations for wave transformation along the coast of India.

3.2.2. Basic formulations

Fully spectral formulations have been applied in the model set up. It is based on the wave action balance equation where the wave field is represented by the wave action density spectrum $N(\sigma, \theta)$. The independent phase parameters have been chosen as the relative (intrinsic) angular frequency, $\sigma=2\pi f$ and the direction of wave propagation, θ. The relation between the wave energy density spectrum $E(\sigma, \theta)$ and the wave action density spectrum is given by,

$$N(\sigma,\theta) = {}^{E}/_{\sigma} \quad \text{..... (3.1)}$$

The spectral wave calculation is activated at a start time step relative to the start of the simulation specified.

The simulation time and accuracy can be controlled by specifying the order of the numerical schemes which are used in the numerical calculations. The schemes for discretization in the geographical domain and the spectral domain can be specified. In the present study, a low order fast algorithm has been used as the geographical space discretization. The dependent variable in the spectral mode is the directional-frequency wave action spectrum in each node point. Hence, the discretization has been made on frequency and direction. For frequency discretization, the logarithmic distribution has been considered, which is given by

$$f_n = f_0 c^n, \quad n = 1,2, \ldots \text{ ..... (3.2)}$$

where, f_n is the frequency, f_0 minimum frequency and c the frequency factor (= 1.1). The minimum frequency is set to 0.055 Hz and the number of frequencies is 25. For directional discretization, 360° rose has been considered. The number of directions is set to 16. For wind sea and swell separation, a dynamic threshold frequency scheme is applied by setting a maximum threshold frequency of 0.3 Hz.

The time integration is based on a fractional step approach. Firstly, a propagation step is performed calculating an approximate solution at the new time level by solving the basic conservation equations without the source functions. Secondly, a source function step is performed calculating the new solution from the estimated solution taking into account only the effect of the source functions. The propagation step is carried out by an explicit Euler scheme. To overcome the severe stability restriction, a multi-sequence integration scheme is employed following Vilsmeier and Hänel (1995). Here, the maximum time step is increased by locally employing a sequence of integration steps, where the number of levels (steps) may vary from element to element. The maximum number of levels in the propagation calculation is 32. The source integration step is carried out using the method of Komen et al. (1994) and Hersbach (1997) and the number of time steps in the source calculation is set as 1. A variable time step interval is used in the time integration of the governing equations. The time step is determined so that the CFL number is less than the maximum number of levels in all computational nodes. The number of levels (and thereby the local time step) for each element is then determined so that the local CFL number is

less than 1. The minimum and maximum time steps were set to 0.01 s and 1200 s respectively. The CFL number is defined as

$$CFL = \left|c_x \frac{\Delta t}{\Delta x}\right| + \left|c_y \frac{\Delta t}{\Delta y}\right| + \left|c_\sigma \frac{\Delta t}{\Delta \sigma}\right| + \left|c_\theta \frac{\Delta t}{\Delta \theta}\right| \quad \text{..... (3.3)}$$

where c_x , c_y , c_σ and c_θ are the propagation velocities of a wave group in the four-dimensional phase spaces x, y, σ and θ. Δx and Δy are characteristic length scale in the x- and y-directions for an element, $\Delta\sigma$ and $\Delta\theta$ are discrete intervals in the direction and frequency spaces and Δt is the time step interval.

3.2.3. Input parameters

Wind is the basic input parameter for wave simulation. Successful wave hindcast and forecast depend on accurate wind fields deduced from meteorological models and analysis. In the present study, NCEP winds, IFREMER/CERSAT blended winds, NCMRWF winds and QuikScat winds have been used. In the MIKE 21 SW simulations, these winds are directly used according to their temporal and spatial resolutions (as described in Sec 2.2.5 to Sec 2.2.8) over the Indian Ocean domain, whereas winds are spatially interpolated to the respective grids to apply in the MIKE 21 OSW simulations. Apart from these sources, AWS winds measured at coastal stations and MM5 winds simulated for the domain were also used for the nearshore wave simulations.

Global winds and MM5 winds are applied as vector components (in the form of u and v velocities) varying in time and space. For the air-sea interaction, a "coupled" formulation is applied according to the formulation of Komen et al (1994). It means the momentum transfer from the wind to the waves or drag depends not only on the wind but also on the waves. The applied background roughness Charnock parameter is 0.01. The Charnock parameter is defined as,

$$z_{ch} = g.z_0/u_*^2 \quad \text{..... (3.4)}$$

where u_*, is the friction velocity and z_0 is the sea roughness.

The wind input source term is parameterized following Janssen's formulation (Komen et al., 1994). For a given wind speed and direction, the growth rate of waves of a given frequency and direction depends on the friction velocity, u_*, and sea roughness z_0. In principle, if the sea roughness is known or assumed (e.g. the Charnock parameter may be assumed), the wind friction speed can be estimated using the logarithmic wind profile. Thus, the growth rate of waves due to wind input can be calculated. Komen et al. (1994)

made a formulation by assuming a dimensionless sea roughness (z_{ch}) of 0.0144, to fit the observations compiled by Plant (1982).

3.2.4. Energy transfer

The nonlinear energy transfer amongst the different wave components of a directional-frequency spectrum plays a crucial role for the temporal and spatial evolution of a wave field. A quadruplet-wave interaction, which is described by the accepted approximate Discrete Interaction Approximate (DIA) (Komen et al. (1994), has been applied in the present study. The quadruplet-wave interaction controls (i) the shape-stabilization of the high-frequency part of the spectrum, (ii) the downshift of energy to lower frequencies and (iii) frequency-dependent redistribution of directional distribution functions.

3.2.5. Calibration parameters

3.2.5.1. White capping

The source function describing the dissipation due to white-capping is based on the theory of Hasselmann (1974). With the description of wind input introduced by Janssen (1989), it was realized that the dissipation source function needs to be adjusted in order to obtain a proper balance between the wind input and the dissipation at high frequencies. The dissipation source function,

$$S_{ds}(\sigma,\theta) = -C_{ds}(\bar{k}^2 m_0)^2 \left\{(1-\delta)\frac{k}{\bar{k}} + \delta(\frac{k}{\bar{k}})^2\right\} \bar{\sigma} N(\sigma,\theta) \quad \text{..... (3.5)}$$

Where, C_{ds} and δ are calibration parameters. The values applied for C_{ds} and δ in the present study are 4.5 and 0.5 respectively. $\bar{k}$ is the mean wave number and m_0 is the zeroth moment of the spectra.

3.2.5.2. Bottom friction

As waves propagate into shallow water, the orbital wave velocities penetrate the water depth, and the source function due to wave-bottom interaction becomes important. The dissipation source function is based on the quadratic friction law and linear wave kinematic theory (Johnson and Kofoed-Hansen, 2000).

$$S_{bot}(\sigma,\theta) = -C_f \frac{k}{sinh2kh} E(\sigma,\theta) \quad \text{..... (3.6)}$$

where C_f is a dissipation coefficient ($= f_w U_{bm}$), which depends on the hydrodynamic and sediment conditions. Here f_w is the wave friction factor and U_{bm} is the maximum near-bed particle velocity.

In the present study, the bottom friction is considered according to Nikuradse roughness, k_N. It is a calibration factor and the value applied in the present study is 0.04 m.

3.2.5.3. Wave breaking

Depth-induced breaking occurs when waves propagate into very shallow areas, and the wave height can no longer be supported by the water depth. The formulation of wave breaking is based on the breaking model by Battjes and Janssen (1978).

The source term due to depth-induced breaking can be written as,

$$S_{surf}(\sigma,\theta) = -\frac{\alpha Q_b \bar{\sigma} H_m^2}{8\pi} \frac{E(\sigma,\theta)}{E_{tot}} \quad \ldots\ldots\ldots\ldots \quad (3.7)$$

where, α (=1.0) is a calibration constant, Q_b is the fraction of breaking waves, $\bar{\sigma}$ is the mean relative frequency, E_{tot} is the total wave energy and $H_m = \gamma d$ is the maximum wave height. Here, γ is the free breaking parameter (a wave height to depth ratio). The alpha (α) controls the rate of dissipation and is a proportional factor to the wave breaking source function. Kaminsky and Kraus (1993) found that γ values are in the range between 0.6 and 1.59 with an average of 0.79. In the present study, $\gamma = 0.8$ has been applied.

3.2.6. Initial conditions

The initial conditions are applied by calculating the spectra from empirical formulations. In the present study, JONSWAP fetch growth expression has been applied to calculate the spectra. The following values are used for various parameters:

maximum fetch length: 100 km; maximum peak frequency: 0.4 Hz; maximum Philip's constant: 0.0081; shape parameter, σ_a : 0.07; shape parameter, σ_b: 0.09; peakedness parameter, γ: 3.3 .

3.2.7. Boundary conditions

For wave simulations in the Indian Ocean, all the boundaries were closed assuming that the influence of wave energy into the Indian Ocean from the rest of the Oceans has negligible impact along the Indian coastal regions. It means, no waves enter the model domain through this boundary and the outgoing waves are fully absorbed. However, for wave simulations in the local models, the wave parameters obtained from the Indian Ocean model were applied as the boundary conditions. For this purpose, wind sea and swell parameters were extracted from the coarser model outputs at the open boundaries of the

local models. The integral parameters applied are significant wave height (m), peak wave period (s), mean wave direction (deg) and directional standard deviation (deg).

3.2.8. Output parameters

The basic outputs from the simulations are integral wave parameters and spectral parameters. The integral wave parameters obtained from the simulations are listed in Table 3-1. The integral parameters are determined for the total spectrum, for the wind sea part of the spectrum and for the swell part of the spectrum. The distinction between wind sea and swell are estimated using dynamic threshold frequency. Here, the swell components are defined as those components fulfilling the following wave-age based criterion,

$$\frac{U_{10}}{c}\cos(\theta - \theta_w) < 0.83 \quad \text{..... (3.8)}$$

Where, U_{10} is the wind speed, c the phase speed and θ and θ_w are the wave direction and wind direction, respectively.

The important integral parameters used in the present study are significant wave height (H_{m0}), peak wave period (T_p), mean wave period (T_{m02}), mean wave direction (θ_m) and directional standard deviation (DSD).

Significant wave height, $H_{m0} = 4\sqrt{m_0}$ ..... (3.9)

Peak wave period, $T_p = 1/f_p$ ..... (3.10)

The peak frequency f_p is calculated from the one-dimensional frequency spectrum using a parabolic fit around the discrete peak.

Mean wave period, $T_{02} = \sqrt{m_0/m_2}$ ..... (3.11)

Mean wave direction, $\theta_m = 270 - tan^{-1}(b/a)$ ..... (3.12)

where, $a = \frac{1}{m_0}\int_0^{2\pi}\int_0^{\infty} cos(270-\theta)\, E(f,\theta)\, df\, d\theta$ ..... (3.13)

$$b = \frac{1}{m_0}\int_0^{2\pi}\int_0^{\infty} sin(270-\theta)\, E(f,\theta)\, df\, d\theta \quad \text{..... (3.14)}$$

The directional standard deviation *DSD* is defined by,

$$DSD = 180/\pi \sqrt{2(1-\sqrt{a^2+b^2})} \quad \text{..... (3.15)}$$

One-dimensional and two-dimensional spectra are obtained from numerical simulations. Directional spectrum or frequency spectrum is one-dimensional, whereas directional-

frequency spectrum is two-dimensional. The directional energy spectrum is obtained by integration over the discretized frequencies and, frequency energy spectrum is obtained by integration over the discretized directions. However, the 2D spectrum is obtained by integration over the discretized frequencies.

Table 3-1. Integral wave parameters obtained from wave simulations

Wave parameters	Symbol	SI unit
Significant wave height	H_{m0}	m
Maximum wave height	H_{max}	m
Peak wave period	T_p	m
Mean wave period	T_{01}	m
Mean wave period (Zero-crossing wave period)	T_{02}	m
Wave energy wave period	T_{-10}	m
Peak wave direction	θ_p	°N
Mean wave direction	θ_m	°N
Directional standard deviation	DSD	°
Wave velocity components	$H_{m0} \cdot \cos(\theta_m)$ $H_{m0} \cdot \sin(\theta_m)$	m/s
Radiation stresses	S_{xx}, S_{xy}, S_{yy}	m^3/s^2
Particle velocities	$U_{max}(z=-d)$, Umax(z=0), Wmax(z=0), Umax(z=z_0), Wmax(z= z_0)	m/s

3.3. Model validation

Model results have been validated with measurements at one deep water location and two nearshore locations in the Indian Ocean. The measurement locations are DS1 (deep water), B1 and B8 (nearshore regions) as shown in Figure 2-1. Continuous 16 months time series data are available at B1, whereas 9 months data were available at DS1 and B8. In addition to DS1 data, Jason-1 significant wave heights at two deep water locations (in the Arabian Sea and Bay of Bengal) have been used to compare with modelled significant wave heights.

3.3.1. Validation at deep water locations

Measured wave data at DS1 is available for the period Jan. – Sep. 2001. Hence, the wave simulation has been carried out for the Indian Ocean using NCEP winds for the above period. The simulated wave parameters have been extracted at location DS1 and compared with measured parameters. Figure 3-7 shows the comparison between measured and modelled wave parameters. The modelled H_s and T_m show close match with the measured wave parameters. The extreme waves observed during the study period are well reproduced in the simulations.

The statistical parameters estimated between measured and modelled wave parameters at DS1 are listed in Table 3-2. Measured and modelled H_s and T_m are well correlated. The correlation coefficient of H_s and T_m are 0.96 and 0.85, respectively. There is no marginal bias between measured and modelled H_s, however, the r.m.s. error is 0.37 m. The mean wave period is slightly under estimated (bias = 0.32 s) and the corresponding r.m.s. error is 0.8 s. The scatter indices estimated for H_s and T_m are 0.2 and 0.14, respectively, which shows good linear fit between measured and modelled parameters. It is evident from the scatter plots (Figure 3-8) that the scatter points of H_s and T_m are linearly well packed. The statistical parameters confirm the excellent performance of the model and reliability of the simulation results.

Waves simulated using NCEP winds of 2005 are compared with Jason-1 data at two deep water locations: one in the Arabian Sea (G1) and another in the Bay of Bengal (P1). The geographical co-ordinates of G1 is 69° E, 15° N and that of P1 is 91° E, 18° N (Figure 2-3). The corresponding water depths are 3800 m and 2200 m at G1 and P1, respectively. Comparison between Jason-1 and model significant wave heights are shown in Figure 3-9. It shows that the modelled significant wave heights match very well with the remotely sensed observations (Jason-1). For larger waves, an underestimation has been observed in

the model significant wave heights. The gaps seen in Jason-1 H_s curve indicate missing values.

Table 3-3 shows the statistical parameters calculated between Jason-1 and model significant wave heights at locations G1 and P1. Good correlation is found between the two at both the locations with correlation coefficients 0.96 and 0.90 at G1 and P1, respectively. There is a slight overestimation of 0.12 m at G1 and an underestimation of 0.07 m at P1. The r.m.s. error calculated at G1 and P1 are 0.44 m and 0.31 m, respectively. The scatter indices (SI) calculated at G1 and P1 are 0.28 and 0.21, respectively. Again the statistical parameters show the reliability of the wave model used, as well as the use of altimeter data for comparison/validation.

Figure 3-10 shows the scatter between Jason-1 and model significant wave heights at G1 and P1. It is clear that the scatter is moderately narrow at both the locations, even though there is slight over estimation at G1 and an under estimation at P1. This shows that the model performs well at deep waters both in the Arabian Sea and the Bay of Bengal.

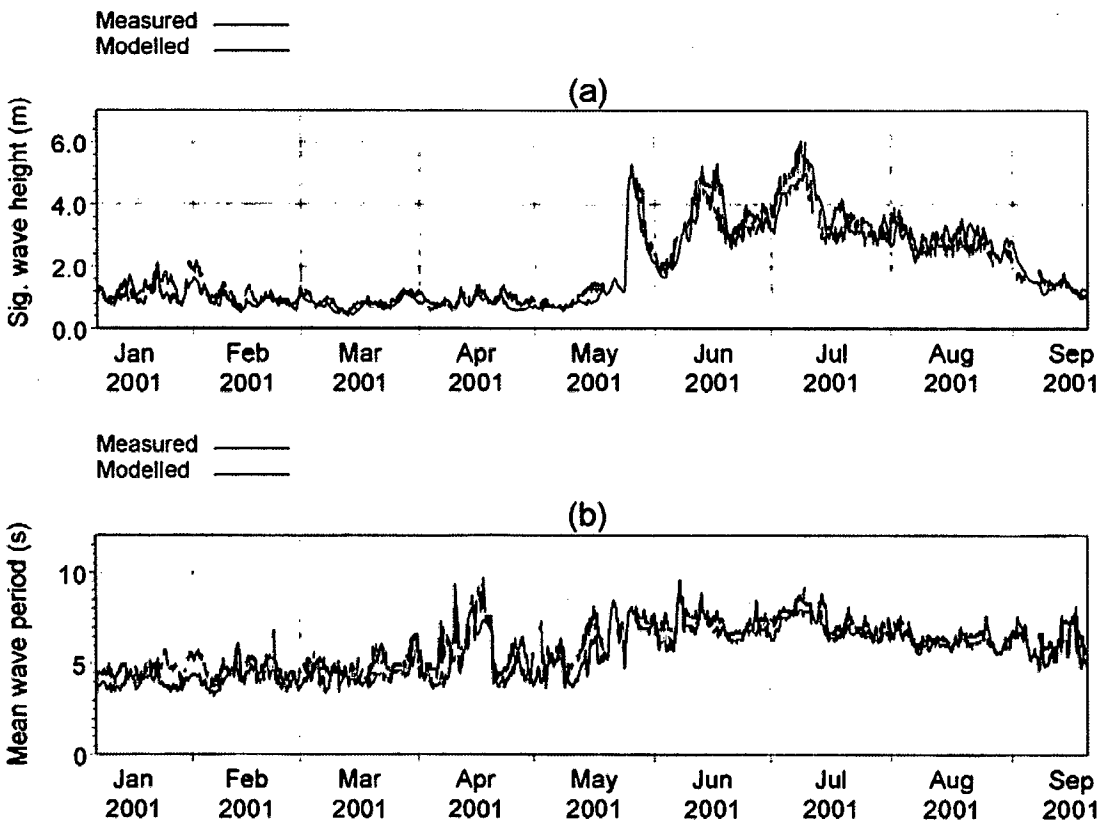

Figure 3-7. Comparison between measured and modelled wave parameters at DS1: (a) significant wave height and (b) mean wave period.

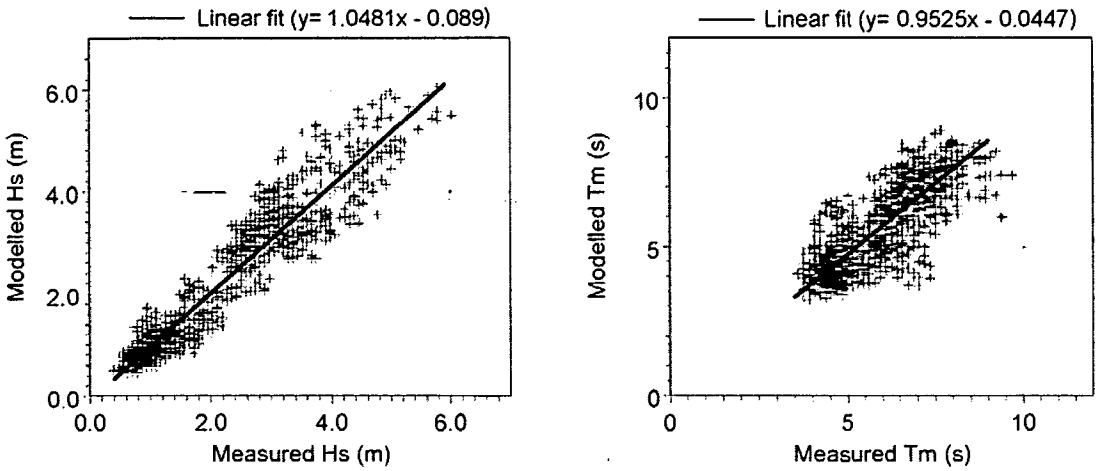

Figure 3-8. Scatter between measured and modelled H_s and T_m at DS1.

Table 3-2. Statistical parameters estimated between measured and model wave parameters at DS1.

Parameters	Correlation coefficient	Bias	r.m.s. error	Scatter Index
H_s (m)	0.96	0.00	0.37	0.20
T_m (s)	0.85	-0.32	0.80	0.14

Table 3-3. Statistical parameters estimated between Jason-1 and model significant wave heights at G1 and P1.

Location	Correlation coefficient	Bias (m)	r.m.s. error (m)	Scatter Index
G1 (off Goa)	0.96	0.12	0.44	0.28
P1 (off Paradip)	0.90	-0.07	0.31	0.21

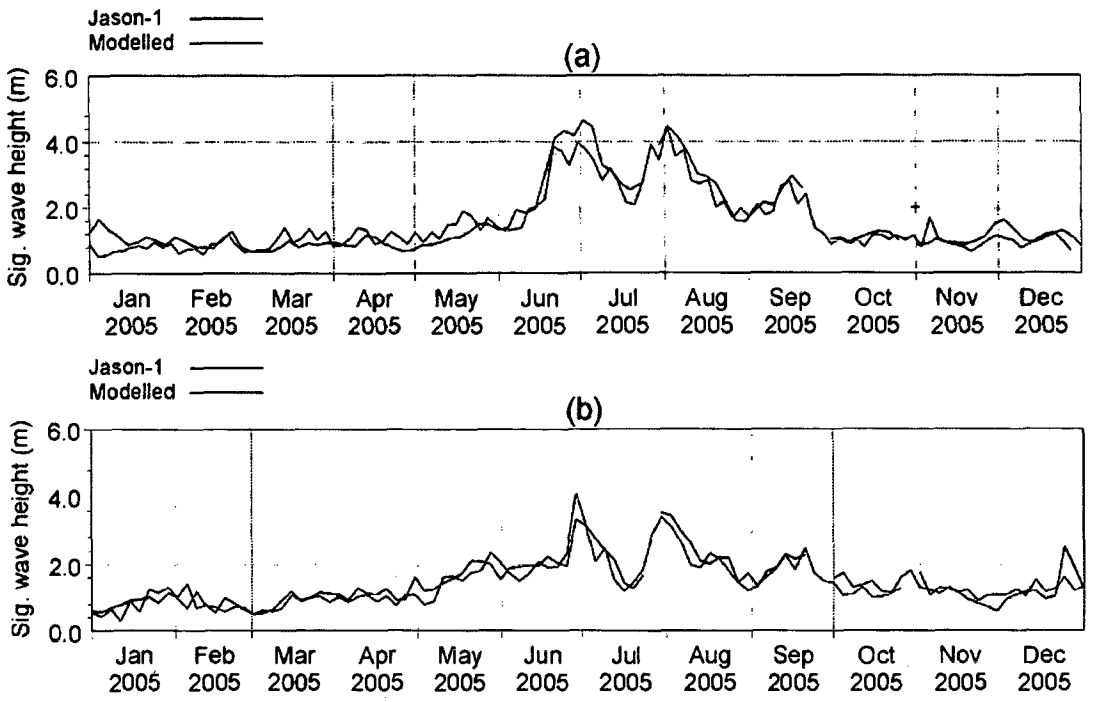

Figure 3-9. Comparison between Jason-1 and modelled H_s off: (a) Goa (at G1) and (b) Paradip (at P1).

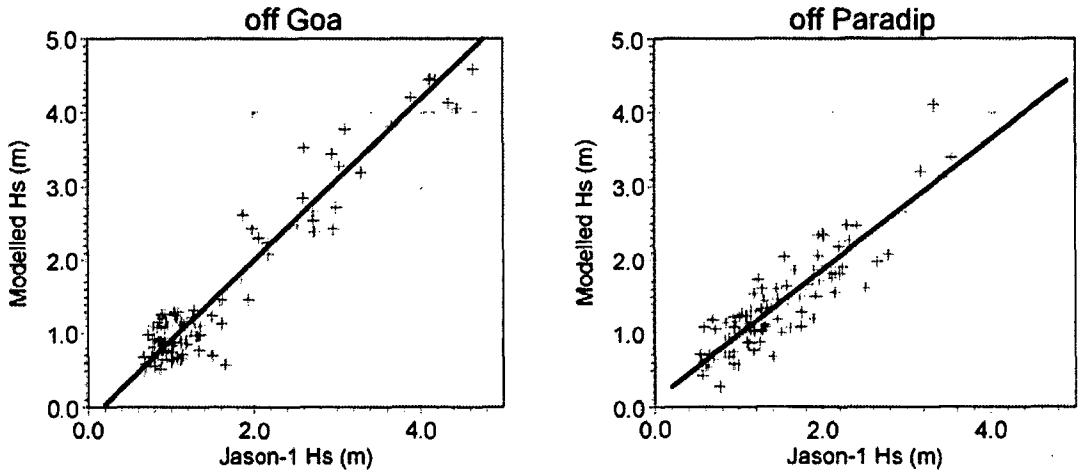

Figure 3-10. Scatter between Jason-1 and modelled H_s at G1 (off Goa) and P1 (off Paradip).

3.3.2. Validation at nearshore regions

The two select nearshore locations are B1 (off Goa) and B8 (off Paradip) as shown in Figure 2-1. Measurements are available during Feb 1996 - May 1997 at B1 and during May 1996 - Jan 1997 at B8. Wave simulations have been carried out using NCEP winds

during 1996 – 1997. The simulated wave parameters have been extracted at the above locations and compared with the measurements.

Figure 3-11 and Figure 3-12 show the comparison between measured and model wave parameters at locations B1 and B8, respectively. Model wave parameters show very good match with measured wave parameters, especially with significant wave height and wave direction at both the locations. The comparison of mean wave period is good at B1 and moderately good at B8.

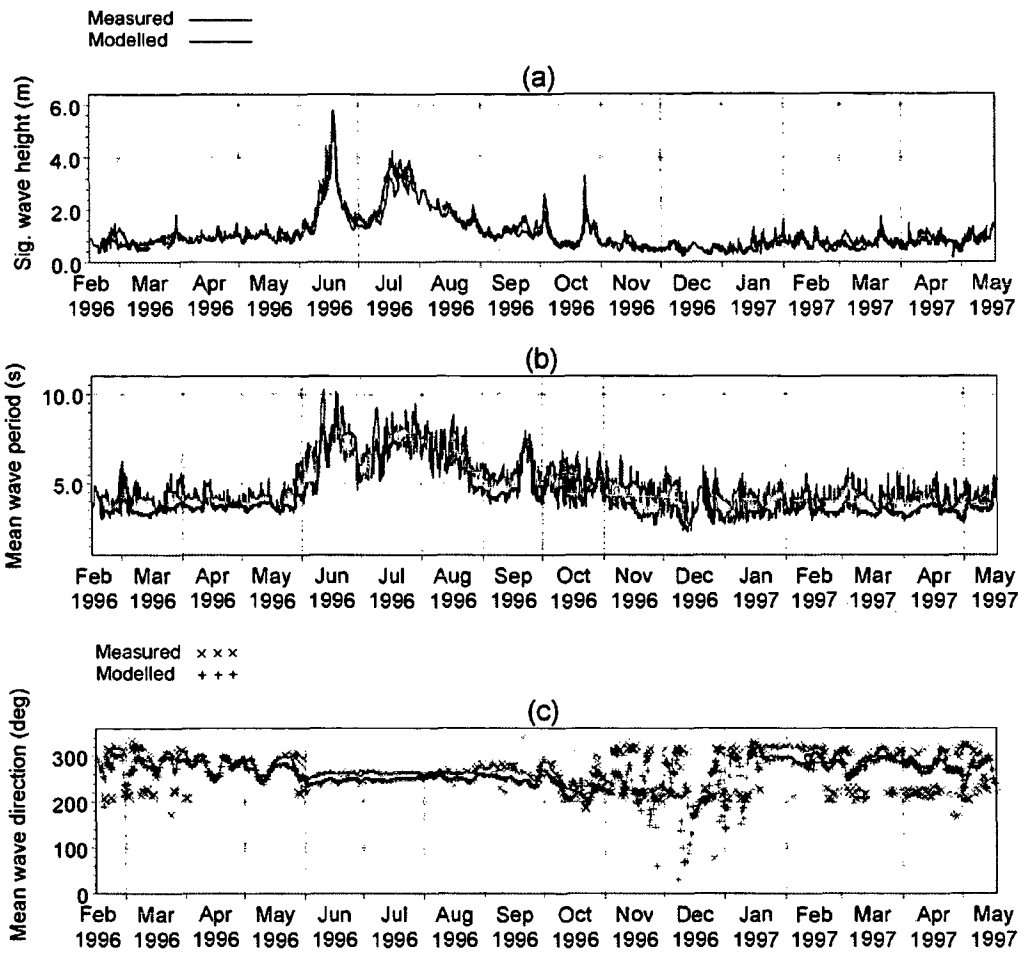

Figure 3-11. Comparison between measured and modelled wave parameters at B1 (off Goa): (a) significant wave height, (b) mean wave period and (c) mean wave direction.

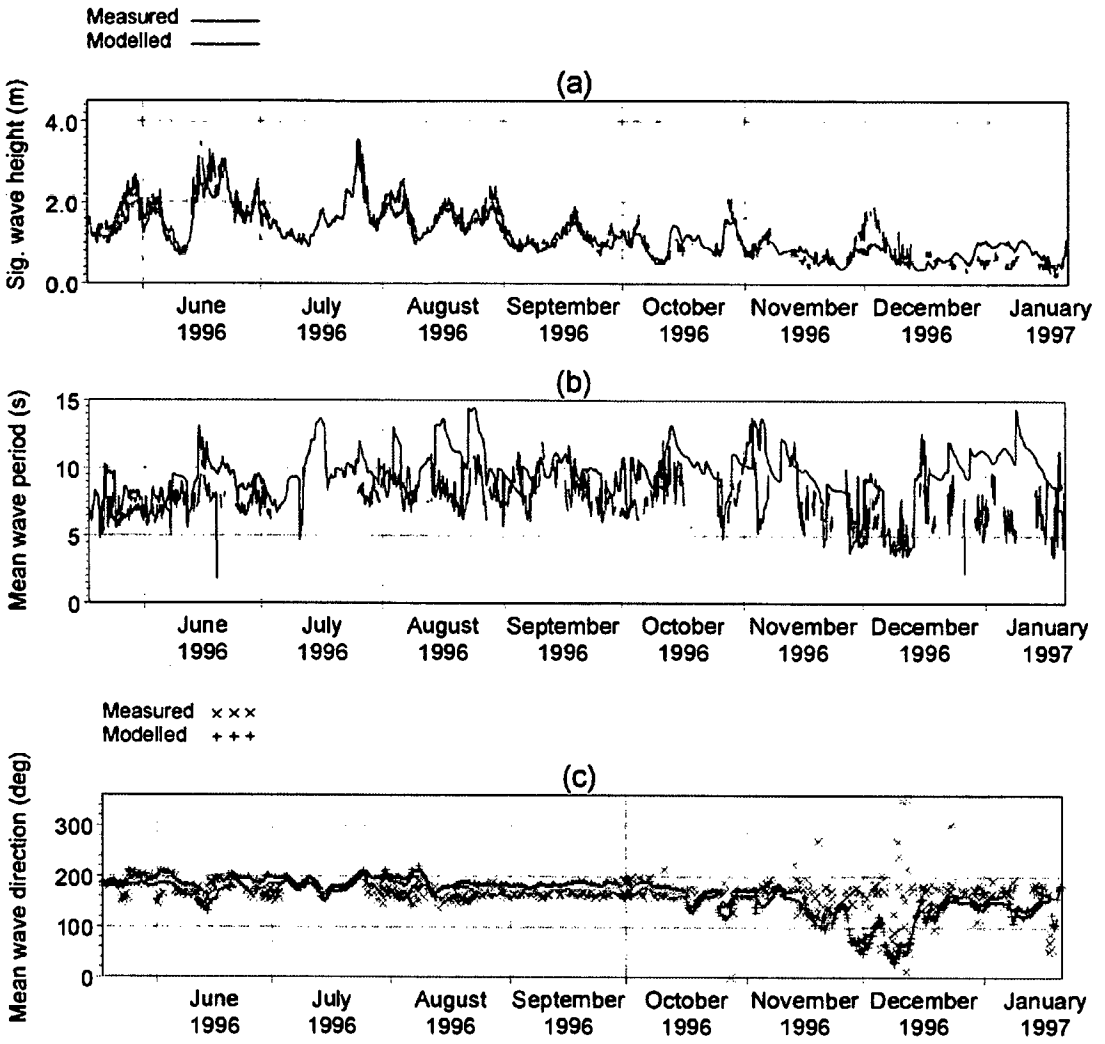

Figure 3-12. Comparison between measured and modelled wave parameters at B8 (off Paradip): (a) significant wave height, (b) mean wave period and (c) mean wave direction.

The statistical analysis of measured and modelled wave parameters have been made separately for wave, swell and wind sea at locations B1 and B8, which are listed in Table 3-4, respectively. Wave and swell are well predicted at both the locations, and not, the wind sea (moderately good). The moderate comparison of winds seas is due to the fact that coarse resolution wind input is applied to the wave model (explained in chapter 4). The correlation coefficients of significant heights of wave, swell and wind sea at location B1 are 0.96, 0.93 and 0.64, respectively, whereas those at B8 are 0.90, 0.84 and 0.63 for wave, swell and wind sea, respectively. The waves and swells are least biased at both the locations; very marginal overestimation in waves (0.06 m and 0.07 m for H_s and 0.1 s and

0.6 s for T_m at B1 and B8, respectively) and underestimation in swells (0.07 m and 0.04 m for H_s and 0.2 s and 0.52 s for T_m at B1 and B8, respectively). The r.m.s. error calculated for H_s (for wave and swell) are in the range of 0.29 - 0.36 m at both the locations. The r.m.s. error in period is low for resultant T_m (between 0.8 – 1.24 s) and larger for swell T_m (between 2.15 – 2.5 s).

The scatter indices are 0.25 and 0.22 for resultant H_s and 0.39 and 0.31 for swell H_s at B1 and B8, respectively. Similar results are observed for resultant T_m (0.17 and 0.22 at B1 and B8, respectively) and swell T_m (0.32 and 0.24 at B1 and B8, respectively). This indicates that the waves are least scattered and swells are moderately scattered. Figure 3-13 and Figure 3-14 show the scatter between measured and modelled wave parameters at locations B1 and B8, respectively. The points are linearly scattered for the waves and swells at B1 and B8, indicating that match is good between measured and modelled wave and swell parameters. The significant swell heights are also linearly correlated, though the mean swell periods show large deviations. The wind sea parameters other than H_s are widely scattered.

Table 3-4. Statistical parameters estimated between measured and model wave parameters at B1 (off Goa) and B8 (off Paradip).

Location	Parameters	Resultant wave		Swell		Wind sea	
		H_s (m)	T_m (s)	H_s (m)	T_m (s)	H_s (m)	T_m (s)
B1	Correlation coefficient	0.96	0.83	0.93	0.45	0.64	0.28
	Bias	0.06	0.1	-0.07	-0.2	0.31	0.3
	r.m.s. error	0.29	0.8	0.36	2.5	0.46	1.6
	Scatter Index	0.25	0.17	0.39	0.32	0.7	0.49
B8	Correlation coefficient	0.9	0.65	0.84	0.68	0.63	0.37
	Bias	0.07	0.6	-0.04	-0.52	0.15	-0.32
	r.m.s. error	0.29	1.24	0.32	2.15	0.12	1.69
	Scatter Index	0.22	0.22	0.31	0.24	0.61	0.43

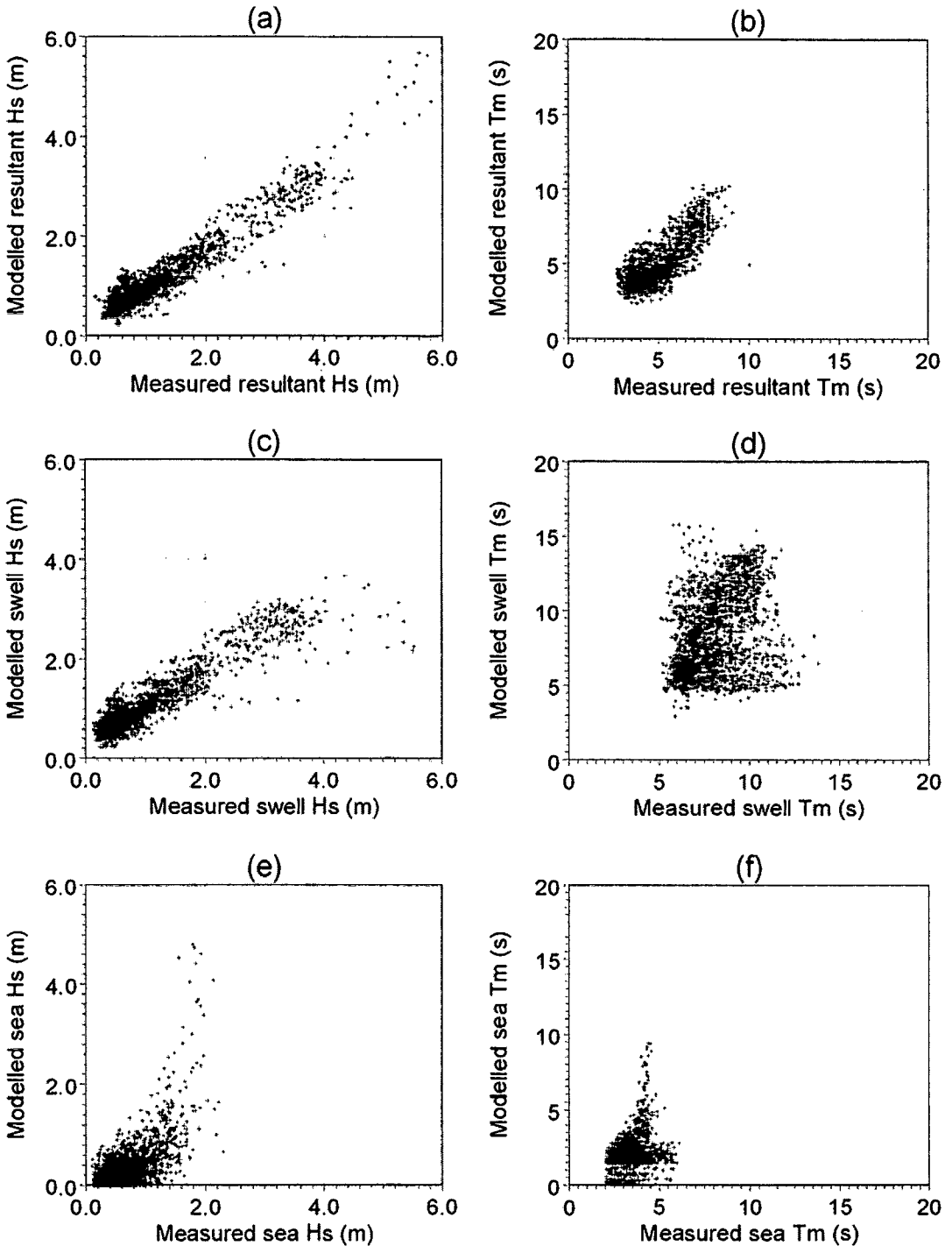

Figure 3-13. Scatter between measured and modelled wave parameters at B1 (off Goa): (a) resultant H_s, (b) resultant T_m, (c) swell H_s, (d) swell T_m, (e) wind H_s sea and (f) wind sea T_m.

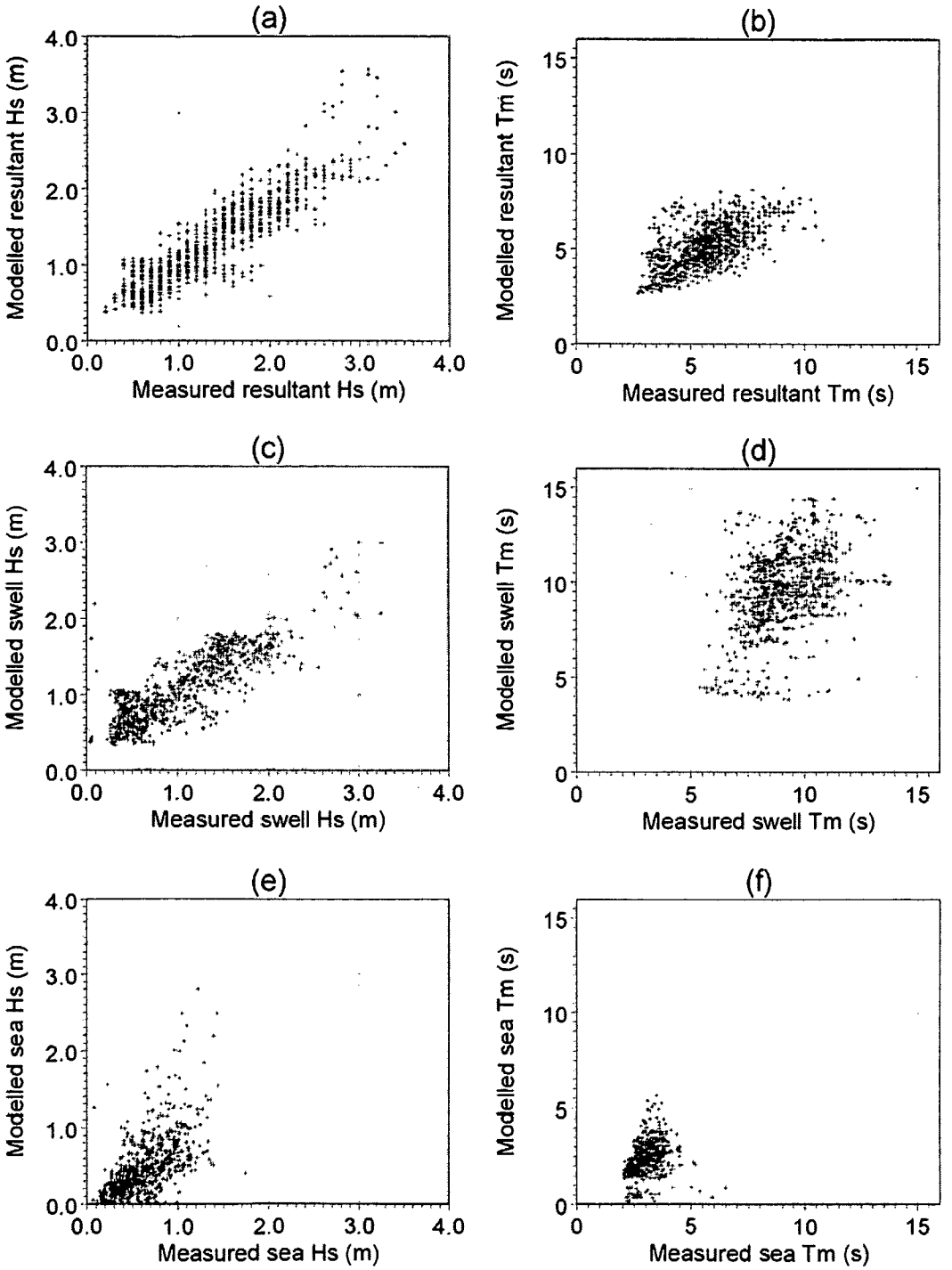

Figure 3-14. Scatter between measured and modelled wave parameters at B8 (off Paradip): (a) resultant H_s, (b) resultant T_m, (c) swell H_s, (d) swell T_m, (e) wind sea H_s and (f) wind sea T_m.

3.3.3. Sensitivity test

The model sensitivity of wave predictions using various wind inputs has been tested as wind is one of the basic input parameters which decide the accuracy of wave prediciton. NCEP, IFREMER/CERSAT blended and QuikScat winds were applied to the simulations. The modelled wave parameters have been extracted at location B2 (off Goa) and compared with measurements available during 01 – 21 May 2005 at B2 (for every 1 hour). Statistical parameters such as correlation coefficient, bias, r.m.s. error and scatter index were also estimated.

Statistical parameters estimated between measured and modelled wave parameters at B2 are listed in Table 3-5. A good match is obtained for the simulation results using NCEP and blended winds, and ,match is relatively poor for QuikScat winds. Since, temporal resolution of the QuikScat winds is coarse (twice daily), the diurnal features along the coast, especially wind waves generated by the sea breeze and land breeze system, could not be reproduced well by the model.

Correlation coefficient and bias of H_s and T_m corresponding to NCEP and blended winds are nearly the same (correlation coefficients of H_s are 0.75 and 0.74, respectively and biases are 0.04 m and 0.09 m, respectively). Correlation coefficients of T_m corresponding to NCEP and blended winds are 0.63 and 0.59, and biases are 0.56 s and 0.47 s, respectively. T_m corresponding to QuikScat winds is poorly correlated (0.20), even though correlation of H_s is moderately good (0.64). The low scatter indices for all cases indicate that there is good linear fit between the measured and modelled parameters.

Since, NCEP winds and blended winds reproduced the near real waves in the simulations, these winds can be chosen for accurate wave predictions in the Indian Ocean. In the sensitivity test, a short duration data has been chosen (01 – 21 May 2005) to calculate the accuracy of wave prediction. However, better results could be obtained with long term observations. Since, the spatial resolution of blended winds is finer (0.25° x 0.25°), characteristics of coastal winds could be incorporated for better wave prediction is expected near the coast.

Table 3-5. Statistical parameters estimated between measured and modelled (using NCEP, Blended and QuikScat winds) wave parameters at B2.

Statistical parameters	NCEP		Blended		QuikScat	
	H_s (m)	T_m (s)	H_s (m)	T_m (s)	H_s (m)	T_m (s)
Correlation coefficient	0.75	0.63	0.74	0.59	0.64	0.20
Bias	0.04	0.56	0.09	0.47	-0.02	0.55
r.m.s. error	0.12	0.75	0.15	1.04	0.11	0.83
Scatter Index	0.15	0.18	0.20	0.25	0.14	0.20

3.4. Simulations using MM5 winds

MM5 winds have been used to simulate wind seas off Goa (local domain) during May 2005, to study wind sea characteristics during pre-monsoon season. Another simulation has been carried out for the local domain considering the wave parameters extracted (at the boundaries of local domain) from the Indian Ocean model as boundary conditions and MM5 winds as input to simulate waves off Goa. The aim of this work is to make use of fine resolution MM5 winds in wave simulations to study coastal wave features due to coastal wind systems.

The wind seas simulated using MM5 winds have been validated with measurements at locations B2 and B3. For this purpose, wind sea and swell parameters at B2 and B3 are separated from the measured wave spectra as described in Sec 2.3.1 (Chapter 2). Figure 3-15 and Figure 3-16 show the comparison between measured and modelled wind sea parameters at B2 and B3, respectively. Modelled wind sea parameters show very good match with measurements. The diurnal pattern of wind seas is well reproduced in the model.

Statistical parameters estimated between measured and modelled wind sea parameters at B2 and B3 are listed in Table 3-6. There is good correlation between measured and modelled wind sea H_s, however, moderate correlation has been obtained between measured and modelled T_m. Correlation coefficients of H_s are 0.70 and 0.73 at B2 and B3, respectively. Biases are less (< 0.1 m for H_s and < 0.5 s for T_m), even though wind sea H_s

and T_m are underestimated by the model. The r.m.s. errors are upto 0.16 m for H_s and 0.55 s for T_m. All the statistical estimates are well within the acceptable limits for the waves.

Figure 3-17 and Figure 3-18 show the scatter between measured and modelled wind sea H_s and T_m at B2 and B3, respectively. There is a good linear fit for H_s, even though a few points are widely scattered. The scatter points of T_m are closely packed with most of the points centered between 2 and 3 s. In fact, these are the wind sea periods exist along the coastal region off Goa during pre-monsoon season.

The wind seas simulated using MM5 winds have been further utilised to study the diurnal variations associated with sea breeze-land breeze systems over the Goa coast during pre-monsoon season (May 2005). The results are discussed in Chapter 4.

Table 3-6. Statistical parameters estimated between measured and modelled wind sea parameters at B2 and B3.

Location	Parameters	Wind sea	
		H_s (m)	T_m (s)
B2	Correlation coefficient	0.70	0.39
	Bias	0.09	0.40
	r.m.s. error	0.16	0.52
	Scatter Index	0.30	0.17
B3	Correlation coefficient	0.73	0.37
	Bias	0.03	0.44
	r.m.s. error	0.12	0.55
	Scatter Index	0.26	0.18

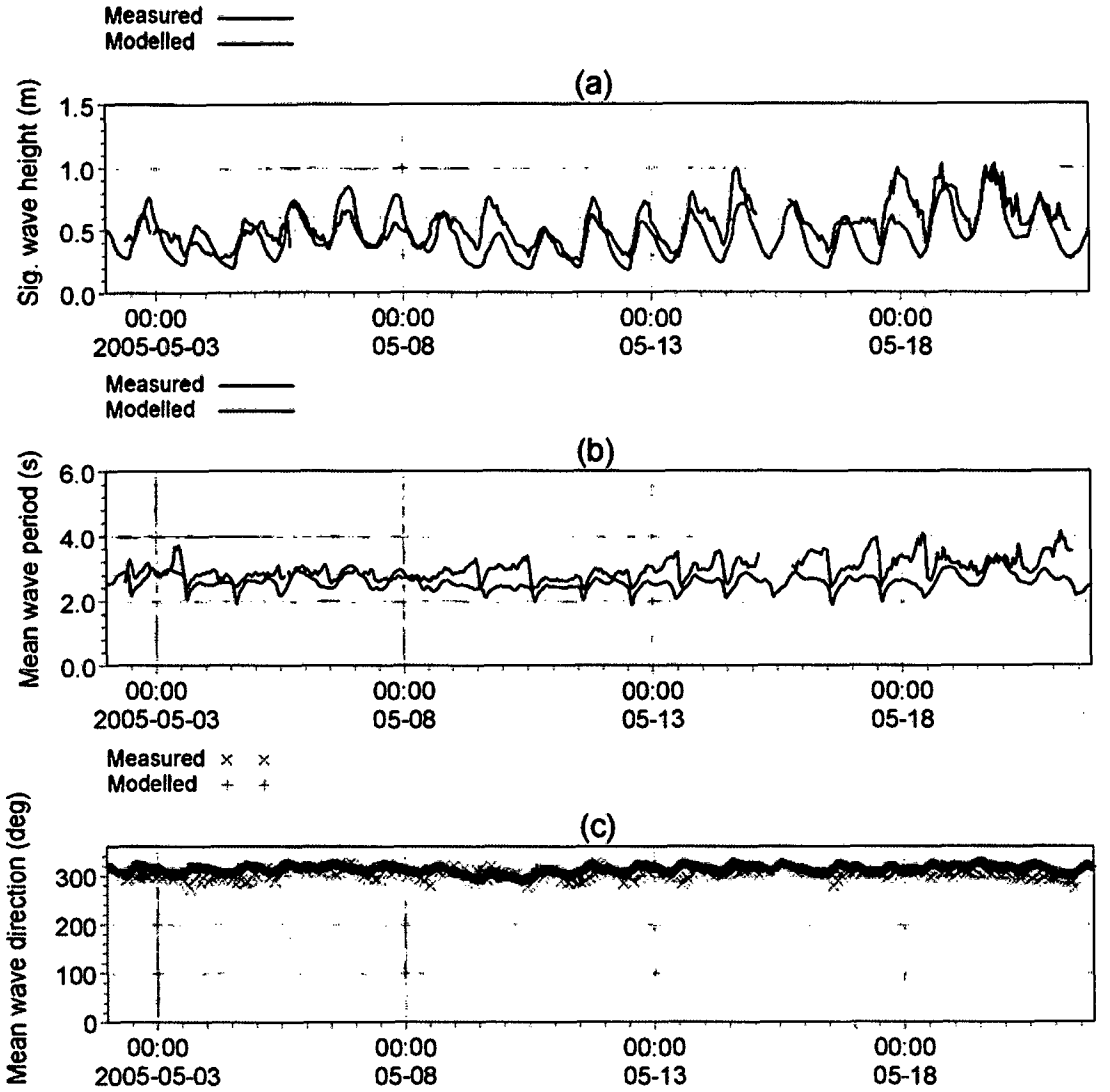

Figure 3-15. Comparison between measured and modelled wind sea parameters at B2: (a) significant wave height, (b) mean wave period and (c) mean wave direction.

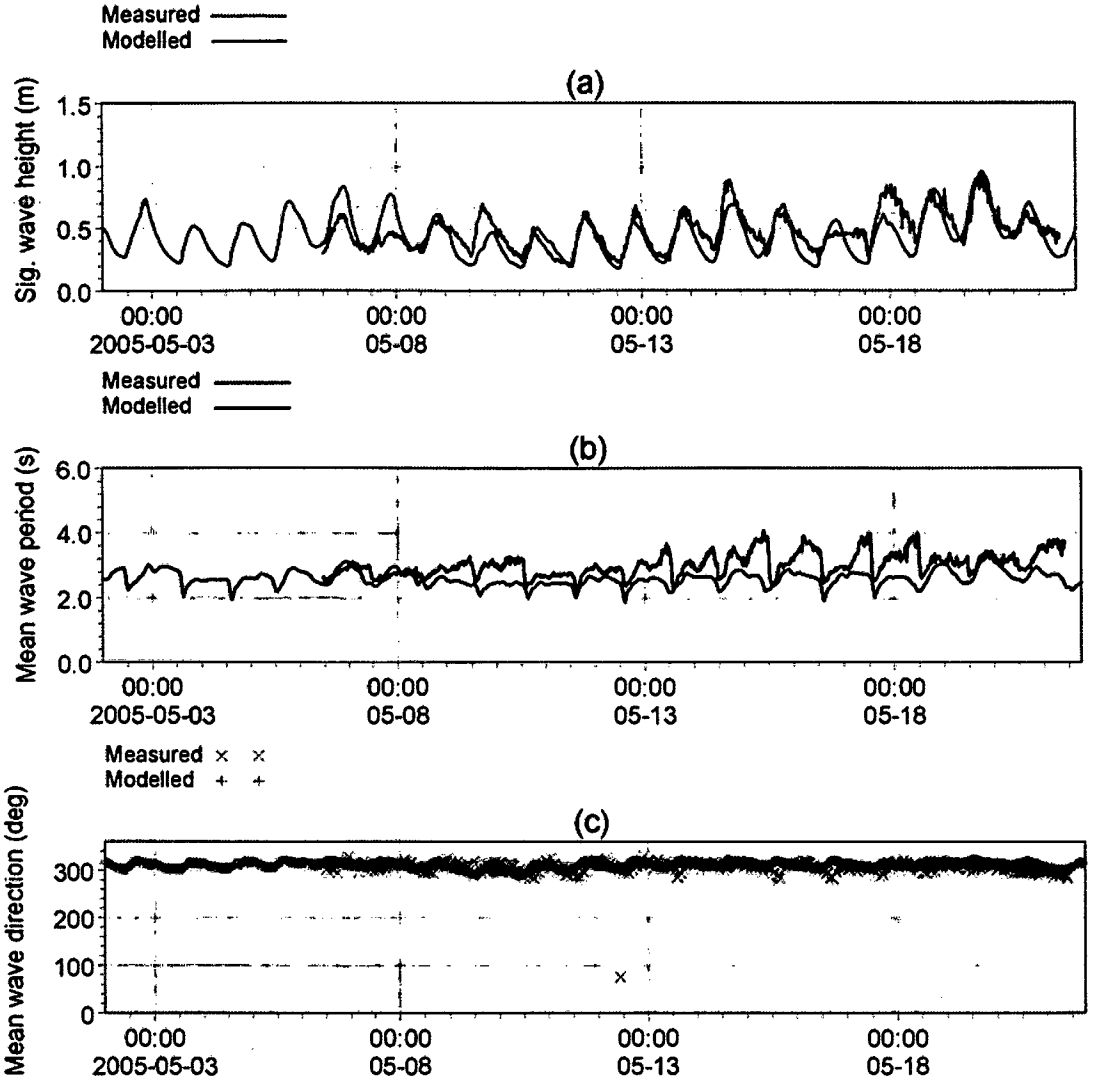

Figure 3-16. Comparison between measured and modelled wind sea parameters at B3: (a) significant wave height, (b) mean wave period and (c) mean wave direction.

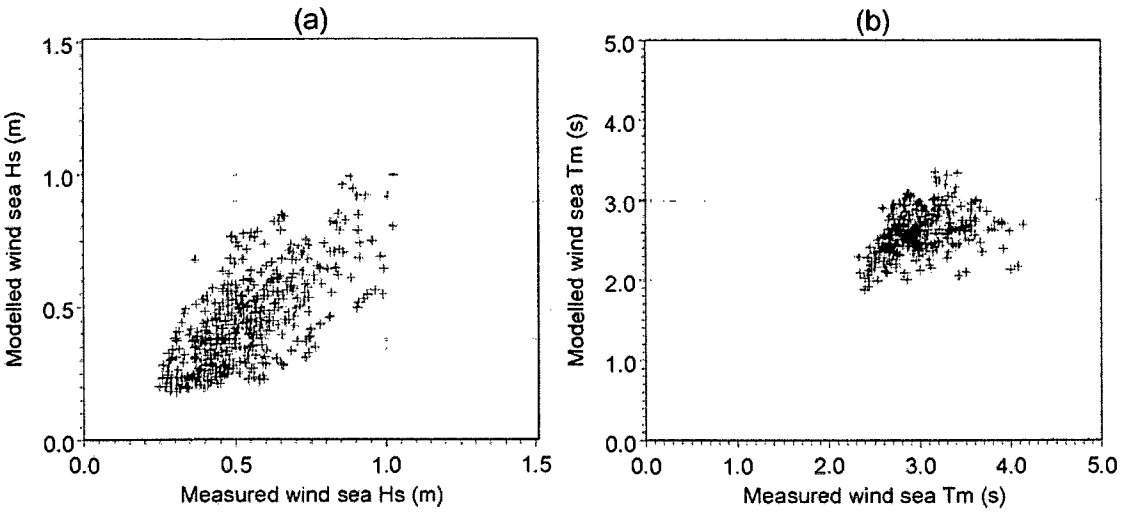

Figure 3-17. Scatter between measured and modelled (a) wind sea H_s and (b) wind sea T_m at B2.

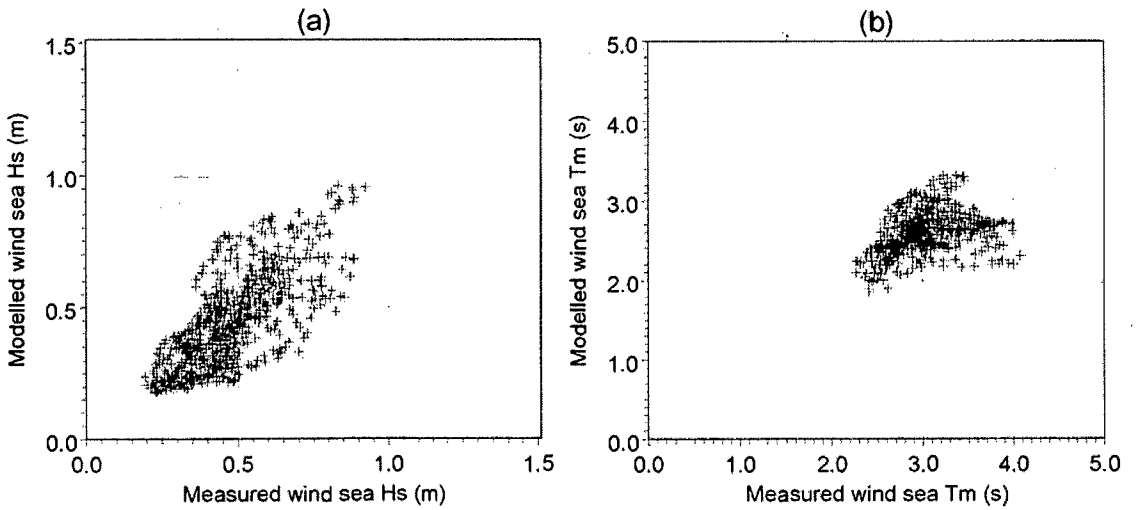

Figure 3-18. Scatter between measured and modelled (a) wind sea H_s and (b) wind sea T_m at B3.

Chapter 4

Seasonal response of coastal waves along the Indian coast: spectral approach

Chapter 4

Seasonal response of coastal waves along the Indian coast: spectral approach

4.1. Introduction

Spectral characteristics of nearshore waves have been analysed using time series wave data measured at select locations along the Indian coast. The directional spectra distinctly separate out the wave conditions prevailed at various locations along the Indian coast during pre-monsoon, SW monsoon and NE monsoon seasons and extreme weather events. Further, dominance of swells and wind seas along the west coast of India has been studied in detail. Potential swell regions, which affect the west coast of India during various seasons, were identified from the analysis of global wind data and wave observations. The findings have been substantiated through numerical simulations. The characteristics of "Shamal swells" have been studied based on measured wave data off Ratnagiri during winter season. Numerical simulations reproduced the generation and propagation of the Shamal swells in the Arabian Sea. Superimposition of pre-existing swells with wind seas generated by the sea breeze during pre-monsoon season has been studied to understand the nature of coastal waves prevailing along the west coast of India.

4.2. Wave characteristics during monsoons and extreme events

Wave data measured at locations B1 (off Goa) and B8 (off Paradip) have been used to study the spectral characteristics of the nearshore waves during monsoons and extreme weather events along the west coast and east coast of India, respectively. Measurements are available for the periods Feb 1996 – May 1997 at B1 and May 1996 – Jan 1997 at B2. Numerical simulations have also been carried out to reproduce the wave characteristics in the Indian Ocean during the measurement periods.

4.2.1. Along the east coast of India

Indian Daily Weather Report (IMD, 1996) reveals the presence of 4 storms/depressions in the Bay of Bengal during the study period. The pressure level data from the Cyclone Detection Radar Centre at Paradip indicates that the pressure dropped from 1003.1 to 996.9 mb during 26–30 May 1996, from 1008.0 to 994.2 mb during 10–21 June 1996 and from

1003.0 to 991.2 mb during 18–26 July 1996 (Figure 4-1), leading to extreme wave conditions. The fourth depression could not intensify, though the pressure level decreased from 1012.3 to 1000.4 mb during 24–28 October 1996. Pressure data from IDWR (IMD, 1996) also indicate the presence of depressions over the region. JTWC reported four storms in the Bay of Bengal during the study period: 11 – 18 June 1996, 21 – 29 Oct 1996, 01 – 07 Nov 1996 and 20 Nov – 07 Dec 1996. However, all of them did not impact the Paradip coast (except the storm during 11 – 18 June 1996), as the tracks were far away from the study region.

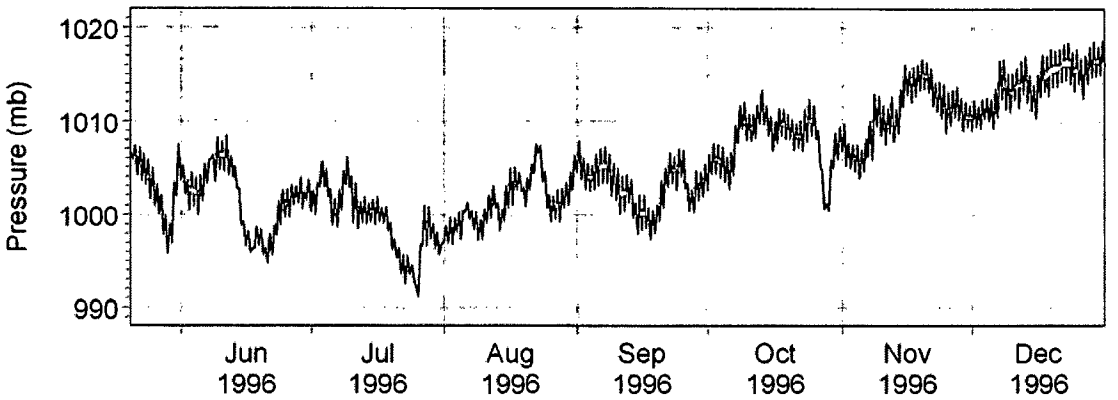

Figure 4-1. Pressure levels during May 1996–December 1996.

In May 1996 (pre-monsoon season), the predominant wave direction was between SSW and SSE with significant wave heights varying between 0.9 and 2.7 m (Figure 4-2). The depression during 26–30 May, 1996 caused the waves to grow and the significant wave height reached up to 2.7 m on 28 May in the SSW direction. On 29 May, the wave direction shifted to S and subsequently wave height reduced. The predominant wave direction during SW monsoon season (June–September) was between S and SSE, and the significant wave height reached a maximum value of 3.8 m and 4.2 m on 16 June and 25 July, respectively. This includes waves during the two depression periods. In NE monsoon (November–January), the predominant wave direction was between SE and NE, and the maximum significant wave height observed was 2.1 m (SE direction) on 28 October due to the depression that occurred in the Bay of Bengal (24–29 October, 1996). Even though the pressure level decreased from 1012.3 to 1000.4 mb, the depression could not intensify further and generate high waves. For the rest of the year, the waves were below 0.8 m in height, and varied between S and SSE directions.

An analysis of several years of wave data from the Bay of Bengal shows that wave parameters such as significant wave height, wave period and mean wave direction vary significantly in various seasons. In general, during fair weather season off Paradip significant wave heights are below 1.0 m, during monsoon below 3.5 m and during extreme weather events of the order of 5.0–7.0 m.

Frequency-energy spectra during extreme events are single peaked, and the maximum energy distribution is in a narrow frequency band (Figure 4-3a) with an average directional spreading of 20°. Spectra for other seasons are multipeaked, and energy is distributed over a wide range of frequencies (Figure 4-3b and 4-3c) in different directions. The type of spectra shown in Figure 4-3b and 4-3c represent the seasonal variation of wave conditions in the Bay of Bengal in the absence of extreme events. Wave spectra of extreme events are distinctly different from that of monsoon or fair weather season. In general, wave spectra along the Indian coast are multi-peaked, often with two peaks (Harish and Baba 1986; Vethamony and Sastry 1986; Rao and Baba 1996). Greenslade (2001) found that when energy shifts from one portion of the spectrum to another, the spectral peak suddenly jumps to a different frequency.

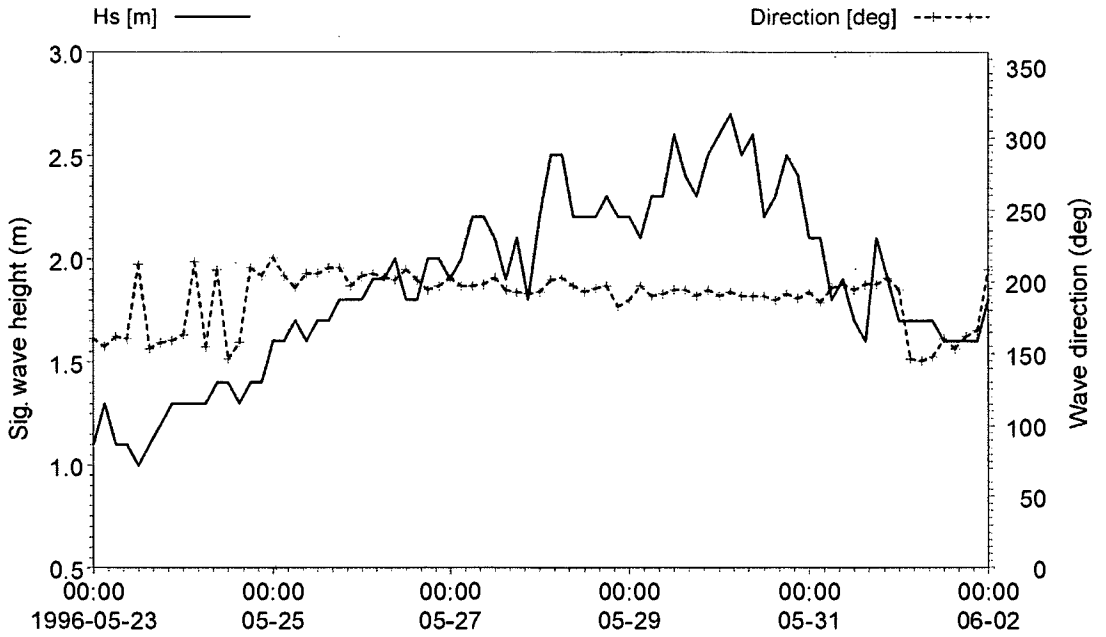

Figure 4-2. Significant wave height pattern during an extreme event (23 May – 02 June, 1996) indicating wave growth and decay.

Sanil Kumar et al. (2004) found that wave spectra during extreme sea states are mainly single-peaked, and the percentage of occurrence of double-peaked spectra is higher for low sea states. In the present case also, the spectra are single-peaked, and the maximum energy is centered in a narrow frequency band. The maximum spectral energy during the two depressions are 30.33 m^2/Hz (15 June) and 31.25 m^2/Hz (26 July), which are very high compared to the energy during normal monsoon months (e.g. 7.63 m^2/Hz (13 June) and 5.68 m^2/Hz (28 July)). It is evident from the spectra that wave energy is higher during SW monsoon season than the NE monsoon. Typical measured directional energy spectra representing SW and NE monsoon seasons are shown in Figure 4-4 and Figure 4-5, respectively.

Bathymetry contours off Paradip are parallel to the coast, and the slope is very gentle. In general, winds are either southwesterlies or northeasterlies. Sufficient fetch is available for both the winds.

During extreme events, long waves with higher amplitudes are generated and most of the energy is concentrated in the low frequency region. So, typically the spectra will be single-peaked. When swells reach the region where the locally generated waves are present, the spectra show double- or multi-peaks. Normally during fair weather season, the sea states are swell dominated. Hence, the primary peak will be in the low-frequency region and secondary peak will be in the high-frequency region, depending on the locally generated wind seas.

During monsoons, the sea off Paradip is usually 'sea' dominated. Distant swells from different directions also propagate to this region and form a complex sea state. Hence, the peak energy shifts from low- to high-frequency region depending on the strength of the prevailing winds.

Modelled directional energy spectra during 26 July are shown in Figure 4-6. The spectra show single-peakedness as in the measured spectra due to extreme event prevailed in the region. The modelled wave directions are between SSW and SSE from May to September and between N and NW in November and December. Mean wave period ranges from 4 to 10 s in SW monsoon and from 2 to 8 s in NE monsoon. The highest measured significant wave height is 4.2 m, whereas the corresponding modelled value is 3.4 m (22 July 1996, due to the extreme event that prevailed in the region).

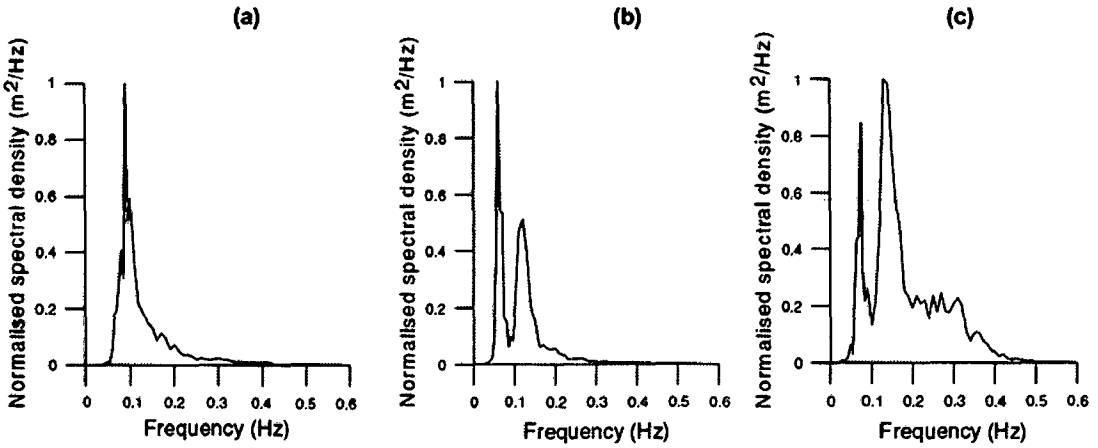

Figure 4-3. Typical wave spectra during (a) 26 July at 09 h, (b) 3 Aug 1996 at 09 h and (c) 3 July 09 h.

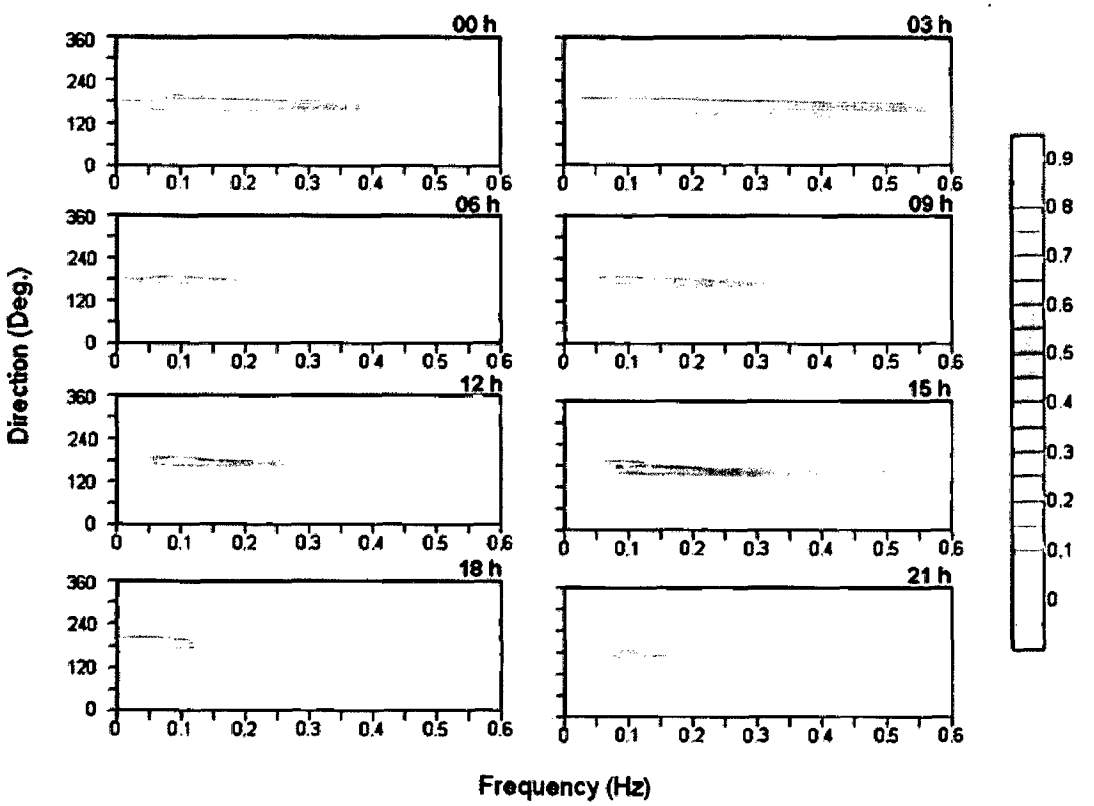

Figure 4-4. Measured directional energy spectra from 00 h to 21 h (for every 3 h) on 26 July 1996.

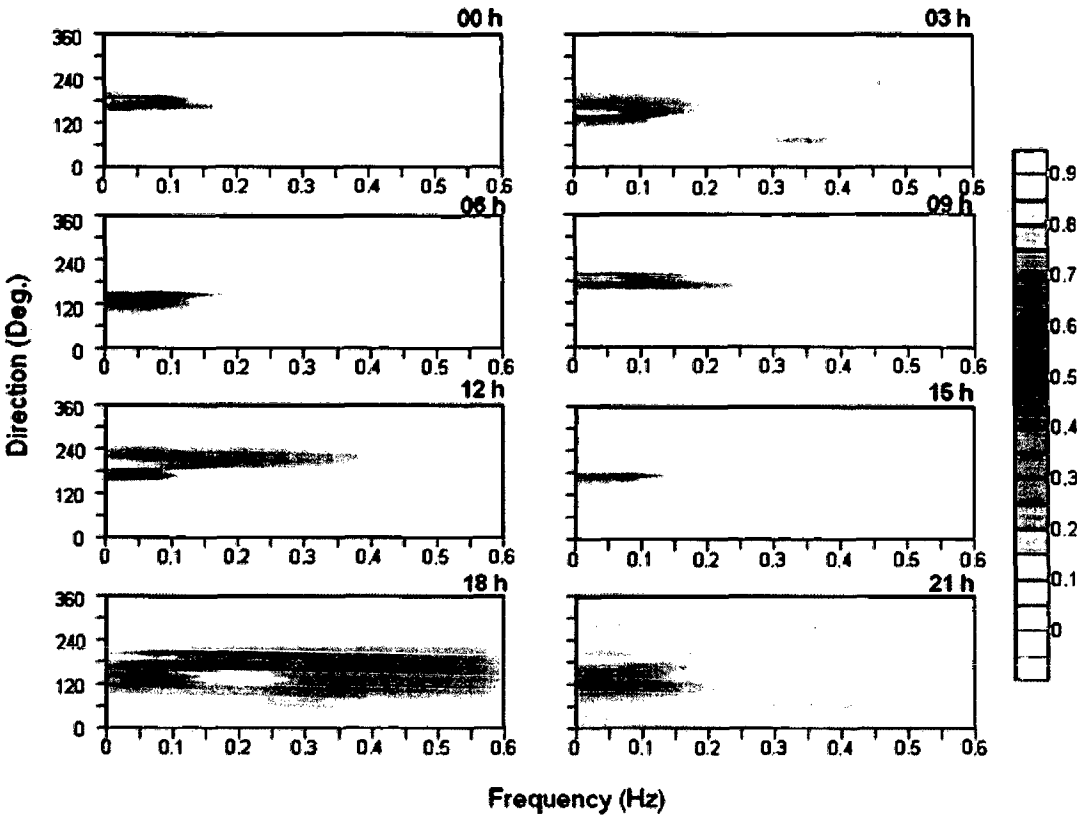

Figure 4-5. Measured directional energy spectra from 00 h to 21 h (for every 3 h) on 15 November 1996.

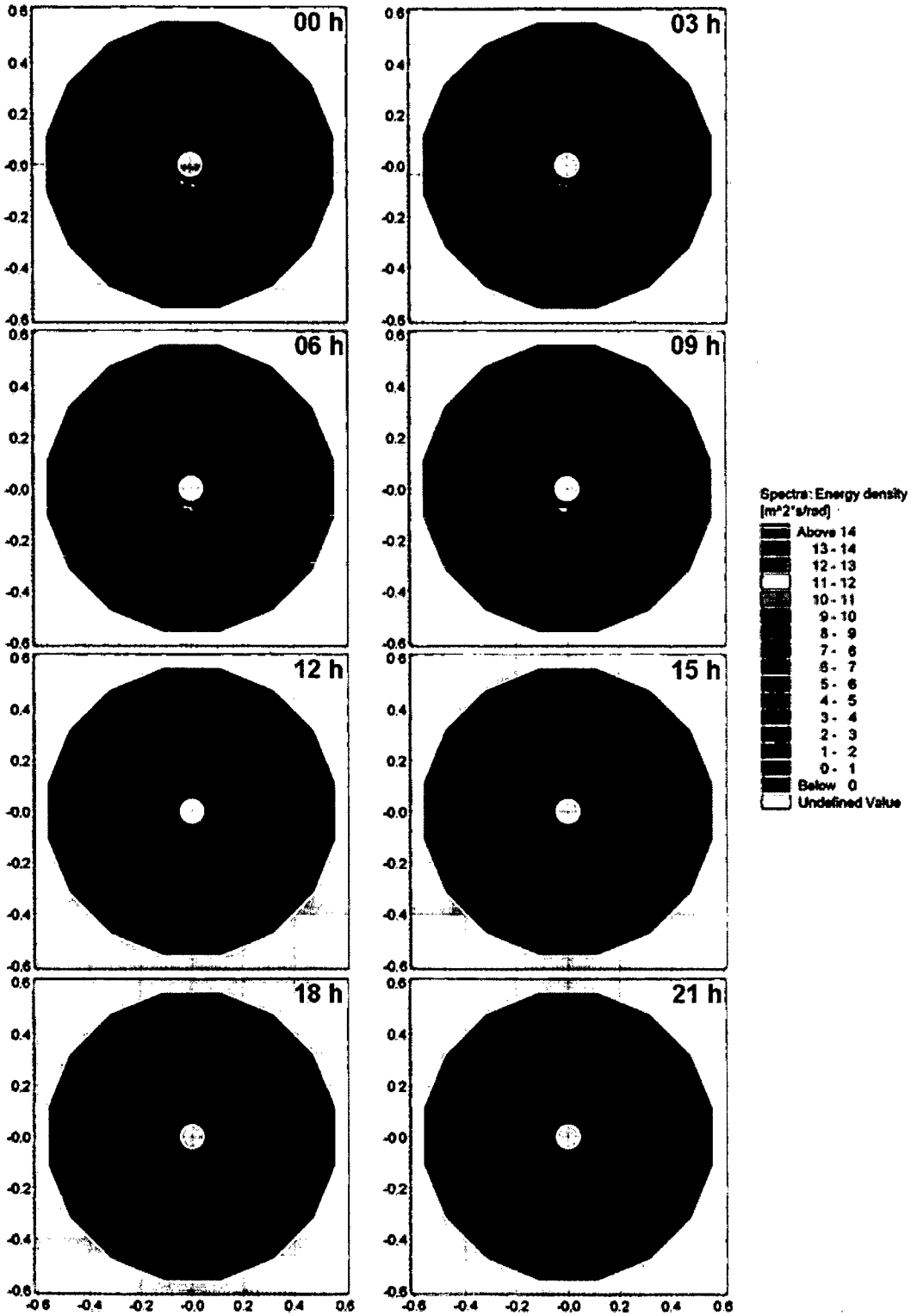

Figure 4-6. Modelled directional energy spectra on 26 July for every 3 h simulations (from 00 h to 21 h).

4.2.2. *Along the west coast of India*

The analysis shows that the wave energy spectra, in general, consist of two/multiple energy peaks - one in the low frequency region (associated with swell) and the other(s) in the high frequency region (associated with seas) indicating the presence of two or more distinct wave systems prevailing in the region. The frequency range of primary and secondary peaks in the spectra varies according to the dominance of different wave systems. During extreme events, the spectra are primarily single-peaked.

The distribution of significant wave height (H_s), mean wave period (T_m) and mean wave direction (θ) of wave, swell and sea for the period February 1996 to May 1997 is shown in Figure 4-7. The maximum H_s observed is 5.85 m and the corresponding T_m is 9.1 s. The maximum swell H_s is 5.53 m and T_m=11.3 s. The maximum wind sea H_s and corresponding T_m are 2.3 m and 4.8 s, respectively. The waves are predominantly from SW, WSW and NW directions. Major part of the swells are from SW, NW and WSW directions with 27%, 23% and 20%, respectively, which constitute 70% of the total swells, whereas, wind seas are distributed over NW, W and WNW directions with 41%, 20% and 16%, respectively, which constitute 77% of the total seas. We find that waves during June – September (SW monsoon season), primarily follow the swell pattern as waves generated in the Arabian Sea/southern Indian Ocean by the strong SW monsoon winds propagate towards the Goa coastal region as swells. During pre-monsoon and NE monsoon seasons, waves follow either swell or wind sea pattern depending on their dominance.

Monthly variations in significant wave height (H_s) and mean wave period (T_m) for the swell and wind sea are presented in Table 4-1. The maximum swell and sea H_s are observed in June, and minimum in December. Larger waves associated with wind seas during January to April, November and December, indicate the influence of local winds on wind sea generation. Long-period swells (T_m > 12 s) are observed during March to May, September, November and December, and these are the swells propagated from higher latitudes (south Indian Ocean). Mean periods of wind seas are generally above 2 s, whereas, those of swells are above 5 s. The observed maximum mean periods are 6.2 s (September) and 13.8 s (December) for wind sea and swell, respectively.

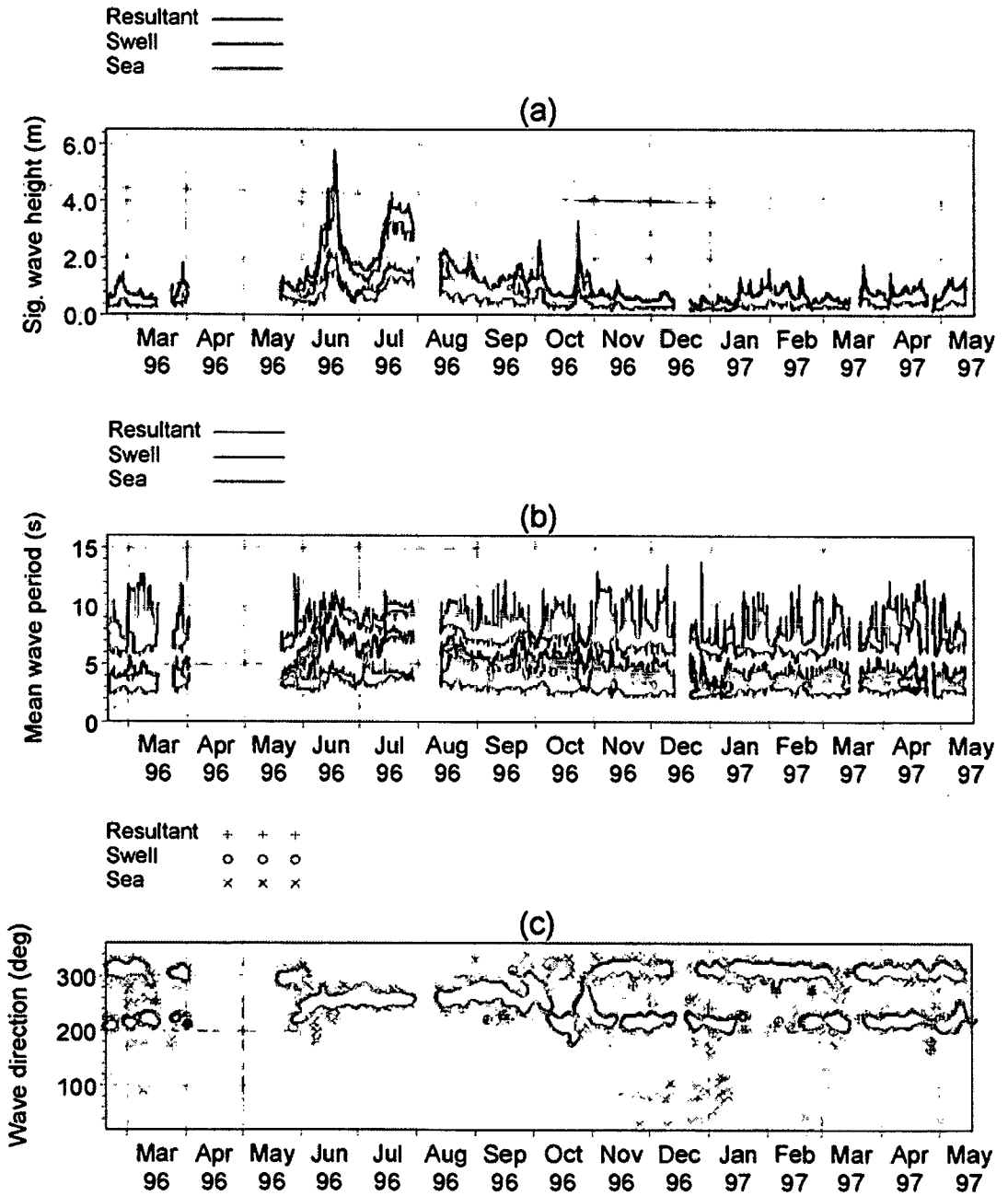

Figure 4-7. Distribution of (a) significant wave height, (b) mean wave period and (c) mean wave direction for the resultant wave, swell and wind sea during February 1996 to May 1997.

Table 4-1. Monthly variations of H_s and T_m for the swell and sea.

Parameters	Significant wave height (m)		Mean wave period (s)	
Month	Swell	Sea	Swell	Sea
January	0.16 - 1.10	0.13 - 1.56	5.3 - 11.3	2.0 - 4.9
February	0.16 - 0.94	0.16 - 1.27	5.1 - 11.9	2.1 - 4.9
March	0.20 - 1.50	0.19 - 1.50	5.6 - 12.7	2.1 - 5.1
April	0.13 - 0.97	0.10 - 1.27	5.7 - 12.3	2.1 - 4.9
May	0.28 - 1.13	0.20 - 1.10	6.0 - 12.7	2.1 - 5.1
June	0.75 - 5.53	0.31 - 2.30	7.3 - 11.3	2.5 - 5.6
July	1.04 - 3.87	0.44 - 1.81	7.5 - 11.3	2.9 - 5.4
August	0.53 - 2.18	0.37 - 1.74	6.7 - 11.0	2.6 - 6.1
September	0.18 - 1.77	0.28 - 1.28	6.3 - 12.2	2.3 – 6.2
October	0.33 - 3.22	0.15 - 1.50	5.8 - 11.5	2.2 - 6.1
November	0.21 - 0.87	0.11 - 0.88	5.5 - 13.0	2.1 - 5.0
December	0.16 - 0.76	0.11 - 0.80	5.4 - 13.8	2.0 - 5.7

In addition to the observations by Kumar and Anand (2004), inferences are made on the seasonal scenario of the nearshore wave characteristics. The mean period of the waves during SW monsoon is generally above 5 s, and it is below 5 s during pre-monsoon and NE monsoon seasons (Figure 4-7). Lower wave periods during pre-monsoon and NE monsoon seasons indicate superimposition of local wind seas with the pre-existing swells. Such effects are relatively less during SW monsoon, and hence waves follow the swell pattern. Figure 4-8 shows typical directional wave energy spectra and wind roses off Goa during pre-monsoon, SW monsoon and NE monsoon seasons. The predominant winds are from

NW, NNW and N directions during pre-monsoon season, from WSW, W and WNW directions during SW monsoon season (swells are mainly from W/WSW) and from NNW and E directions during NE monsoon season. However, swells are mainly from SW /SSW direction (and also from NW), and the predominant wind seas are from NW direction (this is attributed to the local sea breeze, which is absent in the coarse resolution NCEP winds) during pre-monsoon and NE monsoon seasons. Occasionally, low period (and low energy) wind seas from NE and ENE are also present during NE monsoon season.

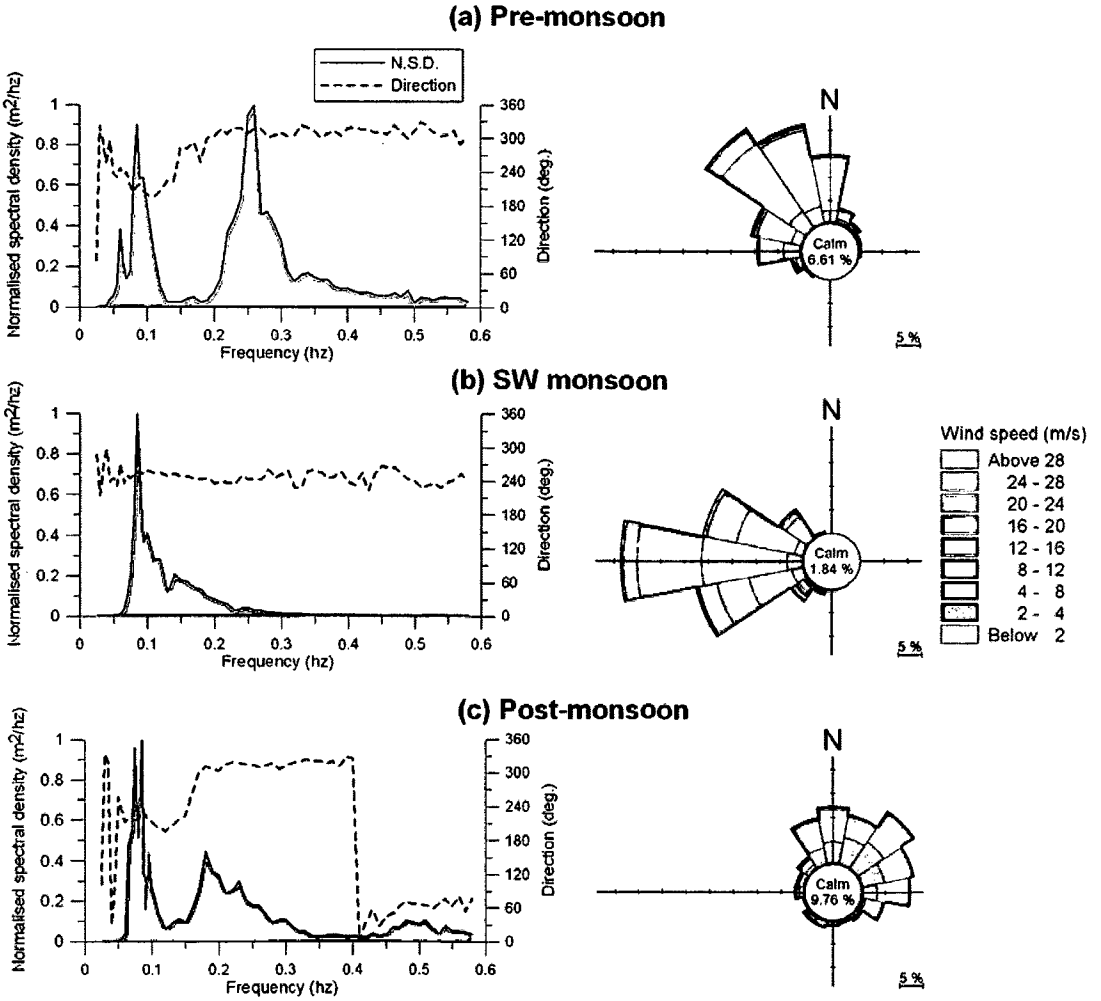

Figure 4-8. Typical directional wave energy spectra and wind rose during (a) pre-monsoon, (b) SW monsoon and (c) NE monsoon seasons.

Joint Typhoon Warning Center (JTWC) reported two extreme events (15 -25 June 1996 and 14 October – 2 November 1996) in the Arabian Sea in 1996. These are subtropical storms of Category 1 with maximum wind speed of 34 m/s. The first storm developed at an

offshore location off Goa; it moved towards north, and changed its direction towards west, and finally hit the Gujarat coast after 3 days. The maximum intensity of the storm was on 19 June 1996, and weakened while travelling further towards the subcontinent. The second storm developed in the Bay of Bengal, moved across the subcontinent towards west and crossed the region between Goa and Mangalore. The maximum speed was observed off Ratnagiri (approx. 200 km north of Goa) on 23 October 1996.

NCEP winds show that wind speeds in the Arabian Sea are of the order of 20 – 34 m/s during the tropical storms (i) 15 -25 June 1996 and (ii) 14 October – 2 November 1996). During evolution of the storms, a gradual increase in wave height is observed along with an increase in wave period (Figure 4-7). Following the peak intensity of the event, maximum H_s of 5.85 m and 3.32 m and maximum T_m of 9.1 s and 6.8 s were observed for the storms (i) and (ii), respectively. The swell H_s are nearly the same as that of waves and the waves follow the pattern of swells. The correlation coefficient between swell H_s and resultant H_s is 0.99, whereas, correlation coefficient between wind sea and resultant swell H_s during both the storm events is 0.87 . Since storm-1 is associated with SW monsoon, the propagation direction of the waves remained the same (SW). Prior to storm-2, the predominant wave direction was W. However, with the evolution of the storm, the wave direction had changed to SSW, and further to SW, following a sudden shift in the cyclone track.

Measured and modelled significant wave heights show very good match during the tropical storm events. For storm-1, the correlation coefficients between measurements and modelling for resultant H_s, swell H_s, and wind sea H_s are 0.93, 0.79 and 0.74, respectively, whereas they are 0.80, 0.74 and 0.7, respectively for storm-2. The swells of storm-1 resemble the same pattern (in terms of propagation direction) of the SW monsoon swells; swells of storm-2 are in different directions (mainly SSW and SW). Off Goa (in deep waters), the significant swell height reached above 6.5 m (Figure 4-9) and mean swell period were 11 -13 s during storm-1. The wave reaches a maximum H_s of 7.9 m at an offshore location off Ratnagiri during storm-1 and 3.6 m off Mumbai during storm-2.

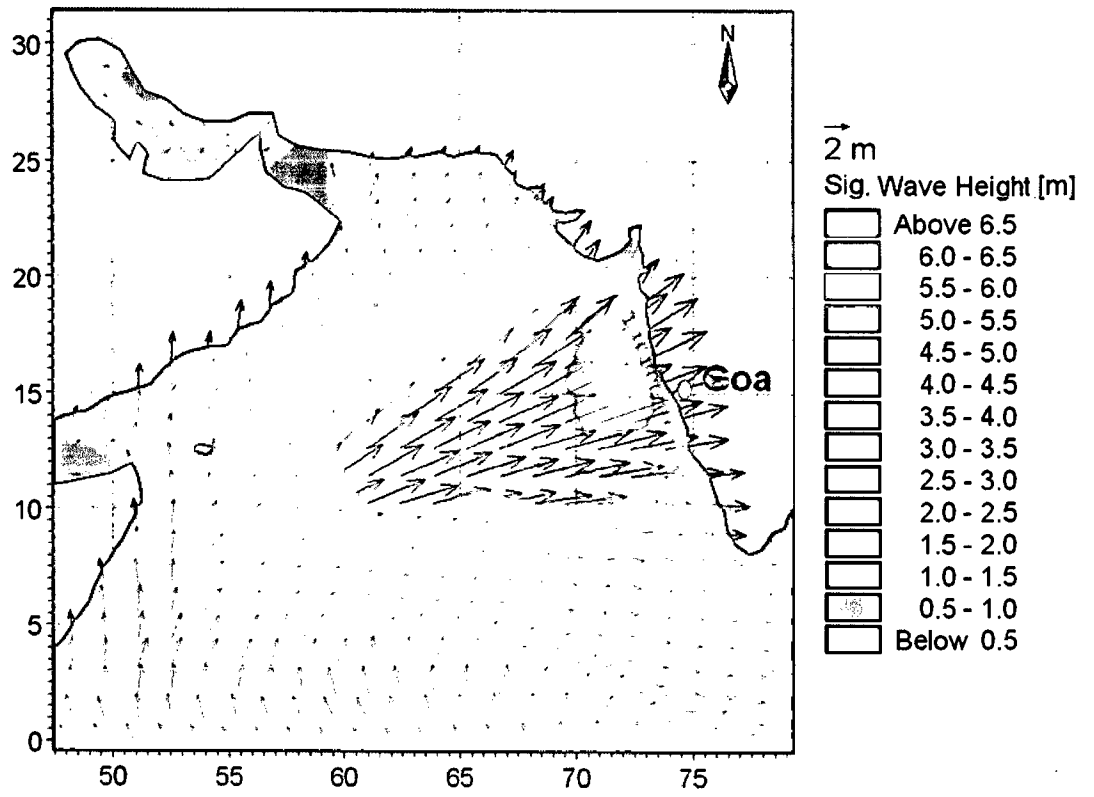

Figure 4-9. Swell patterns during a tropical storm in the Arabian Sea.

4.3. Dominance of swells along the west coast of India

Dominance of wind seas and swells were analysed based on the measured wave data off Goa during Feb 1996 – May 1997. For this purpose, wind sea and swell parameters were calculated from the measured wave energy spectra and analysed.

Monthly dominance of swell and wind sea is presented in Table 4-2. Swells are predominant (above 50 %) during March to December, and wind seas are predominant during January and February. Even though, swells are predominant during March to May, November and December, the role of wind seas is significant (the percentage dominance of wind seas is above 30 % during the above months). Hence, the influence of wind seas along the west coast of India during pre-monsoon and NE monsoon seasons is highly remarkable. During June to July, the waves are fully dominated by swells due to the effect of strong SW monsoon winds. Dominance of wind sea is maximum during February (63 %). Annually, around 70% of the waves are swell dominated. Swells are predominant during SW monsoon and NE monsoon seasons (93 % and 67 %, respectively), whereas, wind seas are predominant during pre-monsoon season (51 %). The dominance of wind

seas during pre-monsoon season is primarily due to prevailing sea breeze along the west coast of India. Numerical experiments could be done for understanding the interaction of wind seas with pre-existing swells, but it requires fine resolution coastal winds.

Figure 4-10 shows the scatter of resultant H_s against swell H_s and wind sea H_s during pre-monsoon, SW monsoon and NE monsoon seasons. The correlation coefficient between wind sea H_s and resultant H_s during pre-monsoon season is 0.85; whereas, it is 0.79 between swell H_s and resultant H_s. The correlation coefficient between swell H_s and resultant H_s during SW monsoon is 0.99, whereas it is 0.83 between wind sea H_s and resultant H_s. Even though the wind seas contributed sufficiently to the wave, swell contribution exceeds that of seas due to the arrival of SW monsoon swells. The correlation coefficients for swell H_s and wind sea H_s with resultant H_s during NE monsoon season are 0.93 and 0.82, respectively. The swell contribution is higher than that of wind sea, and hence it follows mostly the same pattern of swell during the NE monsoon season. It has been noted that irrespective of seasons, the correlation coefficient between the wind seas and wave is 0.82 to 0.85, and this indicates that wind seas are consistent in all seasons. However, the swell contribution varies from season to season.

Figure 4-11a shows the locations of NCEP winds extracted in the Arabian Sea and Figure 4-11b shows wind speed and direction off Goa (at W1) during February 1996 – May 1997. The selected locations are at 72.5° E, 15° N (W1); 65° E, 12.5° N (W2) and 55° E and 5° N (W3). The NCEP winds at W1 during February 1996 – May 1997 have been used to analyse the correlation with wave parameters. At W1, Wind direction varies according to seasons - between west-southwest (WSW) and north (N) during pre-monsoon, between northwest (NW) and east (E) during NE monsoon and between SW and NW during SW monsoon. We find that wind sea direction matches very well with the wind direction in all seasons, except when winds from NE and E are present. Since the measurement location is close to the coast, these winds can contribute only to the wave generation towards offshore (away from measurement location). Hence, wind seas from NE and E are not present at the measurement location. However, these winds (NE/E) could have influenced on the generation and propagation of swells towards the southwestern Arabian Sea.

Table 4-2. Monthly percentage dominance of swell and sea.

Month	Swell dominance (%)	Sea dominance (%)
January	48.5	51.5
February	36.8	63.2
March	55.7	44.3
April	50.5	49.5
May	52.9	47.1
June	99.6	0.4
July	100.0	0.0
August	87.0	13.0
September	85.7	14.3
October	87.9	12.1
November	60.0	40.0
December	69.6	30.4

Figure 4-12 produces scatter diagrams of (i) wind speed against wind sea H_s and (ii) wind direction against wind sea direction. Wind speed gives good linear fit with wind sea H_s and a correlation coefficient of 0.72 is obtained between wind speed and wind sea H_s (Figure 4-12a), which indicates that major part of the local wind contribution to the wind sea generation off the Goa coast has been captured in the NCEP winds. A very good match is obtained between wind and wind sea directions, except when land breeze from N and NE dominates - indicating the influence of local winds on wind sea generation. There exist two distinct wind directions: (i) between SW and N and (ii) between N and E. Major part of wind seas is between SW and N. Though there exists wind between N and E, wind seas from these directions are not present (winds are from land to sea and wave rider buoy was

deployed very close to the coast). It may be noted that NE monsoon winds are not very active over this part of the coast. Hence, low energy waves generated due to NE winds are only present during NE monsoon season. Detailed investigation on the local wind sea contribution to the wind sea generation in the coastal regions demands the use of fine resolution (both temporal and spatial) wind fields, which are not available during the measurement period.

Figure 4-12b shows that there exist wind seas in the NW direction, when there was no NW winds (as seen in NCEP winds), and this may be due to sea breeze, which is hardly captured in NCEP because of its coarse spatial resolution. The offshore extension of the local winds controls the wind sea generation mechanism along the west coast of India. The winds during pre-monsoon season along the west coast of India are dominated by sea breeze. According to Aparna et al. (2005), the seaward extension of the sea breeze is 180 km off Goa during February – April. The selected NCEP grid (close to the coast) covers the entire limit of the sea breeze extension. Neetu et al., (2006) observed that the peak sea breeze speed at Goa coast during pre-monsoon season is 5 m/s and sea breeze generated wind seas have considerable amount of energy in the wave spectra. Masselink and Pattiaratchi (1998) observed that sea breeze typically produces a 1 – 1.5 m high wave with periods ranging between 6 and 9 s.

Figure 4-13 shows the scatter between swell H_s and wind sea H_s during pre-monsoon, SW monsoon and NE monsoon seasons. The correlation coefficients between swell H_s and wind sea H_s are 0.36, 0.74 and 0.56 during pre-monsoon, SW monsoon and NE monsoon seasons, respectively. It is evident that during SW monsoon season, the wind sea also follows the same pattern of the swell (Figure 4-7); however, the energy associated with swells is much higher than that of wind seas. Major part of the swells during pre-monsoon season is propagating far from the southern Indian Ocean in the SW direction, and occasionally from northern Arabian Sea in NW direction. However, the local wind seas are mainly from NW direction. The swells are generally weak during pre-monsoon and NE monsoon seasons. It may be noted that sea breeze is very active during pre-monsoon season. Hence, the weakening of distant swells together with effect of sea breeze on wind sea generation results in the dominance of wind seas along the west coast of India during pre-monsoon season. The moderate correlation during NE monsoon season indicates that even though there exist long period swells propagating from the southern Indian Ocean, there are swells from other areas (swells propagating from NW) in which the directions of swells and wind seas coincide. Hence, there exist multi-directional swells and local wind

seas concurrently. The dynamics associated with the interaction between the multi-directional swells and the superimposition of these swells with the local wind seas is to be investigated in detail.

Waves along the entire west coast of India follow the same distribution in all seasons to a large extent (Figure 4-14). Since Goa is in the central west coast, measurements from this region are taken as representative data for the entire west coast for validation: modelled wave parameters match very closely with measurements. Hence, modelled wave parameters at various other locations along the west coast of India have been extracted and analysed for their distributions. Figure 4-14 shows the modelled significant wave heights at 25m depths off Kochi, Mangalore, Goa, Ratnagiri and Mumbai during pre-monsoon, SW monsoon and NE monsoon seasons. It has been found that the significant wave heights follow nearly the same pattern at all locations in any season though there are time lags due to arrival times of the swells. Hence, it is concluded that swell dominates during SW monsoon and NE monsoon seasons and wind sea dominates during pre-monsoon season at all locations along the west coast of India and their distribution (swell and wind sea) is relatively the same at all locations as observed in the Goa region.

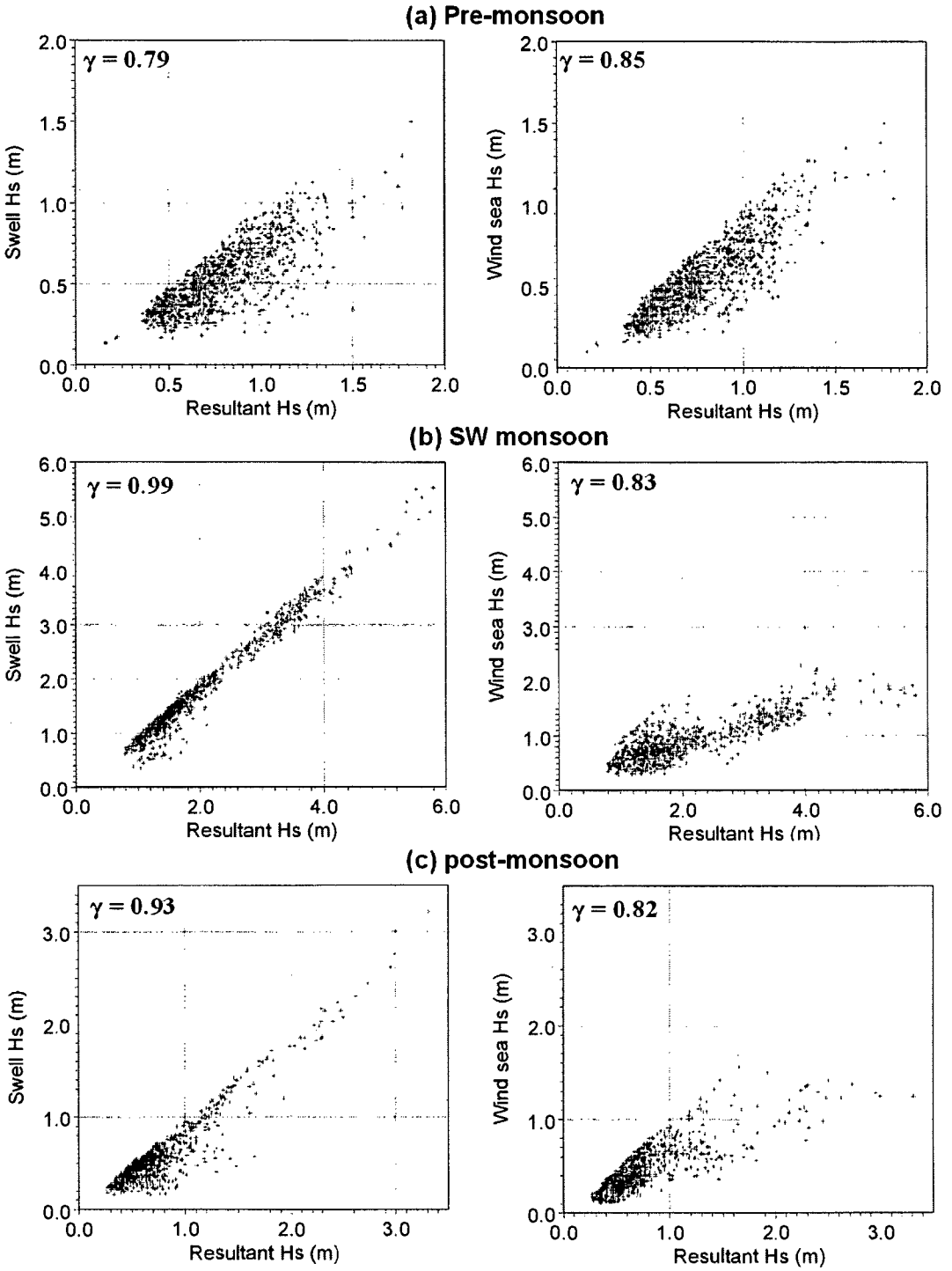

Figure 4-10. Scatter diagrams of resultant H_s vs. swell H_s and resultant H_s vs. wind sea H_s during (a) pre-monsoon, (b) SW monsoon and (c) NE monsoon seasons.

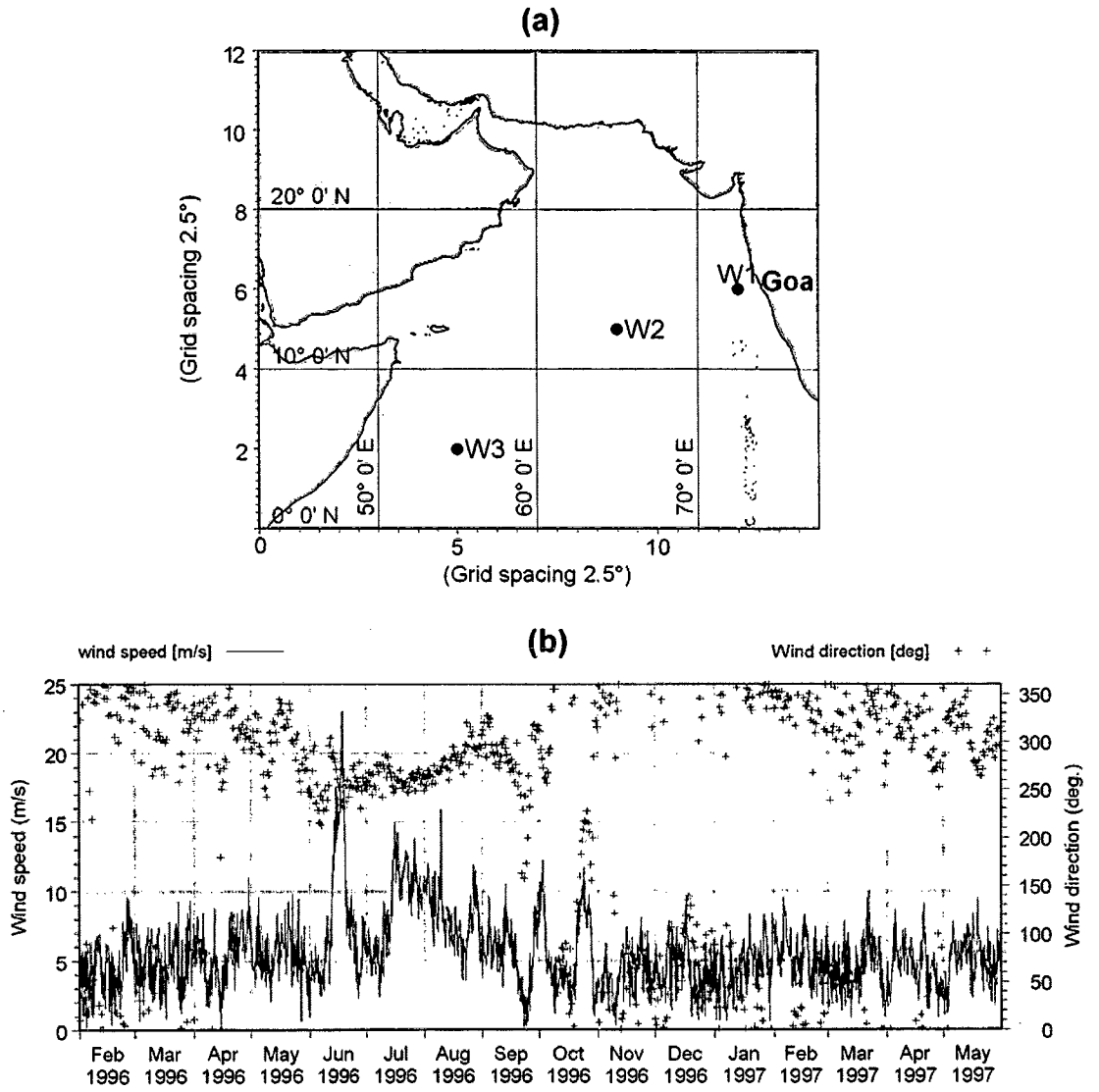

Figure 4-11. (a) Locations of NCEP wind extracted and (b) wind speed and direction at W1 (off Goa) during Feb 1996 to May 1997.

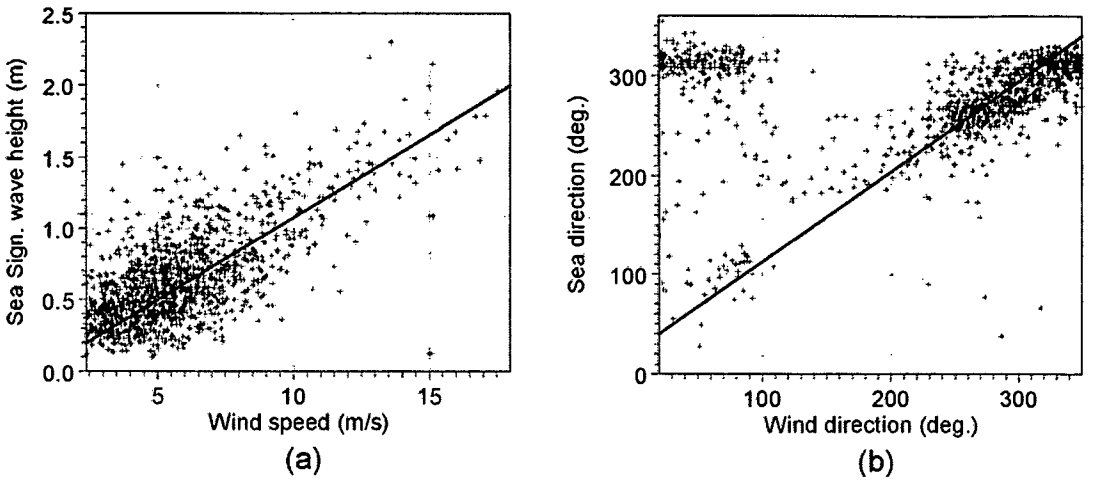

Figure 4-12. Scatter diagrams (a) wind speed vs. wind sea H_s and (b) wind direction vs. wind sea direction.

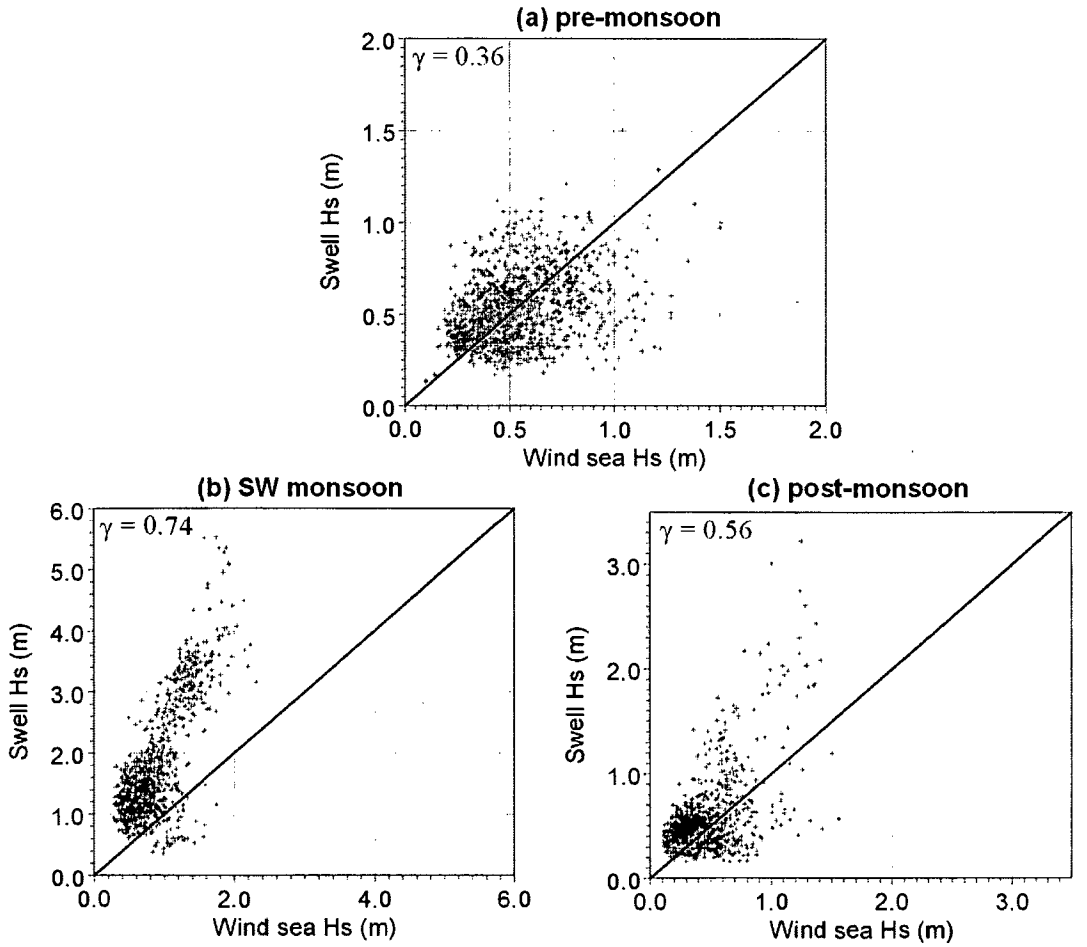

Figure 4-13. Scatter diagram of significant wave heights showing the dominance of wind sea and swell during (a) pre-monsoon, (b) SW monsoon and (c) NE monsoon seasons.

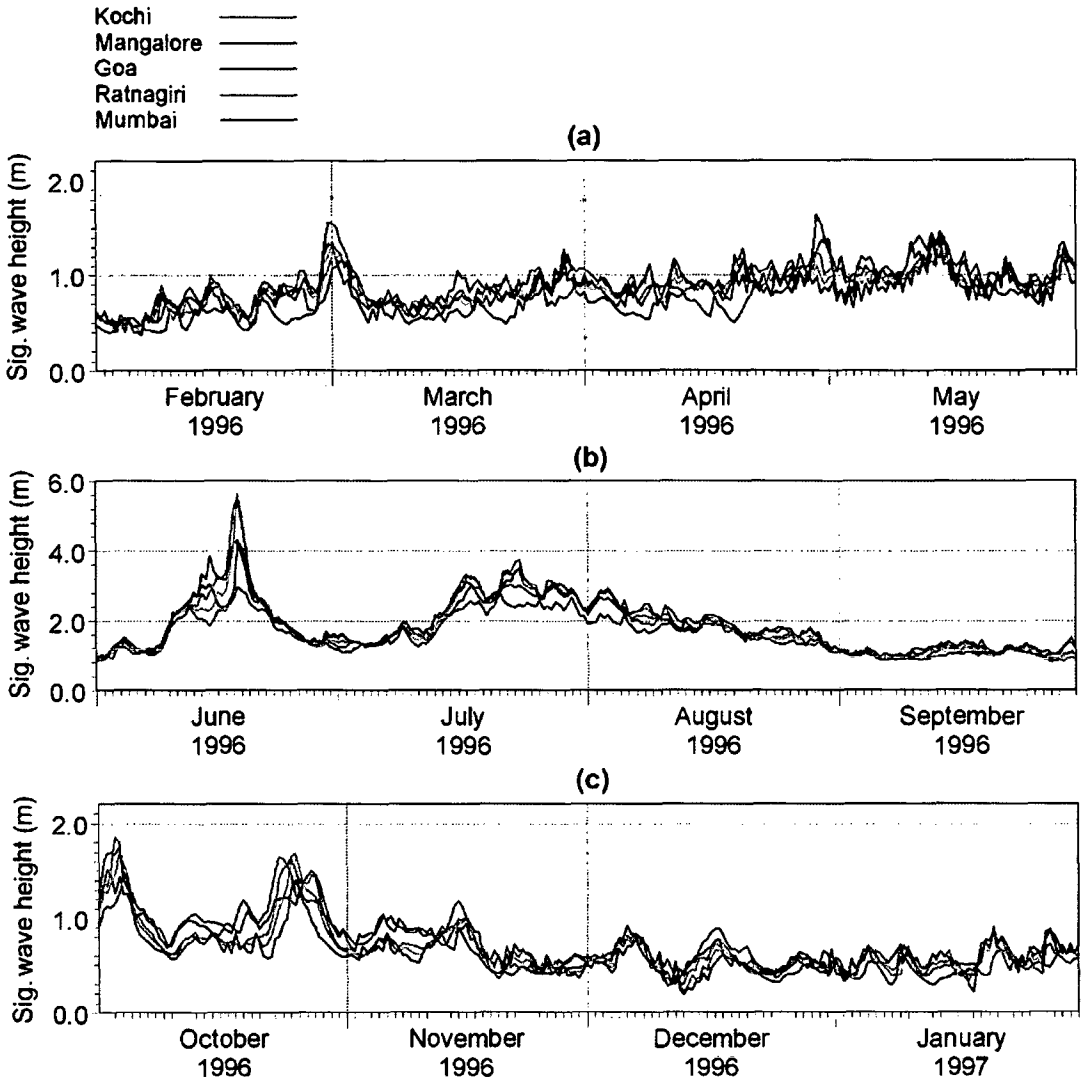

Figure 4-14. Significant wave heights off Kochi, Mangalore, Goa, Ratnagiri and Mumbai during (a) pre-monsoon, (b) SW monsoon and (c) NE monsoon seasons.

4.4. Potential swell generation regions

In this section, winds over the Indian Ocean have been analysed to identify potential areas which generate the swells that influence the west coast of India. These potential swell generation areas have been identified and confirmed through numerical modelling. Propagation of these swells to the west coast of India has been discussed below.

4.4.1. Wave observations

In order to identify potential swell originating areas, NCEP winds at 3 cells, namely, W1, W2 and W3 (Figure 4-11a) have been analysed. During SW monsoon season, wind direction at W3 is predominantly between SW and WSW, at W2, between SW and W with dominating WSW direction and at W1, between SW and NW with dominating W direction. Winds in the south Indian Ocean, say around 20° S, are predominantly in SE direction during SW monsoon season, which generate swells in SE direction. Below 40° S, winds from W are predominant and SW/SSW winds are rarely occur during SW monsoon season, hence SW/SSW swells from these areas are relatively weak as compared to those generated in the north Indian Ocean. Wave measurements show that swells off Goa are predominantly between WSW and W with dominating WSW direction during June – Sept. This indicates that the potential swell generating area during SW monsoon season is between W3 and W2, probably around 60° E, 10° N. The mean swell periods are predominantly 8 to 10 s during June – July, and 7 to 9 s during August – September, which also shows that the swell generating area during the second half of the season are relatively closer to the Goa coast, since these swells are generated over a relatively small fetch.

During pre-monsoon season, winds at W3 (Figure 4-11a) are predominantly between NNE and E in February – April and between SW and WNW in May; at W2, between N and NE in February – March and between W and NE in April – May, and at W1, between W and N with dominant NW direction. Two distinct swells from SW or SSW and NW were observed off Goa during pre-monsoon season. The mean swell periods associated with SW or SSW swells are predominantly 8 to 11 s, whereas, those associated with NW swells are 6 to 8 s. The swells generated by the winds from N, NE and E could not reach the west coast. Hence, swells generated by winds from SW or SSW and NW could impact well. The observed longer period waves also indicate that these swells are generated at an area, probably around 40° S, where large fetch is available for stronger SW or SSW winds with relatively longer duration. It has been found that NW winds are present throughout the season at location W1. Whenever NW winds dominate over the northern Arabian Sea, the generated swells propagate to the Goa coast with relatively low periods (6 to 8 s), since the generation area is relatively close to the measurement location. The potential generation area for NW swells is probably around 65° E, 20° N.

During NE monsoon season, winds at W3 and W2 are predominantly between N and E and at W1, between NW and E. Similar to the observations during pre-monsoon season, there are two distinct swells; SW or SSW and NW swells. The mean periods associated with SW

swells are 8 to 12 s, whereas those associated with NW swells are 6 to 8 s. The long-period SW or SSW swells are generated in the south Indian Ocean, whereas NW swells are generated in the northern Arabian Sea, as observed during pre-monsoon season.

4.4.2. Numerical model results

Wave simulation has been carried out during Feb 1996 – May 1997 (for the same measurement period) using NCEP winds. Swell patterns in the Indian Ocean obtained from the simulations have been analysed. Figure 4-15 shows the typical swell patterns in the Arabian Sea during pre-monsoon and NE monsoon seasons. The simulations indicate that the predominant swells off the west coast of India are from SW or SSW and NW directions during pre-monsoon and NE monsoon seasons. There are various swell systems (other than SW or SSW and NW) in the Arabian Sea during pre-monsoon and NE monsoon seasons which may not propagate towards the west coast as the propagation direction is away from the west coast. NW swells are stronger during pre-monsoon season, as compared to those during NE monsoon season. During SW monsoon season, the predominant swell in the Arabian Sea is from SW and WSW due to the prevailing winds in the same directions. It does have high impact on the nearshore regions off the west coast of India (significant swell heights reach above 4.0 m in the Arabian Sea). The significant swell heights are generally below 2.0m in the Arabian Sea during pre-monsoon and NE monsoon seasons.

The potential swell areas are identified from the simulated swells in the Indian Ocean. It has been found that the SW and SSW swells generated in the area covered by 40° E to 70° E and 30° S to 50° S propagate towards the west coast as long-period swells during pre-monsoon and NE monsoon seasons. However, these swells are relatively weak as compared to those generated in the Arabian Sea during SW monsoon season. Hence, the predominant swells during SW monsoon season are generated in the area covered by 52.5° E to 62.5° E and 5° N to 15° N. During pre-monsoon season, apart from SW swells from southern Indian Ocean, NW swells from northern Arabian Sea have been also found, which are propagating towards the Goa coast. It has been found that these swells are generated in the area bounded by 60° E to 67.5° E and 17.5° N to 25° N. It is evident from wave measurements that wind sea energy dominates over swell energy during pre-monsoon season.

During NE monsoon season, the distant swells play major role in the dominance of swells along the west coast of India. It is clear from Figure 4-15 that the swell patterns in the south Indian Ocean during pre- and NE monsoon seasons are basically the same. However, they

could be distinguished by the influence of NE winds over the north Indian Ocean during NE monsoon season. As explained elsewhere, NE winds cannot generate swells along the west coast of India due to fetch limitation. Majority of the swells during NE monsoon season are generated in the south Indian Ocean, especially in the area bounded by 40° E to 70° E and 30° S to 50° S. Wind sea energies during NE monsoon season are relatively weaker compared to pre-monsoon season. Hence, a well-defined swell dominance has been obtained along the west coast of India during NE monsoon season.

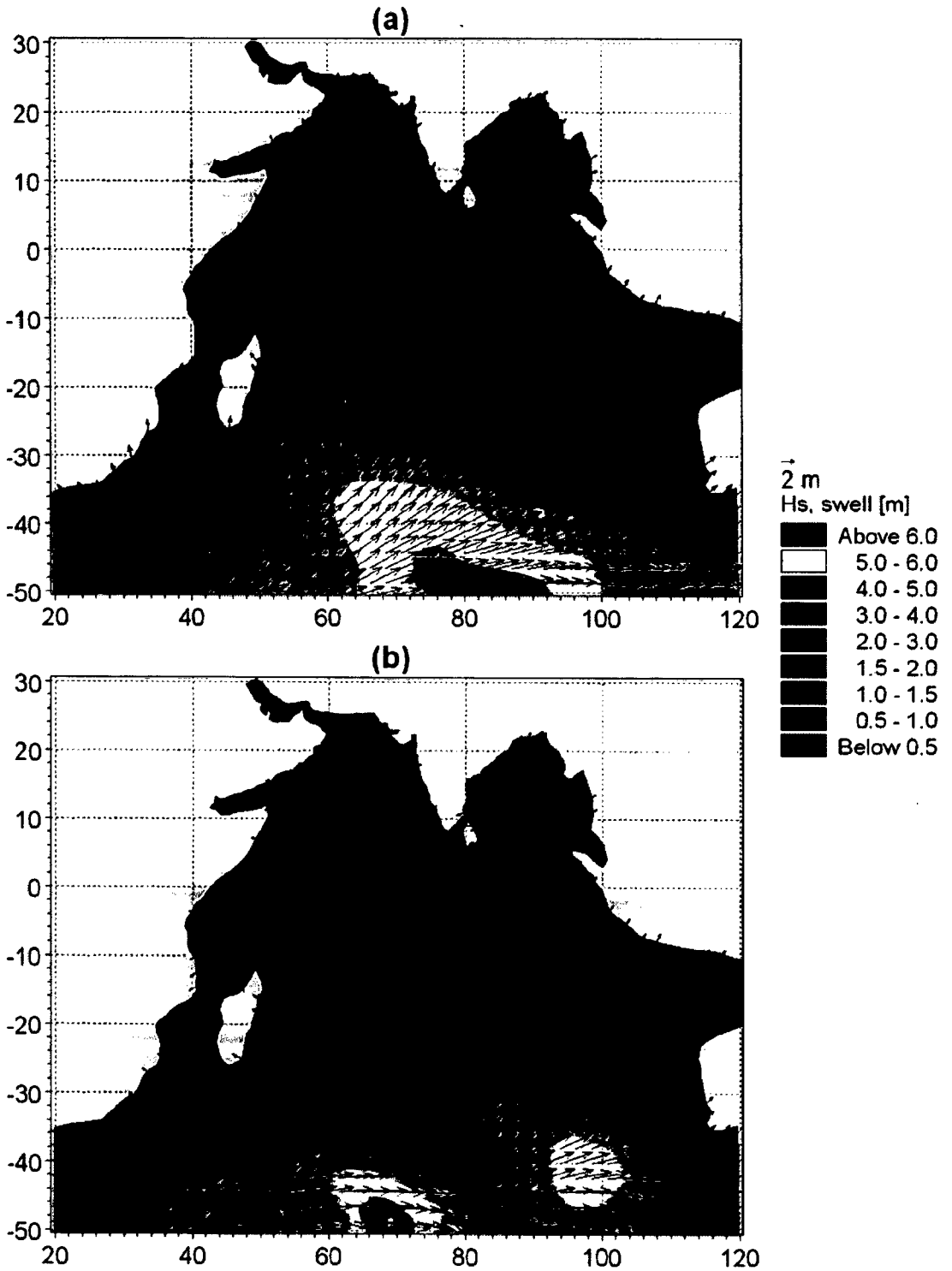

Figure 4-15. Typical swell patterns in the Arabian Sea during (a) pre-monsoon season (12 April 1997) and (b) NE monsoon season (10 December 1996).

4.5. "Shamal" swells in the Arabian Sea

4.5.1. Introduction

Shamal winds are meteorological events associated with winds, which normally occurs in the Arabian Peninsula, especially during the winter season. The word "Shamal" literally means "north" (in Arabic literature) and the winds during Shamal events are named as Shamal winds. Onset, duration and strength of the Shamal winds in winter or summer vary according to the dynamic interaction of the upper air jet streams and the distribution of lower tropospheric pressure zones (Ali, 1994). The summer Shamal events are not very common and the intensity is relatively low. However, the winter Shamal events have high impact on the meteorological conditions over the Arabian Peninsula. The winter Shamal occurs during November to March and is associated with mid-latitude disturbances travelling from west to east (Hubert et al., 1983). It usually occurs following the passage of cold fronts and is characterized by strong northwesterly winds. Based on the intensity, the periodicities are classified as follows: (i) 24 to 36 hours and (ii) 3 to 5 days. The associated wind speeds during the events are higher, of the order of 20 m/s. It can generate surface waves as high as 3.0 – 4.0 m in the Persian Gulf (Arabian Gulf).

Studies on the wave characteristics and storm surges due to Shamal winds are very limited and restricted to the Arabian/Persian Gulf region only (e.g., El-Sabh, 1989 and Parvaresh et al., 2005). Impacts of Shamal events on the Arabian Sea or along the west coast of India are not studied so far. It could have significant role on the meteorological and oceanographic conditions of the Arabian Sea. Rapid changes in wind patterns during the Shamal events can alter the associated wave characteristics in the Arabian Sea. This motivated us to take up the present study with the following objectives: (i) generation and propagation of "Shamal" swells in the Arabian Sea, and (ii) influence of "Shamal" swells on the wave characteristics along the west coast of India. Figure 4-16 shows the study area and wave measurement locations (B1, B4 and B6).

The general swell patterns in the Arabian Sea are known from the literatures (e.g., Sanil Kumar et al. 2000; Rajkumar et al., 2009 and Kurian et al., 2009). The predominant swells are from the SW or S directions, propagating from the south Indian Ocean. On several occasions we have observed weaker swells propagating from the northwest.

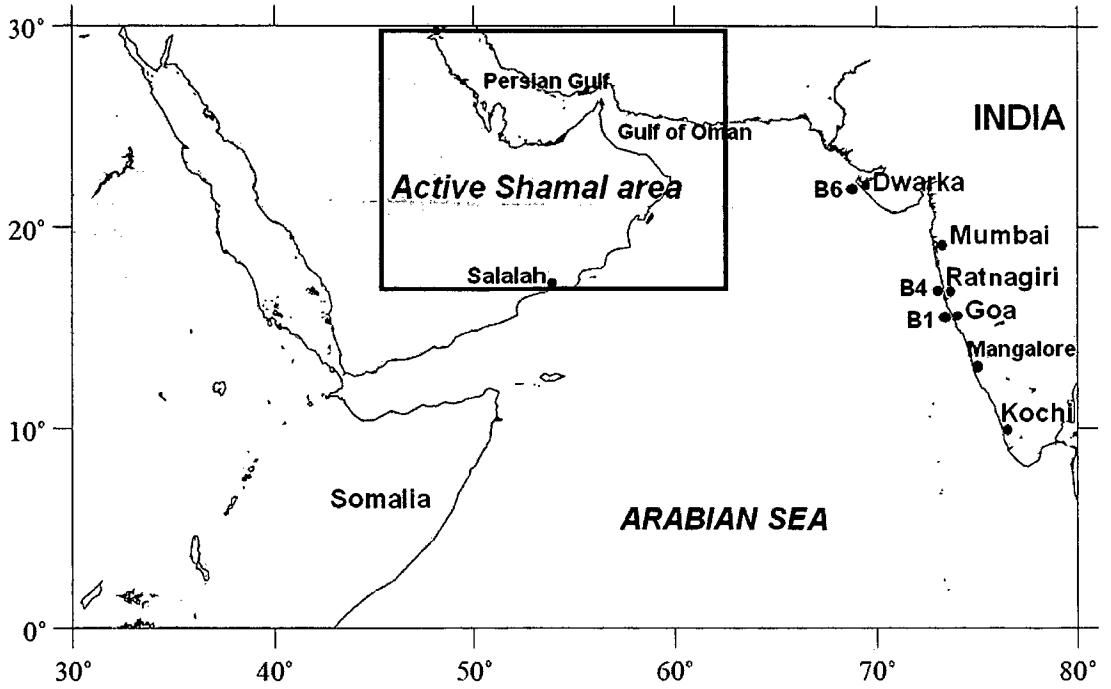

Figure 4-16. Study area and measurement locations.

4.5.2. Characteristics of "Shamal" swells

Measured waves off Ratnagiri show systematic variations in the wave parameters during several occasions (Figure 4-17). During NE monsoon and early pre-monsoon seasons, nearshore waves along the west coast of India are generally low (say, < 1.0 m). However, in 2008 waves with significant wave heights of the order of 1.0 - 2.0 m were observed at several occasions. Further analysis shows that wave parameters exhibit distinct characteristics: increase in wave heights associated with decrease in swell period and a common propagation direction (NW) for wind sea, swell and waves (Figure 4-17a, 4-17b and 4-17c). Measured winds at Ratnagiri coast also show systematic variations during the above periods (Figure 4-17d). The systematic features observed in the wind and wave parameters are indicated as (1) to (6), during which the significant wave heights are in the range 1.0 to 2.0 m, mean swell periods between 6.0 and 8.0 s and predominant wind and wave directions in NW.

The directional energy spectra show peak energies in the swell region, and most of the energies are concentrated between the frequencies 0.1 and 0.2 Hz in the NW direction, contrary to the normal swell conditions along the west coast of India, wherein energy is distributed between 0.05 and 0.15 Hz in the direction SW or S (e.g., Vethamony et al.,

2009). Typical directional energy spectra measured off Ratnagiri during Shamal period and non-Shamal period are shown in Figure 4-18a and 4-18b. Swells from the south Indian Ocean (S or SW direction) are generally observed along the west coast of India, which are mostly "old swells". However, NW swells generated at the northern Arabian Sea can propagate to the west coast within relatively shorter duration, and that is the reason for observing mostly "young" or "matured" swells from the NW direction. On an average, "young", "matured" and "old" swells (NW swells) are 76%, 21% and 3% respectively, during the study period.

The predominant winds in the Arabian Sea during NE monsoon and early pre-monsoon seasons are from NE, and the wind speeds are in the order of 5 to 10 m/s. On several occasions, it was observed that the NE winds become weak, and NW winds become stronger, especially in the north-western Arabian Sea and in the Arabian Peninsula. These NW winds are associated with Shamal events (active Shamal area is marked in Figure 4-16). Typical wind vectors in the Arabian Sea during NE monsoon and associated Shamal events are shown in Figure 4-19a and 4-19b. The wind speeds associated with Shamal events normally range between 10 and 20 m/s. As evident from the AWS winds at Ratnagiri coast (Figure 4-17d), at times, Shamal winds extend upto the west coast of India, though the magnitudes are relatively less along the coastal regions. These winds are stronger at the northern part of the west coast of India extending up to Karachi in Pakistan. The period as well as duration of the Shamal events closely matches with the systematic features observed in the measured wave parameters and AWS winds. Considering the above facts, it has been concluded that the systematic features observed in the wave parameters are primarily duc to the impact of Shamal winds, which generate strong waves and propagate to the west coast of India as swells. These swells are hereafter named as "Shamal" swells.

Waves measured at B1 (off Goa) during Feb 1996 – May 1997 also shows similar features. Such well-defined features are observed between November and March, and more frequently in January and February. These features are not evident in other seasons. Winds associated with summer Shamal events are relatively weaker, and their impact on the wave characteristics along the west coast of India is negligible due to the prevailing stronger SW monsoon winds, and the corresponding larger waves during this season.

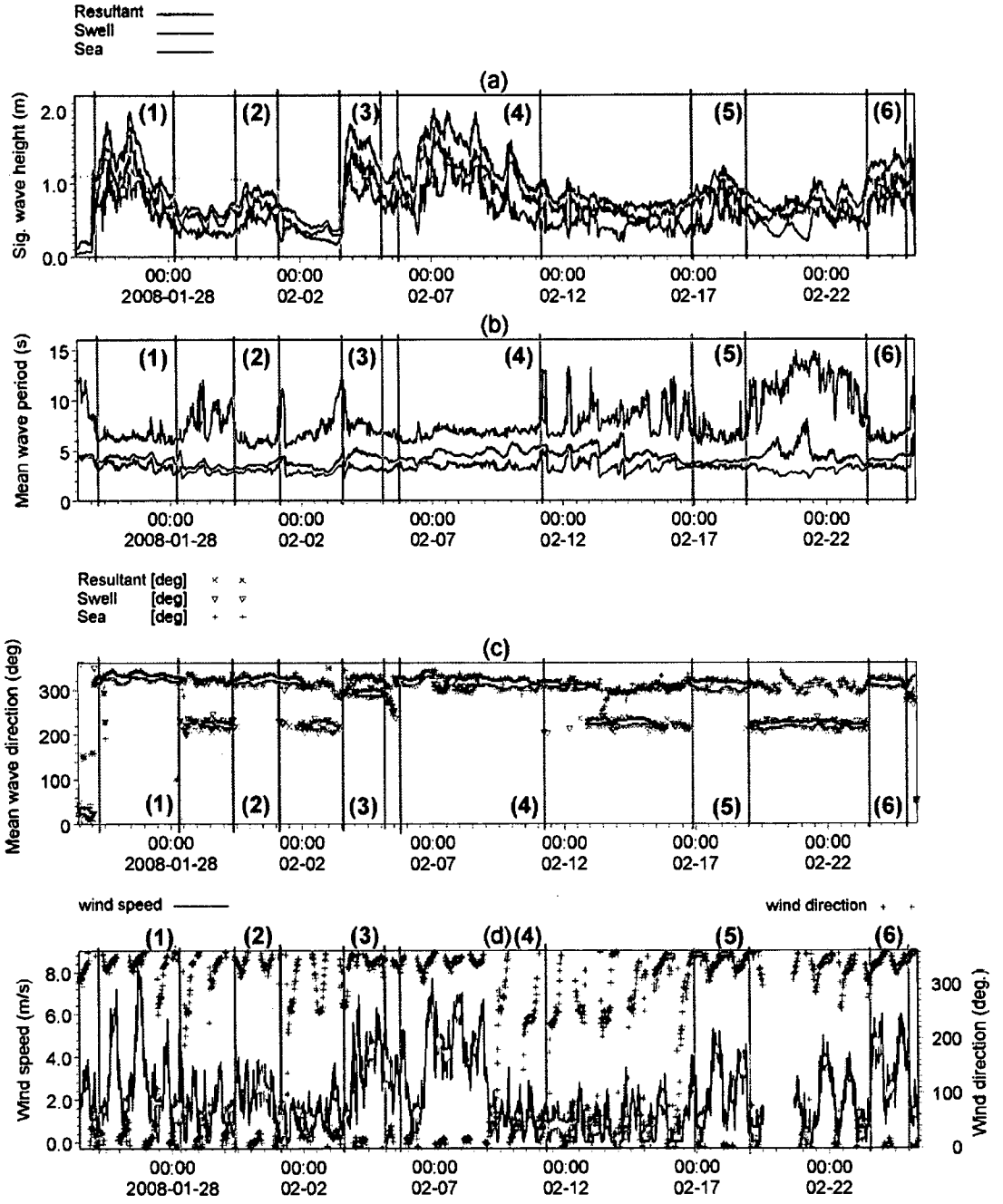

Figure 4-17. Measured wave and wind parameters off Ratnagiri; (a) significant wave height, (b) mean wave period, (c) mean wave direction and (d) AWS wind speed and direction. Well-defined features on wave and wind parameters are marked from (1) to (6).

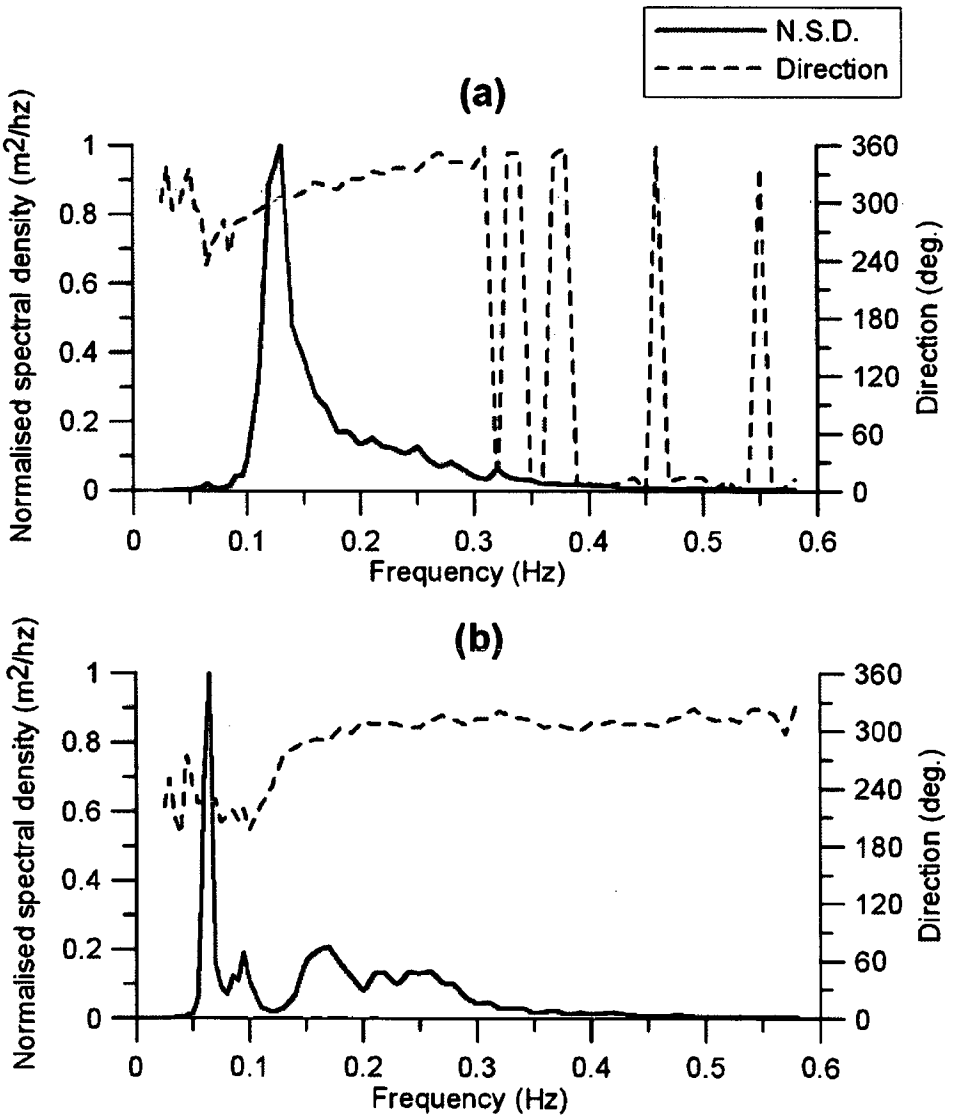

Figure 4-18. Typical directional energy spectra during (a) Shamal period and (b) non-Shamal period.

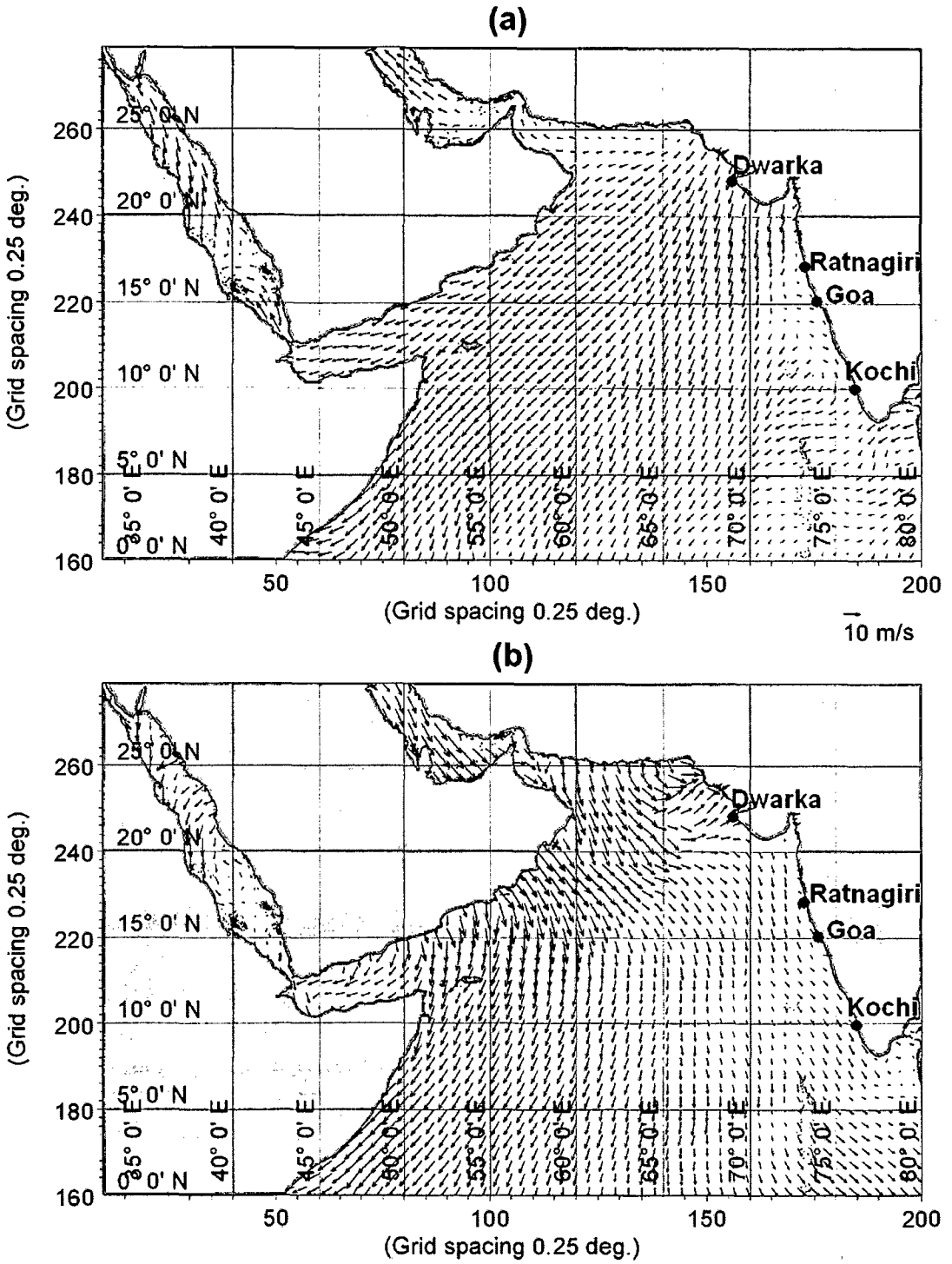

Figure 4-19. Typical wind vectors over the Arabian Sea associated with (a) NE monsoon and (b) Shamal event.

4.5.3. Generation and propagation

Numerical simulations carried out using IFREMER/CERSAT blended winds during Jan – Feb 2008 reproduced the generation and propagation characteristics of Shamal swells in the Indian Ocean. The analysis indicates that waves generated due to strong Shamal winds at the northwestern Arabian Sea propagate in the NW direction towards the west coast of India. A gradual wind wave growth has been observed with respect to the increase in wind speed during Shamal events. Significant wave height reaches upto 4.3 m in the Persian Gulf. However, propagation of the waves generated in the Persian Gulf to the rest of the Arabian Sea is obstructed at Hormuz Strait due to narrow opening and low water depths. It has been found that the Shamal winds generate higher waves in NW direction at the northwestern Arabian Sea (excluding Persian Gulf). The associated significant wave height reaches upto 3.7 m within a fetch of around 300 km. Once leave the generating area, they propagate in NW direction as Shamal swells.

Figure 4-20 shows significant wave height vectors in the Arabian Sea, representing the generation and propagation of Shamal swells for every 12 h during 02-04 Feb 2008. It is evident that larger waves are generated in the Persian Gulf, Gulf of Oman and off the east coast of Oman due to strong Shamal winds. The swells generated in the Gulf of Oman and east coast of Oman propagate in the NW direction. Another swell system also formed at an offshore area close to the Salalah coast (Figure 4-20) and propagates in the NNW direction. Since, the present study aims at understanding the influence of Shamal swells along the west coast of India, importance is attached to the NW swells generated in the northwestern Arabian Sea (Gulf of Oman and off the east coast of Oman).

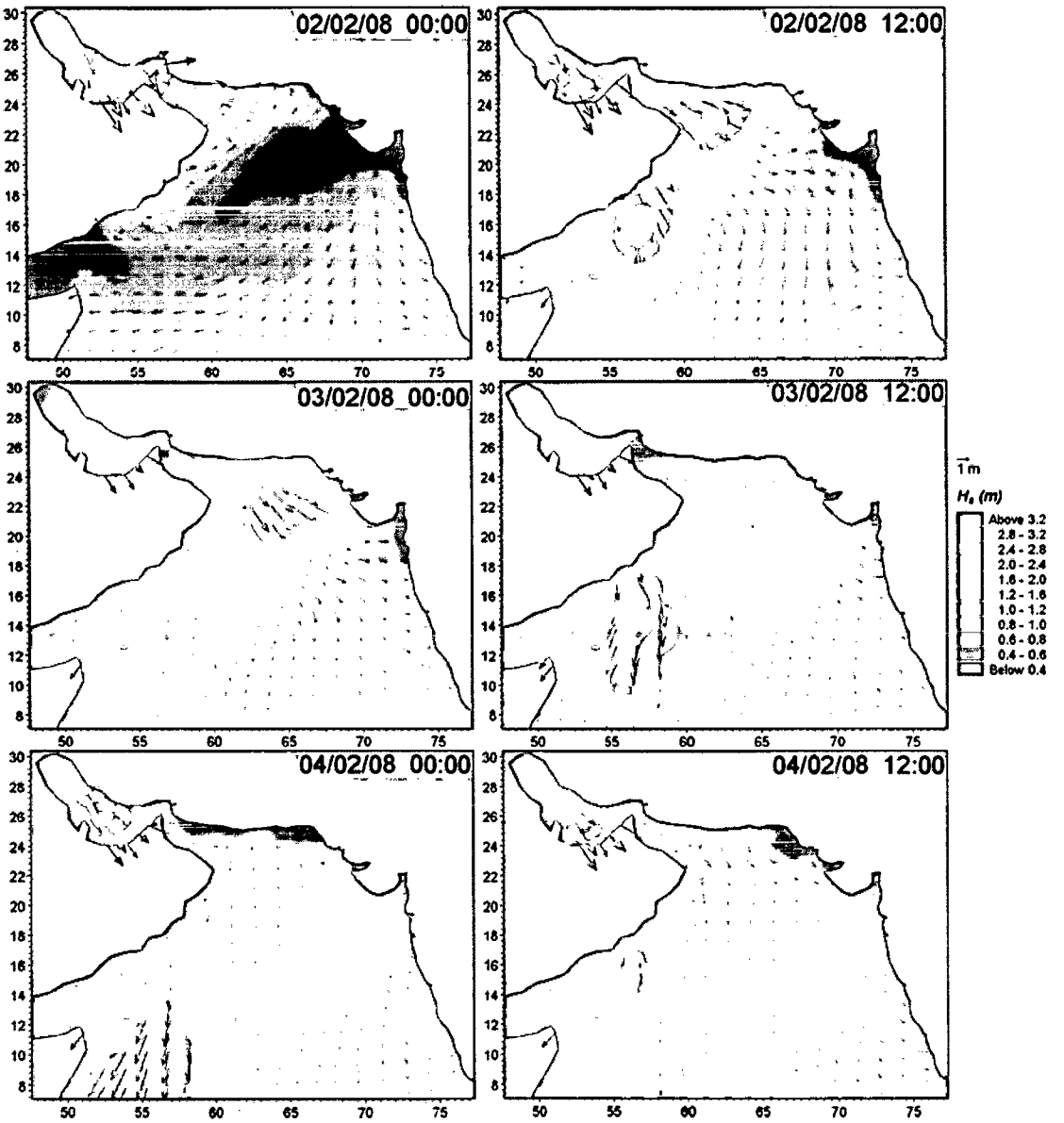

Figure 4-20. Significant wave height vectors in the Arabian Sea during 02-04 Feb 2008 representing the generation and propagation of Shamal swells.

It is evident that the Shamal swells propagate towards the west coast of India in the NW direction. They arrive at different times depending on the distance of propagation to various locations along the west coast of India. The swells reach first (in less than 20 h) along the Gujarat coast and later (around 48 h) along the Kerala coast. The swells observed off Gujarat coast have higher energy than those observed in the Kerala coast, indicating that the coastal region of Gujarat would be having high impact due to Shamal swells. The

Shamal swells measured off Ratnagiri coast has a mean period around 7 s and a wavelength of approximately 76 m. The travel distance of swell to the Ratnagiri coast is around 1200-1500 km. Hence, it takes 30-38 h to reach the Ratnagiri coast.

4.5.4. Influence along the west coast of India

Swell heights extracted from the simulation results at 25 m water depth off Kochi, Mangalore, Goa, Ratnagiri, Mumbai and Dwarka during the study period are presented in Figure 4-21. Variations in swell heights associated with Shamal events indicate that all the above locations along the west coast of India are influenced by the Shamal swells, though there are changes in patterns and heights according to the intensity and duration of the event. The swell heights are higher off Dwarka, indicating that the coast of Gujarat is highly influenced by the Shamal swells. Similar pattern is observed off Mumbai, but swell heights are relatively low compared to those off Dwarka. The swell pattern off Ratnagiri, Goa, Mangalore and Kochi are nearly the same, but with time lags as discussed earlier.

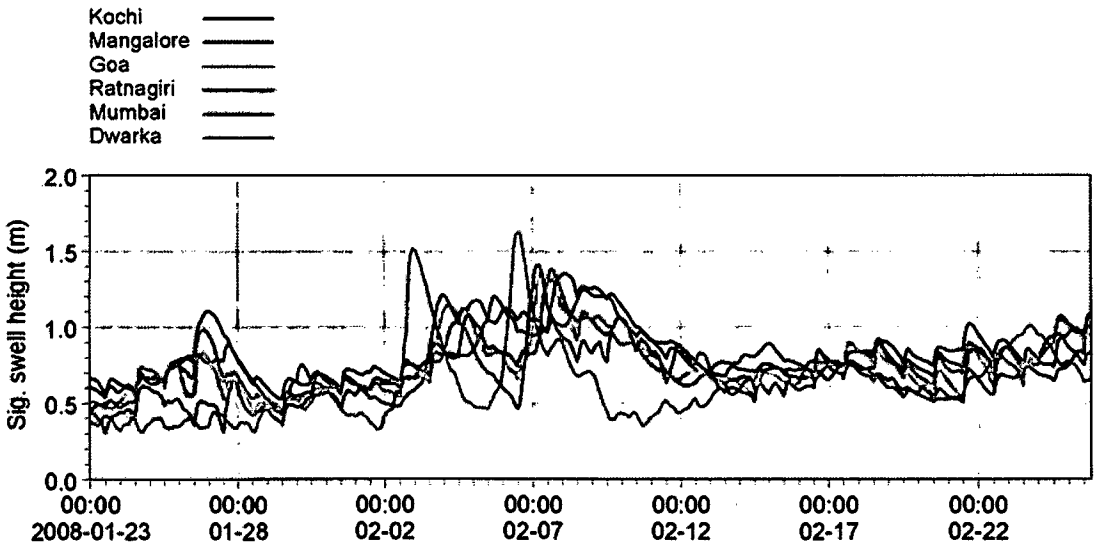

Figure 4-21. Significant swell heights off Kochi, Mangalore, Goa, Ratnagiri and Mumbai at 25 m water depth, extracted from the simulation results.

An analysis of measured waves off Dwarka (at B6) during 05 Dec 2007 – 05 Jan 2008 indicates that the Shamal swells are present, but relatively weaker compared to those during 24 Jan – 25 Feb 2008 (Figure 4-22). The predominant swells during this period are from S or SSW direction. However, short duration (< 24 h) Shamal swells have been observed in the NW direction; the swell heights are significantly higher and the mean swell

periods are between 6 and 8 s. It has been found from measurements that wind seas are dominated off Dwarka during non-Shamal events.

Figure 4-23 shows the wave parameters off Goa (at B1) during January 1997. Increase in wave height associated with decrease in swell period and propagation of wind sea and swell in the NW direction are prominent during the Shamal events. Even though Shamal swells exist, at times, the wind sea energies in NW direction (generated by Shamal winds) dominate over the swell energies, which provide an indication to the extension of Shamal winds up to the west coast of India. However, this has to be confirmed through detailed investigations.

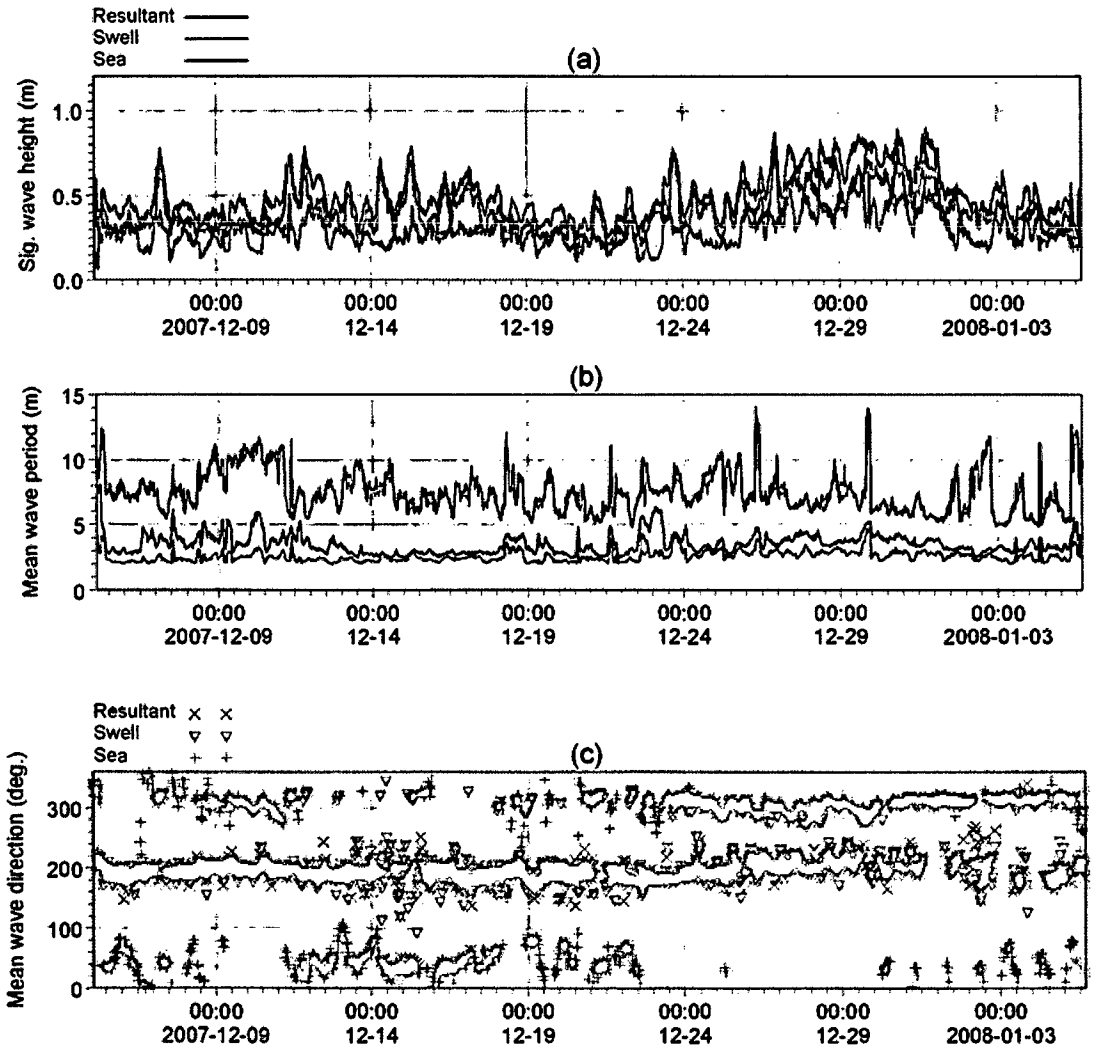

Figure 4-22. Measured wave parameters off Dwarka at B6 during 05 Dec 2007 – 05 Jan 2008: (a) significant wave height, (b) mean wave period and (c) mean wave direction.

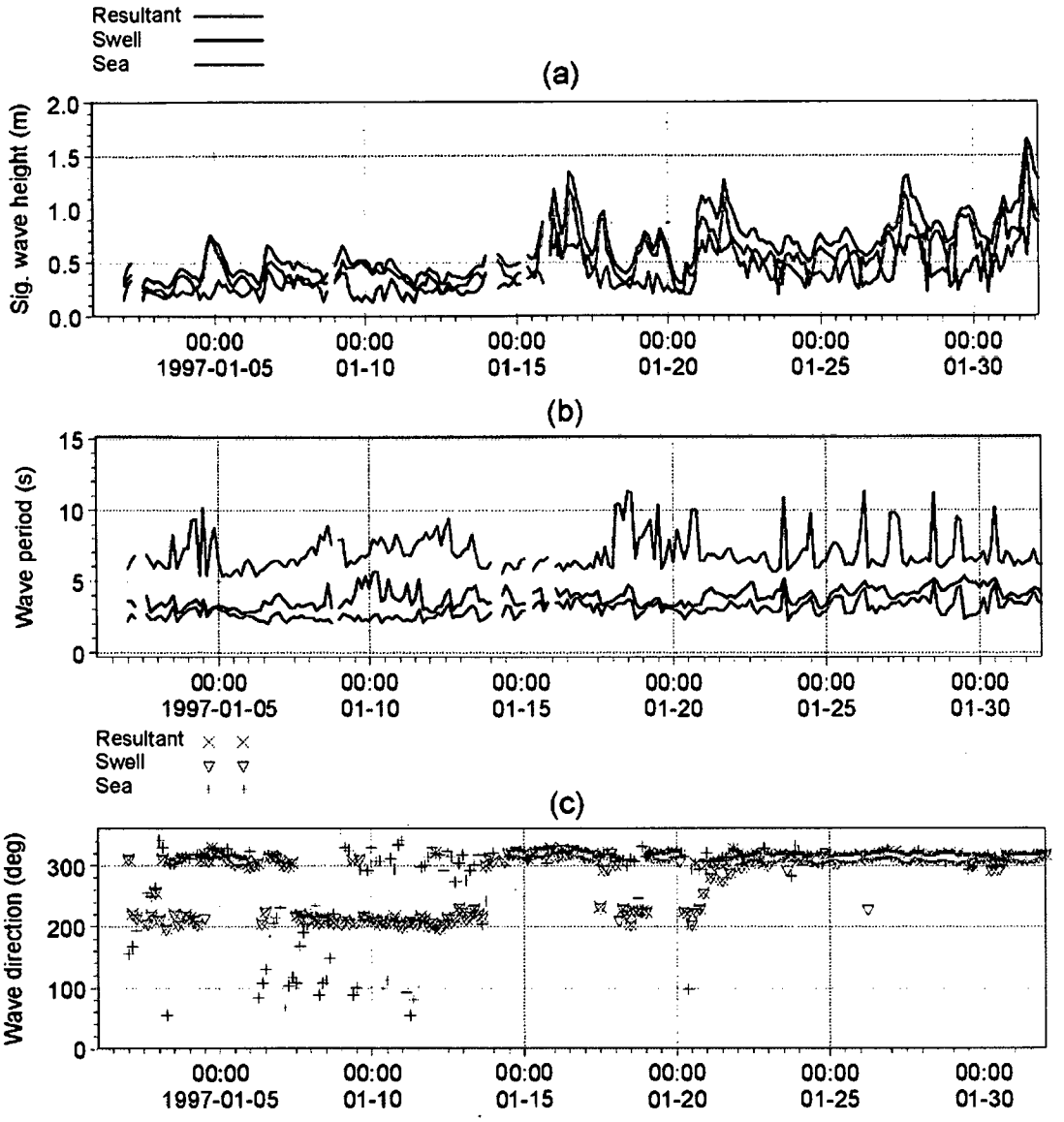

Figure 4-23. Measured wave parameters off Goa at B1 during January 1997: (a) significant wave height, (b) mean wave period and (c) mean wave direction.

4.6. Superimposition of coastal wind seas on pre-existing swells

It has been found that wind seas are dominated along the west coast of India during pre-monsoon season. Sea breeze has prominent role in the generation of relatively stronger wind seas along the west coast. Superimposition of these wind seas with pre-existing swells leads to typical variations in the waves on a diurnal cycle. To understand these variations, wind and wave data measured off Goa, west coast of India, during May 2005 have been analysed.

Masselink and Pattiaratchi [1998] studied the effect of sea breeze on wave characteristics of the coastal regions of Sydney and found that during sea breeze, the addition of locally generated short-period wind waves to the background swell, resulted in an increase in wave height, a decrease in wave period and an intensification of nearshore currents. After the cessation of the sea breeze, the wind-wave energy level gradually decreased and the associated wind-wave period increased. Ten hours after the sea breeze had stopped blowing, significant amount of wind-wave energy was still present. Sonu et al. (1973) noticed that after the onset of sea breeze, the wave height increases, wave period decreases and wave direction changes. Interestingly, similar variations have been found in the wave data measured off Goa at B2 and B3 during May 2005.

4.6.1. Sea breeze along the west coast

The west coast of India is characterized by sea breeze and land breeze systems which are prominent in calm seasons especially during pre-monsoon months (Aparna et al., 2005). The seaward extension of the sea breeze is around 180 km off Goa, while it is 160 km and 190 km off Kochi and Mangalore, respectively during February – April, and the speed decreases towards offshore.

Winds from the AWS for the coastal region off Goa show nearly semi-diurnal variations both in their magnitude and direction (Figure 4-24). The prominent wind directions are NW (from sea to land) and NE (from land to sea). The speeds are relatively higher for northwesterlies. The sea breeze and land breeze systems are nearly perpendicular to each other, the former is roughly parallel and the latter is perpendicular to the orientation of the Goa coast. Sea breeze starts around 11h, and continues to blow in the NW direction; wind speed is maximum between 15h and 18h. Very early in the morning, the wind shifts its direction to NE (land to sea) and continues till 11h; wind speeds are relatively lesser compared to sea breeze. These variations are found to be systematic throughout the study period, and consistent with the results of earlier studies (e.g., Masselink and Pattiaratchi, 1998). In general, the maximum wind speeds are observed around 15h and the minimum around 06h. The maximum wind speed observed during the study period (in May 2005) was 4.6 m/s in the NW direction. On several occasions no wind is observed in the early hours of the day.

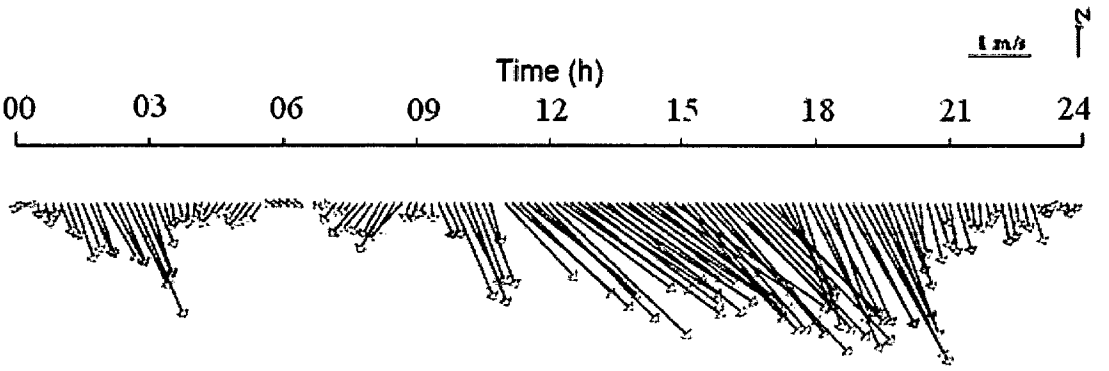

Figure 4-24. AWS wind distribution at Dona Paula during 12 May 2005.

Six –hourly NCEP reanalysis wind data present the existence of two different wind systems in this region: (i) relatively stronger southwesterlies / westerlies in the open ocean throughout the day and (ii) relatively weaker northwesterlies in the coastal region. The analysis of wind speeds obtained from QuikSCAT along a section upto 200 km from the coast (Figure 4-25) indicates that wind speeds increase towards the coast in a constant NW direction. Since QuikSCAT data is available twice daily, i.e., 06h and 18h (local time) and data is not accurate within 25 km from the coast, the land breeze effect could not be noticed. Wind at 06h from the coastal AWS station is NE and relatively weaker, and that at 18h is NW and stronger. A typical vector plot (6-hourly) of the IFREMER/CERSAT blended winds in and around Goa during 05 May 2005 is shown in Figure 4-26. Weaker winds from N and NE (land breeze) are present close to the coast during 00h and 06h, whereas stronger NW winds (sea breeze) are observed during 18h. The speed of northwesterly winds is found to be lower between 00h and 06h as seen in the measurements (Figure 4-24) and direction remains nearly constant throughout the day.

The modelled MM5 winds, clearly show the sea breeze – land breeze distribution at the Goa coast during pre-monsoon season. Figure 4-27 shows the typical wind vectors plotted for every 6 hour. The initial phase of the sea breeze generation is clearly visible around 12h, increases the magnitude with the maximum around 18h and gradually decreases towards 24h (00h). It is evident that NW winds (sea breeze) are stronger at the Goa coast around 18h. Gradual increase in the intensity of the sea breeze towards the coast from offshore area has been observed. While entering the land, sea breeze gets weakened due to the topographic effects. The extension of sea breeze over the land area is clearly visible during this time. Land breeze is observed along the coast around 06h. The magnitude of

land breeze is relatively low and its extension towards offshore is limited to a few kilometer from the coast.

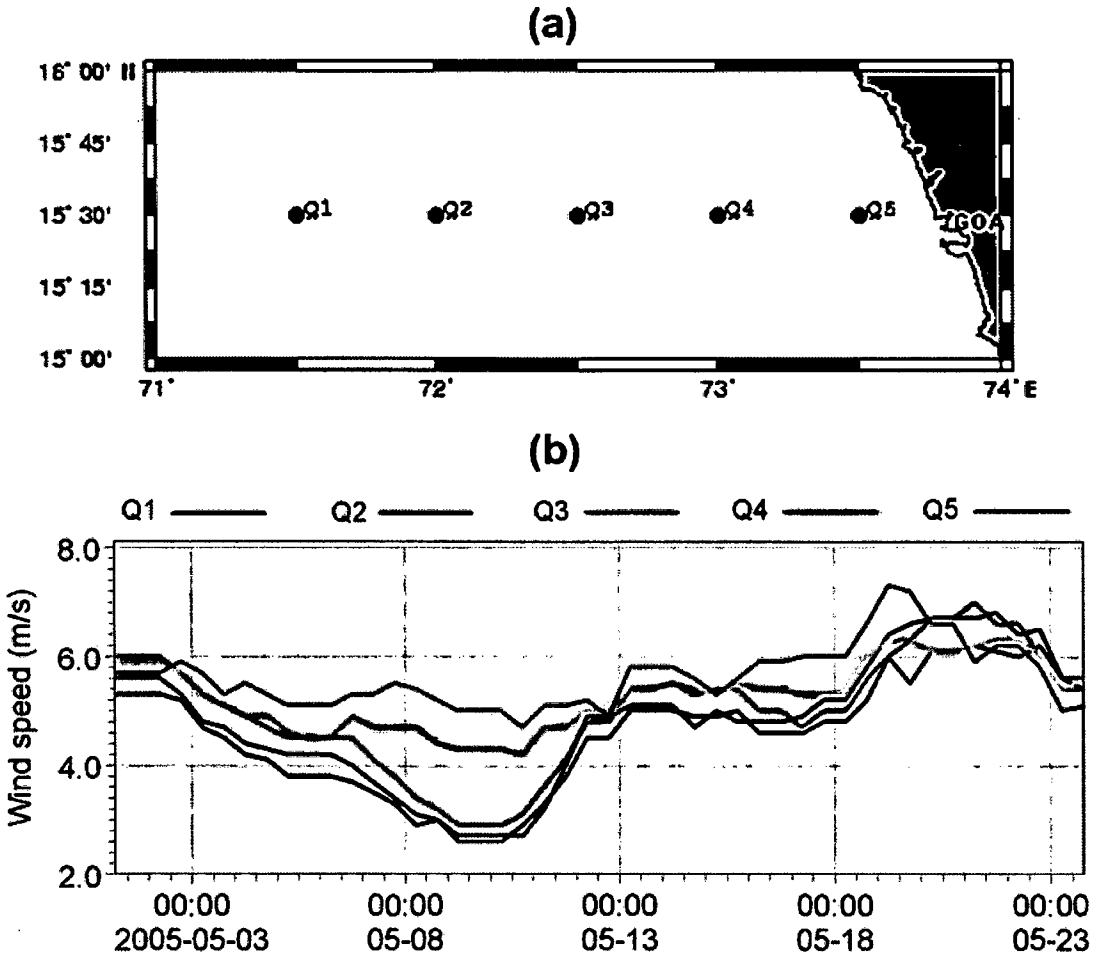

Figure 4-25. QuikSCAT winds off Goa: (a) locations from offshore to coast (Q1 to Q5) and (b) wind speed distribution at the locations Q1 to Q5.

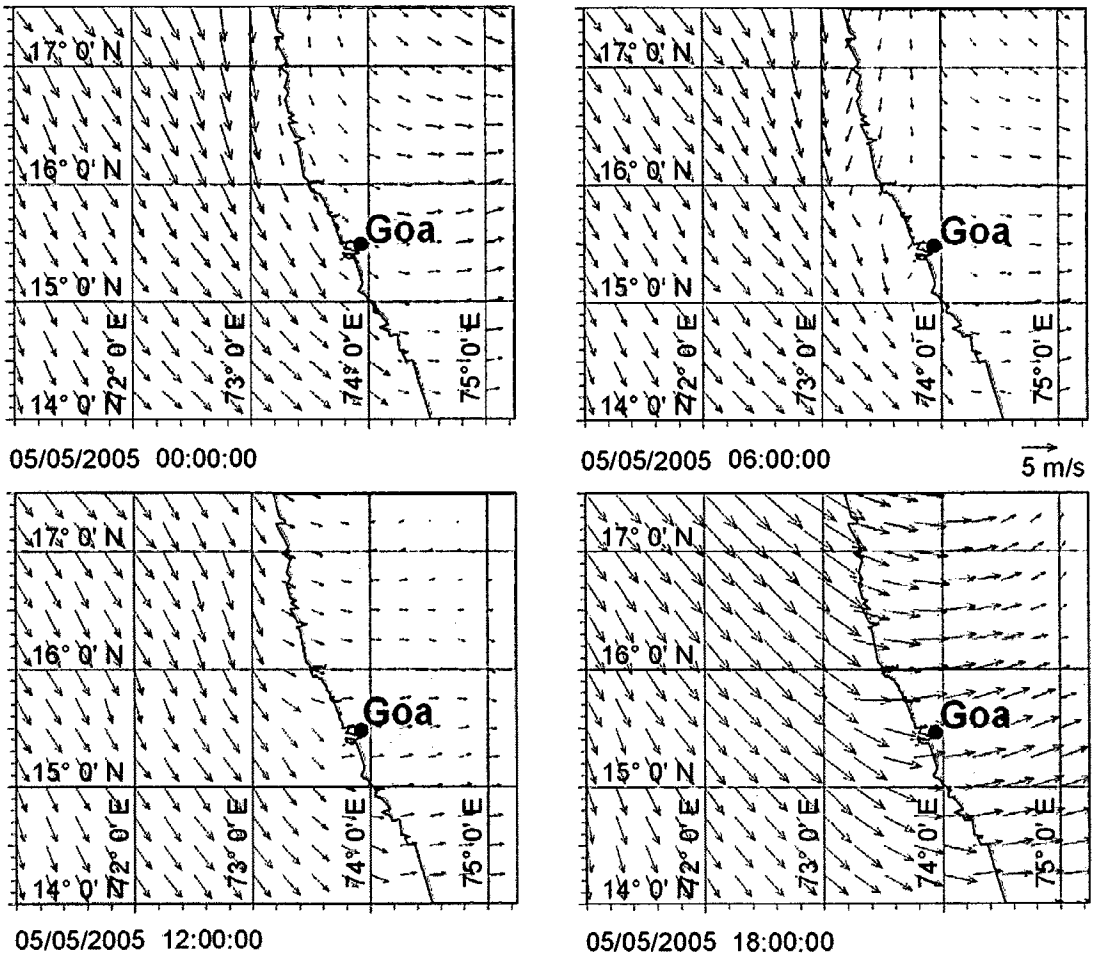

Figure 4-26. Typical wind vectors (CERSAT/IFREMER blended winds) in and around Goa region during 05 May 2005.

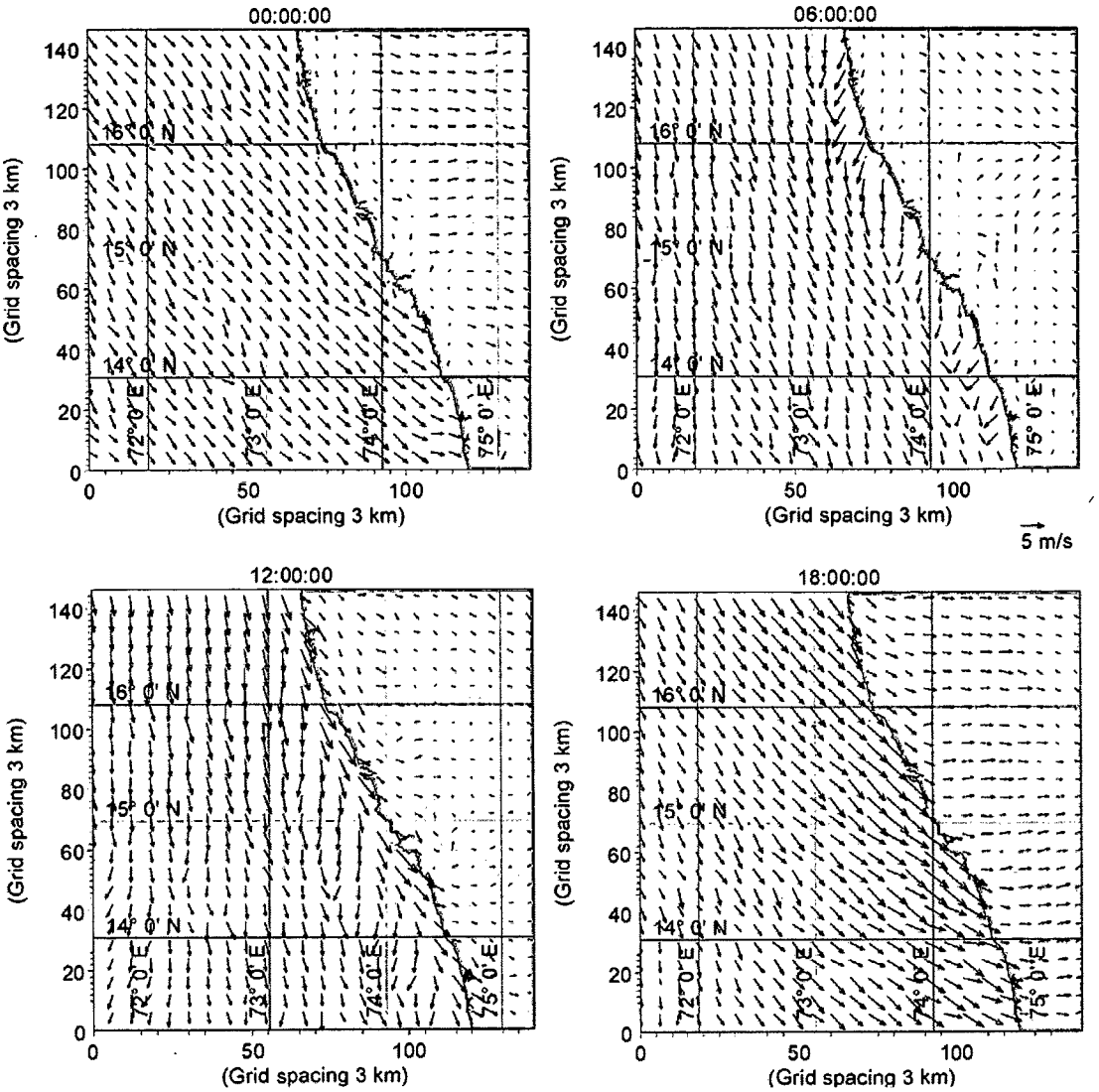

Figure 4-27. Typical wind vectors on a daily cycle during pre-monsoon season, as simulated in MM5.

4.6.2. Diurnal variations in the nearshore waves

The sea-land breeze system leads to a typical cycle of local waves. Following the onset of sea breeze, a wind wave system grows in time, following the progressive extension of the sea breeze area towards offshore. While, once begun, the wind speeds present close to the coast remain relatively constant, the consequent increase of fetch with respect to the coastal area leads to an increase of the derived wave height (Figure 4-28 and Figure 4-29). Although relatively limited, the increase of significant wave height shows that the local wind sea has energy comparable to or larger than the permanent background swell.

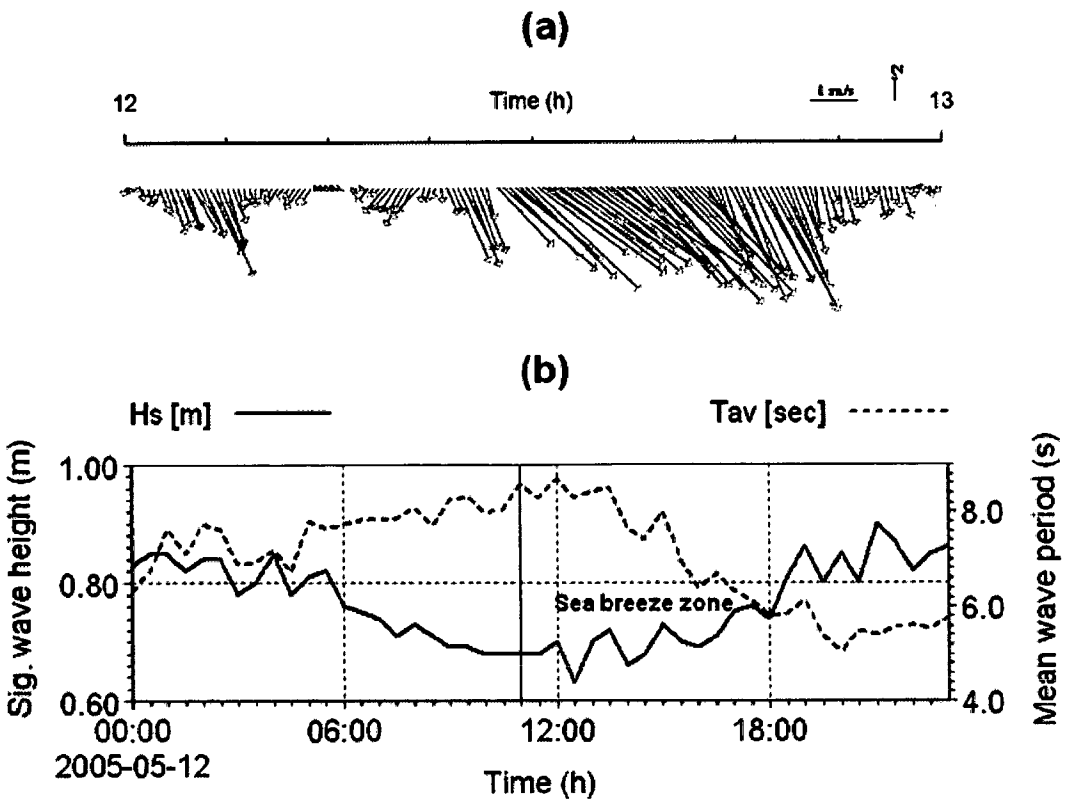

Figure 4-28. (a) AWS wind distribution at Dona Paula and (b) significant wave height and mean wave period at B2 during 12 May 2005.

The time evolution of the sea breeze implies a time lag between the onset of the sea breeze and the maximum wave conditions experienced along the coast. Interestingly, the local experience has led to a practical rule used by the local mariners, indicating that the maximum H_s is reached between 3 and 4 hours after the sea breeze begins, as seen clearly in the measurements (Figure 4-28 and Figure 4-29). Combined with the wave generation rules (see, e.g., SWAMP group, 1985), this suggests a substantial offshore extension of the area, which is affected by the sea breeze.

An indication of the offshore extension where the sea breeze is strong enough to generate waves, is derived from the decay of the wave conditions. During a typical daily cycle, the wave height reaches its peak early in the afternoon, then it decays progressively back to the swell conditions within 5 or 6 hours. Given the typical sea breeze speed between 4 and 5 m/s, the wind sea has a significant wave height (not the overall significant wave height) of the order of 0.5 – 0.6 m. This is very close to the fully developed conditions (for the breeze speed) requiring a minimum fetch of 40 - 50 km. This is not useful for our purpose as the

area affected by the sea breeze is known to be larger. However, another consideration is possible. The typical peak period of sea breeze wave is between 3 and 4 s. This corresponds to about 16 m wavelength (fully consistent with wind sea H_s of 0.5 to 0.6 m), whose energy travels at about 10 km/h. So, the decay time plus the necessary fetch for the most offshore generation suggests an overall extension of the wave generation active zone between 70 and 80 km. An analysis of MM5 winds indicates that the maximum offshore extension of the sea breeze can be around 150-180 km, consistent with the observations of Aparna et al (2005).

Measured spectra clearly show the evidence of the daily cycle of the waves off Goa during pre-monsoon season. Figure 4-30 and Figure 4-31 show the 2D and 1D spectra, respectively. Figure 4-30 clearly shows that at 3-hour intervals, the onset of sea breeze waves around 300° incoming direction, while the swell from 220° - 230° are at much lower frequency, and permanently present. The energy associated with the two different wave systems, wind sea and swell, is derived from Figure 4-31. The onset of sea breeze leads to a decrease of mean period. From the maritime safety point of view, the presence of cross-sea conditions (here represented by the SW swell and NW wind sea), is more difficult than a single wave system with the same overall wave height. These cross conditions are typical of the central and southern part of the west coast of India, because of its exposure to long distance swell from the SW direction. No similar conditions are found along the east coast of India (off Paradip and Nagapattinam).

Notwithstanding the limitations of the coarse wind, a first order understanding of the process can be provided by the wave model results obtained using both the large scale NCEP winds and the AWS data for the local area. Figure 4-33 shows a comparison between modelled and measured significant wave heights at location B2. While there are local differences that we associate with the crude wind data (used as input to the wave model), results are consistent with the measured ones, as seen in the related scatter diagram shown in Figure 4-34. The gridded significant wave heights from Jason-1 also match with the modelling and measurements, even though they are averaged (both spatially and temporally).

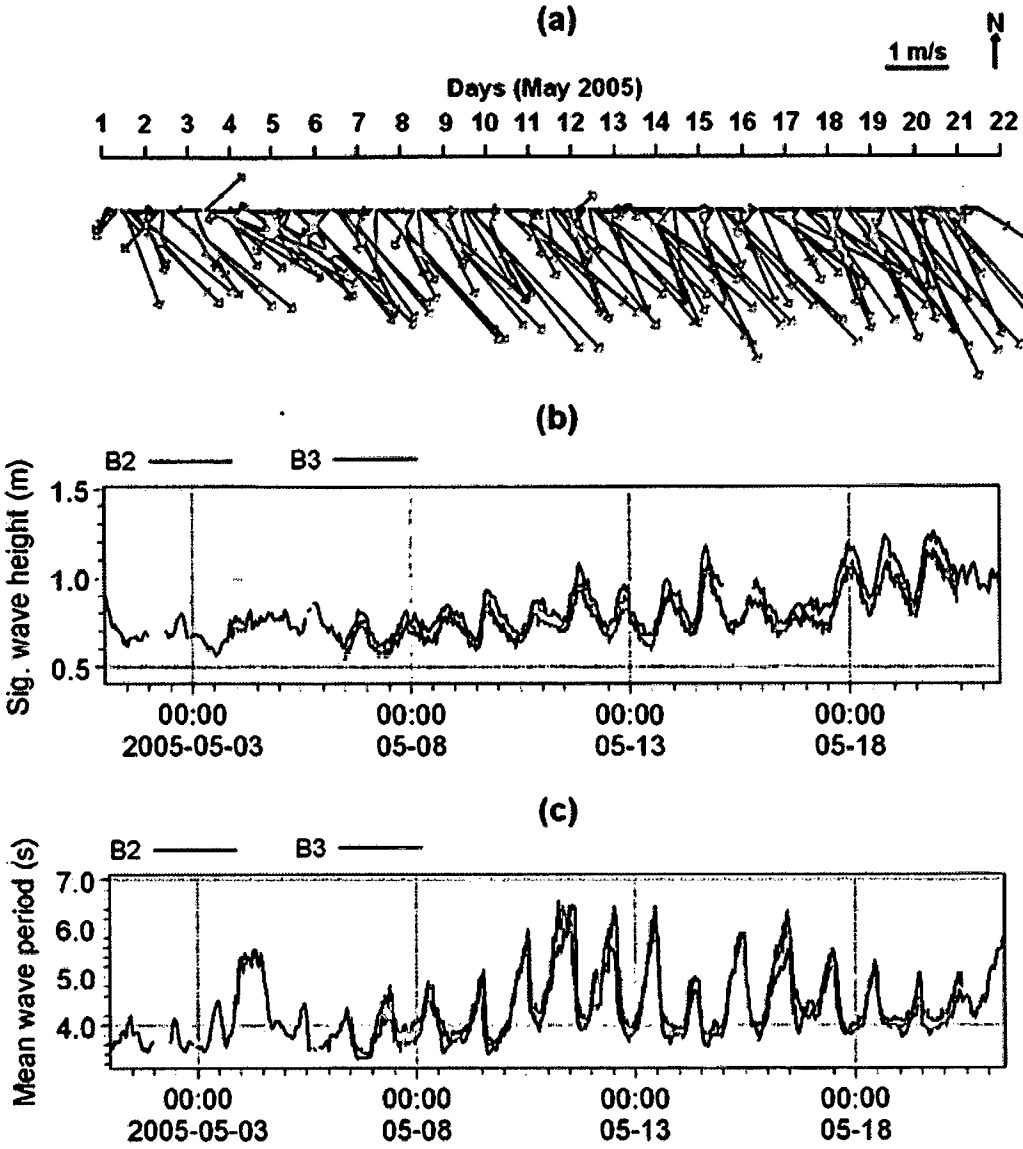

Figure 4-29. Distribution of (a) AWS winds at Dona Paula coastal station, (b) Significant wave height at B2 and B3 and (c) Mean wave period at B2 and B3.

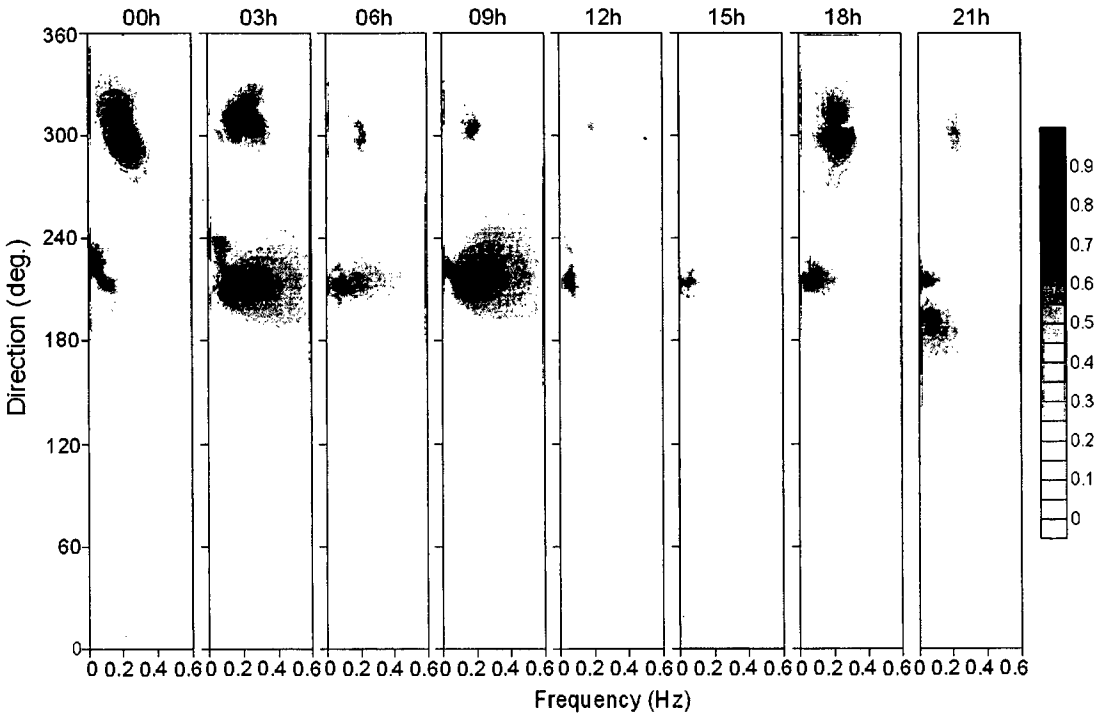

Figure 4-30. Directional energy spectra during 00h to 21h (for every 3 hour) on 19 May 2005.

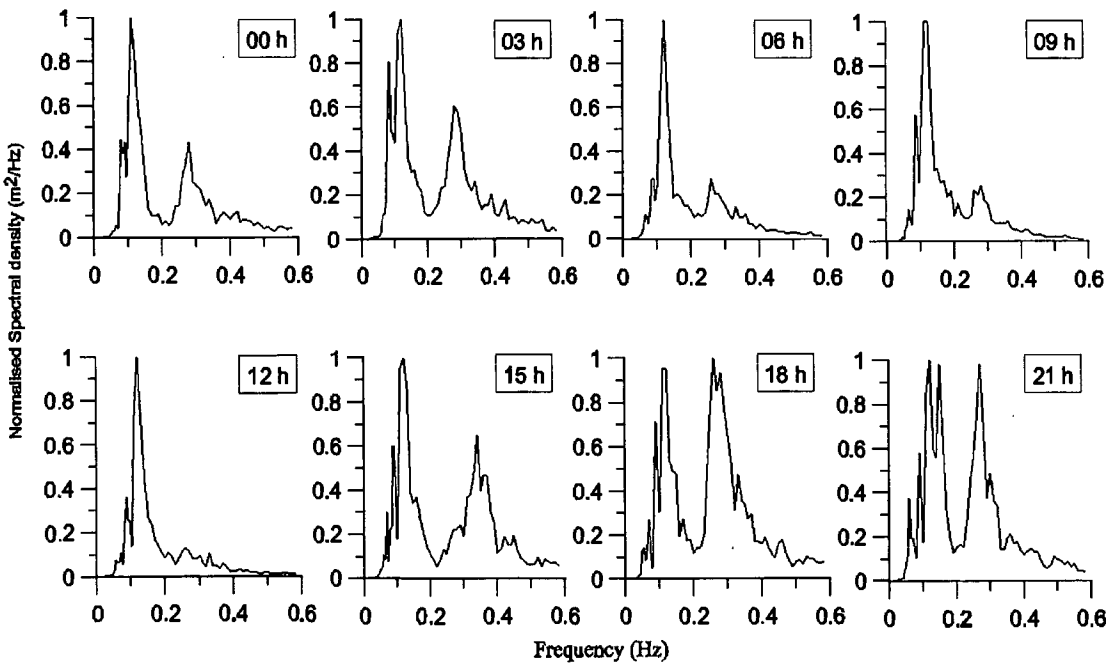

Figure 4-31. Typical 1D spectra during May 2005.

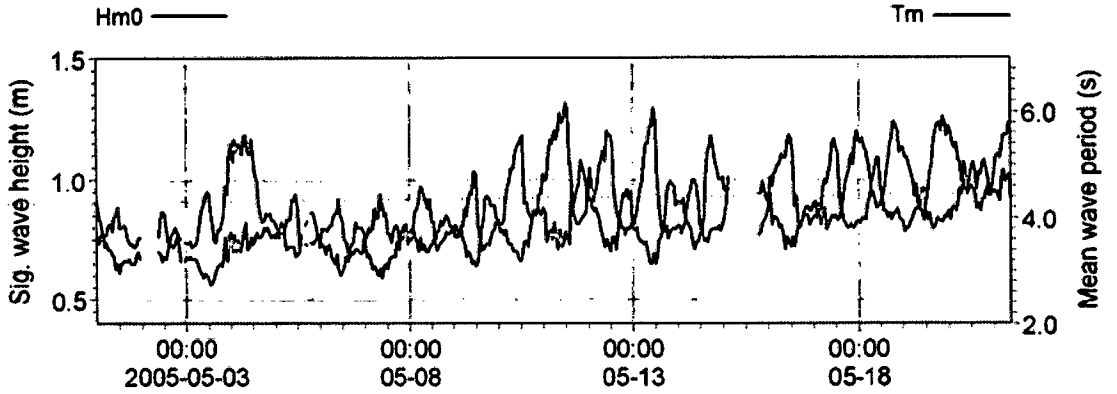

Figure 4-32. Measured significant wave height and mean wave period during May 2005 at B2, showing an inverse proportion among their variations.

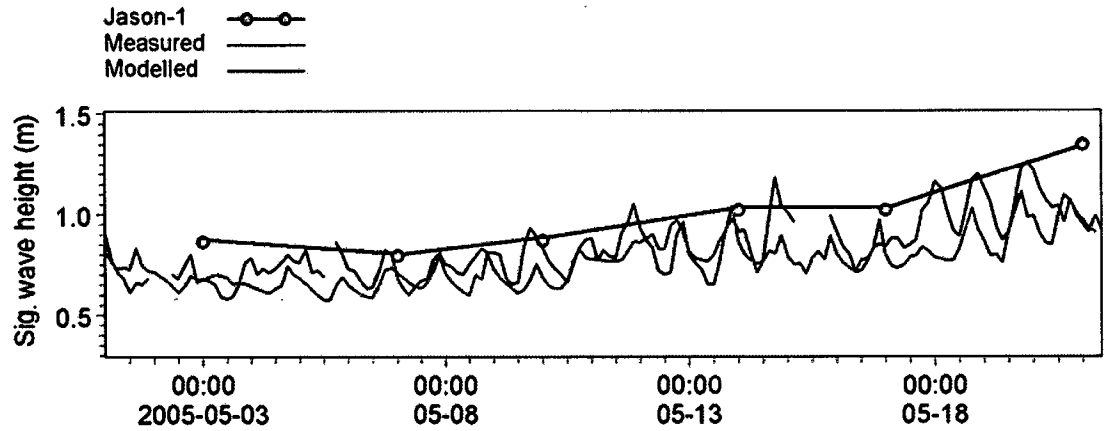

Figure 4-33. Significant wave heights during 1-21 May 2005 : (i) Jason-1 (1 degree x 1 degree grid resolution) extracted at 15^0 N, 73^0 E on an alternate 3 and 4 days average, (ii) Measured at B2 (iii) Modelled data extracted at B2.

Clearly, a deeper quantitative analysis of the local generation requires fine resolution winds capable of resolving the details of the wind speed gradient when moving progressively from the Goa coast towards offshore. In this respect, an attempt has been made using MM5 winds to simulate the wind seas off Goa and to analyse the spatial variations according to the wind speed gradient. Figure 4-35 shows the wind sea H_s vectors off Goa during a sea breeze dominated period. It is evident that the wind sea H_s gradually increases toward the coast from offshore, and the maximum wind sea H_s has been observed close to the Goa coast. The wind sea growth towards the coast is proportional to the wind speed gradient, available fetch and sea breeze duration. After cessation of the sea breeze, the associated wind sea energy starts to reduce, and hence a decrease in wind sea H_s has been observed.

The waves simulated by coupling the boundary conditions obtained from the overall simulations for Indian Ocean using NCEP winds, and the MM5 winds for the Goa region, clearly shows diurnal variations in resultant H_s and T_m. A comparison between measured and modelled H_s and T_m at location B2 is shown in Figure 4-36. The interaction of pre-existing swells with the wind seas results in an overall increase of the resultant H_s (as compared to the above wind seas), keeping similar diurnal patterns as observed in the wind seas. However, the diurnal pattern in T_m becomes more systematic for the wave due to the interaction of pre-existing swells. It has been found that the mean wave period decreases, as wind seas dominate. Hence, an inverse proportion has been found between H_s and T_m. Figure 4-37 shows the resultant H_s vectors during sea breeze dominated period, as simulated using MM5 winds and with offshore boundary conditions.

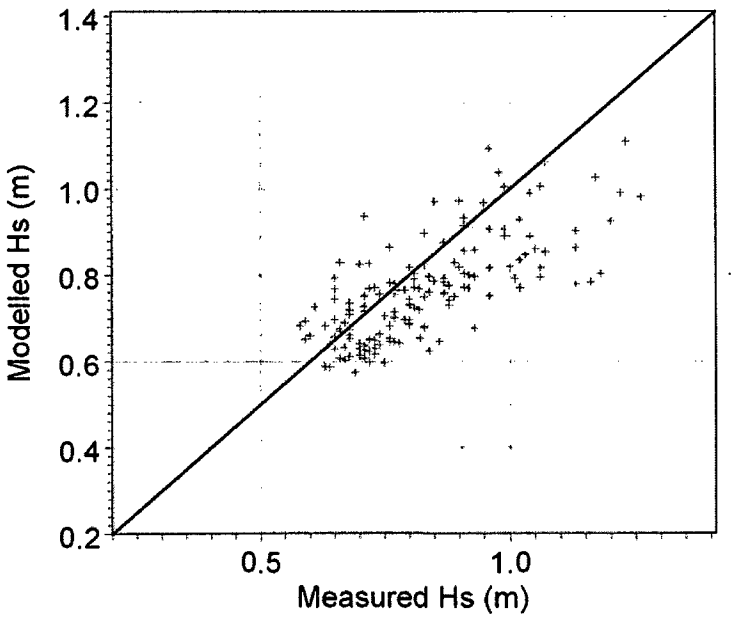

Figure 4-34. Scatter between measured and modelled significant wave heights.

The present theories of wave generation embedded in the various spectral models (e.g., WAM, WAVEWATCH III, etc.) consider the input by wind to a given spectral component (specified in frequency and direction) as independent of energy present in other components. The process of energy transfer from wind to waves is based on a relationship between the wind speed close to the surface and the wave phase speed. However, the latter is bound to change, alternatively in positive and negative direction, when superimposed to a much longer swell. The typical 8 s swell arriving from SW off Goa coast has a

wavelength close to 100m. Therefore, it is likely to affect the local generation of wind waves associated with swell in both wave height and period.

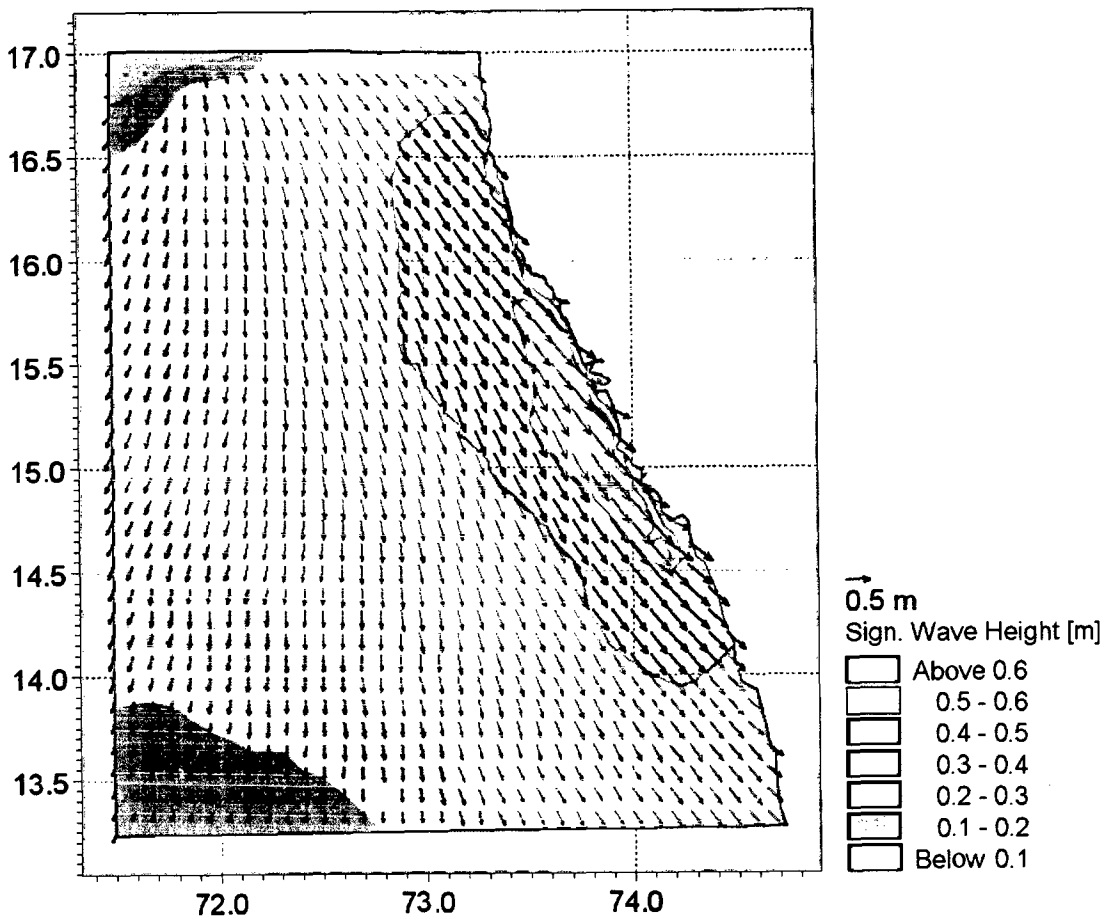

Figure 4-35. Typical wind sea H_s vectors during sea breeze dominated period, simulated using MM5 winds.

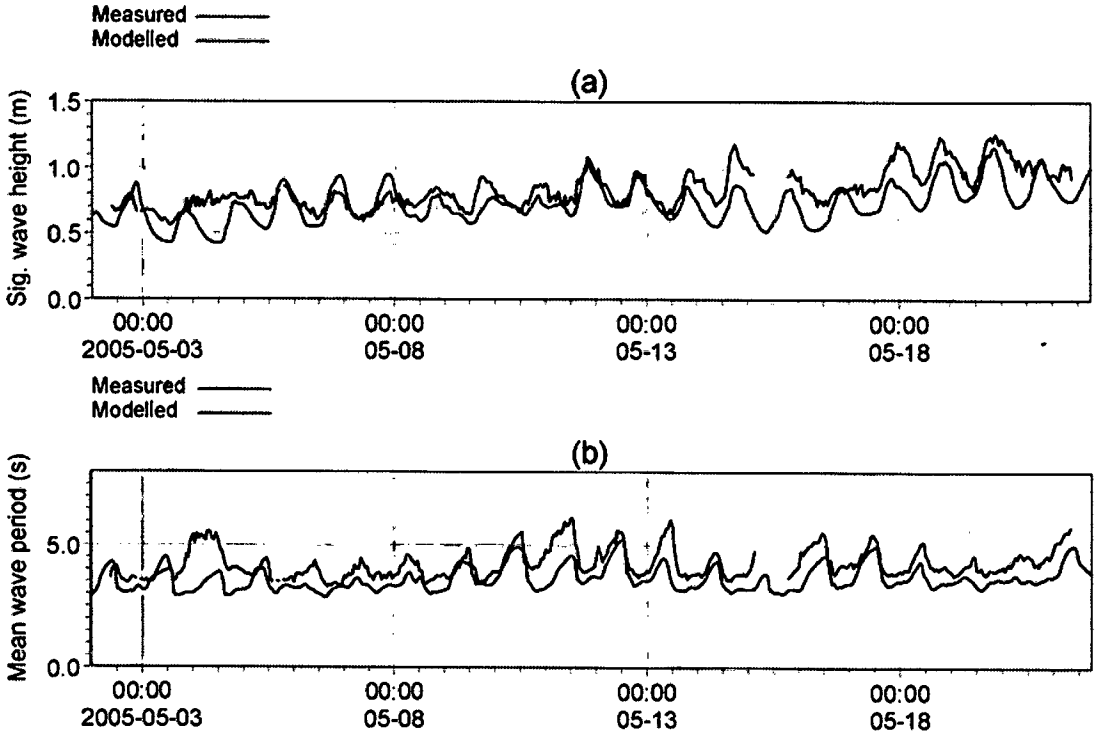

Figure 4-36. Measured and modelled significant wave height and mean wave period at location B2.

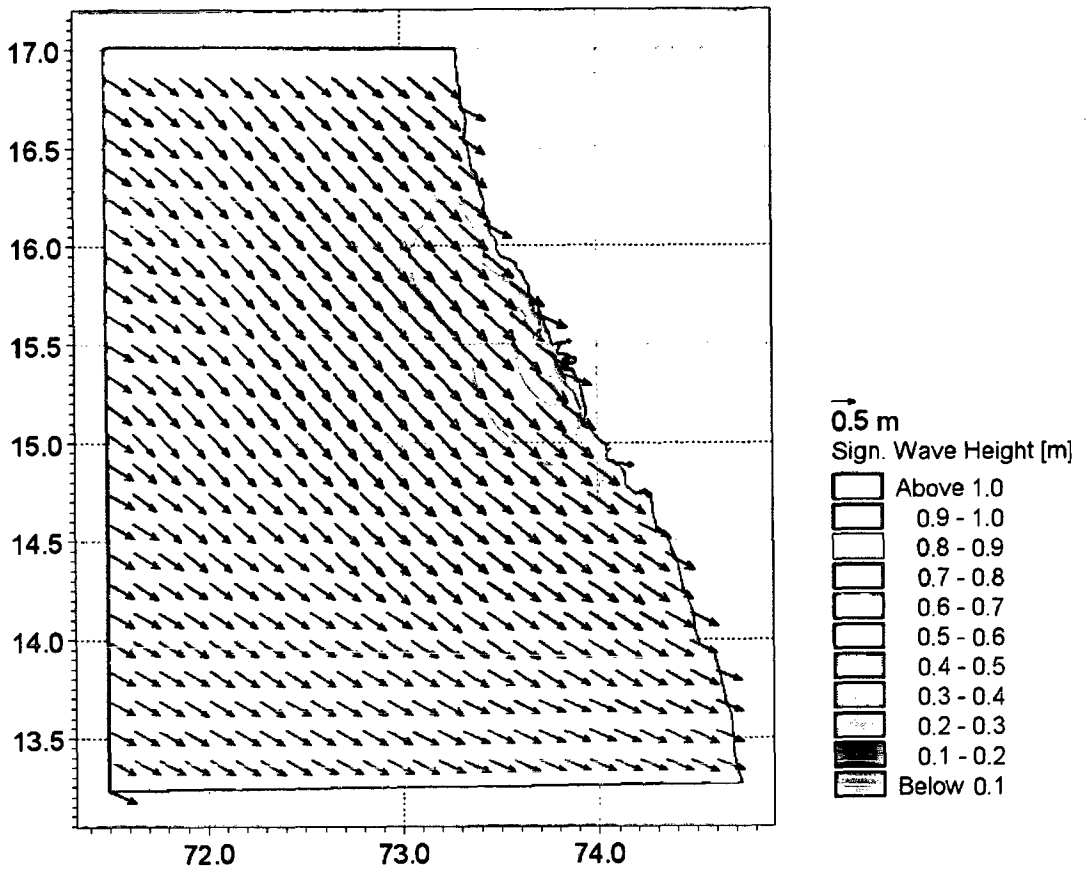

Figure 4-37. Typical H_s vectors during sea breeze dominated period.

Chapter 5

Wave transformation along open coasts and semi-enclosed regions

Chapter 5

Wave transformation along open coasts and semi-enclosed regions

5.1. Introduction

Wave transformation along select open coasts and semi-enclosed regions has been studied using in situ, model and remote sensing wave data have been used in the analysis. Significant wave heights obtained from Jason-1 altimeter (Quilfen et al, 2004) have been analysed to study the deep water wave characteristics. Since, the above data are not reliable at nearshore regions, results from numerical simulations were taken into account. Sec. 5.2 describes wave transformation along select open coasts, and Sec. 5.3 describes the transformation along semi-enclosed areas, which are naturally and artificially protected. Furthermore, a case study has been carried out to revise the inland vessel's limit (IVL) of Mormugao Port based on the distribution of significant wave heights, which illustrates the applicability of a wave transformation model in the nearshore regions. The results are analysed and discussed in Sec. 5.4.

5.2. Wave transformation along open coasts

In order to study wave transformation in the intermediate waters, altimeter data, model results and measured data have been used, depending on the data availability. However, for the nearshore region, measurements and model results have been used as satellite data (altimeter) has inherent limitations.

5.2.1. Deep water waves from Jason-1

Significant wave heights obtained from Jason-1 altimeter during 2005 were analysed to understand the deepwater wave characteristics. Two regions were selected: off Goa (along the west coast of India) and off Paradip (along the east coast of India). At each region, significant wave heights from two grid points were selected. One grid is close to the coast and the other one is approximately 450 km away from the coast (Figure 2-3).

Jason-1 significant wave heights off Goa and off Paradip at deep waters during 2005 are shown in Figure 5-1. Significant wave heights off Goa are relatively low (< 2.0 m) during pre-monsoon and post-monsoon seasons and higher (reach upto 4.6 m) during SW

monsoon. Sanil Kumar et al. (2000) reported that waves along the west coast of India are higher during southwest monsoon. Significant wave heights off Paradip are low (< 2.0 m) during pre-monsoon and NE monsoon seasons and higher (reached up to 3.6 m) during SW monsoon. However, extreme events such as cyclones are more prevalent in the Bay of Bengal, and during such event, higher waves prevail along the east coast of India (Sanil Kumar et al., 2004c; Prasad Kumar et al., 2000 and Aboobacker et al., 2009). Since, the temporal resolution of Jason-1 data is very coarse, the extreme events are not well represented. There are no significant changes in wave heights between the grids G1 and G2 off Goa or between the grids P1 and P2 off Paradip.

The major limitations of Jason-1 data are: (i) data cannot be used at a region very close to the coast, and (ii) its temporal resolution is very coarse (alternate 3 and 4 days). Therefore, wave measurements and modelling results are considered to study wave transformation in shallow waters.

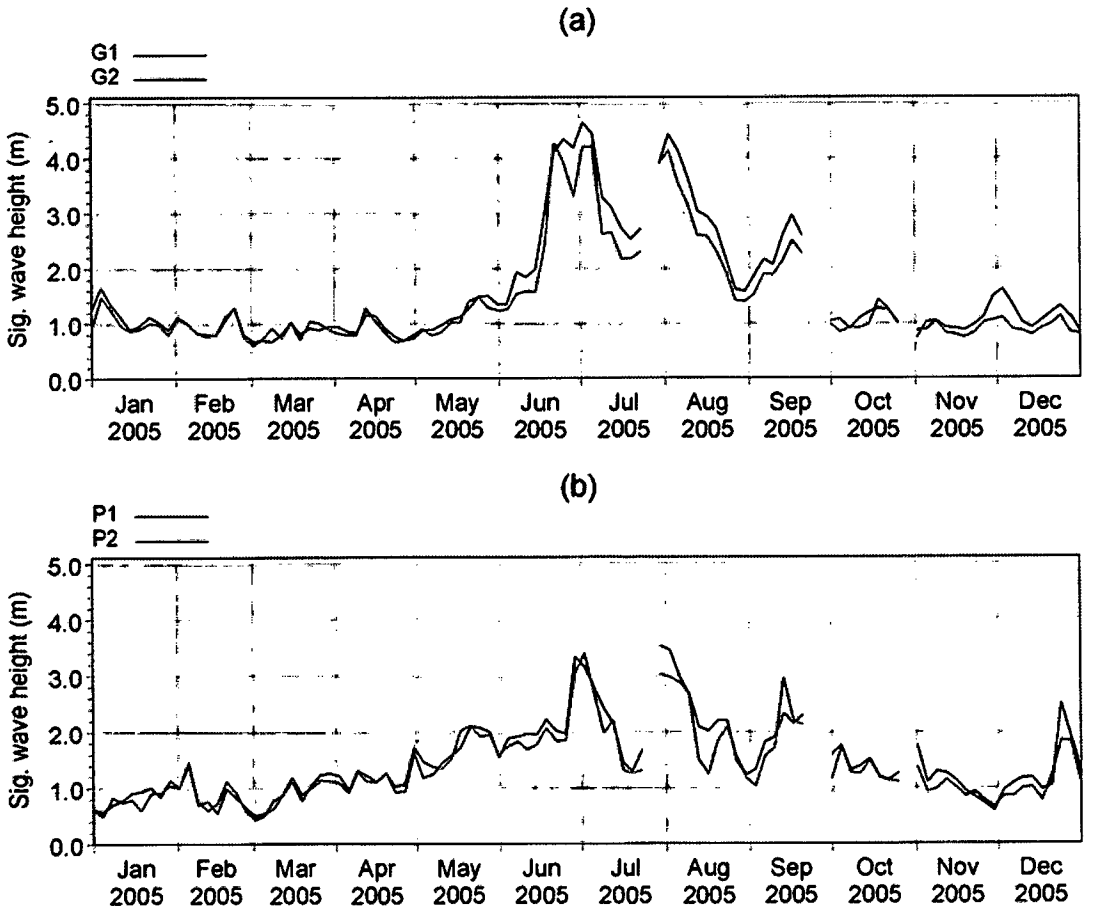

Figure 5-1. Jason-1 significant wave height distribution during 2005: (a) off Goa and (b) off Paradip.

5.2.2. Waves along nearshore regions

Local winds such as seas breeze play a major role in generating wind seas at the nearshore regions. Interaction of these wind seas with pre-existing swells modulates the waves in the nearshore regions. However, the resultant waves propagate into shallow waters. Once they begin to feel the bottom, significant changes occur in wave characteristics because of shoaling, refraction, etc.. To understand the characteristic changes that occur due to wave transformation, measured and modelled wave parameters at 2 different depths normal to coast are analysed. The results are discussed in the following sections.

5.2.2.1. Measurements

Wave data measured at two depths each off Goa, Ratnagiri and Dwarka have been analysed to study transformation in nearshore depths. Measurement points and bathymetry contours at each location are shown in Figure 5-2. Significant wave heights at these two depths off Goa, Ratnagiri and Dwarka are shown in Figure 5-3. It is found that gradients in water depths (offshore to nearshore) led to reduction in wave heights to some extent. But, the patterns are similar, since the bathymetry contours are nearly parallel to the coast at the measurement locations.

Wave attenuation at each location is estimated and given in Table 5-1. Mean values of significant wave heights, differences and percentage reduction in wave heights are calculated separately for wind sea, swell and resultant wave. The reduction in wave heights at 15m depth off Goa (9.3%) and Ratnagiri (9.4%) are nearly the same, whereas, it is much higher off Dwarka (22%). It has been found that the waves off Dwarka are dominated by wind seas during the study period, and the predominant wind seas are from NE (land to sea). The 15m depth contour off Dwarka is very close to the coast, and the fetch available is very limited. However, a fetch of approx. 9 km is available for NE winds at 30m depth, which is sufficient to generate moderate wind seas. Hence, wind seas in the NE direction (away from the coast) resulted in increase in H_s at 30 m depth.

The reduction in swell and wind sea heights at each location has been analysed. The least reduction in swell heights among the two water depths is observed off Goa (4.7%) and higher off Dwarka (15.6%). The reduction in swell H_s off Ratnagiri is 10.6%. This wave height reduction is explained only partially by refraction of waves that propagate onshore at large oblique angles (approx. 45°) with the depth contours (predominant swells are from SW/SSW). As described earlier (in Chapter 4), these are the longer swells propagating from south Indian Ocean. Interaction of waves with bottom produces a boundary layer,

which results in the loss of wave energy to the bed due to bottom friction (Bagnold, 1946). Small-scale bottom features contribute to the roughness of the bottom and determine the dissipation of wave energy in the bottom boundary layer (Zhukovets, 1963). Formation of vortex ripples and their feedback on the waves through enhanced bottom roughness are the primary mechanisms for wave attenuation across a sandy continental shelf. Sediments along the central west coast of India vary between fine sand and medium sand (Sanil Kumar et al., 2003c). The large reduction in wave heights off Dwarka indicates that bottom attenuation is higher compared to Ratnagiri and Goa regions.

The reduction in wind sea H_s off Goa, Ratnagiri and Dwarka are 16.1%, 9.0% and 27.8%, respectively. During sea breeze period, the waves off Goa are dominated by winds seas from NW (as described in Chapter 4). The reduction in short-period wind seas off Goa is much higher than the reduction in long-period swells (it is only 4.7% for swells). This suggest that the reduction is not due to direct wave-bottom interactions, but possibly due to heavy sediment suspension over the entire water column affecting the hydrodynamics of short-period waves (Sheremet and Stone, 2003). Since the observations have been made during pre-monsoon season, the prevailing sea breeze activity can cause sediment re-suspension (Masselink and Pattiaratchi, 1998). However, this has to be confirmed through detailed field study of distribution of bottom sediments and suspended sediments during pre-monsoon season. The large reduction in wind seas off Dwarka is attributed to the generation of NE wind seas, and their growth is towards offshore. Sufficient fetch is available at 30 m depth for NE wind seas compared to 15 m water depth.

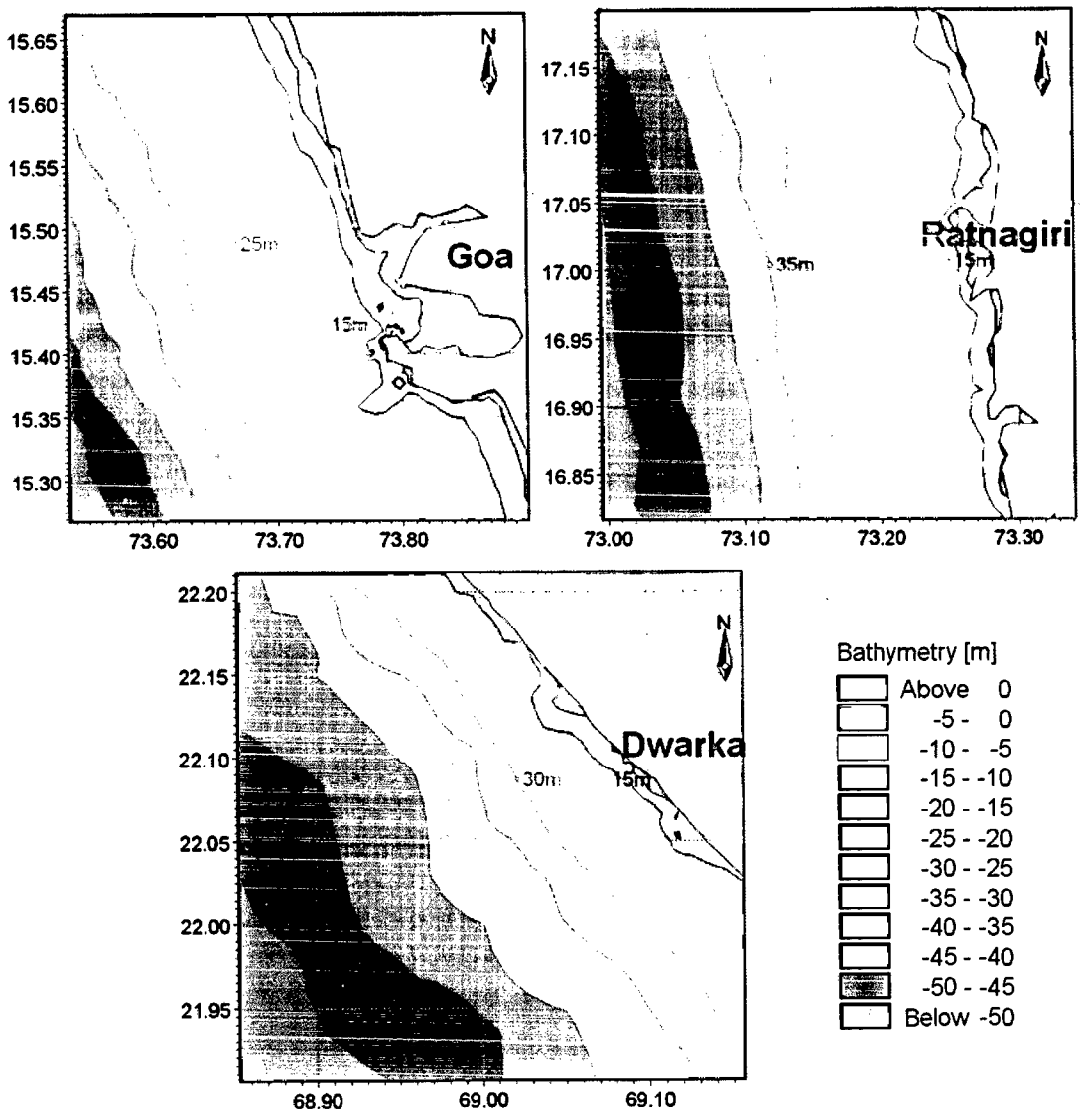

Figure 5-2. Measurement locations and bathymetry contours off Goa, Ratnagiri and Dwarka.

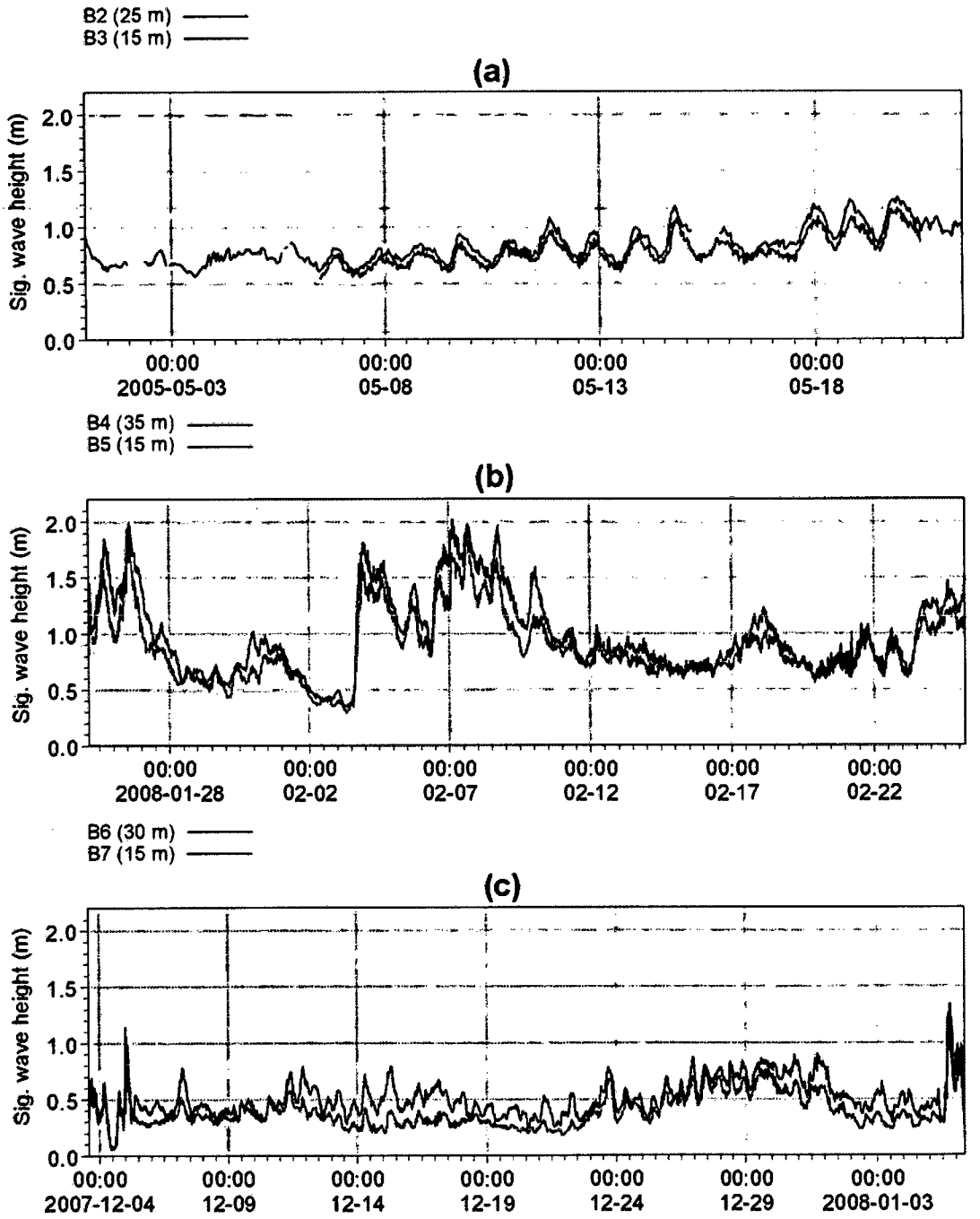

Figure 5-3. Significant wave heights measured at nearshore depths off: (a) Goa, (b) Ratnagiri and (c) Dwarka (locations are marked in Figure 2-2).

Table 5-1. Mean H_s and % reduction at various measurement locations along the west coast of India.

Regions		off Goa		off Ratnagiri		off Dwarka	
Locations		B2 (25 m)	B3 (15 m)	B4 (35 m)	B5 (15 m)	B6 (30 m)	B7 (15 m)
Resultant wave	Mean Hs (m)	0.86	0.78	0.96	0.87	0.50	0.39
	Difference (m)	0.08		0.09		0.11	
	% reduction	9.3		9.4		22.0	
Swell	Mean Hs (m)	0.64	0.61	0.66	0.59	0.32	0.27
	Difference (m)	0.03		0.07		0.05	
	% reduction	4.7		10.6		15.6	
Wind sea	Mean Hs (m)	0.56	0.47	0.67	0.61	0.36	0.26
	Difference (m)	0.09		0.06		0.10	
	% reduction	16.1		9.0		27.8	

5.2.2.2. Modelling results

Modelled wave parameters at various depths (100 m, 50 m, 30 m, 20 m, 10 m and 5 m) off Mumbai, Goa and Kochi (along the west coast of India) and off Nagappattinam, Visakhapatnam and Paradip (along the east coast of India) were analysed. Figure 5-4 shows significant wave heights at various depths off Mumbai, Goa and Kochi during 2005. The pattern of wave transformation is nearly the same. During the southwest monsoon, the significant wave heights show an increasing trend from the south to the north (Kochi to Mumbai). The wave dissipation between deep and shallow depths (100 m and 5 m) is higher for larger waves, since these waves start feeling the bottom at relatively deeper depths. Significant reduction in wave height is occurred at shallow depths for moderate and small waves. Kurian et al. (2009) reported that the sediments along the southwest coast of

India are fine sands (0.25 mm), and further north they are confined to the fine to medium sand (0.5 mm) category. It has been found that the reduction in wave height is minimum off Kochi and maximum off Mumbai, which is attributed to the varying bottom attenuation. This supports the observations by Kurian and Baba (1987) that the frictional attenuation increases towards north, though their study is limited to Kerala coast.

Significant wave heights off Mumbai, Goa and Kochi during pre-monsoon season are further illustrated in Figure 5-5. The diurnal variation in wave heights is found during pre-monsoon season (as described in Chapter 4) at all depths off Mumbai, Goa and Kochi, which is typical for the west coast of India. However, magnitude of variation reduces from the north to the south, indicating that sea breeze and its effect on wind sea generation decreases from the north to the south.

Seasonal and annual statistics (mean and standard deviation) of significant wave heights at various depths off Mumbai, Goa and Kochi are listed in Table 5-2. The seasonal variations in mean H_s are graphically represented in Figure 5-6. Significant reduction in wave heights due to bottom dissipation has been observed at shallow depths. Large waves off Mumbai and Goa, and relatively lower waves off Kochi are observed. The mean H_s during pre-monsoon and NE monsoon seasons off Kochi are nearly the same and relatively low compared to the SW monsoon waves as well as waves off Goa or Mumbai. However, H_s is marginally higher off Goa and Mumbai during the pre-monsoon season compared to NE monsoon waves. It is evident that sea breeze adds up sufficient energy to the waves prevailing in the nearshore region off the west coast of India during pre-monsoon season, and it is highly visible off Mumbai and Goa regions.

Significant wave heights at various water depths off Nagappattinam, Visakapattinam and Paradip during 2005 are shown in Figure 5-7. Waves are small during pre-monsoon season and higher during SW and NE monsoon seasons. Significant wave height is maximum (around 3.0 m) during southwest monsoon season. Wave patterns are nearly the same all along the east coast of India. Wave heights show increasing trend during pre-monsoon and SW monsoon seasons, and decreasing trend during NE monsoon season (October – January) from south to north (Nagappattinam to Paradip). During extreme events, the wave heights are even higher. Sanil Kumar et al. (2004c) found that during the passage of a cyclone in November 1998, the maximum wave height observed off Visakhapatnam was 5.74 m. Aboobacker et al (2009) reported that significant wave height off Paradip during another cyclone in May 1996 was 4.2 m.

During the NE monsoon season, the wind wave grows towards south due to energy transfer from NE winds to the waves. Hence, higher waves are observed along the southeast coast of India during the NE monsoon season. Significant reduction in wave height due to bottom dissipation is noticed when the significant wave heights at depths 100, 50, 30, 20, 10 and 5 m off Nagappattinam, Visakapattinam and Paradip are analysed. However, the reduction among various depths is relatively less as compared to those along the west coast of India, as the depth contours along the east coast of India are more closer than those along the west coast of India (continental shelf is narrow along the east of India). Bottom dissipation causes higher reduction in wave heights over a wide continental shelf (Ardhuin et al., 2003).

Figure 5-8 shows the significant wave heights off Nagappattinam, Visakapattinam and Paradip during pre-monsoon season. Even though, there are variations in wave heights, a well-defined diurnal pattern (as seen along the west coast of India) is not present along the east coast of India during the pre-monsoon season.

Seasonal and annual mean and standard deviation of significant wave heights at various depths off Nagappattinam, Visakapattinam and Paradip are listed in Table 5-3. Seasonal distribution of mean H_s is graphically represented in Figure 5-9 also. The mean H_s is relatively low at all locations along the east coast of India compared to those along the west coast of India. Significant reduction due to bottom dissipation is occurred at lower depths (below 20 m) during all the seasons. The waves off Paradip and Visakapattinam are higher during SW monsoon season, and waves off Nagappattinam are higher during the NE monsoon season. It is evident that wave heights are in the increasing order of magnitude during SW monsoon season from Nagappattinam to Paradip (south to north), and in the decreasing order of magnitude during NE monsoon season. A slight increase in wave height is noticed from south to north during pre-monsoon season.

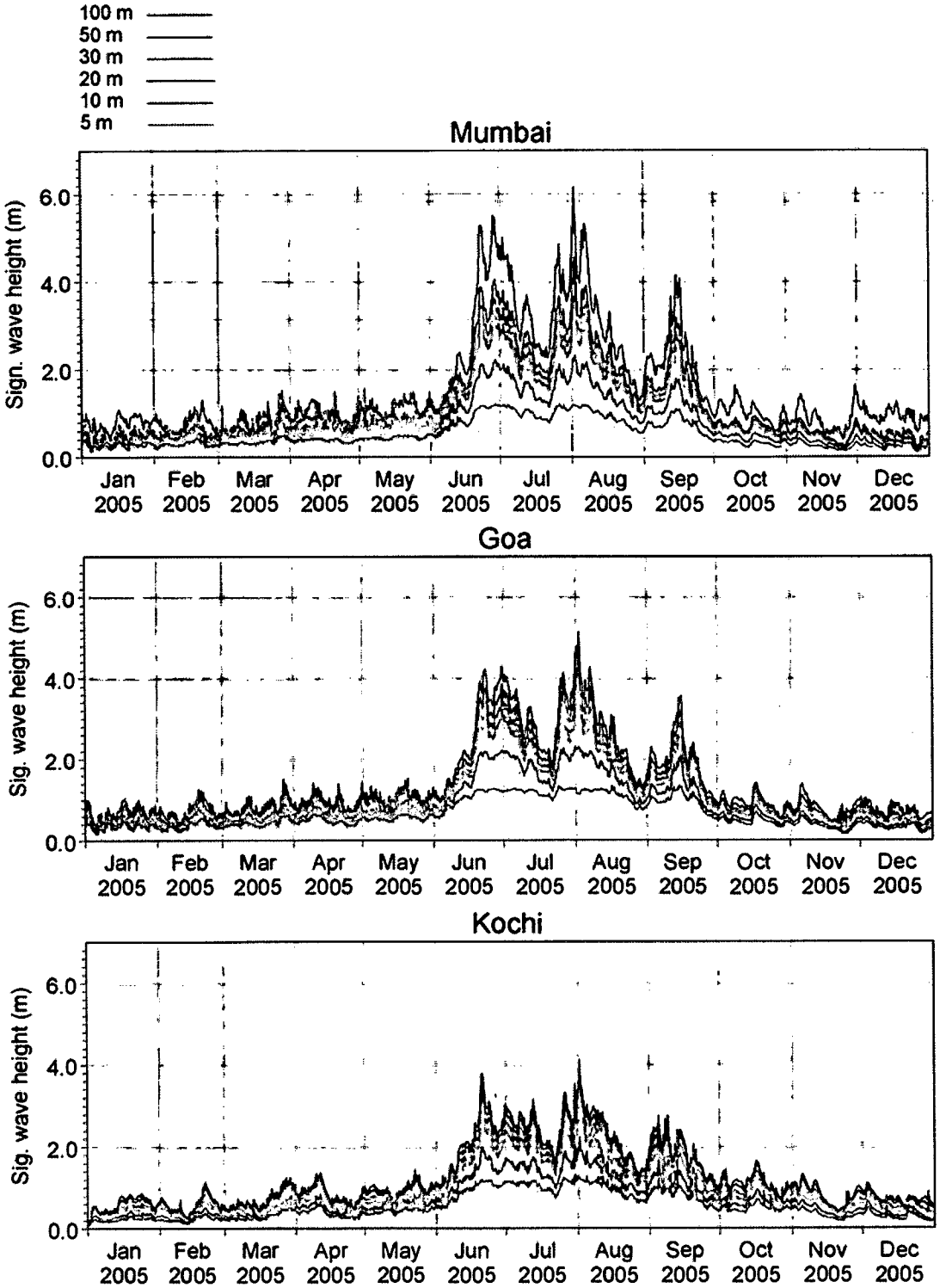

Figure 5-4. Significant wave heights at various water depths off Mumbai, Goa and Kochi during 2005.

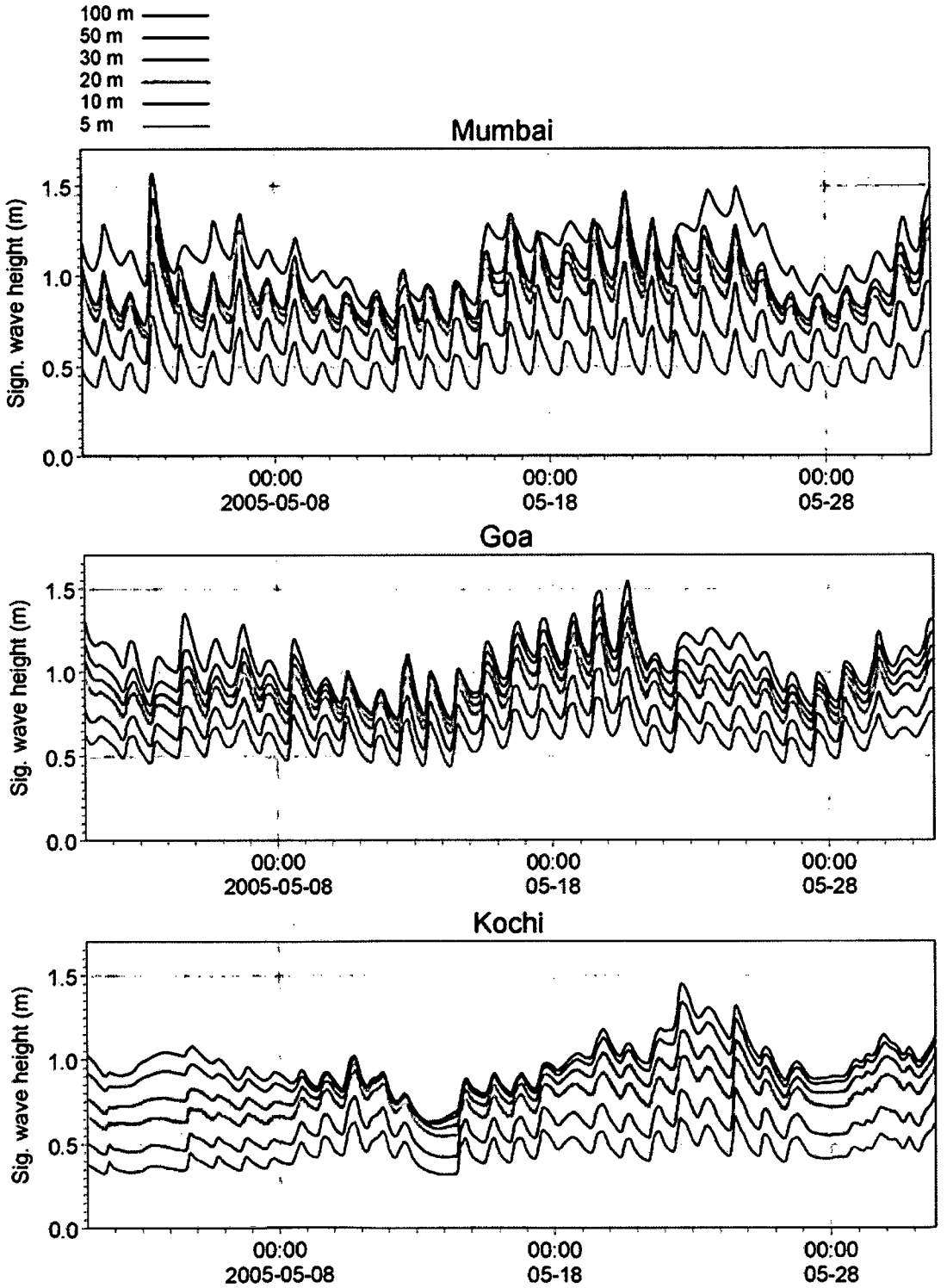

Figure 5-5. Diurnal variations in significant wave heights at various water depths off Mumbai, Goa and Kochi during pre-monsoon season (May 2005).

Table 5-2. Seasonal and annual mean and standard deviation of significant wave heights at various depths off Mumbai, Goa and Kochi.

Seasons	Water depth (m)	Significant wave height (m)					
		Mumbai		Goa		Kochi	
		Mean	S.D.	Mean	S.D.	Mean	S.D.
Pre-monsoon	100	0.92	0.24	0.89	0.22	0.79	0.24
	50	0.77	0.22	0.81	0.21	0.74	0.23
	30	0.75	0.21	0.76	0.20	0.66	0.21
	20	0.71	0.20	0.70	0.18	0.59	0.19
	10	0.58	0.15	0.59	0.15	0.45	0.15
	5	0.42	0.11	0.49	0.13	0.34	0.12
SW monsoon	100	2.88	1.19	2.56	0.96	2.18	0.63
	50	2.29	0.86	2.33	0.84	2.07	0.59
	30	2.09	0.75	2.14	0.76	1.91	0.55
	20	1.89	0.66	1.95	0.69	1.72	0.49
	10	1.38	0.44	1.55	0.47	1.28	0.34
	5	0.89	0.22	1.07	0.20	0.93	0.21
NE monsoon	100	0.90	0.23	0.78	0.20	0.82	0.27
	50	0.57	0.16	0.68	0.18	0.76	0.26
	30	0.52	0.15	0.61	0.16	0.67	0.24
	20	0.48	0.13	0.55	0.15	0.59	0.21
	10	0.38	0.10	0.45	0.13	0.45	0.17
	5	0.27	0.07	0.37	0.10	0.33	0.13
Annual	100	1.57	1.18	1.42	1.00	1.26	0.77
	50	1.21	0.93	1.27	0.91	1.19	0.74
	30	1.12	0.83	1.17	0.83	1.08	0.69
	20	1.03	0.74	1.07	0.76	0.97	0.63
	10	0.78	0.51	0.86	0.57	0.72	0.46
	5	0.52	0.30	0.64	0.34	0.54	0.32

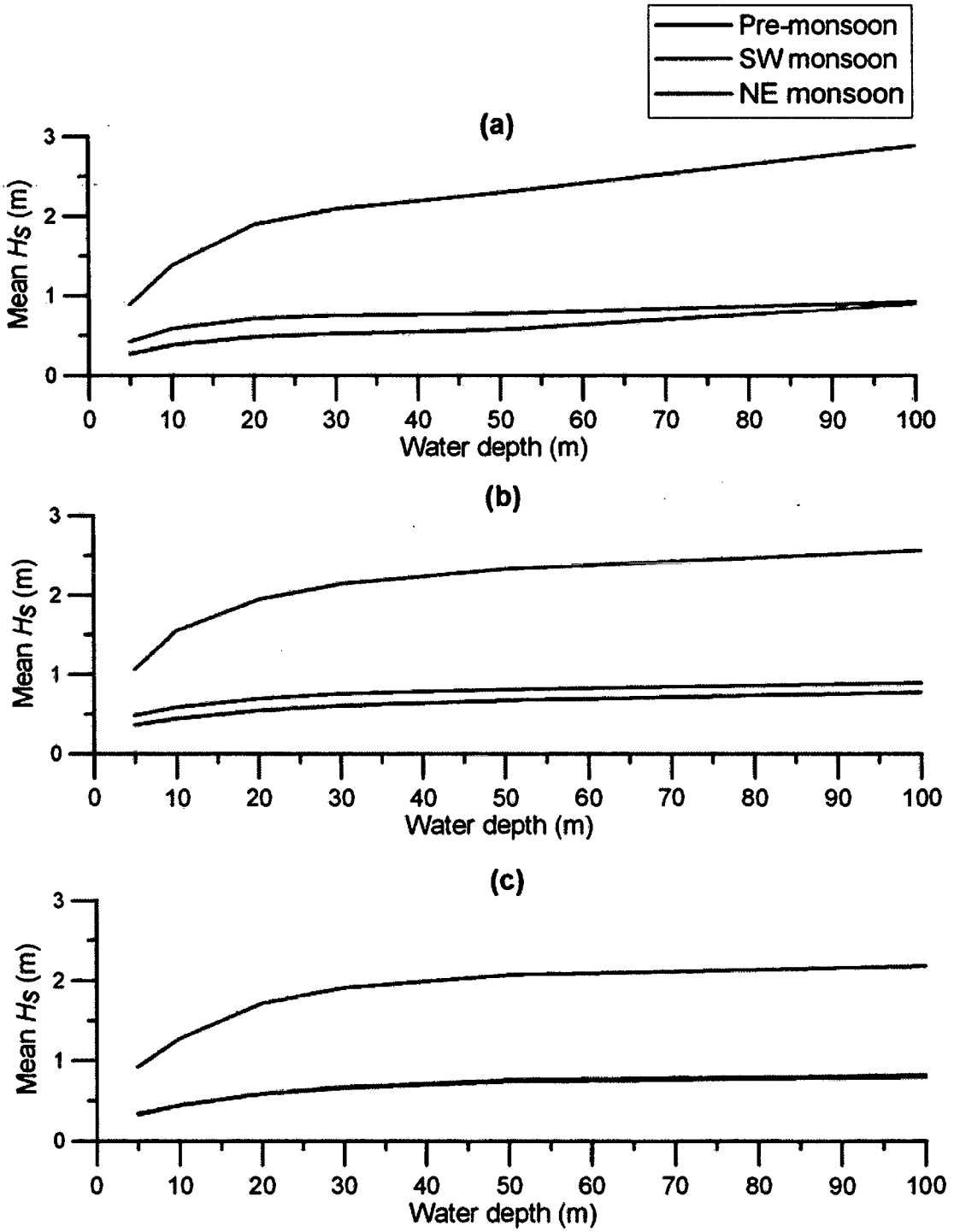

Figure 5-6. Mean H_s at various depths ranging from 100 to 5 m during pre-monsoon, SW monsoon and NE monsoon seasons off: (a) Mumbai, (b) Goa and (c) Kochi.

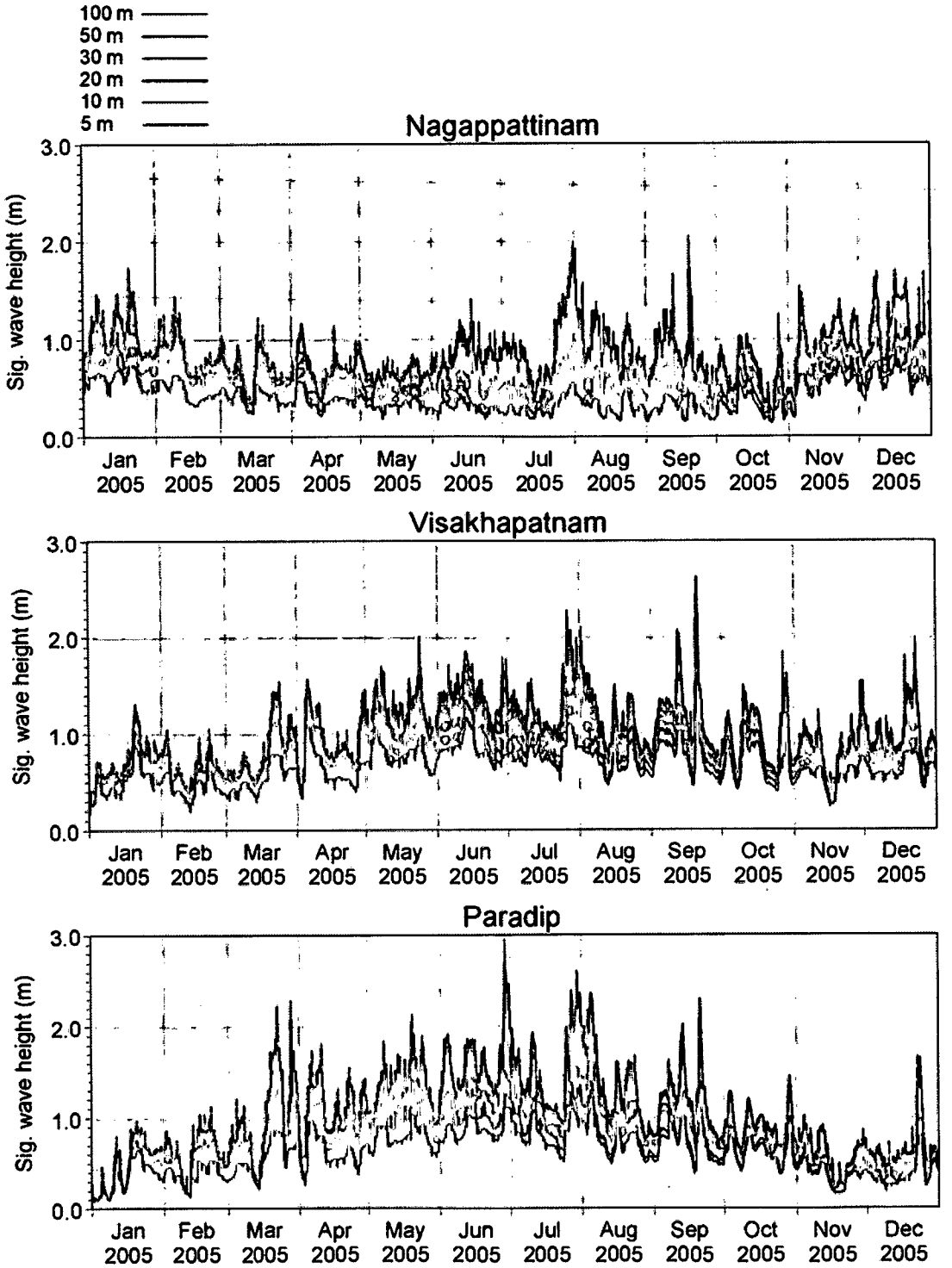

Figure 5-7. Significant wave heights at various water depths off Nagappattinam, Visakhapatnam and Paradip during 2005.

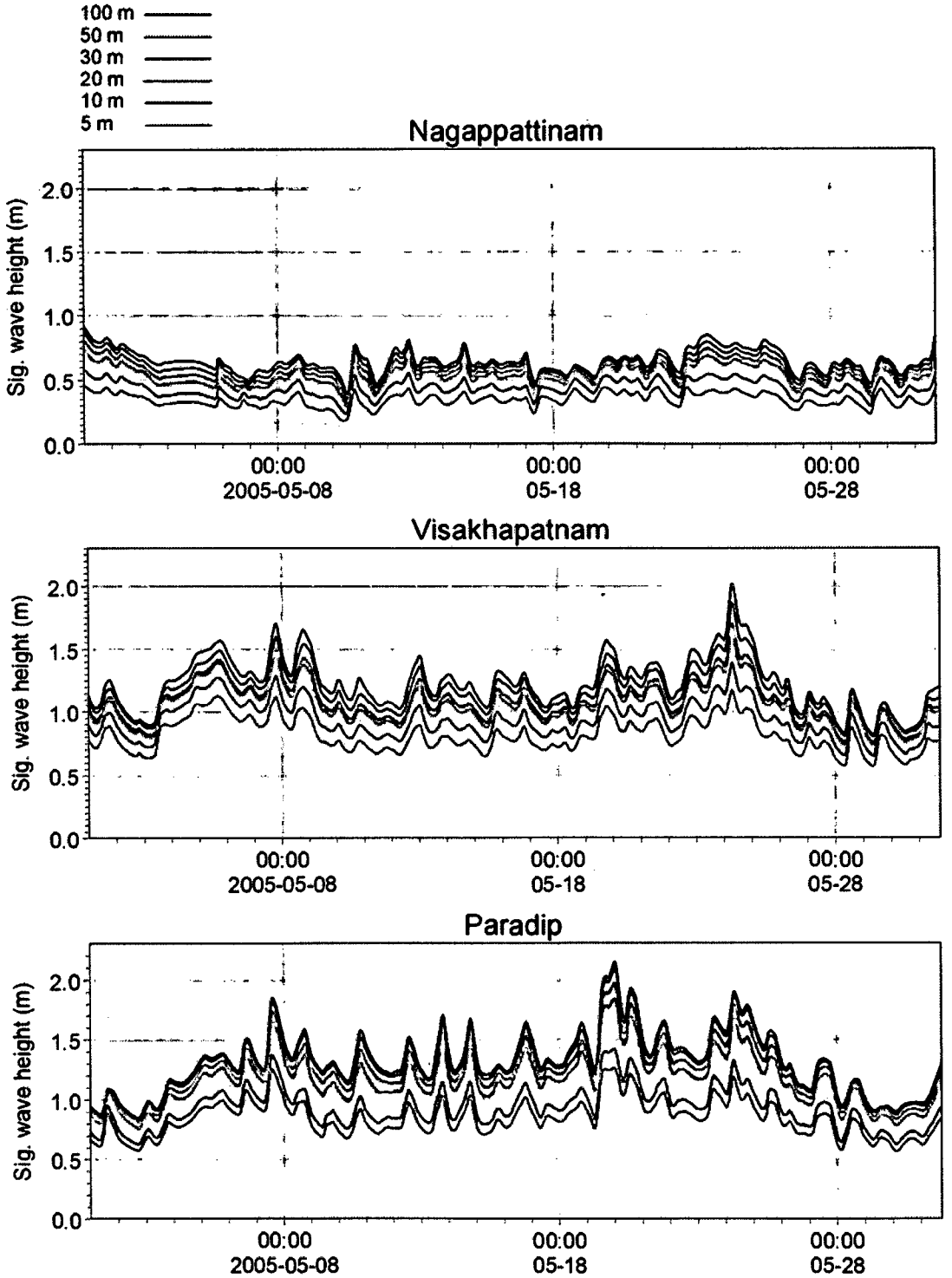

Figure 5-8. Significant wave heights at various water depths off Nagappattinam, Visakhapatnam and Paradip during pre-monsoon season (May 2005).

Table 5-3. Seasonal and annual mean and standard deviation of significant wave heights at various depths off Nagappattinam, Visakapattinam and Paradip.

Seasons	Water depth (m)	Significant wave height (m)					
		Nagappattinam		Visakapattinam		Paradip	
		Mean	S.D.	Mean	S.D.	Mean	S.D.
	100	0.71	0.18	0.89	0.32	0.99	0.41
	50	0.69	0.18	0.86	0.30	0.97	0.40
	30	0.66	0.18	0.82	0.28	0.93	0.37
	20	0.63	0.17	0.80	0.27	0.88	0.35
	10	0.53	0.15	0.72	0.23	0.72	0.27
Pre-monsoon	5	0.43	0.12	0.64	0.20	0.66	0.24
	100	0.82	0.26	1.27	0.31	1.41	0.41
	50	0.76	0.24	1.18	0.27	1.37	0.39
	30	0.69	0.22	1.08	0.24	1.27	0.35
	20	0.61	0.20	1.03	0.23	1.17	0.31
	10	0.45	0.15	0.91	0.19	0.90	0.22
SW monsoon	5	0.34	0.11	0.79	0.16	0.80	0.20
	100	0.94	0.30	0.89	0.29	0.65	0.28
	50	0.92	0.30	0.84	0.26	0.64	0.28
	30	0.89	0.30	0.80	0.24	0.61	0.26
	20	0.84	0.29	0.77	0.23	0.57	0.24
	10	0.67	0.23	0.69	0.19	0.47	0.20
NE monsoon	5	0.53	0.18	0.61	0.16	0.43	0.18
	100	0.83	0.27	1.02	0.36	1.02	0.48
	50	0.79	0.27	0.96	0.32	0.99	0.47
	30	0.75	0.26	0.90	0.28	0.94	0.43
	20	0.69	0.25	0.87	0.27	0.87	0.39
	10	0.55	0.20	0.77	0.23	0.69	0.29
Annual	5	0.43	0.16	0.68	0.19	0.63	0.26

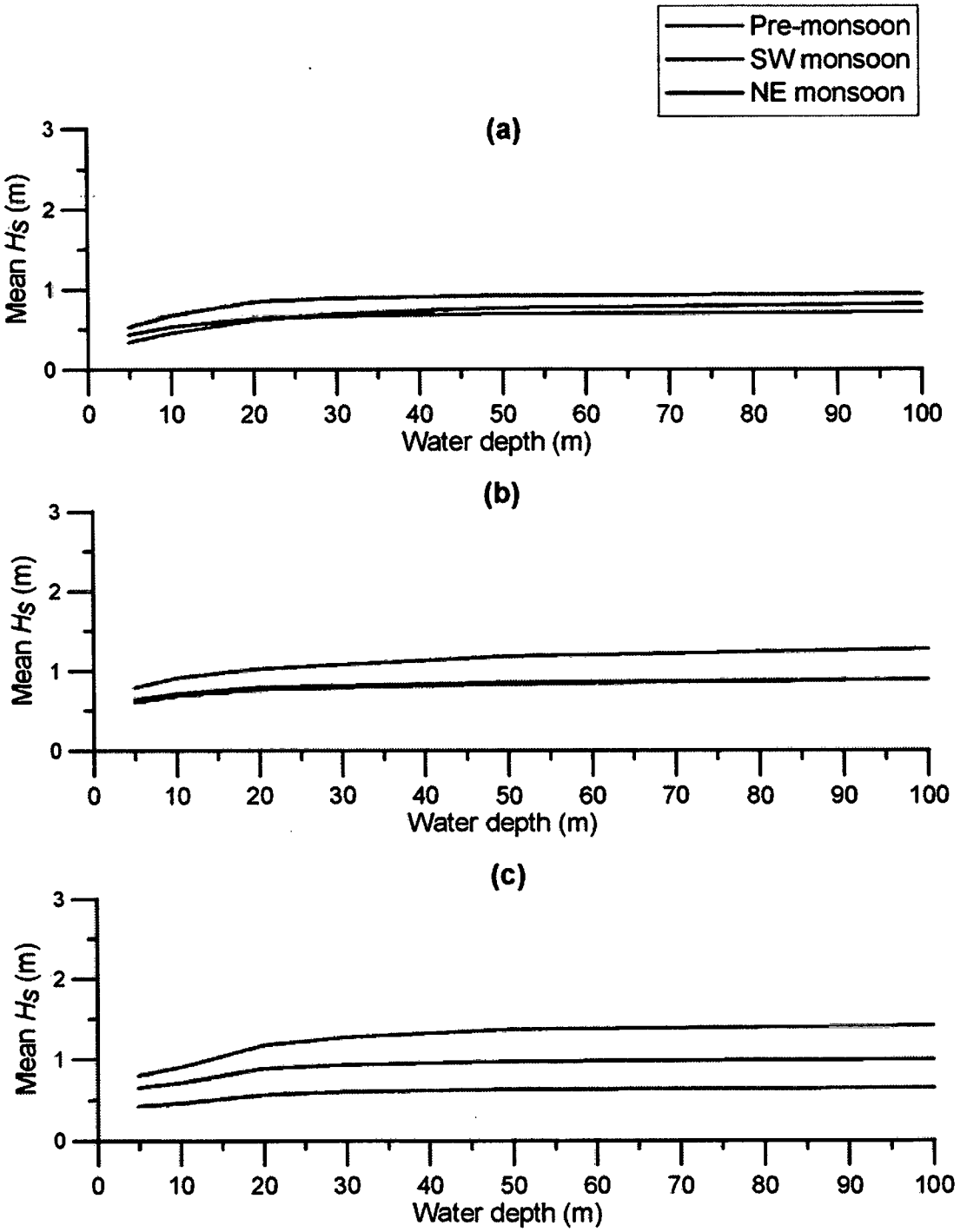

Figure 5-9. Mean H_s at various depths ranging from 100 to 5 m during pre-monsoon, SW monsoon and NE monsoon seasons off: (a) Nagappattinam, (b) Visakapattinam and (c) Paradip.

5.3. Wave transformation at semi-enclosed regions

Wave transformation at two semi- enclosed areas, Dhamra Port (naturally protected), situated on the east coast and Mormugao Port (artificially protected), located on the west coast, has been studied. Non-directional wave gauge data available for the inner channel of the Dhamra Port during 12 July – 13 Aug 2005 has been used for validation; no measurements are available inside the Mormugao Port. Numerical model has been set up for the Dhamra Port and the Mormugao Port regions by including diffraction effects.

5.3.1. Dhamra Port – naturally protected area

Dhamra Port is situated along the northern part of the east coast of India (Figure 1-5). Figure 5-10 show flexible mesh and bathymetry of the Dhamra region. The Port and inner channel are sheltered from the direct impact of waves due to the Dhamra River Delta (Kanika sands), which acts as a natural breakwater. Hence, major part of the wave energy gets dissipated at the delta and the remaining energy propagates towards the Port and surrounding areas.

Waves off Dhamra have been simulated for 2005 (model domain is shown in Figure 3-4b in Chapter 3). The two measurement locations, offshore (B10) and inner channel (C1), are marked in Figure 5-10. A comparison between measured and modelled wave parameters at B10 is shown in Figure 5-11, and the match is very good. Similarly, measured and modelled wave parameters at the inner channel (C1) have been compared, and the match is good (Figure 5-12). This experiment indicates that the model simulates waves in the semi-enclosed regions very accurately.

Wave parameters at three different locations, namely, an open area south of Gahirmatha at 12 m water depth (B10), an open area outside the channel at 11 m depth (O1) and a sheltered area at the inner channel at 6 m water depth (C1), have been analysed. Figure 5-13 shows the significant wave height and mean wave direction at locations B10, O1 and C1. Gahirmatha beach and surrounding mangrove areas prevent the waves fully from SSE to SSW, and partially from ESE to SE direction to reach the Port region. The Kanika sands in front of the Dhamra region, prevent the waves (fully) from ENE to E and the waves (partially) from NNE to NE entering the Port (SW to N are covered by land). It is seen from Figure 5-13 that the waves at an offshore location, say B10, are predominantly from S during pre-monsoon and SW monsoon seasons and between NE and E during NE monsoon season. Waves from these directions are obstructed by the above land forms and mangrove areas. They undergo diffraction while propagating towards the Port region. Hence, the

diffracted waves are predominantly observed at the Port and the inner channel (C1). Due to diffraction and bottom friction, large amount of wave energy gets dissipated, and hence the waves with low heights are observed at C1. The waves at C1 are least attenuated during the NE monsoon season and most attenuated during SW monsoon season.

At O1, the predominant waves are between ESE and SSE during pre-monsoon and SW monsoon seasons and between NE and E during NE monsoon season. Gahirmatha land prevents the waves from S and SW to reach at O1. The bathymetry contours near O1 is normal to ENE direction, and hence large waves will refract and propagate normal to the bathymetry contours. During pre-monsoon season, the predominant waves in deep water location are from S and undergo refraction at O1 upto 30° deviation (from S to SSE). During SW monsoon, the waves are even larger and undergo significant refraction at O1 upto 40° (from S to SE). These waves will refract further while moving towards C1, and in combination with diffraction, a large reduction in wave height has been observed during pre-monsoon and SW monsoon seasons.

During NE monsoon season, the waves are relatively small. Wave heights are nearly the same at locations B10 and O1, since the bottom effects are minimum at these depths for small waves. Significant reduction in wave heights due to diffraction and refraction have been observed at C1, and the predominant propagation directions are between NNE and NE. Maximum, mean and standard deviation of significant wave heights at B10, O1 and C1 are listed in Table 5-4. The maximum values observed at B10, O1 and C1 are 2.3, 1.2 and 0.38 m, respectively, and the mean values are 0.74, 0.4 and 0.07 m with standard deviations of 0.38, 0.19 and 0.06 m, respectively. This indicates that the significant wave heights are reduced significantly while propagating from offshore to the inner channel off Dhamra, mainly due to diffraction and bottom dissipation caused by the natural protection such as Kanika sands and mangroves in the vicinity of Dhamra region.

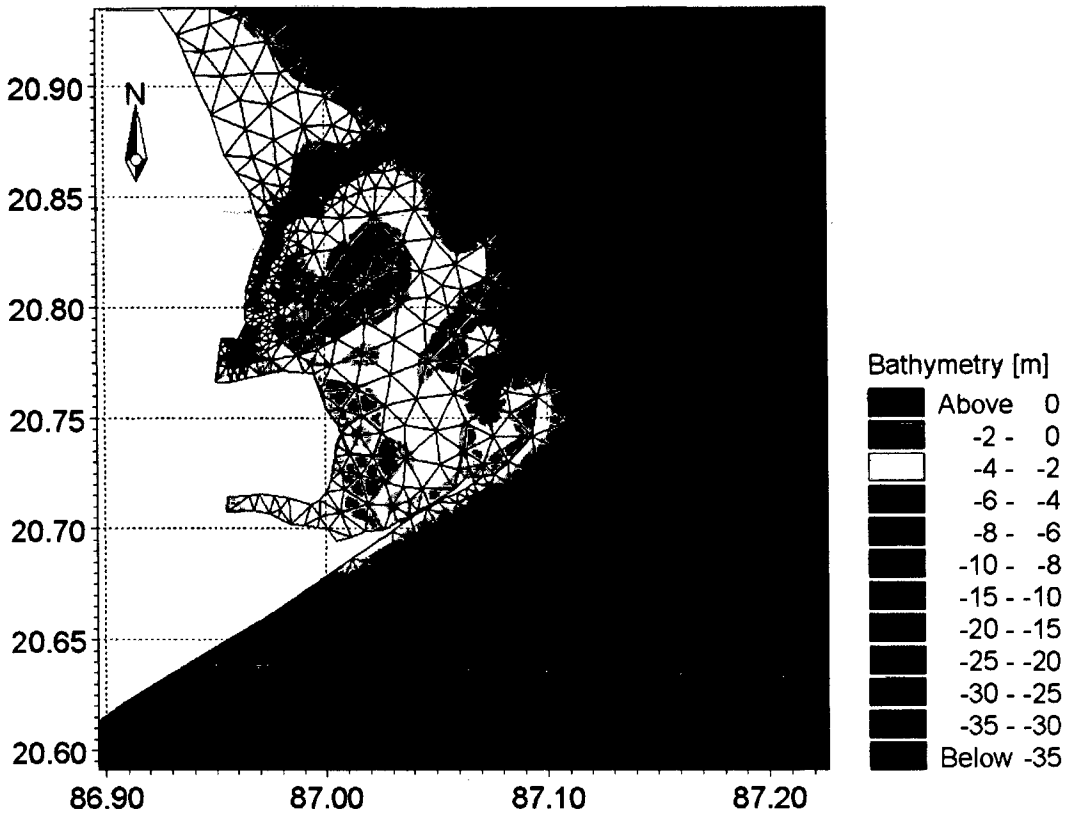

Figure 5-10. Flexible mesh and bathymetry close to the Dhamra region.

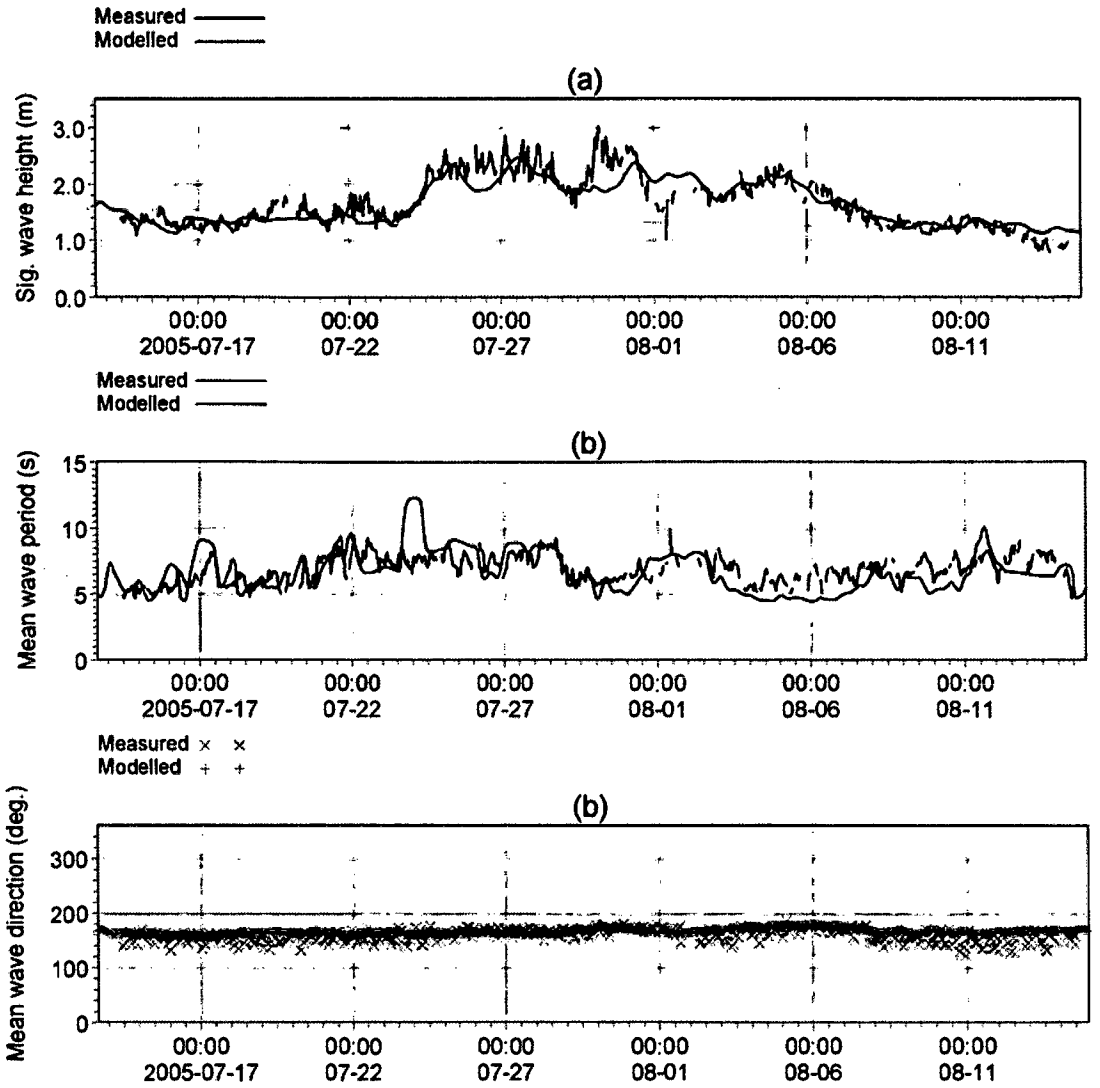

Figure 5-11. Comparison between measured and modelled wave parameters at location B10: (a) significant wave height, (b) mean wave period and (c) mean wave direction.

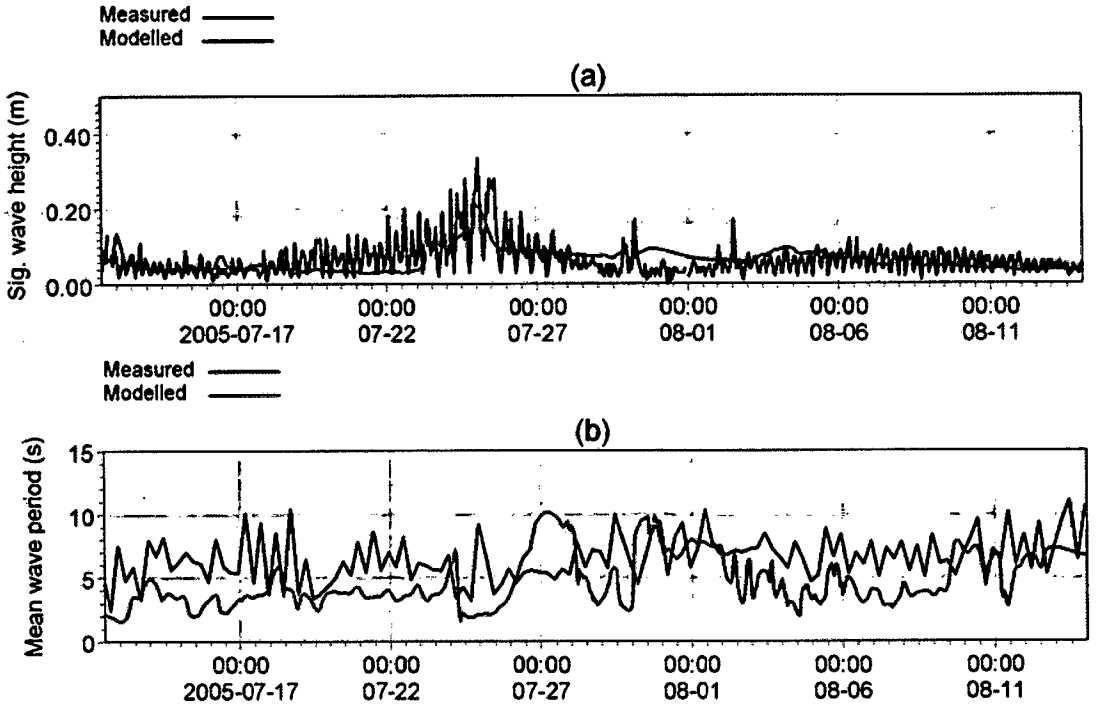

Figure 5-12. Comparison between measured and modelled (a) significant wave height and (b) mean wave period off Dhamra (at C1).

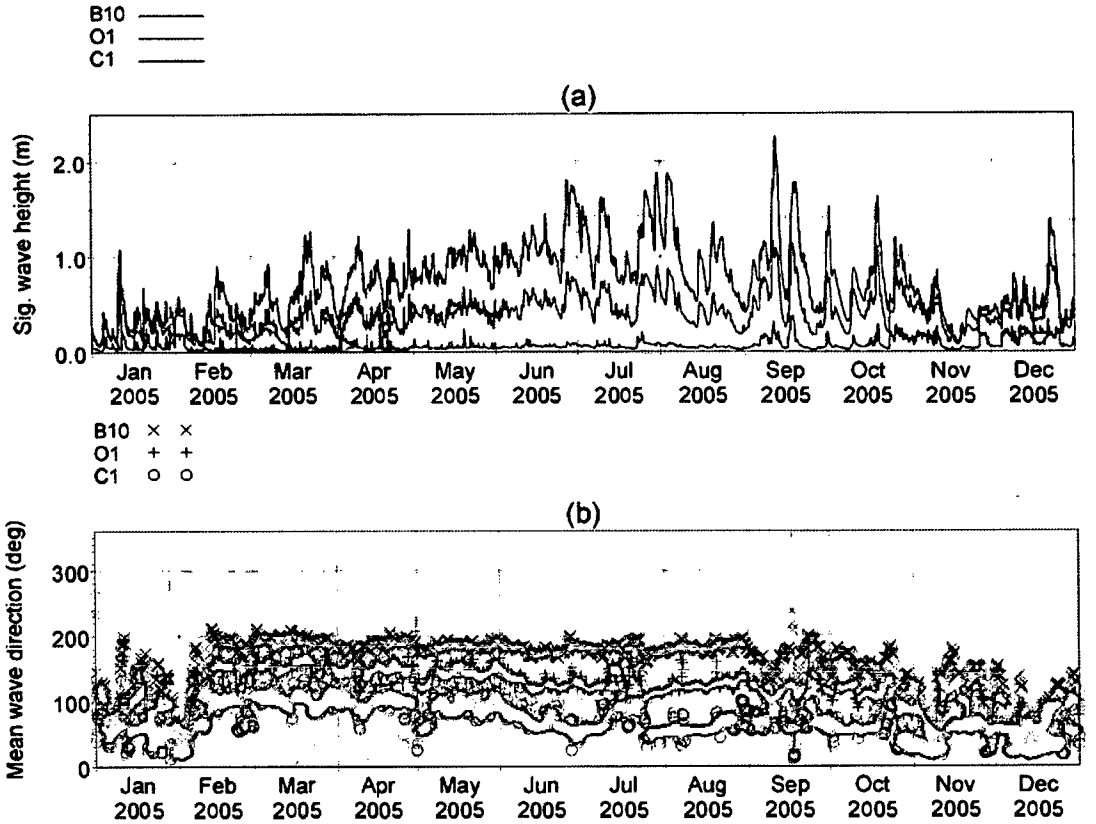

Figure 5-13. (a) significant wave height and (b) mean wave direction, at locations B10, O1 and C1 during 2005.

Table 5-4. Maximum, mean and standard deviation of significant wave heights during 2005 in the vicinity of Dhamra Port.

Location	Significant wave height (m)		
	Maximum	Mean	Standard deviation
B10	2.30	0.74	0.38
O1	1.20	0.40	0.19
C1	0.38	0.07	0.06

5.3.2. Mormugao Port – artificially protected area

Mormugao Port is protected from direct impact of waves due to breakwaters (Figure 1-4b). The breakwaters help to dissipate the wave energy in front of the port; minimum wave

energy only propagates to the area inside the port, which is mainly caused by diffraction. Features like reflection and overtopping are not incorporated in the numerical study.

Since, there are no measurements available inside the Port, the sensitivity of the model has been tested with available data at nearshore depths; measured data at B2 (25 m) and B3 (15 m). Model domain was selected considering the west open boundary at 25 m depth contour; measured data at B2 was used as the boundary conditions. The other two open boundaries (north and south) are considered as symmetrical. Figure 5-14 shows the model domain and flexible mesh bathymetry used for the wave transformation simulations off Mormugao Port region. The waves at B2 during 01-21 May 2005 are subject to transformation. The modelled wave parameters at B3 were extracted and compared with measurements (Figure 5-15) and the match is excellent.

Considering the measured wave parameters at B1 during Feb 1996 – May 1997 as boundary conditions, the waves at Mormugao Port region were simulated to study the transformation in all seasons. The wave parameters at three different locations, outside the breakwater (OP) and inside the Port (IP1 and IP2), were extracted. The extraction locations are marked in Figure 5-14b.

Figure 5-16 shows the significant wave height and mean wave direction at locations B1 (the boundary data), OP, IP1 and IP2 during Feb 1996 – May 1997. The location B1 is open to the waves from all directions, and OP is open to the waves between SW and NW. Diffracted and refracted waves from other directions also propagate towards OP. Since water depth at OP is shallow (9 m), larger waves will get dissipated due to bottom friction to some extent. The bottom contours at OP are normal to the west. Hence, the waves tend to travel in the W direction due to refraction. Even though, significant reduction in wave heights occurs at OP, the waves are still larger for carrying out the port operations. Diffraction takes place around the breakwater and diffracted waves with low energy propagate into the port. Wave heights at IP1 and IP2 are significantly low during any season and extreme events. The highest significant wave height observed at 23 m depth off Goa during a tropical cyclone in the Arabian Sea is 5.8 m. However, simulations show that the associated significant wave heights at OP, IP1 and IP2 are 2.62, 0.89 and 0.33 m, respectively. Maximum, mean and standard deviation of the significant wave heights during February 1996 – May 1997 at locations OP, IP1 and IP2 are given in Table 5-5. The mean significant wave heights at OP, IP1 and IP2 are 0.66, 0.23 and 0.08 m, respectively, and the corresponding standard deviations are 0.47, 0.17 and 0.06, respectively.

Larger waves are experienced during southwest monsoon and relatively low during pre-monsoon and post-monsoon seasons. The waves at B1 during SW monsoon are predominantly in the WSW direction. Due to refraction, it has been aligned to W at OP with a mean deviation of 10°. During pre-monsoon and NE monsoon seasons, the waves at B1 are predominantly in the SW and NW directions. The mean deviations in the predominant direction at OP are 20° from SW to WSW and 10° from NW to WNW, which are due to refraction (bathymetry contours are oriented to W).

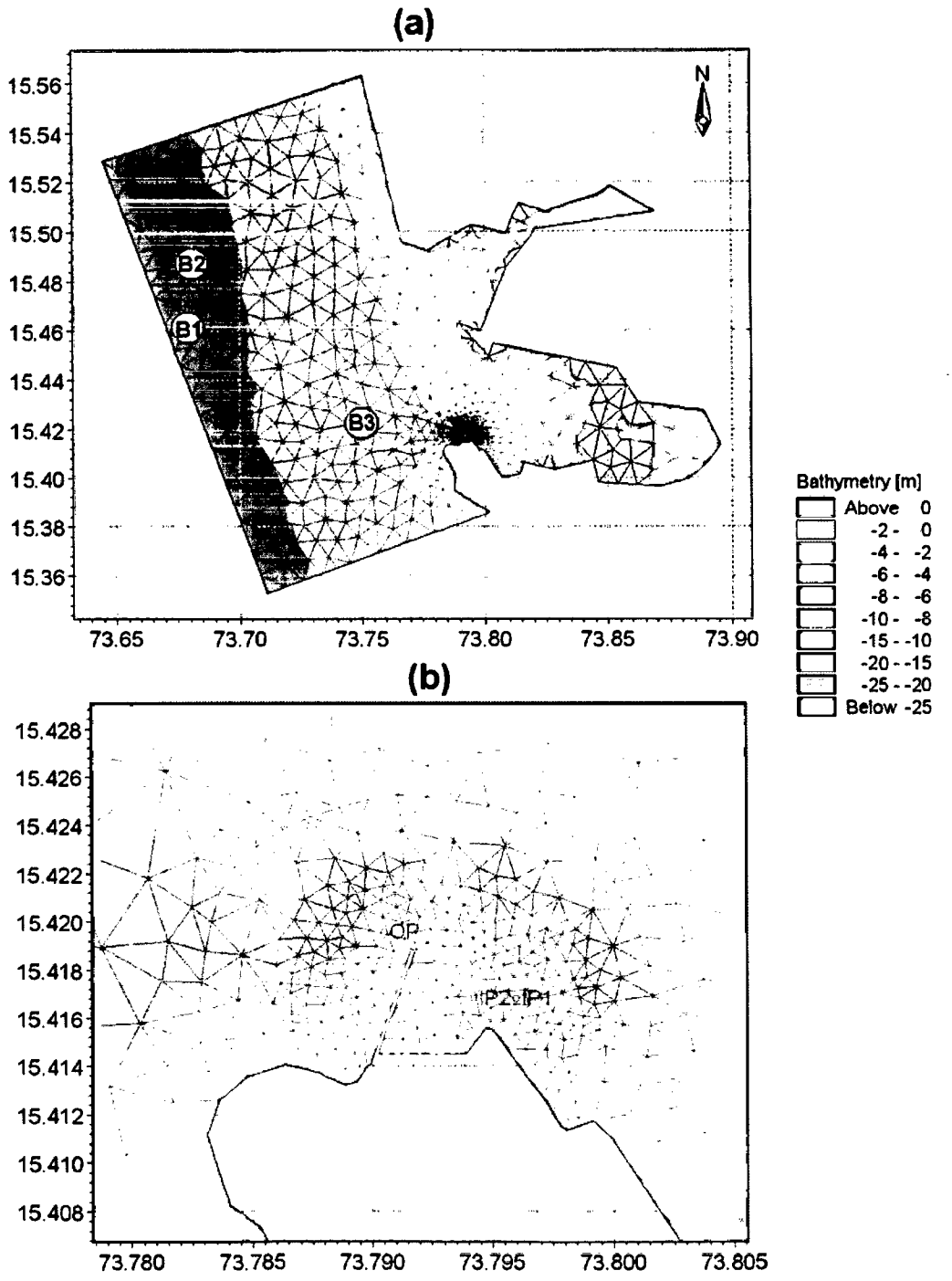

Figure 5-14. (a) Model domain and flexible mesh selected for the wave transformation simulations off Goa and (b) Flexible mesh and bathymetry close to the Port and extraction locations - outside breakwater (OP) and inside breakwater (IP1 and IP2).

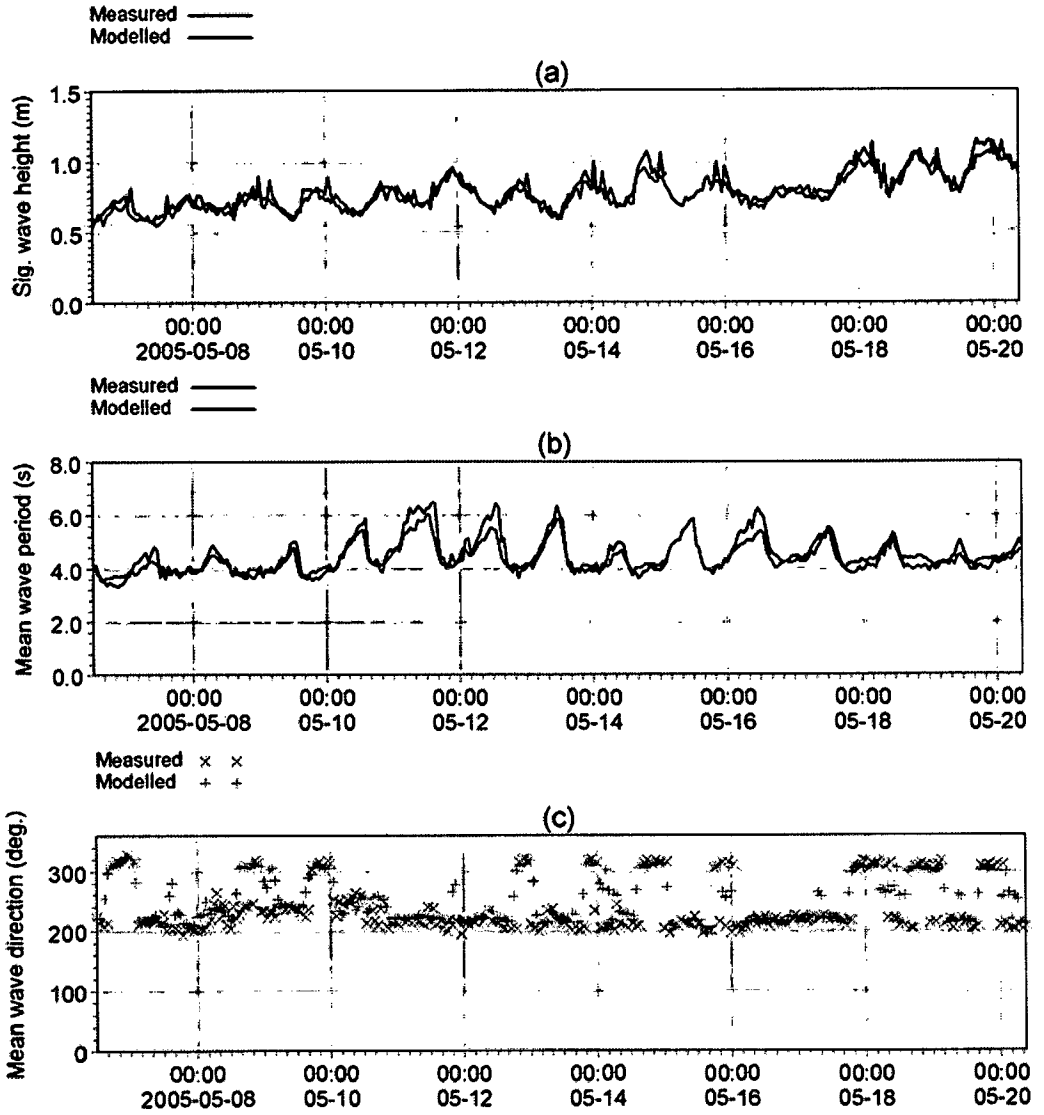

Figure 5-15. Comparison between measured and modelled wave parameters at location B3.

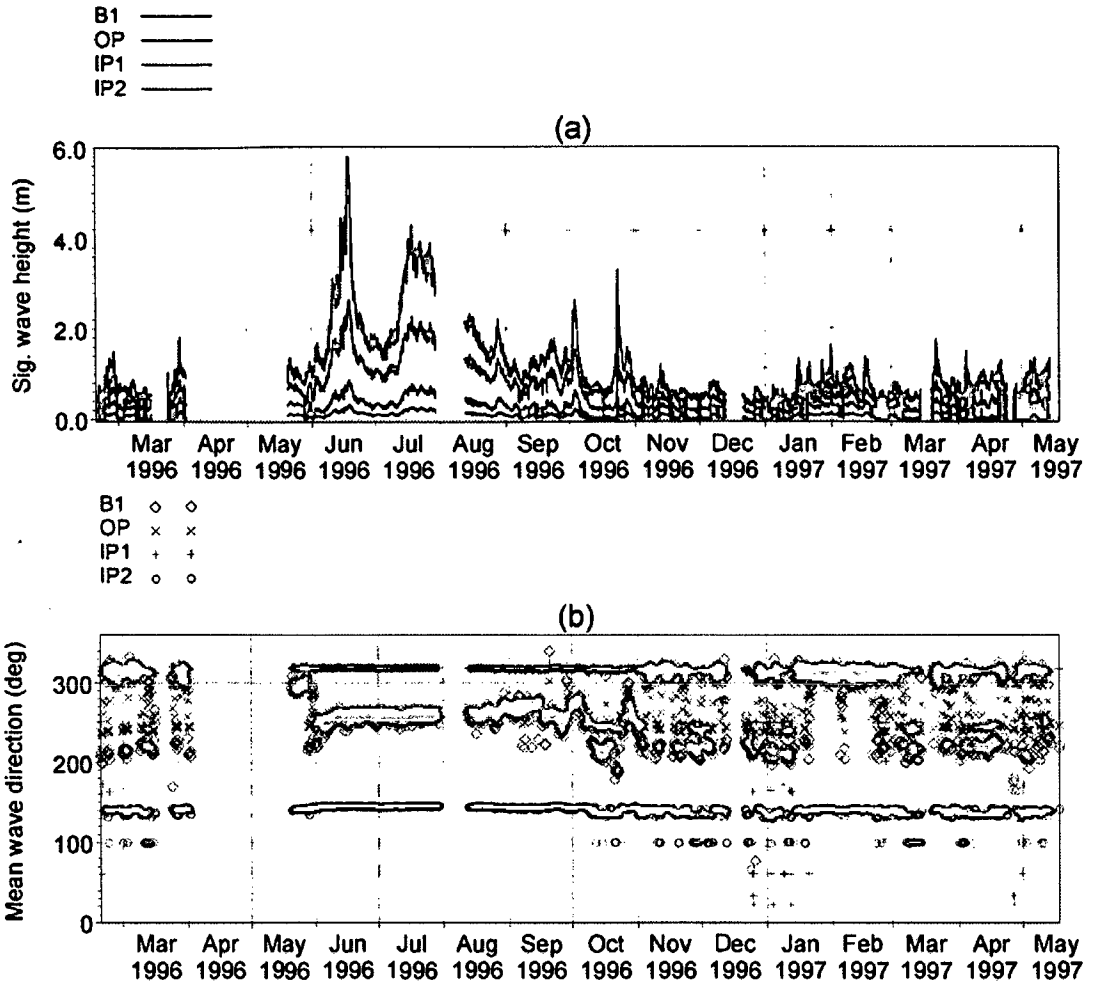

Figure 5-16. Significant wave height and mean wave direction obtained at locations OP, IP1 and IP2 during Feb 1996 – May 1997.

Table 5-5. Maximum, mean and standard deviation of significant wave heights during February 1996 – May 1997 in the vicinity of Mormugao Port.

Location	Significant wave height (m)		
	Maximum	Mean	Standard deviation
OP	2.62	0.66	0.47
IP1	0.89	0.23	0.17
IP2	0.33	0.08	0.06

5.4. Inland vessel's limit off Mormugao Port – a case study

5.4.1. Introduction

Winds, waves and currents are the important driving forces which generate several oceanic phenomena in the coastal and open ocean. Information on winds and waves are very essential for activities such as exploitation of natural resources, ship-routing, design of harbours, breakwaters and jetties, loading & unloading of products from the vessels and navigation of different types of vessels in the coastal region. The lack of adequate reliable wind and wave data has long been recognized as a major limiting factor to such activities along the Indian coast and port & harbour regions. The Ministry of Shipping desires to revise the IVL (inland vessels' limit) notification based on scientific rationale for the following reasons: (i) area of operation of ports has been extended towards the offshore and (ii) new major and minor ports have been developed since 1972. One of the objectives of this initiative is to improve the safety of vessels and onboard personnel. This limit is necessary to prevent damage to any vessel or loss of life.

The study region including the Mormugao Port limit is shown in Figure 1-4a (Chapter 1). The port of Mormugao is formed by a breakwater and a mole. It provides 11 alongside berths and several mooring buoys. The Mandovi river flows into the head of Aguada Bay. The bar at the Mandovi river mouth is subject to frequent change. During southwest monsoon, large breakers break across the bar and river mouth, and makes navigation in and out across the mouth very difficult. The present work is primarily concerned with finding out significant wave heights of the region off Mormugao port. AWS winds, moored buoy winds, NCEP analysed winds and NCMWRF winds are used as input to MIKE 21 - OSW and NSW models.

5.4.2. Data and Methods

In order to get an overall picture of the waves off Goa, the wave data measured off Mormugao (at B1) during February 1996 - May 1997 are analysed. The waves measured off Goa during May 2005 at B2 and B3 are used to study the wave transformation and to analyse the effect of local winds on the generation of wind seas over the region. Moored buoy data, which consists of wind and waves, at a deep water location (DS1) during July - November 1999, May - July 2000, January 2001 and May - September 2001 and at a shallow water location (SW3) during May - September 2001 and October 2004 - March 2005 are also utilised in this study. The location details are given in Table 2-1 and Table 2-2 and marked in Figure 2-3 (in Chapter 2).

AWS winds measured at Dona Paula coastal station during May - September 2004 and April - May 2005 have been analysed to study wind characteristics off Goa during pre-monsoon and SW monsoon periods. In order to predict offshore waves in the north Indian Ocean, the NCEP reanalysis winds and NCMRWF winds are utilised.

Regional (MIKE 21 OSW) and local model (MIKE 21 NSW) domains are selected as given in Figure 3-2 and Figure 3-5 (described in Chapter 3). The wave parameters for the boundary of local model are extracted from the regional model outputs. Significant wave heights derived from simulations have been used to draw IVL limit as follows: (i) regions where significant wave heights (H_s) < 0.6m, (ii) regions where 0.6m ≤ H_s ≤ 1.2m and (iii) regions where 1.2m ≤ H_s ≤ 2.0m.

5.4.3. Results and Discussion

Table 5-6 shows monthly variations in the significant wave height and mean wave period off Goa during February 1996–May 1997. The analysis shows that H_s vary from 0.16 to 5.85 m throughout the measurement period. The highest H_s value of 5.85 m and the maximum wave height of 10.47 m were observed in June 1996 when a monsoon depression was formed over the Arabian Sea. An analysis of waves measured at 25 and 15 m water depths off Mormugao, Goa, during May 2005 shows that H_s varies from 0.56 to 1.26 m and from 0.54 to 1.16 m, and mean wave period from 4.4 s to 9.3 s and from 4.4 s to 8.6 s, respectively. The relative changes in wave parameters at these two locations could be attributed to wave transformation due to refraction, shoaling and bottom friction.

A few typical 3 h interval wave spectra for 13 May 2005 are shown in Figure 5-17. The two major peaks present in the wave spectra at two different frequency bands can be attributed to wave trains coming from two different directions. This is a combination of short period wind seas generated due to local winds and long period swells generated far away. Vethamony and Sastry (1986), Rao and Baba (1996) and Sanil Kumar et al. (2004) also observed multi-peaks in wave spectra along the Indian coast.

It has been found from the analysis of AWS winds during May–September 2004 and April–May 2005 that the local winds dominate in pre-monsoon period (April and May), and there exists diurnal variations in wind speed and direction due to localized convective activity. A typical case for 12 May 2005 was highlighted in Figure 4-24. It is evident from the analysis of local winds measured at the coastal station and wave spectra measured off Goa that the diurnal variations in the wave parameters are mainly due to the co-existence of locally generated wind seas over the pre-existing swells.

Table 5-7 shows the statistics of significant wave heights exceeding 2.0 m during southwest monsoon of various years of measurements. Table 5-8 shows the ranges of H_s derived from available moored buoy data off Goa. It has been observed that H_s exceeds 2.5 m during June - August 2004, whereas it is below 2.0 m in September and does not exceed 1.2 m during October 2004 - May 2005. The highest value of 4.30 m obtained in May 2001 was due to an extreme event prevailed in the region. H_s are the highest during June - August and below 2.0 m during the rest of the period. Hence, it is very evident that Mormugao port and Panaji coastal region are safe from large waves, except during June - August.

Figure 5-18 shows a typical H_s distribution off Mormugao port during southwest monsoon. It is very clear that most of the region is influenced by large monsoon waves having H_s greater than 2.5 m. As the inland vessels are smaller in size and they are permitted to ply only during non-monsoon months, especially when H_s are less than 2.0 m, IVL is required to be fixed for non-monsoon months. The outer boundary of the 2.0 m decides the extreme IVL. Accordingly, IVL contours were fixed for all the months. These results will be used by the Ministry of Shipping (MoS) for implementing the IVL. A typical H_s distribution along with IVL contours for a non-monsoon month is shown in Figure 5-19. The existing smooth and partially smooth waterlines (practiced now by the inland vessels) and the port limit are also shown in Figure 5-19. The present study gives hope for larger area of movement for the vessels as seen by the existing waterlines and the proposed IVL.

Table 5-6. Monthly variations in the significant wave height and mean wave period off Goa during February 1996 - May 1997.

Year	Month	Significant wave height (m)	Mean wave period (s)
	February	0.33 - 1.50	3.0 - 5.0
	March	0.42 - 1.82	3.0 - 5.7
	April	--	--
	May	0.75 - 1.37	3.7 - 6.3
	June	0.93 - 5.85	4.6 - 9.1
	July	1.32 - 4.29	5.2 - 8.7
	August	1.20 - 3.25	4.4 - 7.5
	September	0.80 - 1.80	4.1 - 8.0
	October	0.47 - 3.31	3.6 - 6.9
	November	0.36 - 1.20	3.1 - 6.5
1996	December	0.29 - 0.96	2.7 - 6.5
	January	0.27 - 1.65	2.7 - 5.6
	February	0.38 - 1.39	3.1 - 5.3
	March	0.39 - 1.77	3.1 - 5.7
	April	0.16 - 1.50	2.8 - 5.7
1997	May	0.38 - 1.36	2.9 - 6.1

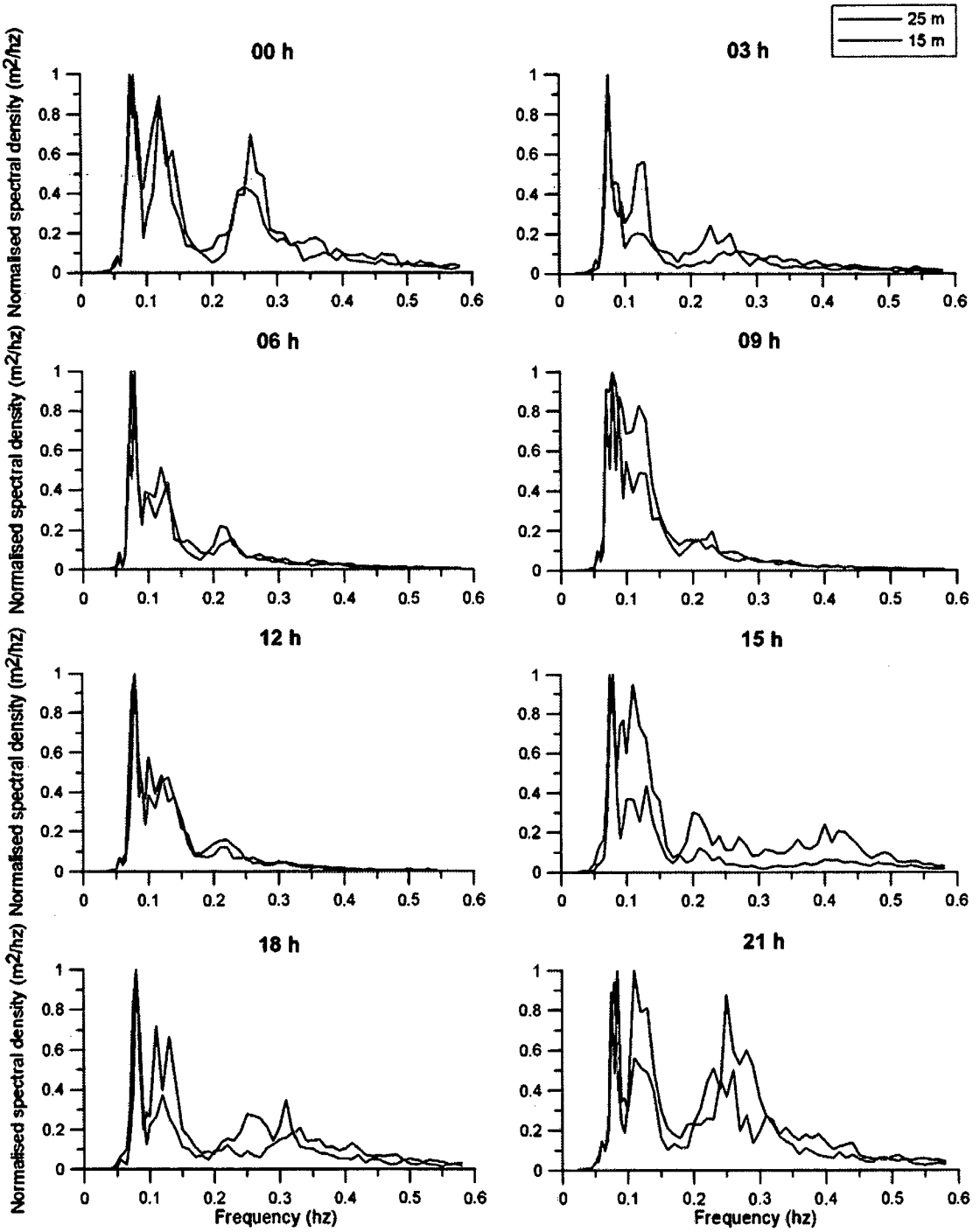

Figure 5-17. Typical wave spectra at 2 locations off Goa during 13 May 2005 (00 h, 03 h, 06 h, 09 h, 12 h, 15 h, 18 h, 23and 21 h respectively).

Table 5-7. Statistics of significant wave heights exceeding 2.0 m during SW monsoon season.

Month	May		June			July		Aug.		Sep.
Year	2001	2004	2001	2002	2003	2001	2003	2001	2003	2001
Total wave heights	237	247	178	124	240	145	246	218	118	230
H_s >2.0 m	59	20	120	36	151	71	228	78	52	0
% of H_s > 2.0 m	24.9	8.1	67.4	29	62.9	49	92.7	35.8	44.1	0

Table 5-8. Range of significant wave height derived from available moored buoy data off Goa.

Months	Years				
	2001	2002	2003	2004	2005
Jan		0.23 -1.41	0.33 -1.15	0.23 -1.25	0.33 -1.8
Feb	0.31 -1.41	0.31 -1.41	0.38 -1.50	0.39 -1.02	0.35 -1.45
Mar	0.31 -1.56	0.47-1.09	0.30 -1.87	0.16 -1.17	0.41-1.21
Apr				0.55 -1.17	
May	0.55 - 4.30	0.53 -1.87	0.46 -1.53	0.63 -2.27	
Jun	0.80 - 3.91	0.96 - 4.41	0.78 -3.80		
Jul	1.48 - 2.81		1.61 -3.78		
Aug	1.56 - 2.97		1.26 -2.52		
Sep	0.55 -1.88				
Oct	0.39 -1.48	0.42 - 1.42		0.31-1.31	
Nov	0.31 - 0.78	0.38 -0.76		0.29 -1.05	
Dec	0.23 - 0.70	0.30 -1.29	0.23-1.02	0.31-0.96	

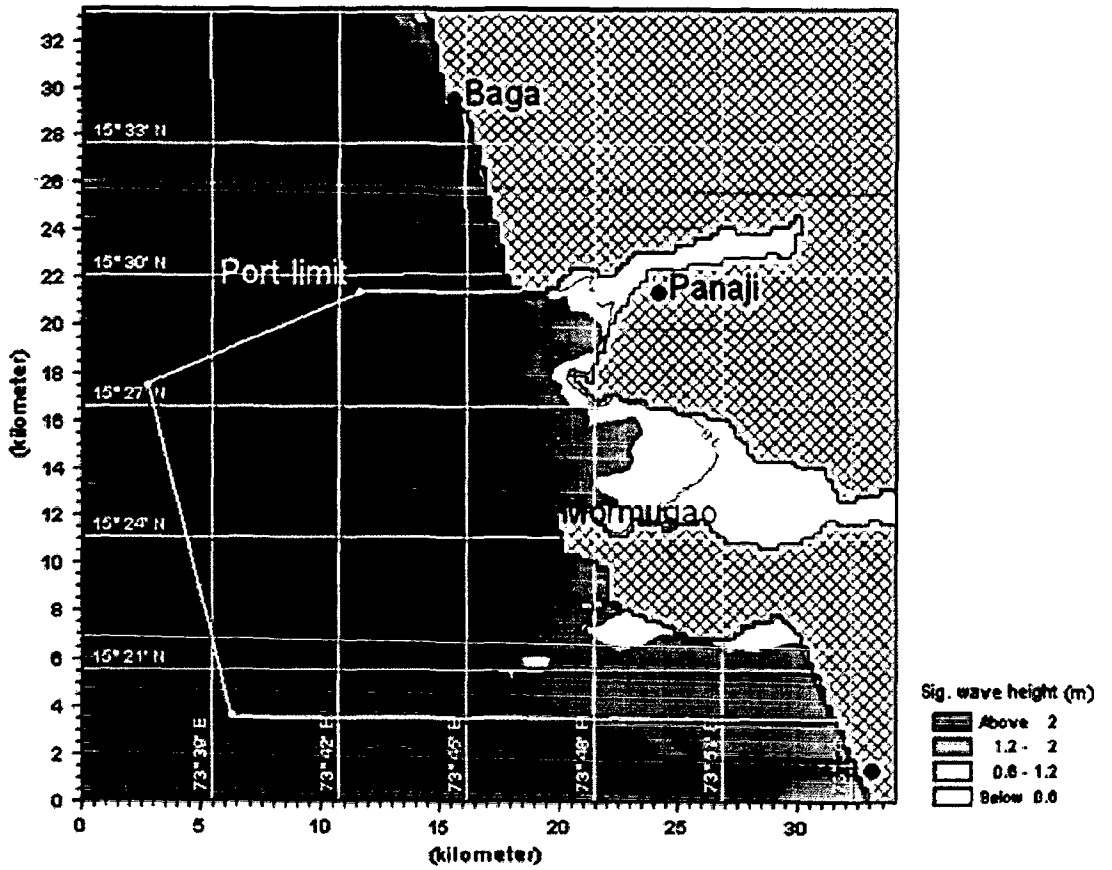

Figure 5-18. Typical significant wave height distribution off Mormugao Port during southwest monsoon (region showing the Mormugao Port limit is marked).

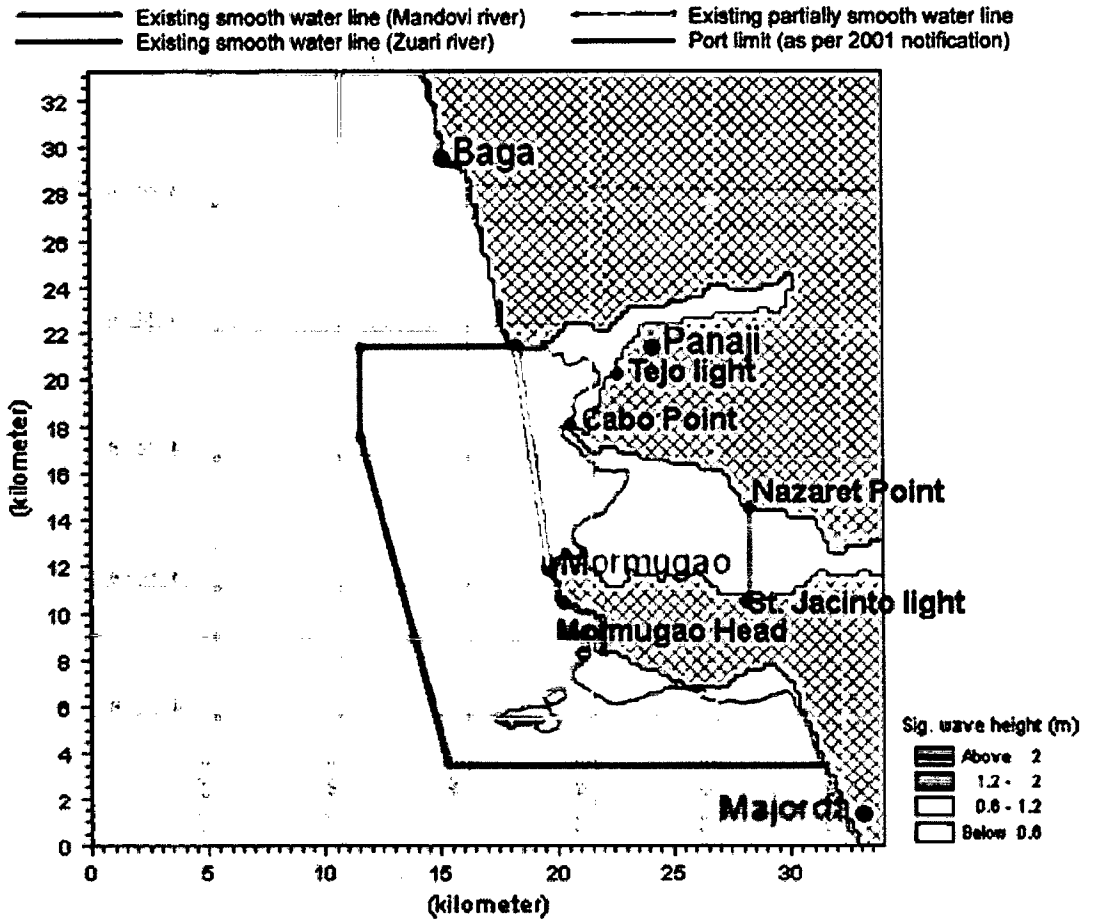

Figure 5-19. IVL regions demarcated based on wave heights (April 2005) with existing smooth and partially smooth waterlines.

Chapter 6

Summary and conclusions

Chapter 6

Summary and conclusions

6.1. Summary

Wave characteristics along the Indian coast have been studied by several researchers. Probably, this may be the first attempt to study seasonal response of coastal waves and wave transformation along the Indian coast using measurement, modelling and remote sensing. The broad objectives of the present study are:

- understanding the wave generation and propagation processes in the select nearshore regions along the Indian coast through measured data
- validation of wave modelling results of deep and shallow waters using measurements and remote sensing data
- to study the interaction between pre-existing swells and wind seas generated by coastal winds
- prediction of wave transformation along the select Indian coasts using high resolution winds such as MM5

Wave data collected using directional wave rider buoys, moored data buoys and non-directional wave recorder have been analysed. Wind data were measured using Autonomous Weather Station (AWS) at various coastal stations. Apart from measurements, significant wave heights (H_s) derived from Jason-1 altimeter were used for deep water wave analysis as well as model validation/comparison. Wind data from QuikScat scatterometer and re-analysed winds such as NCEP, CERSAT/IFREMER blended and NCMRWF were considered for the analysis, and applied as input to numerical wave simulations. Fine resolution coastal winds off Goa have been simulated using Mesoscale Model (MM5) to study the wind sea generated by sea breeze – land breeze system during pre-monsoon season.

The specific investigations carried out in the present study are as follows:

i) analysis of spectral wave characteristics along the Indian coast during monsoons and extreme events

ii) dominance of swells over wind seas along the west coast of India

iii) setting up of a numerical model for the Indian Ocean, and validation of model results with measurements and remote sensing data

iv) identification of potential swell generation areas, and propagation of these swells in the Arabian Sea and their impact on the west coast of India

v) characteristics of "Shamal" swells – generation and propagation, and their influence along the west coast of India

vi) superimposition of pre-existing swells over wind seas off Goa coast during pre-monsoon season

vii) wave transformation along select open coasts and semi-enclosed regions

Spectral characteristics during monsoons and extreme events have been studied using wave spectra measured off Paradip and Goa, along the east coast and west coast of India, respectively. Multi-peaked spectra with spectral peaks in the low and high frequency regions have been observed, indicating the presence of different wave systems in the region. The spectral peak in the low frequency region indicates the dominance of distant swells and that in the high frequency region indicates the dominance of wind seas. During extreme events, the spectra are single-peaked and the energy is centred on a narrow band in the low-frequency region with an average directional spreading of 20°. It is evident from the spectra that wave energy during the southwest monsoon season is higher than the northeast monsoon season along the east coast as well as west coast of India.

Wind sea and swell energies have been separated, and the respective parameters have been calculated from the wave energy spectra using the methodology proposed by Gilhousen and Hervey (2001). It has been found that swells are dominated along the west coast of India during SW monsoon (93%) and NE monsoon (67%) seasons; however, wind seas are dominated during pre-monsoon season (51%). Annually, the dominance of swells is around 70%. The mean wave periods (T_m) during SW monsoon season are generally above 5 s, whereas, T_m are below 5 s during other seasons, indicating the superimposition of local wind seas over pre-existing swells during the pre-monsoon and NE monsoon seasons. The predominant swells observed along the west coast of India during pre-monsoon and NE monsoon seasons are in the SW/SSW directions, which are mostly propagated from the south Indian Ocean. However, the predominant swells during SW monsoon season are generated from the north Indian Ocean. NE monsoon winds could have negligible impact along the west coast of India, as waves generated due to these winds propagate away from the coast. Wind seas are predominantly in the NW direction during pre-monsoon and NE

monsoon seasons, and those during pre-monsoon season are generated by sea breeze. It has been found that the nearshore waves during extreme events are dominated by swells.

Numerical models were set up for large domain (the Indian Ocean region) and small domains (off Goa, Ratnagiri, Dwarka, Paradip and Dhamra) to simulate waves during various seasons. Model results have been validated with measurements at deep water locations as well as nearshore depths, and the match is very good. Correlation coefficients of model and measured H_s and T_m at a deep water location off Goa are 0.96 and 0.85, respectively, and at a nearshore location off Goa are 0.96 and 0.83, respectively. The bias and r.m.s. error between measured and model wave parameters are as follows: H_s: 0.00 and 0.37 m, respectively in deep water; 0.06 m and 0.29 m, respectively in a nearshore depth; T_m: -0.32 s and 0.80 s, respectively in deep water, and 0.10 s and 0.80 s, respectively in a nearshore depth.

Coastal wind seas off Goa simulated using MM5 winds are validated with measured wind sea parameters off Goa and the match is very good. The correlation coefficient, bias and r.m.s. error between measured and modelled wind sea H_s are 0.73, 0.03 m and 0.12 m, respectively. Diurnal variations associated with winds are evident in the simulated wind sea parameters also.

Analysis of winds and simulated waves in the Indian Ocean revealed the areas of potential swell generation; these swells propagate in the Arabian Sea and effect the west coast of India. Predominant swells are in the SW direction during SW monsoon season and in the SW/SSW and NW directions during both pre-monsoon and NE monsoon seasons. The potential swells are generated primarily in the following areas: (i) area covered by 52.5° E to 62.5° E and 5° S to 15° S for SW swells during SW monsoon season, (ii) area covered by 40° E to 70° E and 30° S to 50° S for SW/SSW swells during pre-monsoon and NE monsoon seasons and (iii) area covered by 60° E to 67.5° E and 17.5° N to 25° N for NW swells during pre-monsoon and NE monsoon seasons.

Shamal winds are meteorological events associated with winds, which normally occurs in the Arabian Peninsula, especially during the winter season. They generate large swells in the Persian Gulf and in the Arabian Sea. Characteristics of the "Shamal" swells were studied by analyzing measured wave parameters along the west coast of India during winter season. Increase in wave heights associated with decrease in swell periods and a common propagation direction (NW) for wind sea and swell are the distinct features of the Shamal swells. The associated significant wave heights and mean swell periods are between 1.0

and 2.0 m and between 6.0 and 8.0 s, respectively. Numerical simulations reproduced the Shamal swells in the Arabian Sea. It has been found that the Shamal swells are generated in the Gulf of Oman and off the east coast of Oman, which propagate to the west coast of India in the NW direction. The analysis of swell parameters extracted at 6 locations (Dwarka, Mumbai, Ratnagiri, Goa, Mangalore and Kochi) along the west coast of India indicates that the swell heights are larger off Dwarka and relatively smaller off Kochi, i.e., in the decreasing order of magnitude from north to south. The swells reach first along the Gujarat coast and then on the Kerala coast with time lags according to their arrivals.

Superimposition of coastal wind seas with pre-existing swells during pre-monsoon season was investigated. A distinct and systematic diurnal variation in wind speed, wave height and wave period, especially increase in wave height and decrease in wave period following the increase in the intensity of coastal winds due to sea breeze system has been observed. During the onset of sea breeze, a wind wave system grows in time, following the progressive extension of the sea breeze area towards offshore. After cessation of the sea breeze, wave energy level gradually decreased and the associated wave period increases. During a typical daily cycle, the wave height reaches its peak early in the afternoon, then it decays progressively back to the swell conditions within 5 or 6 hours. It is evident from the wind sea that the wind sea H_s gradually increases towards the coast from offshore, and the maximum wind sea H_s has been observed close to the Goa coast. The wind sea growth towards the coast is proportional to the wind speed gradient, available fetch and sea breeze duration.

Wave transformation along the open coasts and semi-enclosed regions has been studied using measurements and simulations. Reduction in significant wave heights among two nearshore water depths measured off Goa, Ratnagiri and Dwarka were estimated. Least reduction is observed off Goa and maximum off Dwarka. In fact, a wind sea growth in the NE direction (away from the coast) off Dwarka has been observed, which sufficiently contributes to the prevailing waves at 30 m depth location. Simulated wave parameters at water depths of 100 m, 50 m, 30 m, 20 m, 10 m and 5 m off Mumbai, Goa and Kochi (along the west coast of India), and off Nagappattinam, Visakapattinam and Paradip (along the east coast of India) were analysed. Wave patterns along the west coast of India are nearly the same, but in increasing order of wave heights from south to north. It is found that wave dissipation is high off Mumbai and low off Kochi along the west coast of India. Wave heights along the east coast of India are in the increasing order during pre-monsoon and SW monsoon seasons, and in the decreasing order during NE monsoon season, from

south to north (Nagappattinam to Paradip), and the reduction among various depths are relatively less as compared to those along the west coast of India. Bottom dissipation causes higher reduction in wave heights over wide continental shelf, and the continental shelf of west coast is wider compared to east coast of India.

Wave transformation at naturally protected (Dhamra Port) and artificially protected (Mormugao Port) semi-enclosed regions has been studied. The Dhamra port is protected from direct waves by Kanika sands, Gahirmatha beach and surrounding mangroves, and is only partially open to the waves from NNE to NE and from ESE to SE. Diffraction and bottom dissipation play major role in controlling the wave energy while propagating towards the Port. The Mormugao Port is protected from waves by breakwaters, and during any season, wave height inside the port is very low, and only diffracted waves propagate towards the port. During an extreme event prevailed in the Arabian Sea, the significant wave height observed inside the port was only 0.33 m.

A case study was carried out to demarcate inland vessels' limit (IVL) limit off Mormugao Port region for demonstrating the operational use of wave model results. It has been found that during September – May, significant wave heights do not exceed 2.0 m off Mormugao port and coastal regions. Based on the significant wave height distribution around the coastal region, the IVL has been demarcated.

6.2. Conclusions

- Time series wave data measured off Goa (west coast of India) and off Paradip (east coast of India) distinctly show the response of coastal waves to the seasons and extreme events.
- Monthly, seasonal and annual characteristics of wind seas and swells off Goa have been separated from the measured wave spectra using the separation frequency method. The wave pattern primarily follows swell pattern during most part of the year, especially during SW monsoon and NE monsoon seasons. Wind seas are dominated during pre-monsoon season.
- Numerical model results have been validated with measurements in deep water as well as nearshore locations, and the match is very good.
- MM5 winds have been simulated for Goa region during pre-monsoon season, and applied to simulate coastal waves off Goa. Significant improvement in simulated wave

parameters was observed, urging the need of using high resolution winds for coastal wave predictions.

- Superimposition of locally generated waves from NW with the pre-existing swells from SW along the west coast of India results in diurnal variations in waves. Increase in wave height and decrease in wave period with increase in wind speed, especially during fair weather season, are the important effects of dominance of sea breeze.
- Though waves during southwest monsoon season have high impact on the west coast of India, the wind seas super-imposed on pre-existing swells do cause geomorphological changes during non-monsoon months. The role of distant swells in modulating the wave generation along the west coast of India, where the impact of sea breeze is dominant during pre-monsoon season, is yet to be understood.
- The "Shamal" swells were identified along the west coast of India during winter season. Increase in wave heights associated with decrease in swell periods and common propagation direction (NW) for wind sea and swell are the distinct characteristics of Shamal swells. Shamal swells are generated in the northwestern Arabian Sea, especially in the Gulf of Oman and off the east coast of Oman, and propagate towards the west coast of India in the NW direction. Influence of Shamal swells is the maximum along the Gujarat coast and the minimum along the Kerala coast.
- Shamal winds can influence the wind-induced circulation in the Arabian Sea. Study on Shamal wind extension and their distribution along the west coast of India require fine resolution winds (e.g. MM5 winds). Even though swells from the south Indian Ocean are always present along the west coast of India, the presence of Shamal swells cannot be ignored.
- Transformation of wave parameters in the nearshore depths at various locations along the Indian coast has been assessed. Wave height reduction is higher along the west coast compared to the east coast, since bottom dissipation causes higher reduction over wide continental shelf. Along the west coast of India, the wave dissipation increases from south to north (Kochi to Mumbai). Attenuation due to bottom friction varies along the west coast of India according to the size of the bottom sediments, and it is in the increasing order from the south to the north.
- Wave patterns along the west coast of India are nearly the same, with wave heights increasing from south to north (Kochi to Mumbai). Wave heights along the east coast

of India increase from south to north (Nagappattinam to Paradip) during pre-monsoon and SW monsoon seasons and decrease during NE monsoon season. Diurnal variations are evident at nearshore depths along the west coast of India during pre-monsoon season, but in the decreasing order of magnitude from north to south (Mumbai to Kochi).

- Wave modelling results have been applied to an operational use: based on the distribution of significant wave heights, inland vessel's limit (IVL) of the Mormugao port has been demarcated.

6.3. Future perspective

The present work can be extended further to study the following aspects:

- ✓ Role of distant swells in modulating wave generation along the west coast of India, where the impact of sea breeze is dominant during pre-monsoon season, is yet to be understood – a detailed investigation is required.
- ✓ Shamal winds can influence the wind-induced circulation in the Arabian Sea. Shamal wind extension along the west coast of India has to be analysed in detail utilsing fine resolution atmopsherics models.
- ✓ Since, swells (SW/SSW) from south Indian Ocean are always present along the west coast of Inida, they interact with Shamal swells (NW) during Shamal events. The interaction of these multi-directional swells deserves special attention in future research.
- ✓ A detailed field study should be carried out to understand the nature of attenaution of short period wind seas observed at the nearshore depths off Goa during pre-monsoon season.

References

References

Abdalla, S. and L. Cavaleri, 2002: Effect of wind variability and variable air density on wave modeling, *J. Geophys. Res.*, 107 (C7), 17-1/17-17.

Abhijit Sarkar, M. Mohan and Raj Kumar, 1997: Inter-comparison of model-predicted wave heights with satellite altimeter measurements in the north Indian Ocean, *Ocean Eng.*, 24(9), 879-885.

Aboobacker, V.M., P. Vethamony, K. Sudheesh and S.P. Rupali, 2009: Spectral characteristics of the nearshore waves off Paradip, India during monsoon and extreme events, *Nat. Hazards,* 49, 311-323.

Aboobacker, V.M., Vethamony, P., Sudheesh, K., 2005: Wave characteristics off Paradip during monsoons as evident from measurements and modelling, *Proceedings of the National Workshop on Oceanographic Features of the Indian Coastal Waters, held at Naval Physical & Oceanographic Laboratory, Kochi,* 46-53.

Ali, A.H., 1994: Wind regime of the Arabian Gulf, *The Gulf War and the environment, Taylor & Francis,* 206 pp.

Al-Zanaidi, M.A. and W.H. Hui, 1984: Turbulent air flow water waves, *J. Fluid Mech.*, 148, 225-246.

Aparna, M., S.R. Shetye, D. Shankar, S.S.C. Shenoi, P. Mehra, and R.G.P. Desai, 2005: Estimating the seaward extent of sea breeze from QuikSCAT scatterometry, *Geophys. Res. Lett.,* 32, L13601, doi:10.1029/2005GL023107.

Ardhuin, F. and T. Herbers, 2002: Bragg scattering of random surface gravity waves by irregular seabed topography, *J. Fluid Mech.*, 451, 1-33.

Ardhuin, F., L. Berotti, J.R. Bidlot, L. Cavaleri, V. Filipetto , J.M. Lefevre and P. Wittmann, 2007: Comparison of wind and wave measurements and models in the Western Mediterannean Sea, *Ocean Eng.,* 34, 526-541.

Ardhuin, F., W.C. O'Reilly, T.H.C. Herbers and P.F. Jessen, 2003: Swell transformation across the continental shelf. Part I: Attenuation and directional broadening, *J. Phys. Oceanogr.,* 33 (9), 1921-1939.

Baba, M., J. Dattatri and S. Abraham, 1989: Ocean wave spectra off Cochin, west coast of India, *Indian J. Mar. Sci.,* 18, 106-112.

Baba, M., N.P. Kurian, K.V. Thomas, M. Prasannakumar, T.S.S. Hameed and C.M. Harish, 1983: Study of the waves and their refraction in relation to beach erosion along the Kerala coast, *Centre for Earth Science Studies, Technical Report*, No.29, 28 pp.

Bagnold, R. A., 1946: Motion of waves in shallow water - interaction between waves and sand bottoms, *Royal Society of London*, 187, 1-18.

Barber, N.F. and F. Ursell, 1948: The generation and propagation of ocean waves and swell, *Philosopical Transactions of the Royal Society of London*, 240A, 527-560.

Barnett, T.P. and J.C. Wilkerson, 1967: On the generation of ocean wind waves as inferred from airborne measurements of fetch-limited spectra, *J. Mar. Res.*, 25, 292-328.

Battjes, J. A. and J. P. F. M. Janssen, 1978: Energy loss and set-up due to breaking in random waves, *Proc. 16th Coastal Engineering Conference, Hamburg, Germany*, 569-587.

Belcher, S.E. and J.C.R. Hunt, 1993: Turbulent shear flow over slowly moving waves, *J. Fluid Mech.*, 251, 109-148.

Bentamy, A., D. Croize-Fillon, P. Queffeulou, C. Liu, and H. Roquet, 2009: Evaluation of high-resolution surface wind products at global and regional scales, *Journal of Operational Oceanography*, 2(2), 15-27.

Bentamy A., H.L. Ayina, P. Queffeulou, and D. Croize-Fillon, 2006: Improved near real time surface wind resolution over the Mediterranean Sea, *Ocean Sci. Disc.*, 3, 435-470.

Bhatt, V., R. Kumar, S. Basu, V.K. Agarwal, 2005: Assimilation of altimeter significant wave height into a third generation global spectral wave model, *IEEE Trans Geosci. Rem. Sens.*, 43, 110-117.

Bhowmick, S.A., R. Kumar, S. Basu, A. Sarkar and V.K. Agarwal, 2009: Improvement in wave forecast using data assimilative coastal wave model, *Indian J. Mar. Sci.*, 38(2), 142-150.

Bonnefond, P., B. Hanes, G. Born, P. Exertier, S. Gill, G. Jan, E. Jeansou, D. Kubitschek, O. Laurain, Y. Menard and A. Orsoni, 2003: Calibrating the Jason-1 measurement system: Initial results from the Corsica and Harvest verification experiments, *Adv. Space Res.*, 32 (11), 2135-2140.

Booij, N., L.H. Holthaijsen and R.C. Ris, 1999: A third-generation wave model for coastal regions. 1. Model description and validation", *J. Geophys. Res.*, 104(C4), 7649-7666.

Bretschneider, C.L., 1963: Significant wave hindcast for station I. North Atlantic Storm, Dec. 1959, *Tech Report,* No. SN-77-1.

C2-MUT-W-03-IF, 2002: QuikScat Scatterometer Mean Wind Field Products User Manual, *France, IFREMER,* Version: 1.0.

Cavaleri, L. and M. Sclavo, 2006: The calibration of wind and wave model data in the Mediterranean Sea, *Coastal Eng.* 53, 613-627.

Chalikov, D.V. and V.K. Makin, 1991: Models of the wave boundary layer, *Boundary-Layer Meteorol.,* 56, 83-99.

Chambers, D.P., J.C. Ries and T.J. Urban, 2003: Calibration and verification of Jason-1 using global along-track residuals with TOPEX, *Marine Geodesy,* 26, 305-317.

Chandramohan, P., V. Sanil Kumar and B.U. Nayak, 1991: Wave statistics around the Indian coast based on ship observed data, *Indian J. Mar. Sci.,* 20, 87-92.

Coleman, J.M. and L.D. Wright, 1971: Analysis of major river systems and their deltas: procedures and rationale with two examples, *Louisiana State University, Coastal Studies Institute, Technical Report,* 95, 125 pp.

Combes, J.A., A. Grossmann and Ph. Tchamitchian, 1989: Wavelets, Time-Frequency Methods and Phase space, *Springer-Verlag, Berlin,* 315.

Darbyshire, J., 1961: Prediction of wave characteristics over the North Atlantic, *J. Inst. Navigation,* 14, 339-347.

Datawell BV, 2006: Datawell wave rider reference manual, *Datawell BV, Zumerlustraat 4, 2012 LM Haarlem, The Netherlands.*

Datawell, 2001: The W@ves21 spectral analysis tool, developed for analysis of the directional Wave Rider buoys from Datawell in the Netherlands, www.datawell.nl.

Dhanya, P., P. Vethamony, K. Sudheesh, G. Smitha, M.T. Babu and T.M. Balakrishnan Nair, 2010: Simulation of coastal winds along the central west coast of India using the MM5 mesoscale model, *Meteorology and Atmospheric Physics.* (Article in Press).

DHI, 2001: MIKE 21 Wave modelling user guide, *DHI Water & Environment, Denmark,* 66 pp.

Dobson, F.W., 1971: Measurement of atmospheric pressure on wind-generated sea waves, *J. Fluid Mech.,* 48, 91.

Dobson, F.W., S.D. Smith, and R.J. Anderson, 1994: Measuring the relationship between wind stress and sea state in the open ocean in the presence of swell, *Atmosphere-Ocean,* 32, 237-256.

Dobson, R.S., 1967: Some applications of a digital computer to hydraulic engineering problems, *Dept. of Civil Engineering, Stanford University, Technical Report,* No. 80, 115p.

Donelan, M.A., 1982: The dependence of the aerodynamic drag coefficeint on wave parameters, *Proc. Of the first international conference on meteorological and air/sea interaction of the coastal zone; Amer. Meteor. Soc., Boston, Mass,* 381-387.

Donelan, M.A., W.M. Drennan and E.A. Terray, 1999: Wavenumber spectra of wind waves in the range of 1–50 m, *In: Banner, M.L. (Ed.), The Wind-Driven Air–Sea Interface. School of Mathematics, The University of New South Wales, Sydney,* 35-42.

Donelan, M.A., W.M. Drennan, and K.B. Katsaros, 1997: The air-sea momentum flux in conditions of wind sea and swell, *J. Phys. Oceanogr.,* 27, 2087-2099.

Drennan, W.M., H.C. Graber and M.A. Donelan, 1999: Evidence for the effects of swell and unsteady winds on marine wind stress, *J. Phys. Oceanogr.,* 29, 1853–1864.

Duchossois, G., 1991: The ERS-1 mission objectives, *ESA Bull.,* 65, 16-25.

Earle, M.D., 1984: Development of Algorithms for separation of sea and swell, *National Data Buoy Centre Tech. Rep.,* MEC-87-1, 53 pp.

Ebuchi, N., H.C. Graber and M.J. Caruso, 2002: Evaluation of wind vectors observed by QuikSCAT/SeaWinds using ocean buoy data, *J. Atmos. Oceanic Technol.,* 19, 2049-2062.

Elgar, S. and R.T. Guza, 1985: Observations of bispectra of shoaling surface gravity waves, *J. Fluid Mech.,* 161, 425-448.

El-Sabh, M.I. and T.S. Murty, 1989: Storm surges in the Arabian Gulf, *Nat. Hazards,* 1, 371-385.

Fabrikant, A.L., 1976: Quasilinear theory of wind-wave generation, *Izv. Atmos. Ocean. Phys.* 12, 524-526.

Freilich, M.H. and Guza, R.T., 1984: Nonlinear effects on shoaling surface gravity waves, *Philosophical Transactions of the Royal Society of London,* A 311, 1-41.

Freilich, M.H., R.T. Guza and S. Elgar, 1990: Observations of nonlinear effects in directional spectra of shoaling gravity waves, *J. Geophys. Res.*, 95, C6, 9645-9656.

Fu, L.L., E.J. Christenses, C.A. Yamarone, M. Lefebvre, Y. Menard and P. Escudier, 1994: TOPEX-POSEIDON mission overview, *J. Geophys. Res.*, 99 (C12), 24369-24381.

Gelci, R., H. Cazale´ and J. Vassal, 1957: Pre´vision de la houle. Lame´thode des densite´s spectroangulaires, *Bull. Inf. Comite´ Central Oce´anogr. Etude Coˆtes,* 9, 416-435.

Gerling, T. W., 1992: Partitioning sequences and arrays of directional ocean wave spectra into component wave systems, *J. Atmos. Oceanic Technol.*, 9, 444-458.

Gilhousen, D.B. and R. Hervey, 2001: Improved Estimates of Swell from Moored Buoys. *Proc. of the Fourth International symposium WAVES 2001, ASCE: Alexandria, VA,* 387-393.

Gille, S. T., S. G. Llewellyn Smith, and S. M. Lee, 2003: Measuring the sea breeze from QuikSCAT Scatterometry, *Geophys. Res. Lett.,* 30(3), 1114, doi:10.1029/2002GL016230.

Goodberlet, M.A., C.T. Swift and J.C. Wilerson, 1992: Validation of ocean surface wind fields and wave height measurements derived from data of the ERS-1 scatterometer and radar altimeter (early results), *Proc. Of the workshop on ERS-1 Geophysical Validation, Penhors, France, 27-30 April 1992; ESA WPP-36, European Space Agency, Paris,* 61-64.

Graber, H. C., N. Ebuchi, and R. Vakkayil, 1996: Evaluation of ERS-1 scatterometer winds with wind and wave ocean buoy observations, *University of Miami Tech. Rep.,* RSMAS 96-003, 78 pp.

Greenslade, D.J.M., 2001: The assimilation of ERS-2 significant wave height data in the Australian region. *J. Mar. Syst.*, 28: 141-160.

Grell, G., J. Dudhia, and D.R. Stauffer, 1994: A description of the fifth-generation Penn State/NCAR Mesoscale Model (MM5), *NCAR Tech. Note, NCAR/TN398+STR,* 138 pp.

Guedes Soares, C., 1984: Representation of double-peaked sea wave spectra, *Ocean Eng.,* 11, 185-207.

Guedes Soares, C., 1991: On the occurrence of double peaked wave spectra, *Ocean Eng.,* 18, 167-171.

Gunther, H., P.Lionello and B. Hansen, 1993: The impact of the ERS-1 altimeter on the wave analysis and forecast, *Report No. GKSS 93/E/44, GKSS, Germany*, 56p.

Hanson, J. L., and O. M. Phillips, 2001: Automated analysis of ocean surface directional wave spectra, *J. Atmos. Oceanic Technol.*, 18, 277-293.

Hanson, J.L. and O.M. Phillips, 1999: Wind sea growth and dissipation in the open ocean, *J. Phys. Oceanogr.*, 29, 1633-1648.

Hanson, J.L., 1996: Wave spectral partitioning applied to the analysis of complex wave conditions in the North Pacific Ocean, Pre-prints, *Eight Conf. on Air-Sea Interactions and Symp. On Goals, Atlanta, GA, Amer. Meteor. Soc.*, 61-65.

Harish, C.M. and M. Baba, 1986: On spectral and statistical characteristics of shallow water waves, *Ocean Eng.*, 13(3), 239-248.

Hasselmann, D.E. and J. Bosenberg, 1991: Field measurements of wave-induced pressure over wind sea and swell, *J. Fluid Mech.*, 230, 391-428.

Hasselmann, K. and S. Hasselmann, 1985: The wave model EXACT-NL, In: The SWAMP Group (Eds.), *Ocean Wave Modelling, PlenumPress, New York and London*, 256 pp.

Hasselmann, K., 1962: On the non-linear energy transfer in a gravity-wave spectrum, Part 1. General theory, *J. Fluid Mech.*, 12, 481-500.

Hasselmann, K., 1974: On the spectral dissipation of ocean waves due to white capping, *Boundary-Layer Meteorol.*, 6, 107-127.

Hasselmann, K., T.P. Barnett, E. Bouws, H. Carlson, D.E. Cartwright, K. Enke, J.I. Ewing, H. Gienapp, D.E. Hasselmann, P. Kruseman, A. Meerburg, P. Muller, D.J. Olbers, K. Richter, W. Sell and H. Walden, 1973: Measurements of wind–wave growth and swell decay during the Joint North Sea Wave Project (JONSWAP), *Deutsche Hydrographische Zeitschrift*, A 8 (12), 1-95.

Hasselmann, S., K. Hasselmann, J.A. Allender and T.P. Barnett, 1985: Computations and parameterizations of the non-linear energy transfer in a gravity-wave spectrum. Part 2: parameterizations of the non-linear transfer for application in wave models, *J. Phys. Oceanogr.*, 15, 1378–1391.

Herbers, T.H.C., M. Orzech, S. Elgar and R.T. Guza, 2003: Shoaling transformation of wave frequency-directional spectra, *J. Geophys. Res.*, 108 (C1), 3013, doi:10.1029/2001JC001304.

Herbers, T.H.C., N.R. Russnogle and S. Elgar, 2000: Spectral energy balance of breaking waves within the surf zone, *J. Phys. Oceanogr.*, 30, 2723-2737.

Hersbach. H., 1997: Application of the adjoint of the WAM model to inverse wave modelling, *J. Geophys. Res.*, 103, C5, 10469-10487.

Holthuijsen, L.H. and S. De Boer, 1988: Wave forecasting for moving and stationary targets. In: Schrefler, B.A. and Zienkiewicz, O.C., Editors, 1988, *Computer Modelling in Ocean Eng.*, 231-234.

Hristov, T.S., S.D. Miller, C.A. Friehe, 2003: Dynamical coupling of wind and ocean waves through wave-induced air flow, *Nature,* 442, 55-58.

Hubert W.E., D.R. Morford, A.N. Hull, and R.E. Englebretson, 1983: Forecasters handbook for the middle east/arabian sea, *Naval Environmental Prediction Research Facility Monterey, California*, CR83-06.

IMD, 1996: Indian Daily Weather Reports, *India Meteorological Department, Pune*, India.

Jacobs, S.J., 1987: An asymptotic theory for the turbulent flow over a progressive water wave, *J. Fluid Mech.*, 174, 69-80.

Janssen, P.A.E.M, 1982: Quasilinear approximation for the spectrum of wind-generated water waves. *J. Fluid Mech.*, 117, 493-506.

Janssen, P.A.E.M., 1989: Wave-induced stress and the drag of air flow over sea waves, *J. Phys. Oceanogr.*, 19, 745-754.

Janssen, P.A.E.M., 1992: Experimental evidence of the effect of surface waves on the airflow, *J. Phys. Oceanogr.*, 22, 1600-1604.

Janssen, P.A.E.M., 2004: The Interaction of Ocean Waves and Wind, *Cambridge University Press, Cambridge, UK*, 300 pp.

Jeffreys, H., 1924: On the formation of waves by wind, *Proc. Roy. Soc.*, A107, 189-206.

Jeffreys, H., 1925: On the formation of waves by wind II, *Proc. Roy. Soc.*, A110, 341-347.

Jenkins, A.D., 1992: A quasi-linear eddy-viscosity model for the flux of energy and momentum to waves, using conservation law equations in a curvilinear system, *J. Phys. Oceanogr.*, 22, 843-858.

Jiang, F. and A.J. Mehta, 1996: Mud banks of the southwest coast of India: V: wave attenuation, *J. Coast. Res.*, 12(4), 890-897.

Johnson, H.K. and H. Kofoed-Hansen, 2000: Influence of bottom friction on sea surface roughness and its impact on shallow water wind wave modelling, *J. Phys. Oceanogr.*, 30, 1743-1756.

Kalney, E., M. Kanamitsu, R. Kistler, W. Collins, D. Deaven, L. Gandin, M. Iredell, S. Saha, G. White, J. Woollen, Y. Zhu, M, Chelliah, W. Ebsuzaki, W. Higgins, J. Janowiak, K. C. Mo, C. Ropelewski, J. Wang, A. Leetma, R. Reynolds, R. Jenne and D. Joseph et al., 1996: The NCEP/NCAR 40-Year Reanalysis Project, *Bull. Amer. meteor. Soc.*, 77, 437-471.

Kaminsky, G. M. and N. C. Kraus. 1993: Evaluation of depth-limited wave breaking criteria, *Proceedings of 2nd International Symposium on Ocean Wave Measurement and Analysis, Waves 93* (ASCE, New York), 180-193.

Kinsman, B., 1965: Wind waves, their generation and propagation on the ocean surface, *Prentice-Hall Inc., Englewood Cliffs, New Jersey*, 676 pp.

Kline, S.A., and J.L. Hanson, 1995: Wave identification and tracking system, *Applied Physics Laboratory, The Johns Hopkins University, Tech. Rep. STD-R-2436, Laurel, MD*, 44 pp.

Komen, G.J., Cavaleri, L., Donelan, M., Hasselmann, K., Hasselmann, S. and P.A.E.M., Janssen, 1994: Dynamics and Modelling of Ocean Waves, *Cambridge University Press, Cambridge,* 532 pp.

Kurian, N.P., K. Rajith, T.S. Shahul Hameed, L. Sheela Nair, M.V. Ramana Murthy, S. Arjun and V.R. Shamji, 2009: Wind waves and sediment transport regime off the south-central Kerala coast, India, *Nat. Hazards*, 49, 325-345.

Kurian, N.P. and M. Baba, 1987: Wave attenuation due to bottom friction across the southwest Indian continental shelf, *J. Coast. Res.*, 3(4), 485-490.

Kurian, N.P., M. Baba and T.S Shahul Hameed, 1985: Prediction of nearshore wave heights using a wave refraction programme, *Coastal Eng.* 9 (4), 347-356.

Linacre, E. and J. Hobbs, 1977: The Australian Climatic Environment, *John Wiley & Sons: Brisbane,* 354 pp.

Liu, P.C., 2000: Is the wind wave frequency spectrum outdated, *Ocean Eng.*, 27, 577-588.

Long, R. B., 1973: Scattering of surface waves by an irregular bottom, *J. Geophys. Res.*, 78 (33), 7861-7870.

Maat, N., C. Kraan and W.A. Oost, 1991: The roughness of wind waves, *Boundary-Layer Meteorol.*, 54, 89-103.

Mac Pherson, H. and P.G. Kurup, 1981: Wave damping at the Kerala mud banks, *Indian J. Mar. Sci.*, 10, pp. 154-160.

Madsen, P. A., and O. R. Sorensen, 1993: Bound waves and triad interactions in shallow water, *J. Ocean Engineering*, 20(4), 359-388.

Makin, V.K., V.N. Kudryavstev and C. Mastenbroek, 1995: Drag of the sea surface. *Boundary-Layer Meteorol.*, 73, 159-182.

Mandal, S. and N. Prabaharan, 2010: Ocean wave prediction using numerical and neural network models, *The Open Ocean Engineering Journal*, 3, 12-17.

Mandal, S., 1985: A numerical wave prediction model DOLPHIN: theory and test results, *Report no. 3-85, Delft. Univ. Tech.*, The Netherlands, 68 pp.

Masselink Gerhard and Charithra B. Pattiarchi, 1998: The effect of sea breeze on beach morphology, surf zone hydrodynamics and sediment resuspension, *Marine Geology*, 146, 115-135.

Mastenbroek, C., 1996: Wind-wave interaction, *Ph.D. Thesis. Delft Tech. Univ.*, 119 pp.

Mastenbroek, C., V.K. Makin, A.C. Voorrips and G.J. Komen, 1994: Validation of ERS-1 altimeter wave height measurements and assimilation in a North Sea wave model, *The Glob. Atm. Oc. System*, 2, 143-161.

Mathew, J., M. Baba and N.P. Kurian, 1995: Mud- banks of southwest coast of India I: Wave characteristics, *J. Coast. Res.*, 11(1), 168-178.

Miles, J.W., 1957: On the generation of surface waves by shear flows, *J. Fluid Mech.*, 3, 185-204.

Mitsuyasu, H., 2002: A historical note on the study of ocean surface waves, *J. Oceanography*, 58, 109-120.

Munk, W. H., 1951: Origin and generation of waves, *Proc. First Coastal Eng. Conference, Long Beach, Calif.*, 1-4.

Neetu, S., S. Shetye and P. Chandramohan, 2006: Impact of sea-breeze on wind-seas off Goa, west coast of India, *J. Earth Sys. Sci.*, 115(2), 229-234.

Nikolayeva. Y.I. and L.S. Tsimring, 1986: Kinetic model of the wind generation of waves by a turbulent wind, Izv. Acad. Sci. USSR, *Atmos. Ocean Phys.*, 22, 102-107.

Oost, W.A., G.J. Komen, C.M.J. Jacobs and C. Van Oort, 2002: New evidence for a relation between wind stress and wave age from measurements during ASGAMAGE, *Boundary-Layer Meteorol.*, 103, 409-438.

Parvaresh, A., S. Hassanzadeh, and M.H. Bordbar, 2005: Statistical analysis of wave parameters in the north coast of the Persian Gulf, *Annales Geophysicae*, 23, 2031-2038.

Pattiaratchi, C., B.J. Hegge, J. Gould and I.G. Eliot, 1997: Impact of sea breeze activity on nearshore and foreshore processes in Southwestern Australia, *Cont. Shelf Research,* 17, 1539-1560.

Peregrine, D.H., 1967: Long waves on a beach, *J. Fluid Mech.*, 27, 815–827.

Philips, O.M., 1957: On the generation of waves by turbulent wind, *J. Fluid Mech.*, 2, 417-445.

Philips, O.M., 1977: The dynamics of the upper ocean, *Cambridge University Press, Cambridge,* 336 pp.

Pierson, W. J. and L. Moskowitz, 1964: A proposed spectral form for fully developed wind-seas based on the similarity theory of S. A. Kitaigorodskii, *J. Geophys. Res.*, 69(24), 5181-5190.

Pierson, W. J. and W. Marks, 1952: The power spectrum analysis of ocean wave record, *Trans. Amer. Geophys. Un.,* 33, 834-844.

Pierson, W. J., G. Neumann and R. W. James, 1955: Practical methods for observing and forecasting ocean waves by means of wave spectra and statistics, *US Navy Hydrographic Office Pub.*, 603.

Plant, W.J., 1982: A relationship between wind stress and wave slope, *J. Geophys. Res.*, 87(C3), 1961-1967.

Portilla, J., J.O. Francisco and J. Monbaliu, 2009: Spectral partitioning and identification of wind sea and swell, *J. Atmos. Oceanic Technol.*, 26, 107-122.

Prasad Kumar, B. and G.W. Stone, 2007: Numerical simulation of Typhoon wind forcing in the Korean Seas using a spectral wave model, *J. Coast. Res.*, 23(2), 362-373.

Prasad Kumar, B., R. Kalra, S.K. Dube, P.C. Sinha, A.D. Rao, R. Kumar and A. Sarkar, 2000: Extreme wave conditions over the Bay of Bengal during a severe cyclone - simulation experiment with two spectral wave models, *Marine Geodesy,* 23(2), 91-102.

Quilfen Y., B. Chapron, F. Collard and M. Serre, 2004: Calibration/Validation of an altimeter wave period model and application to TOPEX/Poseidon and Jason-1 altimeters, *Marine Geodesy, 27,* 3-4, 511-534.

Raj Kumar., S.A. Bhowmick, S. Ray, V. Bhatt, S. Surendran, S. Basu, A. Sarkar and V.K. Agarwal, 2009: Improvement in predictability of waves over the Indian Ocean, *Nat. Hazards*, 49, 275-291.

Rao C.V.K.P. and M. Baba, 1996: Observed wave characteristics during growth and decay: a case study, *Cont. Shelf Res.,* 16(12), 1509-1520.

Resio, D.T. and W. Perrie, 1991: A numerical study of nonlinear energy fluxes due to wave–wave interactions. Part 1: Methodology and basic results, *J. Fluid Mech.*, 223, 609–629.

Richter, K., B. Schmalfeldt, and J. Siebert, 1976: Bottom irregularities in the North Sea. *Dtsch. Hydrogr. Z.,* 29 (1), 1-10.

Rodriguez, G.R., and C. Guedes Soares, 1999: The Bivariate distribution of wave heights and periods in mixed sea states, *Journal of Offshore Mechanics and Arctic Engineering,* 121(2), 102-108.

Roland B. Stull, 1988: An introduction to Boundary Layer Meteorology, Kluwer Academic Publishers, 666 pp.

Sanil Kumar, V. and Ashok Kumar, 2008: Spectral characteristics of high shallow water waves, *Ocean Eng.*, 35; 900-911.

Sanil Kumar, V. and N.M. Anand, 2004a: Variations in wave direction estimated using first and second order Fourier coefficients, *Ocean Eng.,* 31, 2105-2119.

Sanil Kumar, V. and M.C. Deo, 2004b: Design wave estimation considering directional distribution of waves, *Ocean Eng.,* 31; 2343-2352.

Sanil Kumar, V., K. Ashok Kumar and N.S.N. Raju, 2004c: Wave characteristics off Visakhapatnam coast during a cyclone, *Current Science,* 86, 1524-1529.

Sanil Kumar, V., N.M. Anand, K.A. Kumar and S. Mandal, 2003a: Multipeakedness and groupiness of shallow water waves along Indian coast, *J. Coast. Res.*, 19, 1052-1065.

Sanil Kumar, V., S. Mandal and K. Ashok Kumar, 2003b: Estimation of wind speed and wave height during cyclones, *Ocean Eng.*, 30, 2239-2253.

Sanil Kumar, V., N.M. Anand, P. Chandramohan and G.N. Nayak, 2003c: Longshore sediment transport rate – measurement and estimation, central west coast of India, *Coastal Eng.*, 48, 95-109.

Sanil Kumar, V., N.M. Anand and R. Gowthaman, 2002: Variations in nearshore processes along Nagapattinam coast, India, *Current Science,* 82, 1381- 1389.

Sanil Kumar, V., K. Ashok Kumar and N.S.N. Raju, 2001: Nearshore Processes along Tikkavanipalem beach, Visakhapatnam, India, *J. Coast. Res.,* 17(2), 271-279.

Sanil Kumar, V., K. Ashok Kumar and N.M. Anand, 2000: Characteristics of waves off Goa, west coast of India, *J. Coast. Res.,* 16(3), 782-789.

Sanil Kumar,V., M.C. Deo, N.M. Anand and P. Chandramohan, 1999: Estimation of wave directional spreading in shallow water, *Ocean Eng.,* 26, 83-98.

Satheesan, K., A. Sarkar, M. Parekh, M.R. Ramesh Kumar and Y. Kuroda, 2007: Comparison of wind data from QuikSCAT and buoys in the Indian Ocean, *International J. Rem. Sens.*, 28(10), 2375-2382.

Seymour, R.J., 1977: Estimating wave generation on restricted fetches, *Proc. ASCE J. of Waterway Port, Coastal and Ocean Div.*, 103(2), 251-264.

Shahul Hameed, T.S., N.P. Kurian, K.V. Thomas, K. Rajith and T.N. Prakash, 2007: Wave and current regime off the southwest coast of India, *J. Coast. Res.,* 23(5), 1167-1174.

Shemdin, O. H., S. V. Hsiao, H. E. Carlson, K. Hasselman and K. Schulze, 1980: Mechanisms for wave transformation in finite depth water, *J. Geophys. Res.*, 5(C9), 5012-5018.

Sheremet, A. and G. Stone, 2003: Observations of nearshore wave dissipation over muddy sea beds, *J. Geophys. Res., 108 (C11)*, 3357. doi:10.1029/2003JC00188, 21-11.

Short, A. D., and N. L. Trenaman, 1992: Wave Climate of the Sydney Region, an Energetic and Highly Variable Ocean Wave Regime, *Aust. J. Mar. Freshwater Res.,* 43, 765-91.

Simpson, J. E., 1994: Sea breeze and Local Wind, *Cambridge Univ. Press, New York*, 234 pp.

Sindhu, B., I. Suresh, A.S. Unnikrishnan, N.V. Bhatkar, S. Neetu and G.S. Michael, 2007: Improved bathymetric data sets for the shallow water regions in the Indian Ocean, *J. Earth Sys. Sci.*, 116(3), 261-274.

Smith, J.M. and C.L. Vincent, 2002: Application of spectral equilibrium ranges in the surf zone, *Proc. 28th Int. Conf. on Coast Eng., World Scientific*, 269-279.

Smith, S.D., R.J. Anderson, W.A. Oost, C. Kraan, N. Maat, J. DeCosmo, K.B. Katsaros, K.L. Davidson, K. Bumke, L. Hasse and H.M. Chadwick, 1992: Sea surface wind stress and drag coefficients: the HEXOS results, *Boundary-Layer Meteorol.*, 60, 109–142.

Snyder, R.L., 1974: A field study of wave-induced pressure fluctuations above surface gravity waves, *J. Marine Res.*, 32, 497-531.

Snyder, R.L., F.W. Dobson, J.A. Elliot and R.B. Long, 1981: Array measurements of atmospheric pressure fluctuations above surface gravity waves, *J. Fluid Mech.*, 102, 1-59.

Sonu, C.J., S.P. Murray, S.A. Hsu, J.N. Suhayda and E. Waddell, 1973: Sea-breeze and coastal processes, *EOS, Trans.Am.Geophys. Union*, 54, 820-833.

Sudheesh K., P. Vethamony, M.T. Babu and S. JayaKumar, 2004: Assessment of wave modeling results with buoy and altimeter deep water waves for a summer monsoon, *Proceedings of the Third Indian National Conference on Harbour and Ocean Engineering (INCHOE - 2004). NIO, Goa (India),* 184-192.

Sullivan, P., J. McWilliams and C.H. Moeng, 2000: Simulation of turbulent flow over idealized water waves, *J. Fluid Mech.*, 404, 47-85.

Sundara Raman, K.V., M.J. Varkey, P.K. Vijayarajan, V.C. John and M.X. Joseph, 1974: Waves in coastal waters off Mangalore Pt. I: distribution of wave characteristics, *Indian J. Met. Geophys.*, 25, 3&4, 453-460.

Sverdrup, H.U. and W.H. Munk, 1947: Wind sea and swell: Theory of realtions for forecasting, *H.O. Pub. 601, US Navy Hydrographic Office, Washington, DC*, 44 pp.

Swain, J., P.N. Ananth and C.V.K.P. Rao, 1993: Shallow water wave characteristics off Cochin during monsoon 1986, *Indian J. Mar. Sci.*, 22(4), 256-262.

SWAMP Group, 1985: An inter-comparison study of wind wave prediction models. Part I, Principal results and conclusions, In: *Ocean Wave Modelling*, Plenum Press, New York, 256 pp.

Tang, W. and W.T. Liu, 1996: Objective interpolation of scatterometer winds, *JPL publication,* 96, 19, 16 pp.

Thornton, E.B. and R.T. Guza, 1983: Transformation of wave height distribution, *J. Geophys. Res.*, 88, 5925-5938.

Tolman, H.L., V.M. Krasnopolsky and D.V Chalikov, 2005: Neural network approximations for nonlinear interactions in wind wave spectra: direct mapping for wind seas in deep water, *Ocean Model.*, 8 (3), 253-278.

Tolman, H.L., 1999: User Manual and System Documentation of WAVEWATCHIII version 1.18, *NOAA/NWS/NCEP/OMB technical note,* 166, 100 pp.

Tolman H.L, 1998: Validation of NCEP's ocean winds for the use in wind wave models, *Global Atmos. Oc. System*, 6, 243-268.

Torsethaugen K. and S. Haver, 2004: Simplified double peak spectral model for ocean waves, *Proceedings of ISOPE conference,* 3, 76–84.

Vledder, G.Ph., 2001: Extension of the Discrete Interaction Approximation for computing nonlinear quadruplet wave-wave interactions in operational wave models, *4th ASCE International Symp. Ocean Waves, Meas. Anal., San Francisco, California, USA,* 540-549.

Verhagen, H.J. and B. Savov, 1999: Sea breeze generated waves and Coastal Morphology, *Proc. Int. Medcoast conference on Wind and Waves, Antalya, Turkey.*

Vethamony P., V.M. Aboobacker, K. Sudheesh, M.T. Babu and K. Ashok Kumar, 2009: Demarcation of inland vessels' limit off Mormugao Port region, India: a pilot study for the safety for inland vessels using wave modelling, *Nat. Hazards,* 49, 411-420.

Vethamony, P., K. Sudheesh, S.P. Rupali, M.T. Babu, S. Jayakumar, A.K. Saran, S.K. Basu, Raj Kumar and Abhijit Sarkar, 2006: Wave modelling for the north Indian Ocean using MSMR analysed winds, *International J. Rem. Sens.*, 27, 18, 3767-3780.

Vethamony P; K. Sudheesh, Asha Rajan, A.K. Saran, Sujit Basu, Raj Kumar and Abhijit Sarkar, 2003: Wave modelling using MSMR analysed winds, *Report No. NIO/TR/10/2003, February 2003, National Institute of Oceanography, Goa, India.*

Vethamony P. and J.S. Sastry, 1986: On the characteristics of multipeaked spectra of ocean surface waves, *J. Inst. Eng. India*, 66, 129-132.

Vilsmeier R. and D. Hänel 1995: Adaptive solutions for unsteady laminar flows on unstructured grids, *Int. J. Numer. Meth. Fluids*, 22, 85-101.

Violante-Carvalho, N., F.J. Ocampo-Torres and I.S. Robisnson, 2004: Buoy observations of the influence of swell on wind waves in the open ocean, *Applied Ocean Research,* 26, 49-60.

WAMDI Group, 1988: The WAM model - A third generation ocean wave prediction model, *J. Phys. Oceanogr.*, 18, 1775-1810.

Wang, D.W. and P.A. Hwang, 2001: An operational method for separating wind sea and swell from ocean wave spectra, *J. Atmos. Oceanic Technol.*, 18, 2052-2062.

Wilson, B.W., 1955: Graphical Approach to the Forecasting of Waves in Moving Fetches, *U.S. Beach Erosion Board, Corps of Engineers, Dept. of the Army Techn. Memo.*, 73, 1-31.

WISE Group, 2007: Wave modelling – the state of the art, *Progress in Oceanography,* 75, 603-674.

WMO, 1998: Guide to wave analysis and forecasting, *World Meteorological Organization,* WMO-No. 702.

Wright, L. D., J. D. Boon, S. C. Kim, and J. H. List, 1991: Modes of cross-shore sediment transport on the shoreface of the Middle Atlantic Bight, *Marine Geology,* 96, p. 19-51.

Young, I.R., 1999: Wind generated ocean waves, in *Elsevier Ocean Engineering Book Series, Volume 2, Eds. R. Bhattacharyya and M.E. McCromick, Elsevier.*

Zhukovets, A. M., 1963: The influence of bottom roughness on wave motion in a shallow body of water, *Izv. Acad. Sci. USSR Geophys. Ser.*, 10, 1561-1570.

Annexure I

Published papers

"Shamal" swells in the Arabian Sea and their influence along the west coast of India

V. M. Aboobacker,[1] P. Vethamony,[1] and R. Rashmi[1]

Received 5 October 2010; revised 7 January 2011; accepted 10 January 2011; published 8 February 2011.

[1] Wave data collected off Ratnagiri, Goa and Dwarka along the west coast of India during winter season (NE monsoon and early pre-monsoon) present distinct wave characteristics with periodicity ranging between 2 and 5 days associated with shamal events. The notable wave characteristics during these events are: an increase in wave height, decrease in swell period and a common propagation direction (northwest) for wind sea and swell. IFREMER/CERSAT blended winds clearly show the presence of strong northwesterly winds in the Arabian Peninsula and northwestern Arabian Sea, which are associated with the winter shamal events. The winds during such events generate large northwesterly swells (shamal swells) in the northwestern Arabian Sea and propagate towards the west coast of India in the NW direction with mean periods ranging between 6 and 8 s. Numerical simulations reproduce the shamal swells over the Arabian Sea, and they can be traced all along the west coast of India, however, with lesser order of magnitude from north to south. Generation and propagation of shamal swells and their influence along the west coast of India have been described. **Citation:** Aboobacker, V. M., P. Vethamony, and R. Rashmi (2011), "Shamal" swells in the Arabian Sea and their influence along the west coast of India, *Geophys. Res. Lett.*, *38*, L03608, doi:10.1029/2010GL045736.

1. Introduction

[2] The word "shamal" in Arabic literally means "north" and the winds during shamal events are named as shamal winds. Shamal winds normally occur in the Arabian Peninsula during winter (November to March) and summer (June to August). The onset, duration and strength of the shamal winds vary depending on the dynamic interaction of upper air jet streams and distribution of lower tropospheric pressure zones [*Ali*, 1994]. The winter shamal is associated with mid-latitude disturbances travelling from the west to the east, which has a high impact on the meteorological conditions over the Arabian Peninsula [*Hubert et al.*, 1983]. It usually occurs following the passage of cold fronts, and is characterized by strong northwesterly winds. Based on the intensity, shamal periodicities are classified as follows: (i) 24 to 36 hours and (ii) 3 to 5 days. The associated wind speeds can reach up to 20 m/s, and this can generate surface waves as high as 3.0 to 4.0 m in the Arabian/Persian Gulf [*Hubert et al.*, 1983].

[1]National Institute of Oceanography, CSIR, Goa, India.

0094-8276/11/2010GL045736

[3] General swell patterns in the Arabian Sea are from the southwest or south, propagating from the south Indian Ocean [e.g., *Sanil Kumar et al.*, 2000; *Kumar et al.*, 2009; *Kurian et al.*, 2009]. On several occasions, swells propagating from the northwest were also observed. Studies on wave characteristics and storm surges due to shamal winds are very limited and restricted to the Arabian/Persian Gulf region only [e.g., *El-Sabh and Murty*, 1989; *Parvaresh et al.*, 2005]. Shamal winds could have a significant impact on the meteorological and oceanographic conditions of the Arabian Sea, and this has not been studied so far. Rapid changes in wind patterns during these shamal events can alter the wave characteristics of the Arabian Sea. This has motivated us to take up the present study with the following objectives: (i) generation and propagation of shamal swells in the Arabian Sea, and (ii) influence of shamal swells on the wave characteristics along the west coast of India.

2. Area of Study

[4] Figure 1a shows the study area. The Arabian Sea experiences three different seasons: pre-monsoon (February–May), southwest monsoon (June–September) and northeast monsoon (October–January). The winds are stronger during southwest (SW) monsoon season and generally weak during pre-monsoon and northeast (NE) monsoon seasons. Large scale winds are weak during pre-monsoon season and hence sea breeze has an impact on the diurnal cycle of the sea state along the west coast of India [*Neetu et al.*, 2006]. Co-existence of wind seas and pre-existing swells creates diurnal variations on the resultant waves along the west coast of India during pre-monsoon season [*Vethamony et al.*, 2009]. During NE monsoon season, the predominant winds in the Arabian Sea are northeasterlies. The waves generated due to NE winds are relatively weak and propagate away from the coast. However, swells from SW or S dominate along the west coast of India during NE monsoon season.

3. Data and Methodology

[5] Directional waves are measured using a Datawell directional wave rider buoy for the periods 24 January–25 February 2008 (off Ratnagiri at 35 m), 05 December 2007–05 January 2008 (off Dwarka at 30 m) and February 1996–May 1997 (off Goa at 23 m) (Figure 1a). The data was collected at 1 hour interval off Ratnagiri and Dwarka, and at 3 hours interval off Goa with a sampling period of 20 minutes. The wave rider buoy has an accuracy of 3% for wave height and within 0.5–2° for wave direction. Wind sea and swell parameters were calculated from the measured wave energy spectra using the methodology provided by *Gilhousen and Hervey* [2001]. Simultaneous wind mea-

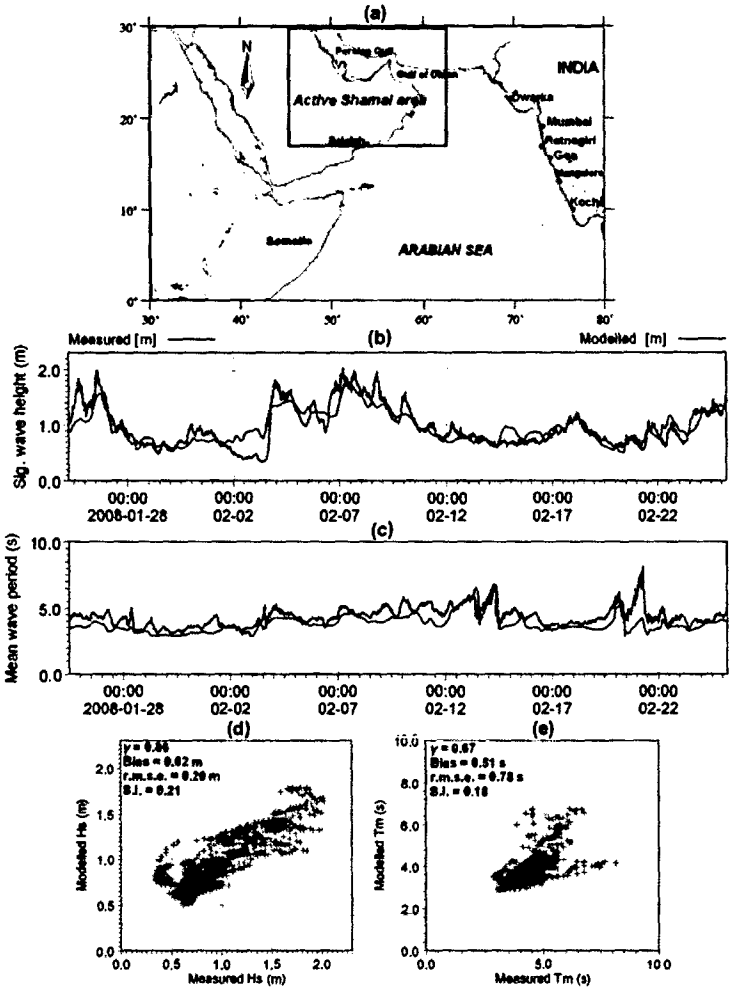

Figure 1. (a) Study area, (b) measured and modelled significant wave height, (c) measured and modelled mean wave period, (d) scatter of significant wave height, and (e) scatter of mean wave period.

surements were carried out at Ratnagiri and Dwarka coastal stations using an Autonomous Weather Station (AWS) of the National Institute of Oceanography (NIO), Goa. The AWS provided wind speed and direction at 10-minutes interval. The accuracy of AWS is: 0.2 m/s for wind speed in the range 0–60 m/s and 3° for wind direction in the range 0–360°.

[6] IFREMER/CERSAT blended winds (U and V components) were analysed and used as input for numerical simulations. These are remotely sensed retrievals from QuikScat [*Ebuchi et al.*, 2002] blended to the operational ECMWF wind analysis over the global oceans by the IFREMER/CERSAT and available for every 6 hours with 0.25° × 0.25° grid spacing [*Bentamy et al.*, 2006, 2009]. The quality of this data has been checked with buoy winds and the match is very good [*Bentamy et al.*, 2007].

[7] Numerical simulations have been carried out to reproduce wind sea, swell and resultant wave characteristics in the Arabian Sea using MIKE 21 SW - a spectral wind wave model developed by the DHI Water & Environment, Denmark [*DHI*, 2007]. The model domain covers the entire Indian Ocean (65° S to 30° N and 20° to 125° E). A flexible mesh has been generated using Etopo 5 bathymetry data obtained from NGDC (National Geophysical Data Center, USA) for deep water and modified bathymetry data from *Sindhu et al.* [2007] for coastal region. The selected resolutions for the flexible mesh bathymetry are: 1.5° in the south Indian Ocean, 0.5° in the north Indian Ocean, 0.25° around the Indian coast and 5 km along the west coast of India. Major outputs from the simulations are integral wave parameters such as significant wave height, mean wave period and mean wave direction.

4. Results and Discussion

4.1. Model Validation

[8] The modelled wave parameters have been validated with measured wave parameters off Ratnagiri during 24 January–25 February 2008. It has been found that the modelled significant wave height (H_s) and mean wave period (T_m) match reasonably well with the measurements (Figures 1b and 1c). The scatter (Figures 1d and 1e) shows that measured and modelled H_s and T_m are linearly correlated. Correlation coefficient, bias, r.m.s. error and scatter

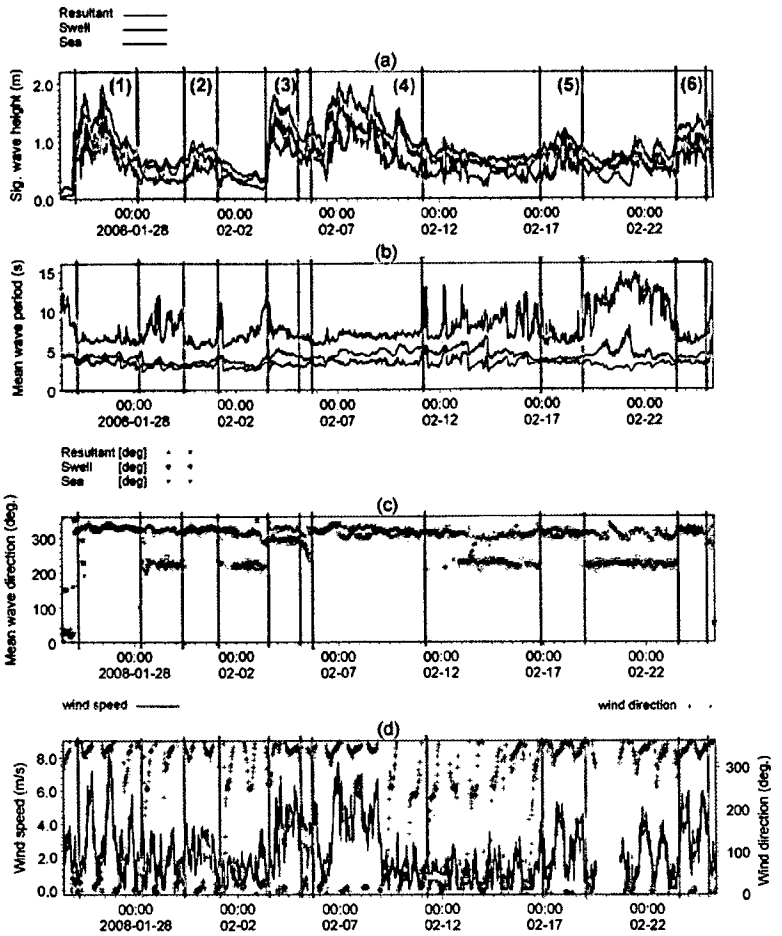

Figure 2. Measured wave and wind parameters off Ratnagiri: (a) significant wave height, (b) mean wave period, (c) mean wave direction, and (d) AWS wind speed and direction. Well-defined features on wave and wind parameters are marked from (1) to (6).

index are 0.86, 0.02 m, 0.20 m and 0.21, respectively for H_s and 0.67, 0.51 s, 0.78 s and 0.18, respectively for T_m.

4.2. Characteristics of "Shamal" Swells

[9] The measured waves off Ratnagiri show systematic variations in the wave parameters during several occasions (Figure 2). During NE monsoon and early pre-monsoon seasons, nearshore wave heights along the west coast of India are generally low (<1.0 m). However, waves with H_s of the order of 1.0–2.0 m were observed at several occasions during 24 January–25 February 2008. Further analysis shows that wave parameters exhibit distinct characteristics, namely, (a) increase in wave heights associated with decrease in swell period and (b) a common propagation direction (NW) for wind sea, swell and resultant waves (Figures 2a–2c). Measured winds at Ratnagiri coast also show systematic variations during the above period (Figure 2d). The systematic features observed in the wind and wave parameters are indicated as (1) to (6) in Figure 2. During this period, the H_s is in the range of 1.0 to 2.0 m, mean swell periods are between 6.0 and 8.0 s and predominant wind and wave directions is NW.

[10] The directional energy spectra show peak energy in the swell region, between the frequencies 0.1 and 0.2 Hz in the NW direction, contrary to the normal swell conditions along the west coast of India, wherein energy is distributed between 0.05 and 0.15 Hz in the SW or S direction [e.g., *Vethamony et al.*, 2009]. Typical directional energy spectra measured off Ratnagiri during shamal period and non-shamal period are shown in Figures 3a and 4b. Swells from the south Indian Ocean (S or SW direction) are generally observed along the west coast of India, which are mostly "old swells" (significant wave steepness, $H_s/L < 0.004$, where L is the wavelength). However, NW swells generated in the northern Arabian Sea can propagate to the west coast within a short duration, and that is the reason for observing mostly "young" ($0.01 \leq H_s/L > 0.025$) or "mature" ($0.004 \leq H_s/L > 0.01$) swells from the NW direction. On an average, "young", "mature" and "old" swells (NW swells) were 76%, 21% and 3%, respectively during the study period.

[11] The predominant winds in the Arabian Sea during the NE monsoon and early pre-monsoon seasons are from NE, and the wind speeds are of the order of 5 to 10 m/s. On several occasions, it was observed that the NE winds become weak, and NW winds become stronger, especially

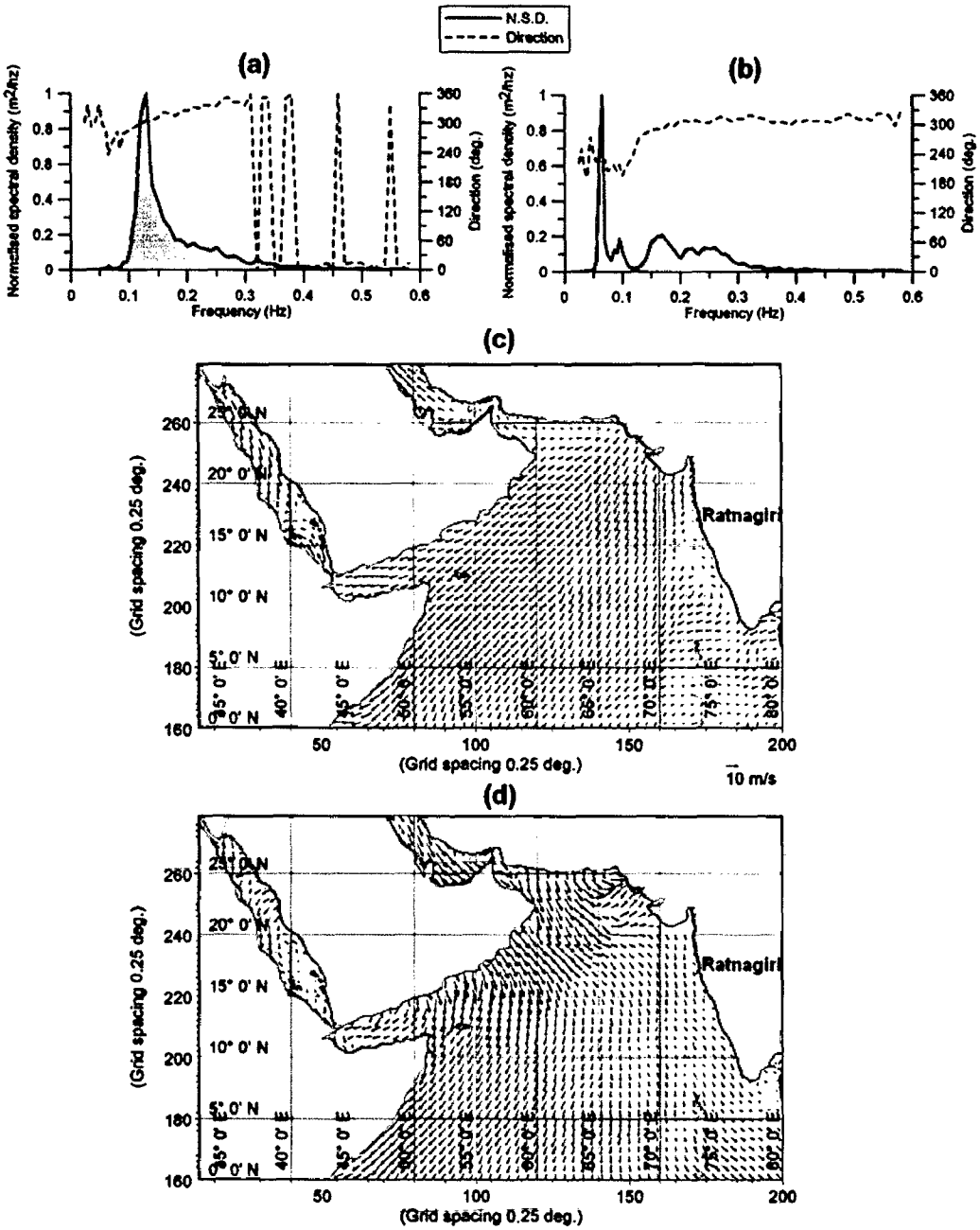

Figure 3. Typical directional energy spectra during (a) shamal period (07-02-2008 03:00) and (b) non-shamal period (15-02-2008 02:00), and Typical wind vectors over the Arabian Sea associated with (c) NE monsoon (12-02-2008 18:00) and (d) shamal event (02-02-2008 06:00).

in the north-western Arabian Sea and in the Arabian Peninsula. These winds are associated with shamal events (active shamal area is marked in Figure 1a). Typical wind vectors in the Arabian Sea during NE monsoon and during shamal events are shown in Figures 3c and 3d, respectively. The wind speeds associated with shamal events range between 10 and 20 m/s. As evident from the AWS winds at Ratnagiri coast (Figure 2d), shamal winds can extend up to the west coast of India, though the magnitudes are relatively less along the coastal regions. These winds are stronger at the northern part of the west coast of India. The period and duration of the shamal events closely match with those of the systematic features observed in the measured wave parameters and AWS winds. Considering the above facts, it has been concluded that the systematic features observed in the wave parameters during the winter season are primarily due to the impact of shamal winds, which generate high energy waves and propagate to the west coast of India as swells. These swells are hereafter referred as "shamal" swells.

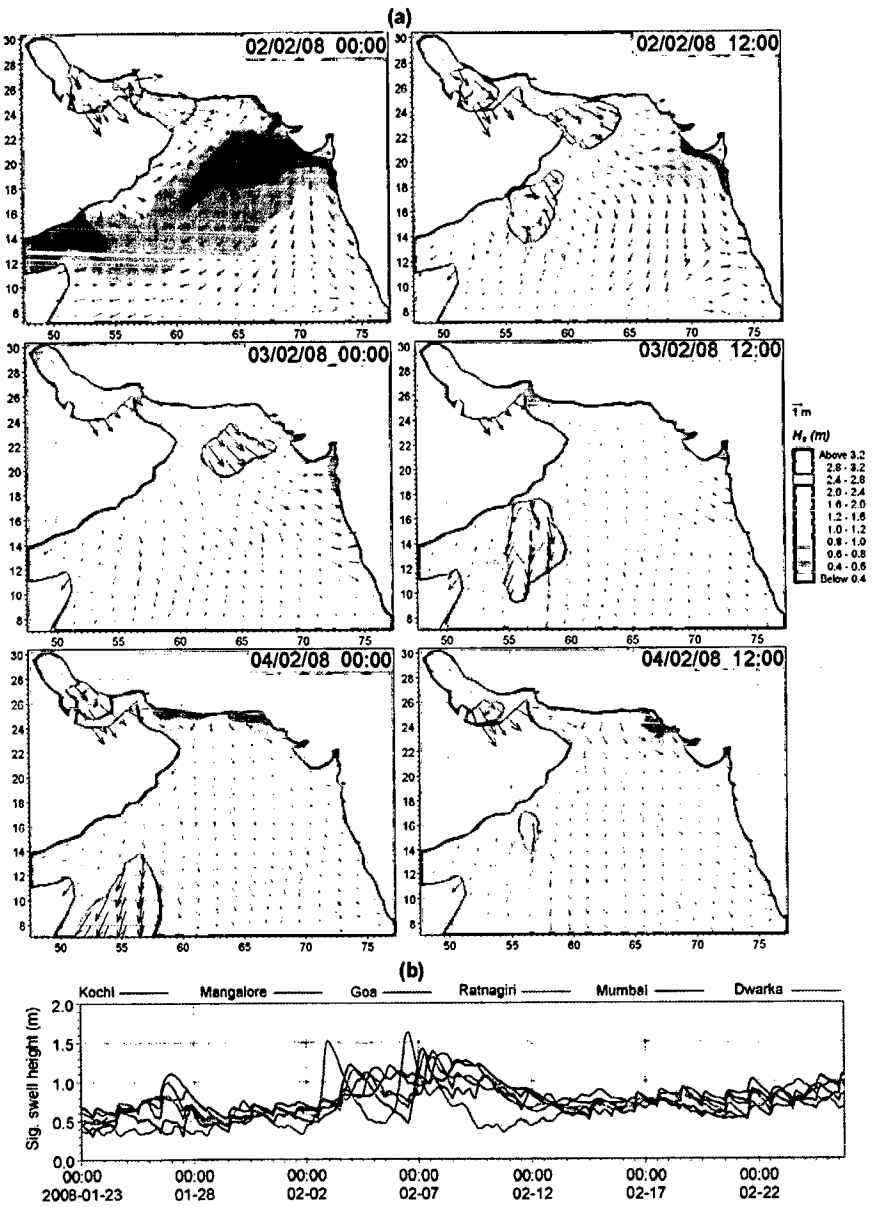

Figure 4. (a) H_s vectors in the Arabian Sea during 02–04 Feb 2008 and (b) swell H_s off Kochi, Mangalore, Goa, Ratnagiri and Mumbai at 25 m water depth.

[12] Waves measured at 23 m water depth off Goa during February 1996–May 1997 also show similar features. It has been noticed that such well-defined features are observed between November and March, and more frequently in January and February. Winds associated with summer shamal events are relatively weaker, and their impact on the wave characteristics along the west coast of India is negligible due to the prevailing SW monsoon winds, which generate higher waves during this season.

4.3. Generation and Propagation

[13] Numerical simulations carried out using IFREMER/CERSAT blended winds during January–February 2008 reproduced the generation and propagation characteristics of shamal swells in the Indian Ocean. Analysis of swell, wind sea and the resultant wave parameters obtained from the simulations indicates that the waves generated due to strong shamal winds over the northwestern Arabian Sea propagate in the NW direction towards the west coast of India. A gradual wind wave growth has been observed with respect to increase in wind speed during shamal events. H_s reaches above 4.0 m in the Persian Gulf. However, propagation of the waves generated in the Persian Gulf to the rest of the Arabian Sea is obstructed at Hormuz Strait due to the narrow opening and shallow water depths. It has also been found that the shamal winds generate higher waves in the NW direction at the northwestern Arabian Sea (excluding the Persian Gulf). The associated H_s reaches above 3.5 m

within a fetch of ≈300 km. Once they leave the generating area, they propagate in the NW direction as shamal swells.

[14] Figure 4a shows the H_s vectors (12 h interval) in the Arabian Sea representing the generation and propagation of shamal swells during 02–04 February 2008. It is evident that larger waves are generated in the Persian Gulf, Gulf of Oman and off the east coast of Oman due to strong shamal winds. The swells generated in the Gulf of Oman and the east coast of Oman propagate in the NW direction. Another swell system formed off Salalah coast (Figure 4a) propagates in the NNW direction. Since the present study aims at understanding the influence of shamal swells along the west coast of India, significance has been attached to the NW swells, generated in the northwestern Arabian Sea (Gulf of Oman and off the east coast of Oman).

[15] It is evident that the shamal swells propagate towards the west coast of India in the NW direction. The arrival time of the swells depends on the distance of propagation to various locations along the west coast of India. The swells arrive early (<20 h) along the Gujarat coast and later (around 48 h) along the Kerala coast. The swells observed off Gujarat coast have higher energy than those observed off the Kerala coast, indicating that the coastal region of Gujarat is impacted by the shamal swells to a high degree. The deep water group velocity of the shamal swells is approximately 9 m/s. The distance of swell propagation to the Ratnagiri coast is around 1200–1500 km. Hence, a propagation time of 37–46 h has been estimated for the shamal swells to reach the Ratnagiri coast.

4.4. Influence Along the West Coast of India

[16] Swell heights obtained from the numerical simulations at 25 m depth off Kochi, Mangalore, Goa, Ratnagiri, Mumbai and Dwarka during the study period are presented in Figure 4b. Variations in swell heights associated with shamal events indicate that all the above locations along the west coast of India are influenced by shamal swells, though there are changes in patterns and heights according to the intensity and duration of the event. The swell heights are higher off Dwarka, indicating that the open coast of Gujarat is highly influenced by shamal swells. A similar pattern is observed off Mumbai, but swell heights are relatively low compared to those off Dwarka. The swell pattern off Ratnagiri, Goa, Mangalore and Kochi are nearly the same; the respective time lags have been estimated for all the locations according to the swell propagation time.

[17] An analysis of the measured waves off Dwarka (at 30 m depth) during 05 Dec 2007–05 Jan 2008 indicates that the shamal swells with short duration (<24 h) are present though their heights are relatively less compared to the shamal swells observed off Ratnagiri during 24 Jan–25 Feb 2008. During non-shamal periods the waves off Dwarka are dominated by wind seas, as evident from the measurements. Measured waves off Goa (at 23 m depth) during November 1996–March 1997 also show the presence of shamal swells. Increase in wave height associated with decrease in swell period and propagation of wind sea and swell in the NW direction are prominent during the shamal events. Even though shamal swells exist, at times, the wind sea energy in the NW direction (generated by shamal winds) dominates over the swell energy, which provides an indication to the extension of shamal winds up to the west coast of India. However, this has to be confirmed through detailed investigations.

5. Conclusions

[18] The characteristics of shamal swells were analysed using the wave data collected off Ratnagiri during the winter season of 2008. An increase in wave heights, decrease in swell periods and common propagation direction (NW) for wind sea and swell were observed during the shamal events. Typical mean periods of the shamal swells are between 6 and 8 s. Measured waves off Goa and Dwarka exhibit similar features during shamal events. It is evident from the numerical simulations that winds during shamal events generate high waves in the northwestern Arabian Sea, which propagate as swells in the NW direction and reach along the west coast of India. The potential swell generating areas are the Gulf of Oman and off the east coast of Oman. The significant wave heights associated with shamal events reach above 3.5 m in the northwestern Arabian Sea and between 1.0 and 2.0 m along the west coast of India.

[19] Shamal winds can influence the wind-induced circulation in the Arabian Sea. Studies on shamal winds extension and their distribution along the west coast of India require fine resolution winds (e.g., MM5 winds). Even though swells from the south Indian Ocean are always present along the west coast of India, the shamal swells dominate over these swells. However, interaction between these multi-directional swells has to be investigated further.

[20] **Acknowledgments.** We thank S.R. Shetye, the Director, National Institute of Oceanography (NIO), Goa for providing necessary facilities and encouragement. We acknowledge all the project participants for their help during data collection. This study is carried out as a part of the partial fulfillment of Ph.D. work of the first author. The NIO contribution number is 4899.

References

Ali, A. H. (1994), Wind regime of the Arabian Gulf, in *The Gulf War and the Environment*, pp. 31–48, Gordon and Breach, New York.

Bentamy, A., H. L. Ayina, P. Queffeulou, and D. Croize-Fillon (2006), Improved near real time surface wind resolution over the Mediterranean Sea, *Ocean Sci. Discuss.*, *3*, 435–470, doi:10.5194/osd-3-435-2006.

Bentamy, A., H. L. Ayina, P. Queffeulou, D. Croize-Fillon, and V. Kerbaol (2007), Improved near real time surface wind resolution over the Mediterrancan Sea, *Ocean Sci. Discuss.*, *3*, 259–271.

Bentamy, A., D. Croize-Fillon, P. Queffeulou, C. Liu, and H. Roquet (2009), Evaluation of high-resolution surface wind products at global and regional scales, *J. Oper. Oceanogr.*, *2*(2), 15–27.

DHI (2007), *MIKE 21 Wave Modelling User Guide*, DHI Water and Environ., Aarhus, Denmark.

Ebuchi, N., H. C. Graber, and M. J. Caruso (2002), Evaluation of wind vectors observed by QuikSCAT/SeaWinds using ocean buoy data, *J. Atmos. Oceanic Technol.*, *19*, 2049–2062, doi:10.1175/1520-0426(2002)019<2049:EOWVOB>2.0.CO;2.

El-Sabh, M. I., and T. S. Murty (1989), Storm surges in the Arabian Gulf, *Nat. Hazards*, *1*, 371–385, doi:10.1007/BF00134834.

Gilhousen, D. B., and R. Hervey (2001), Improved Estimates of Swell from Moored Buoys, in *Proceedings of the Fourth International symposium WAVES 2001*, pp. 387–393, Am. Soc. of Civ. Eng., Alexandria, Va.

Hubert, W. E., D. R. Morford, A. N. Hull, and R. E. Englebretson (1983), *Forecasters Handbook for the Middle East/Arabian Sea*, Naval Environ. Predict. Res. Facil., Monterey, Calif.

Kurian, N. P., K. Rajith, T. S. Shahul Hameed, L. Sheela Nair, M. V. Ramana Murthy, S. Arjun, and V. R. Shamji (2009), Wind waves and sediment transport regime off the south-central Kerala coast, India, *Nat. Hazards*, *49*, 325–345, doi:10.1007/s11069-008-9318-3.

Neetu, S., S. Shetye, and P. Chandramohan (2006), Impact of sea-breeze on wind-seas off Goa, west coast of India, *J. Earth Syst. Sci.*, *115*(2), 229–234, doi:10.1007/BF02702036.

Parvaresh, A., S. Hassanzadeh, and M. H. Bordbar (2005), Statistical analysis of wave parameters in the north coast of the Persian Gulf, *Ann. Geophys.*, *23*, 2031–2038, doi:10.5194/angeo-23-2031-2005.

Kumar, R., S. A. Bhowmick, S. Ray, V. Bhatt, S. Surendran, S. Basu, A. Sarkar, and V. K. Agarwal (2009), Improvement in predictability of waves over the Indian Ocean, *Nat. Hazards*, *49*, 275–291, doi:10.1007/s11069-008-9310-y.

Sanil Kumar, V., K. Ashok Kumar, and N. M. Anand (2000), Characteristics of waves off Goa, west coast of India, *J. Coastal Res.*, *16*(3), 782–789.

Sindhu, B., I. Suresh, A. S. Unnikrishnan, N. V. Bhatkar, S. Neetu, and G. S. Michael (2007), Improved bathymetric data sets for the shallow water regions in the Indian Ocean, *J. Earth Syst. Sci.*, *116*(3), 261–274, doi:10.1007/s12040-007-0025-3.

Vethamony, P., V. M. Aboobacker, K. Sudheesh, M. T. Babu, and K. Ashok Kumar (2009), Demarcation of inland vessels' limit off Mormugao Port region, India: A pilot study for the safety for inland vessels using wave modelling, *Nat. Hazards*, *49*, 411–420, doi:10.1007/s11069-008-9295-6.

V. M. Aboobacker, R. Rashmi, and P. Vethamony, National Institute of Oceanography, CSIR, Dona Paula, Goa, 403004, India.

Nat Hazards (2009) 49:311–323
DOI 10.1007/s11069-008-9293-8

ORIGINAL PAPER

Spectral characteristics of the nearshore waves off Paradip, India during monsoon and extreme events

V. M. Aboobacker · P. Vethamony · K. Sudheesh · S. P. Rupali

Received: 13 May 2008 / Accepted: 5 September 2008 / Published online: 25 September 2008

Abstract Spectral and statistical wave parameters obtained from the measured time series wave data off Paradip, east coast of India during May 1996–January 1997 were analysed along with MIKE 21 spectral wave model (SW) results. Statistical wave parameters and directional wave energy spectra distinctly separate out the wave conditions that prevailed off Paradip in the monsoon, fair weather and extreme weather events during the above period. Frequency-energy spectra during extreme events are single peaked, and the maximum energy distribution is in a narrow frequency band with an average directional spreading of 20°. Spectra for other seasons are multi-peaked, and energy is distributed over a wide range of frequencies and directions. The NCEP re-analysis winds were used in the model, and the results clearly bring out the wave features during depressions. The simulated wave parameters reasonably show good match with the measurements. For example, the correlation coefficient between the measured and modelled significant wave height is 0.87 and the bias −0.25.

Keywords Directional wave spectra · Depressions · Wave measurements · MIKE21 · Wave modelling · Paradip coast

1 Introduction

Wave is the dominant forcing parameter for most of the nearshore processes. Design of coastal structures to a large extent depends on waves than any other environmental factors.

V. M. Aboobacker · P. Vethamony (✉) · K. Sudheesh · S. P. Rupali
National Institute of Oceanography, Dona Paula, Goa 403004, India
e-mail: mony@nio.org

V. M. Aboobacker
e-mail: vmabacker@gmail.com

K. Sudheesh
e-mail: ksudheesh@nio.org

S. P. Rupali
e-mail: rupali@nio.org

When waves generated by storms leave the zone of generation, they couple with locally generated waves, and create complex characteristics in the nearshore region. The east coast of India is characterised by narrow continental shelf width compared to the west coast. The sudden decrease in water depth causes the waves to surge further during extreme events, creating severe coastal hazards (Sanil Kumar et al. 2004). The present study is important because Paradip region houses Paradip Port and several other major industries, and this region is vulnerable to cyclones frequently.

Deepwater waves can be well modelled with third-generation wave models which are driven by predicted wind fields (e.g. WAMDI Group 1988), and based on physical processes rather than empirical formulations. However, as temporal and spatial resolutions of most of the wind models are coarse, some of the major features, such as wind information near the eye of cyclones cannot be incorporated accurately. Also, the impact of locally generated winds on nearshore waves cannot be predicted with coarse resolution wind fields.

The Bay of Bengal (north Indian Ocean) experiences three different weather conditions—fair weather, southwest monsoon and northeast monsoon. During fair weather season, the sea surface is usually calm and the coastal region is dominated by swells and to a smaller extent by locally generated waves. Extreme weather events are common during southwest monsoon (June–September) and northeast monsoon (October–December) seasons.

We have observed that in the Bay of Bengal, in general, the wave spectra are double- or multi-peaked. The double-peaked spectra are mainly due to the existence of wind seas along with the 'young' swells. Multi-peaked spectra are due to complex sea state where the separation of wind seas and swells is complicated. The single-peaked spectra are observed during extreme events, wherein all the energies are concentrated in the low-frequency region.

Low-frequency waves (swells) can propagate faster than the generated wind fields and reach areas not influenced by this wind field. This swell component adds to the locally generated wind sea and create double (or multiple)-peaked spectra.

For swell dominated sea, if the local wind decays, the waves will loose energy for high frequencies. This swell ("old" wind sea) can represent the highest spectral peak if no new local wind seas are generated with sufficient spectral peak density. For wind dominated sea, the secondary system represents an average of swell sea for the area, whereas for swell dominated sea, the secondary sea system represents local wind sea.

In this study, MIKE 21 two-dimensional Offshore Spectral Wave model (OSW) developed by the Danish Hydraulic Institute (DHI), Denmark (Anonymous 2001) has been utilised to simulate offshore waves off Paradip. This model has been used earlier for comparing waves derived from MSMR winds and NCEP reanalysis winds with measured waves of north Indian Ocean (Sudheesh et al. 2004; Vethamony et al. 2006). MIKE 21 Spectral Wave model (SW) has been used to simulate nearshore wave characteristics, taking into account the results of OSW.

2 Data and methods

2.1 Data

Wave measurements were carried out off Paradip (Fig. 1) during May 1996–January 1997 using a Datawell directional wave rider buoy deployed at the location 20°08.57′ N and

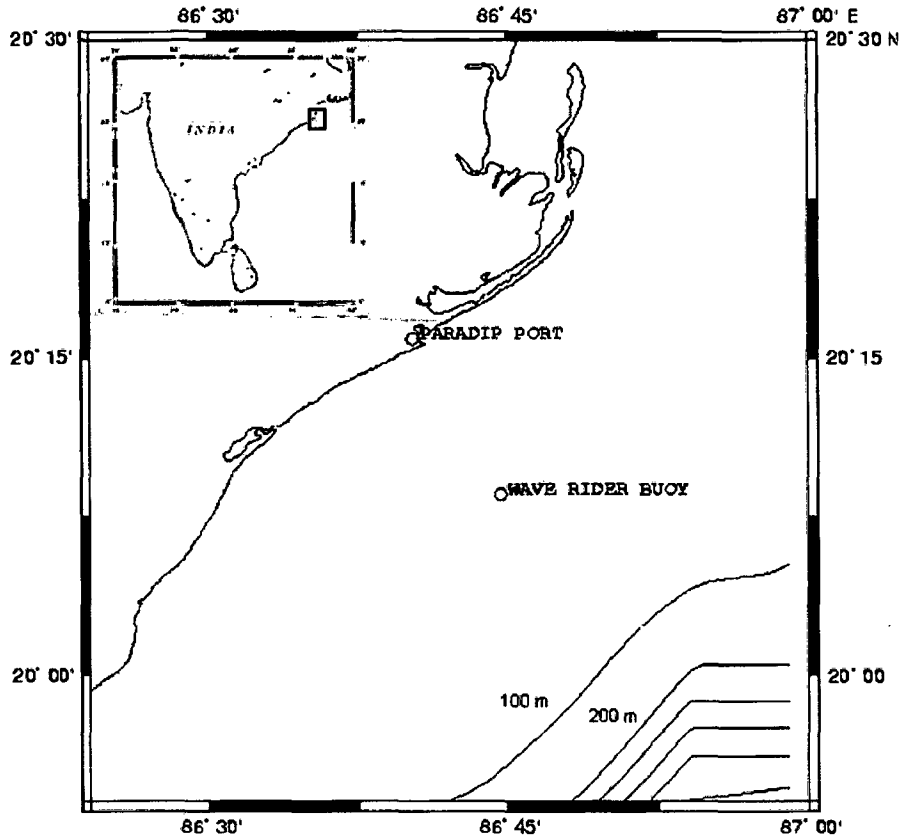

Fig.1 Study area showing the wave measurement location

86°44.67′ E, where the water depth is 30 m. A few data loss are found on the days when the buoy was retrieved for safety during extreme events or maintenance. Wave statistics and directional spectra of the region are discussed for different seasons—pre-monsoon (May), southwest monsoon (June–September) and northeast monsoon (November–January) and extreme events.

Indian Daily Weather Report (Anonymous 1996) reveals the presence of 4 storms/depressions in the Bay of Bengal during the study period. The pressure level data from the Cyclone Detection Radar Centre at Paradip indicates that pressure dropped from 1003.1 to 996.9 mb during 26–30 May 1996, from 1008.0 to 994.2 mb during 10–21 June 1996 and from 1003.0 to 991.2 mb during 18–26 July 1996 (Fig. 2), leading to extreme wave conditions. The fourth depression could not intensify, though the pressure level decreased from 1012.3 to 1000.4 mb during 24–28 October 1996.

Reanalysed NCEP winds available in the form of **U** and **V** components for 2.5° × 2.5° grids and for every 6-h intervals have been interpolated into 0.75° × 0.75° grid size by linear interpolation. The Etopo-5 bathymetry data (National Geophysical Data Centre, USA) available in 5′ × 5′ grid is extracted for every 0.75° × 0.75° grid as OSW requires only coarse resolution. The bathymetry data for the nearshore flexible mesh model is taken from MIKE CMAP of DHI—digitised data of hydrographic charts.

2.2 Offshore spectral wave model (OSW)

The OSW consists of second- and third-generation models, WAM 2G and WAM 3G. The second-generation model WAM 2G is utilised in the present study. It is a spectral

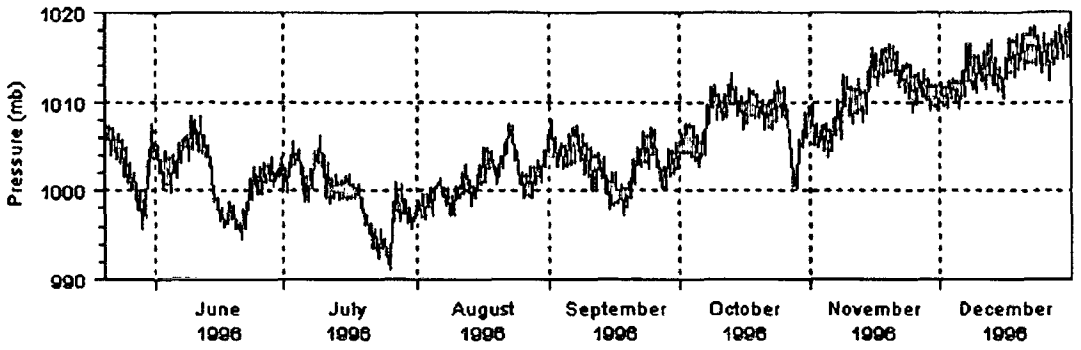

Fig. 2 Pressure levels during May 1996–December 1996

wind-wave model describing the propagation, growth and decay of short-period waves in the offshore areas. The model takes care of the effects of wave generation due to winds, refraction, shoaling due to varying depths and frictional resistance. It also includes the effect of interaction between waves with different frequencies. The model is based on the numerical integration of the spectral energy balance equation formulated in Cartesian co-ordinates. For the calculation of transport of wave energy from one time step to the next, a Lagrangian transport scheme is applied.

The model domain for the MIKE21 OSW ranges from 5° S to 25° N and from 50° E to 95° E, and is divided into 40 × 60 grids in longitude and latitude, respectively, with a grid spacing of 0.75° × 0.75°. The boundary along 5° S latitude is considered as open boundary, and all other boundaries are closed. The model starts with zero energy in all grid points, that is, the model performs a 'cold' start so that it takes a few time steps to perform the actual simulations. To provide an accurate description of the transport of energy, the time steps with 1-h intervals are selected so that the Courant number based on the group velocity is less than unity. Simulations are carried out for the year 1996 and wave parameters are extracted for every 3 h.

2.3 Flexible mesh model

Nearshore wave simulations are carried out using the MIKE 21 flexible mesh SW model. The offshore and alongshore extensions are 150 km and 100 km, respectively, from the origin (Fig. 3). The region including the measurement location is triangulated with a maximum area of 5 km × 5 km and the shallowest region with a maximum area of 1.5 km × 1.5 km. The water points are interpolated in the entire mesh by Natural Neighbourhood method so that output parameters from any desired point can be extracted.

There are three open boundaries—north, east and south, out of which north boundary is considered as lateral boundary. The boundary conditions are extracted from the output of MIKE21 OSW, and applied to the east and south boundaries. The SW model output parameters at the buoy location are compared with the measurements.

The model simulations are made by considering 97092-time steps with an interval of 200 s. The total computational time required is around 14.5 h (52429 s) in 32-bit PC having dual processors. The number of elements in the computational mesh is 1359.

3 Results and discussions

In May 1996 (pre-monsoon season), the predominant wave direction was between SSW and SSE with significant wave heights varying between 0.9 and 2.7 m (Fig. 4). The

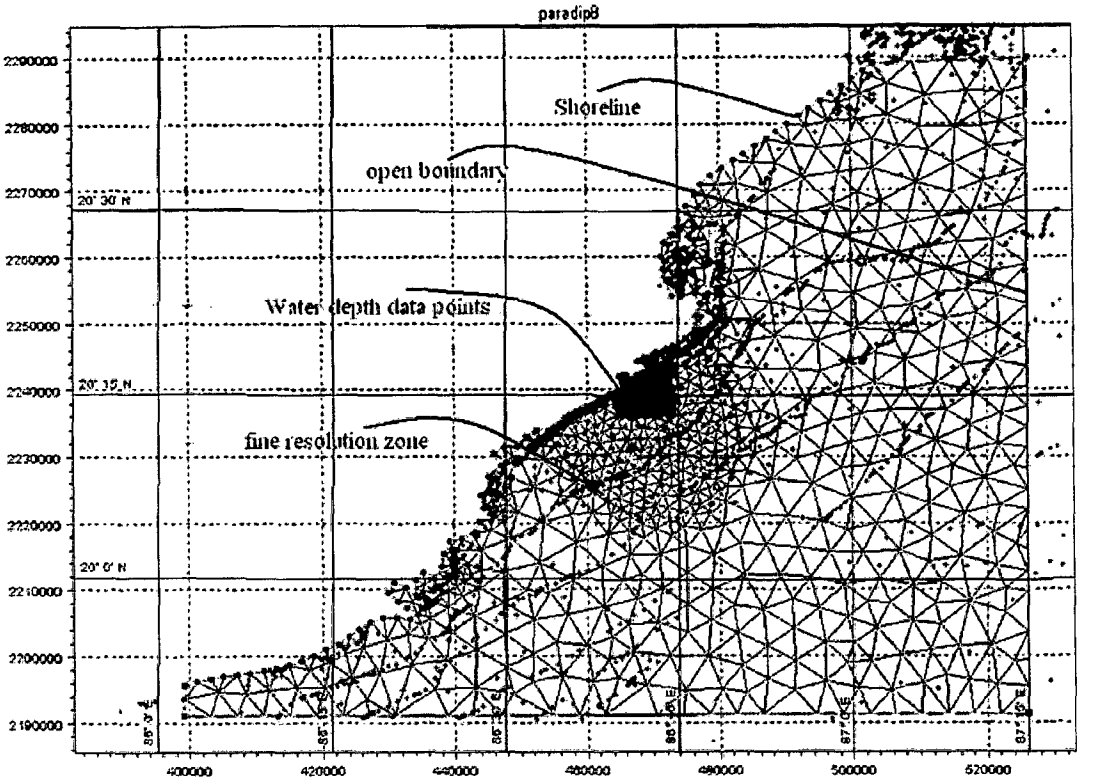

Fig. 3 Triangulated flexible mesh and model domain for nearshore wave prediction using spectral wave model

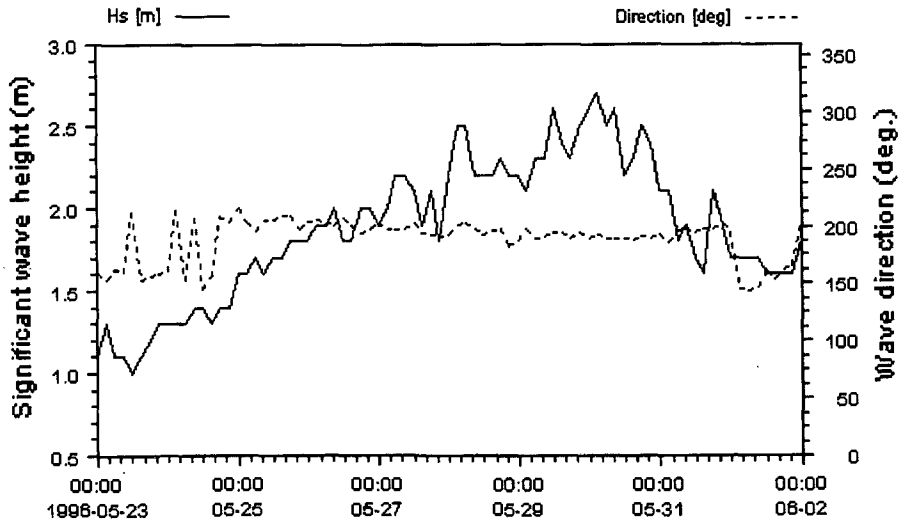

Fig. 4 Significant wave height pattern during an extreme event (23 May–02 June 1996) indicating wave growth and decay

depression during 26–30 May, 1996 caused the waves to grow and the significant wave height reached up to 2.7 m on 28 May in the SSW direction. On 29 May, the wave direction shifted to S and also the height reduced. The predominant wave direction during southwest monsoon season (June–September) was between S and SSE, and the significant wave height reached a maximum value of 3.8 m and 4.2 m on 16 June and 25 July,

respectively. This includes waves during the two depression periods. In northeast monsoon (November–January), the predominant wave direction was between SE and NE, and the maximum significant wave height observed was 2.1 m (SE direction) on 28 October due to the depression that occurred in the Bay of Bengal (24–29 October, 1996). Even though the pressure level decreased from 1012.3 to 1000.4 mb, the depression could not intensify further, and generate high waves. In the rest of the year, the waves were below 0.8 m in height, and varied between S and SSE direction.

An analysis of several years of wave data from the Bay of Bengal shows that wave parameters, such as significant wave height, wave period and mean wave direction are significantly different for various weather events. In general, during fair weather season off Paradip significant wave heights are below 1.0 m, during monsoon below 3.5 m and during extreme weather events of the order of 5.0–7.0 m.

Frequency-energy spectra during extreme events are single peaked, and the maximum energy distribution is in a narrow frequency band (Fig. 5a) with an average directional spreading of 20°. Spectra for other seasons are multipeaked, and energy is distributed over a wide range of frequencies (Fig. 5b, c) in different directions. The type of spectra shown in Fig. 5b and c represent the seasonal variation of wave conditions in the Bay of Bengal in the absence of extreme events. Wave spectra of extreme events are distinctly different from that of monsoon or fair weather season. In general, wave spectra along the Indian coast are multi-peaked, often with two peaks (Harish and Baba 1986; Vethamony and Sastry 1986; Rao and Baba 1996). Greenslade (2001) found that when energy shifts from one portion of the spectrum to another, the spectral peak suddenly jumps to a different frequency.

Sanil Kumar et al. (2004) found that wave spectra during extreme sea states are mainly single-peaked, and the percentage of occurrence of double-peaked spectra is higher for low sea states. In the present case also, the spectra are single-peaked, and the maximum energy is centered in a narrow frequency band. The maximum spectral energy during the two depressions are 30.33 m^2/hz (15 June) and 31.25 m^2/hz (26 July), which are very high compared to the energy during normal monsoon months (e.g. 7.63 m^2/hz (13 June) and 5.68 m^2/hz (28 July)). It is evident from the spectra that wave energy is higher during southwest monsoon season than the northeast monsoon. Typical measured directional energy spectra representing SW and NE monsoon seasons are shown in Figs. 6a, 7a, respectively, and the corresponding wind directions in Figs. 6b, 7b.

Bathymetry contours off Paradip are parallel to the coast, and the slope is very gentle. In general, winds are either southwesterlies or northeasterlies. Sufficient fetch is available for both the winds.

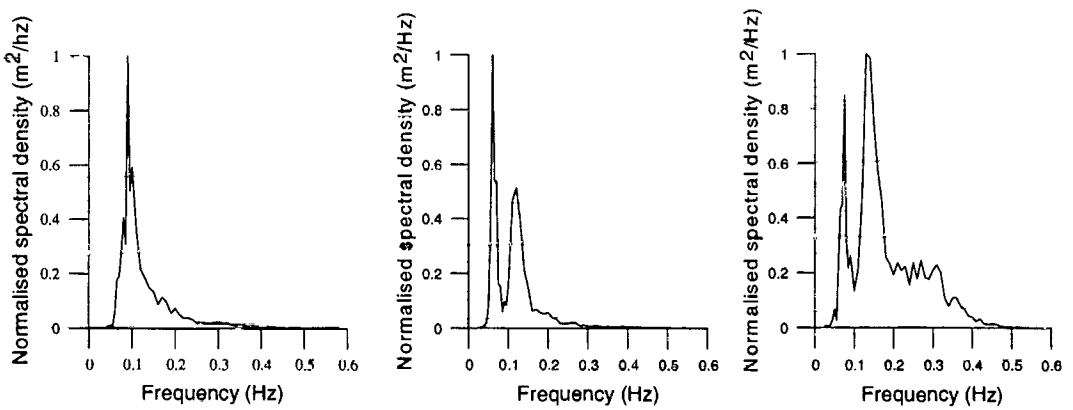

Fig. 5 Typical wave spectra during (**a**) 26 July at 09 h, (**b**) 3 Aug 1996 at 09 h and (**c**) 3 July 09 h

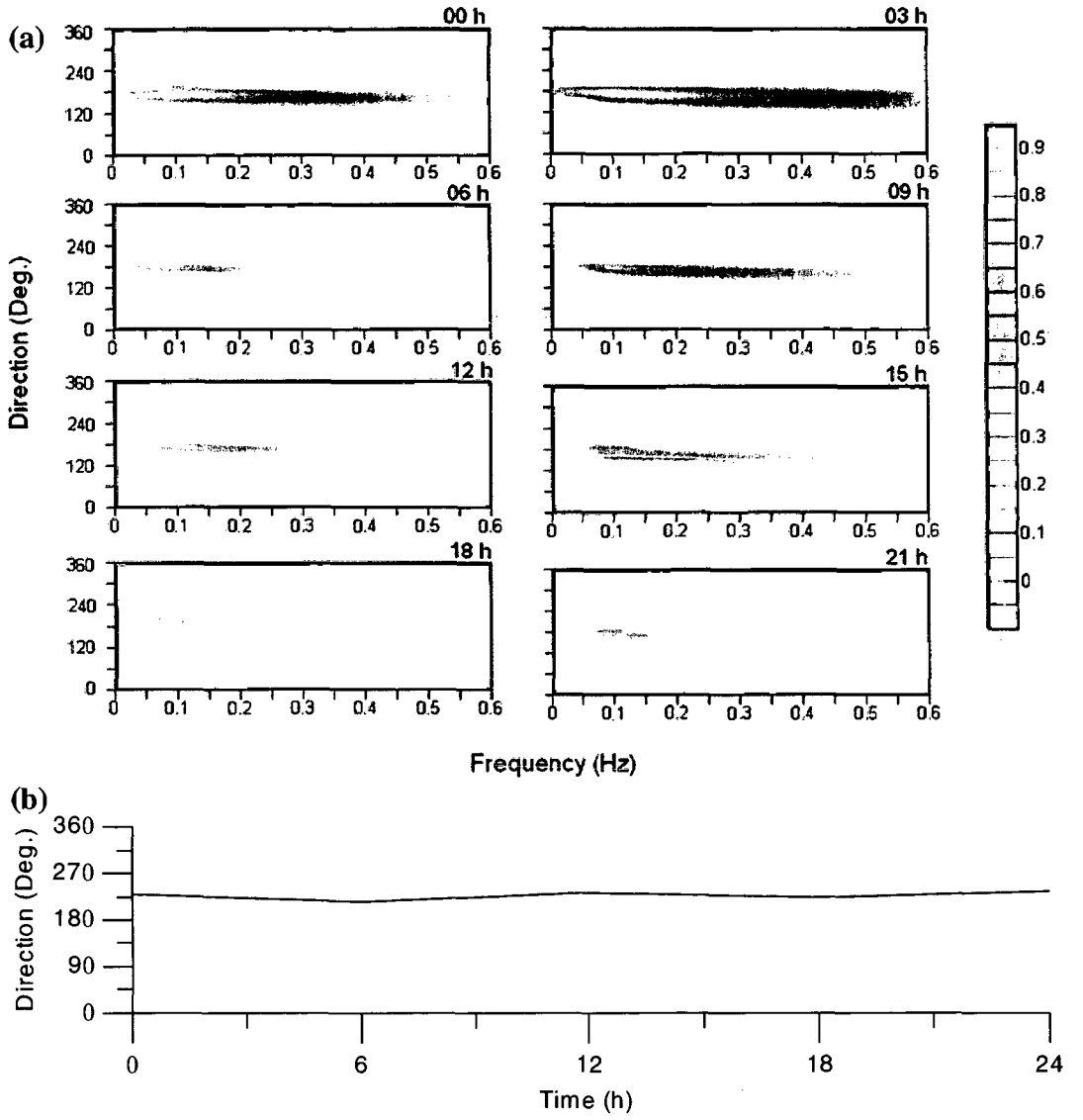

Fig. 6 (**a**) Measured directional energy spectra from 00 h to 21 h (for every 3 h) and (**b**) NCEP wind (for every 6 h) at offshore location near to the study region on 26 July 1996

During extreme events, long waves with higher amplitudes are generated and most of the energy is concentrated in the low frequency region. So, typically the spectra will be single-peaked. When swells reach the region where the locally generated waves are present, the spectra show double- or multi-peaks. Normally during fair weather season, the sea states are swell dominated. Hence, the primary peak will be in the low-frequency region and secondary peak will be in the high-frequency region depending on the locally generated wind seas.

During monsoons, the sea off Paradip is usually 'sea' dominated. Distant swells from various directions also propagate to this region and form complex sea state. Hence, the peak energy will shift from low- to the high-frequency region depending on the strength of the prevailing winds on the region.

The criterion for the single-peakedness is $T_p = T_{pf}$, where T_{pf} is the spectral peak period (period of the highest spectral density) for fully developed sea at the actual location and T_p is the peak wave period (Torsethaugen and Haver 2004). Hence, all the energy will be

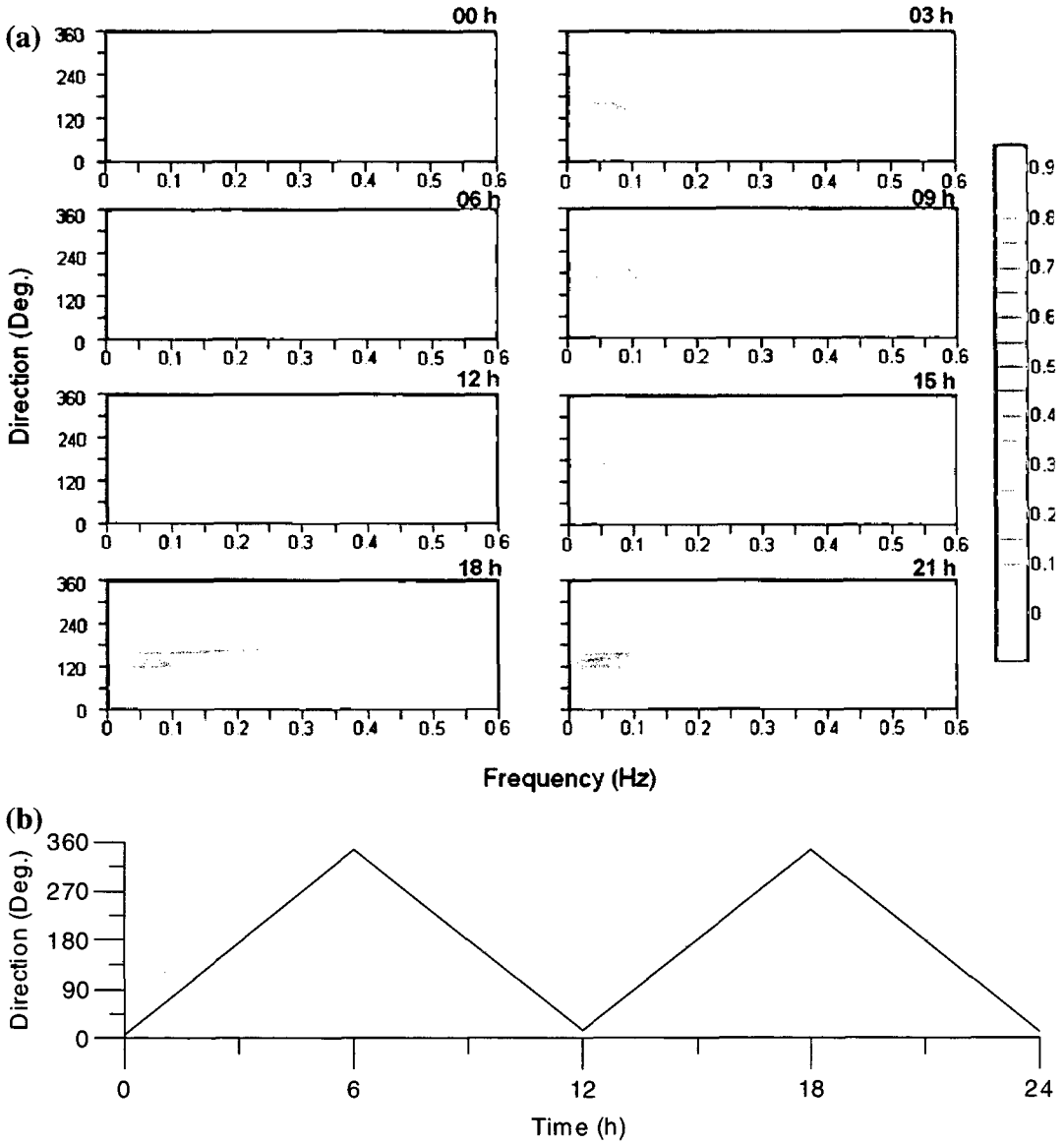

Fig. 7 (**a**) Measured directional energy spectra from 00 h to 21 h (for every 3 h) and (**b**) NCEP wind (for every 6 h) at offshore location near to the study region on 15 November 1996

concentrated into a narrow banded low-frequency region. If $T_p < T_{pf}$, i.e. the sea state is wind sea dominated, the spectral peak will be in the high frequency region and there may be double or multiple peaks in the spectra. The case $T_p > T_{pf}$ is swell dominated, and usually occurs during fair weather season, where the spectral peak is in the low-frequency region.

Modelled directional energy spectra during 26 July are shown in Fig. 8. The spectra show the single-peakedness as in the measured spectra due to the extreme event that prevailed in the region. Modelled wave heights, wave periods and wave directions agree closely with the measured values (Figs. 9, 10, 11). For example, the correlation coefficient between the measured and modelled significant wave height is 0.87 and the bias −0.25. The scatter of measured and modelled significant wave height, mean wave period and mean wave direction are shown in Figs. 12, 13 and 14. The statistical parameters, such as

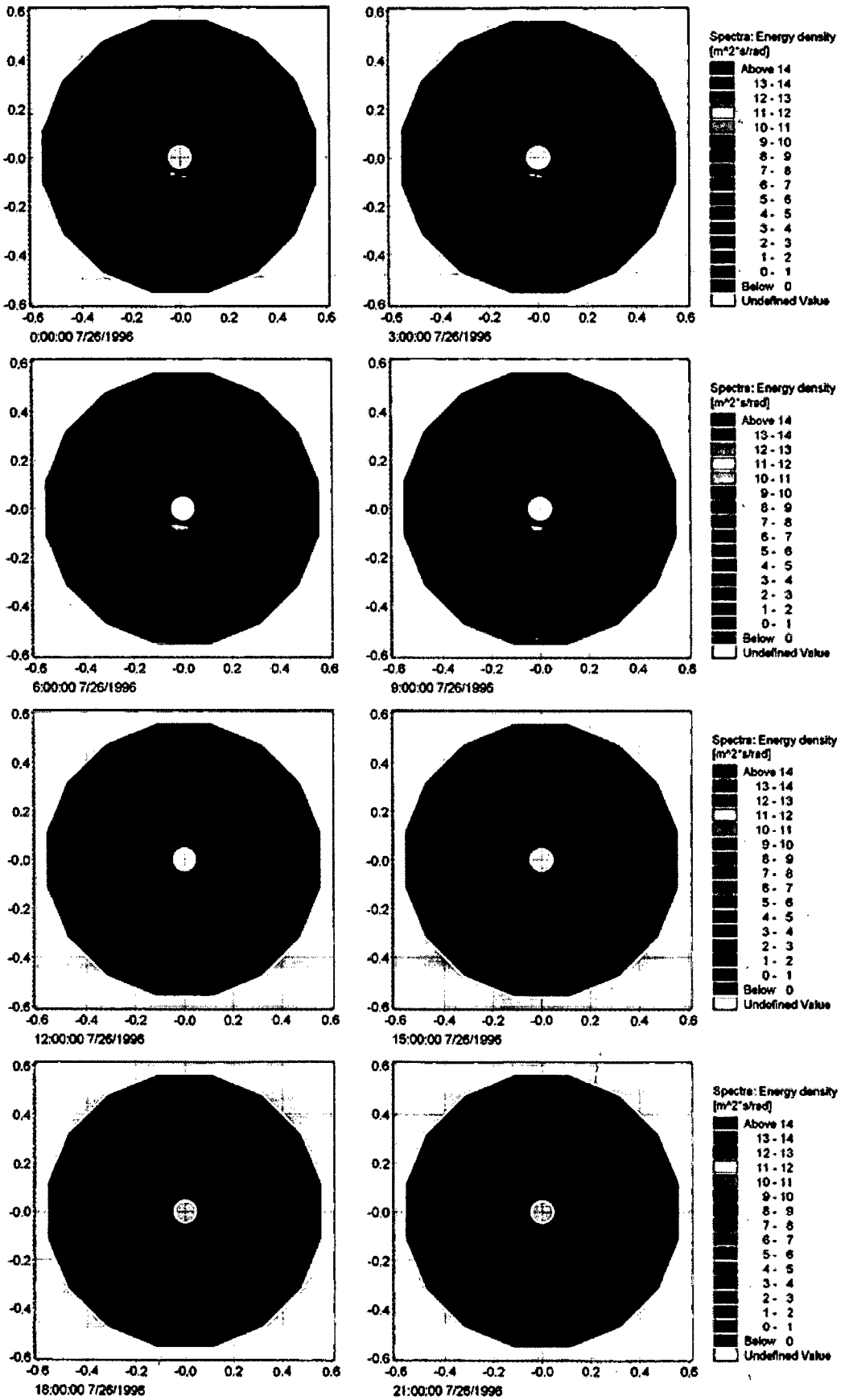

Fig. 8 Modelled directional energy spectra during 26 July for every 3 h simulations (00 h to 21 h)

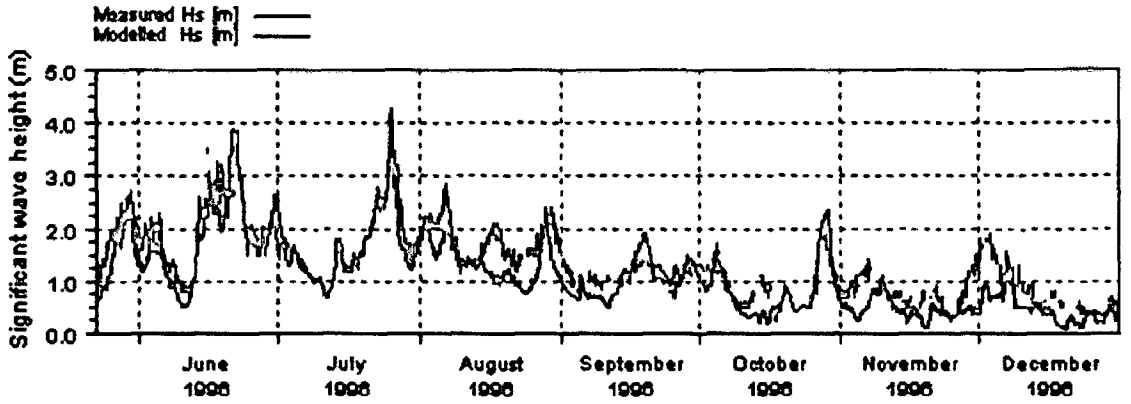

Fig. 9 Measured and modelled significant wave heights (May–December 1996)

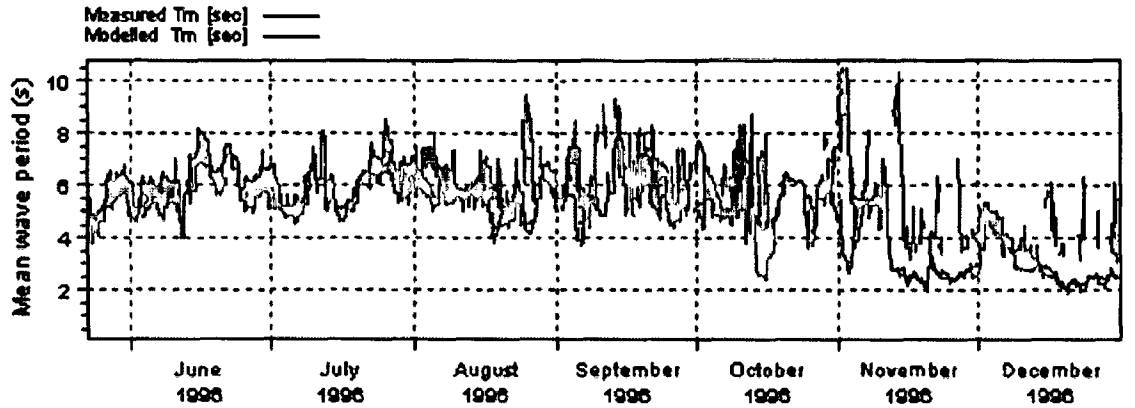

Fig. 10 Measured and modelled mean wave periods (May–December 1996)

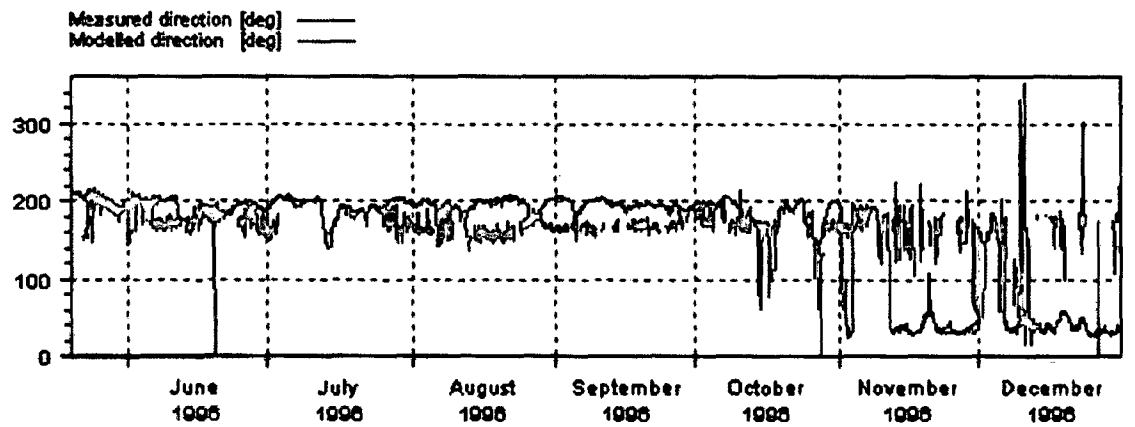

Fig. 11 Measured and modelled mean wave directions (May–December 1996)

correlation coefficient, RMS error and bias between the measured and modelled parameters are given in Table 1. The correlation between measured and modelled wave direction is not good. The discrepancy in the measured and modelled wave direction is mainly due to deficiency in spatial and temporal resolution of wind parameters as the local wind effect inside the model domain is not incorporated in the simulation and the winds used at the boundaries have coarse resolution. The modelled wave directions are between SSW and SSE from May to September and between N and NW in November and December. Mean

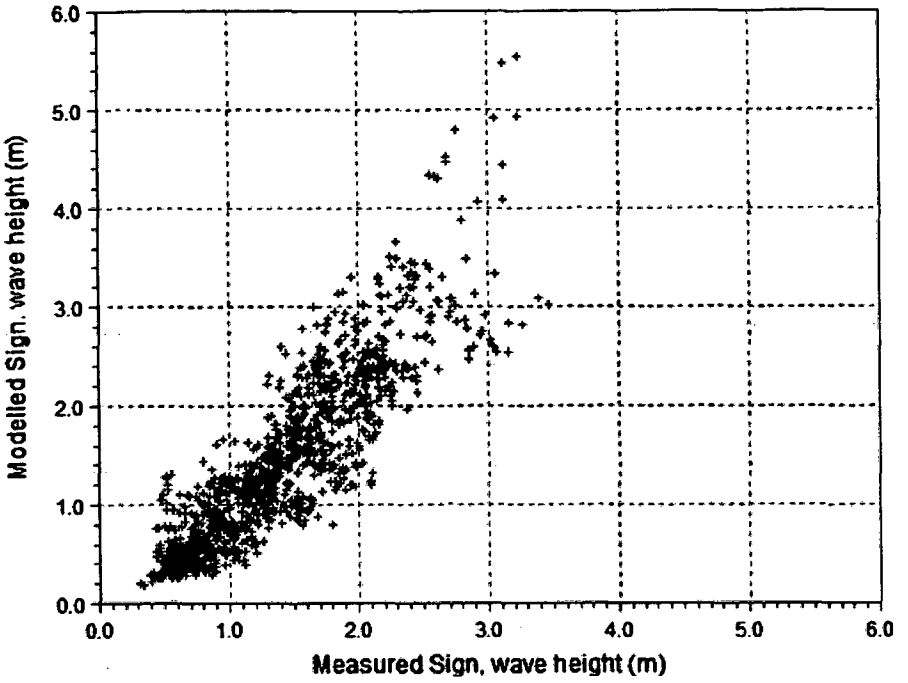

Fig. 12 Scatter showing measured and modelled significant wave heights (May–December 1996)

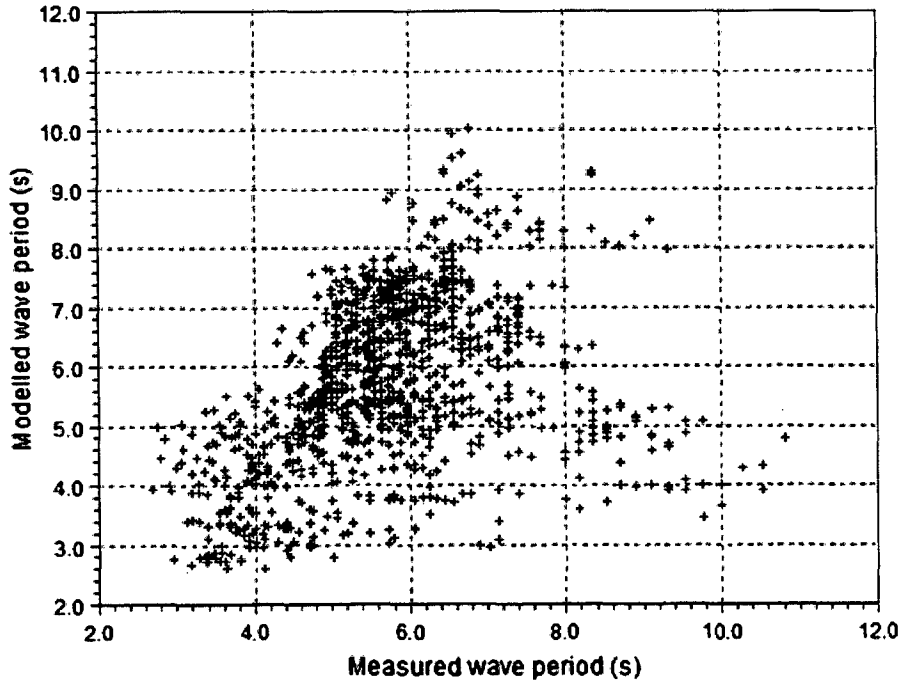

Fig. 13 Scatter showing measured and modelled wave periods (May–December 1996)

wave period ranges from 4 to 10 s during SW monsoon and from 2 to 8 s during NE monsoon. The highest measured significant wave height is 4.2 m, whereas the corresponding modelled value is 3.4 m (22 July 1996, due to an extreme event that prevailed in the region).

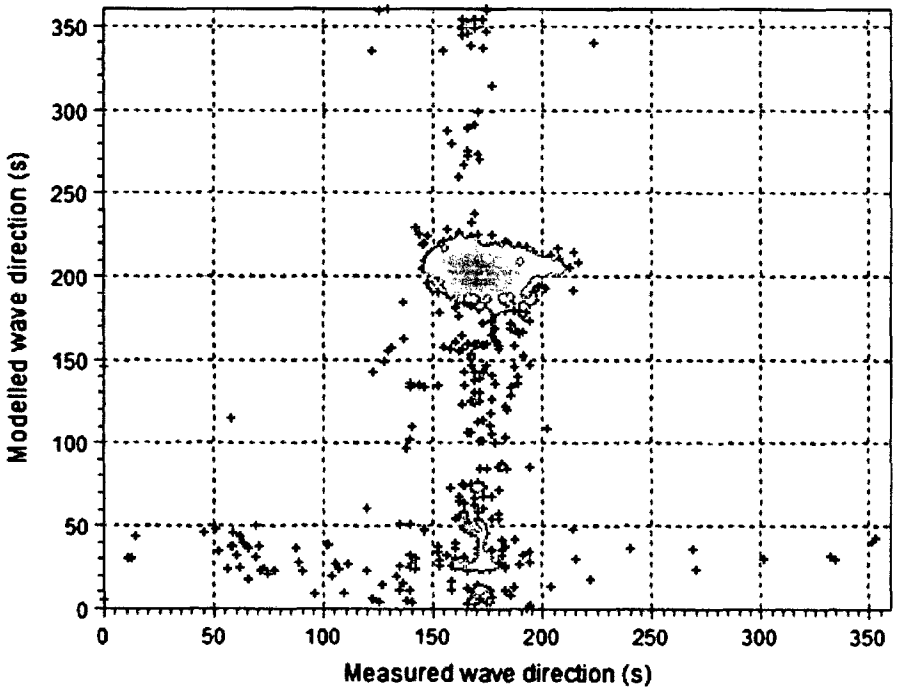

Fig. 14 Scatter showing measured and modelled wave direction (May–December 1996)

Table 1 Statistics of the measured and modelled wave parameters

Statistics	Significant wave height	Wave period	Wave direction
Correlation coefficient	0.87	0.48	0.21
RMS error	0.54	1.7	60
Bias	−0.25	−1.1	−6.9

4 Conclusion

The analysed time series wave data covering all seasons off a typical east coast of India distinctly show the response of coastal waves to the seasons. The model could reasonably reproduce the wave characteristics prevailing off Paradip in different seasons. The accuracy of model results could be improved when fine spatial resolution winds are used. The results of this study are very useful for the design of proposed SPM at the wave measurement location and other coastal activities planned in this region.

Acknowledgements We thank Dr SR Shetye, Director, National Institute of Oceanography (NIO), Goa for providing necessary facilities and the Indian Oil Corporation Ltd (IOCL), New Delhi for funding the project. We acknowledge all the project participants for their help during wave data collection.

References

Anonymous (2001) MIKE 21 Wave modelling user guide. DHI Water & Environment, Denmark, 66 pp
Greenslade DJM (2001) The assimilation of ERS-2 significant wave height data in the Australian region. J Mar Syst 28:141–160

Harish CM, Baba M (1986) On spectral and statistical characteristics of shallow water waves. Ocean Eng 13(3):239–248

Rao CVKP, Baba M (1996) Observed wave characteristics during growth and decay: a case study. Cont Shelf Res 16(12):1509–1520

Sanil Kumar V, Ashok Kumar K, Raju NSN (2004) Wave characteristics off Visakhapatnam coast during a cyclone. Curr Sci 86:1524–1529

Sudheesh K, Vethamony P, Babu MT, JayaKumar S (2004) Assessment of wave modeling results with buoy and altimeter deep water waves for a summer monsoon. Proceedings of the third Indian national conference on harbour and ocean engineering (INCHOE—2004). NIO, Goa (India), pp 184–192

Torsethaugen K, Haver S (2004) Simplified double peak spectral model for ocean waves. Proceedings of ISOPE conference, vol 3, pp 76–84

Vethamony P, Sastry JS (1986) On the characteristics of multipeaked spectra of ocean surface waves. J Inst Eng India 66:129–132

Vethamony P, Sudeesh K, Rupali SP, Babu MT, Jayakumar S, Saran AK, Basu SK, Kumar R, Sarkar A (2006) Wave modelling for the north Indian Ocean using MSMR analysed winds. Int J Remote Sens 27(18):3767–3780

WAMDI Group (1988) The WAM model—a third generation ocean wave prediction model. J Phys Oceanogr 18:1775–1810

Nat Hazards (2009) 49:411–420
DOI 10.1007/s11069-008-9295-6

ORIGINAL PAPER

Demarcation of inland vessels' limit off Mormugao port region, India: a pilot study for the safety of inland vessels using wave modelling

P. Vethamony · V. M. Aboobacker · K. Sudheesh · M. T. Babu · K. Ashok Kumar

Received: 10 June 2008 / Accepted: 10 September 2008 / Published online: 25 September 2008

Abstract The Ministry of Shipping desires to revise the inland vessels' limit (IVL) notification based on scientific rationale to improve the safety of vessels and onboard personnel. The Mormugao port region extending up to the Panaji was considered for this pilot study. Measured winds and wave parameters (AWS and moored buoy) as well as NCEP re-analysis and NCMRWF winds were used for the analysis and input to regional and local models. The results of wave model were validated with measured significant wave heights (SWHs) and the comparison shows a good match. The analysis indicates that SWHs do not exceed 2.0 m during non-monsoon months, and in monsoon months exceed 5.0 m, and even 7.0 m, especially during extreme events. In order to draw IVL contours for Goa coastal region, local model was set up and nearshore waves were simulated for the period May 2004–May 2005. Based on the nearshore SWH distribution, IVL contours have been fixed for the Mormugao port and Panaji coastal regions.

Keywords Mormugao port · Wave modelling · Wave measurements · Inland vessels' limit · Wave spectra

P. Vethamony (✉) · V. M. Aboobacker · K. Sudheesh · M. T. Babu · K. Ashok Kumar
National Institute of Oceanography, Dona Paula, Goa 403004, India
e-mail: mony@nio.org

V. M. Aboobacker
e-mail: vmabacker@gmail.com

K. Sudheesh
e-mail: sudheesh@nio.org

M. T. Babu
e-mail: mtbabu@nio.org

K. Ashok Kumar
e-mail: akumar@nio.org

1 Introduction

Information on winds and waves are very essential for activities such as exploitation of natural resources, ship-routing, design of harbours, breakwaters and jetties, loading and unloading of products to and from the vessels and navigation of different types of vessels in the coastal region. Until a few years ago, the lack of adequate reliable wind and wave data had been recognised as a major limiting factor to such activities along the Indian coast, including port and harbour regions.

The Ministry of Shipping, Govt. of India, desires to revise the inland vessels' limit (IVL) notification based on the scientific rationale for the following reasons: (i) area of operation of ports has been extended towards offshore and (ii) new major and minor ports have been developed since 1972. The primary objective of this initiative is to improve the safety of vessels and onboard personnel. IVL is necessary to prevent the damage to any vessel or loss of life. Mormugao port region, including Panaji port region is considered for the pilot study.

Figure 1 shows the study region including the Mormugao port limit. Mormugao Bay lies between Mormugao Point and Cabo Point. The south of Mormugao Bay is mostly rocky. The port is protected by a breakwater, and it lies on the north of Mormugao Head. The Cabo Point is a 55 m high prominent headland. To the north of Mormugao Bay, and between Cabo Point and Nazaret Point, stretches of sandy and rocky coasts are found.

The Mormugao port provides 11 alongside berths and several mooring buoys. During southwest monsoon season (June–September), when pilots cannot embark, a launch will lead vessels from the breakwater head to a suitable anchorage. Anchorage may be obtained in depths of about 7 m. The movement of small inland vessels is banned through the Mandovi Zuari estuaries during southwest monsoon due to rough weather and closure of Mandovi channel for navigation (bar formation takes place). Large breakers break across the bar and river mouth and make navigation in and out across the mouth very risky.

The present work primarily deals with fixing of IVL contours based on significant wave heights (SWHs) of the region obtained from wave measurements and numerical modelling. AWS (Autonomous Weather Station) and moored buoy winds, NCEP (National Centre for Environmental Prediction, USA) re-analysis winds and NCMRWF (National Centre for Medium Range Weather Forecasting, India) winds were used as input to MIKE 21—OSW and NSW models. The results of the model have been validated with wave parameters, measured using moored data buoys and directional wave rider buoys.

2 Data and methods

Wave data measured using directional wave rider buoys and moored buoys at different locations off Goa during different periods were used to analyse wave characteristics of the region as well as for numerical validation. In order to get a general feel of wave pattern off Goa, waves measured off Mormugao during February 1996–May 1997 were analysed. Waves measured off Goa during May 2005 at two water depths, 15 m and 25 m, respectively, were used to study the wave transformation and the effect of local winds on wind sea generation. Moored buoy data, which consists of winds and waves, at a deep water location during July - November 1999, May–July 2000, January 2001 and May–September 2001 and a shallow water location for May–September 2001 and October 2004–March 2005 were also utilised in this study.

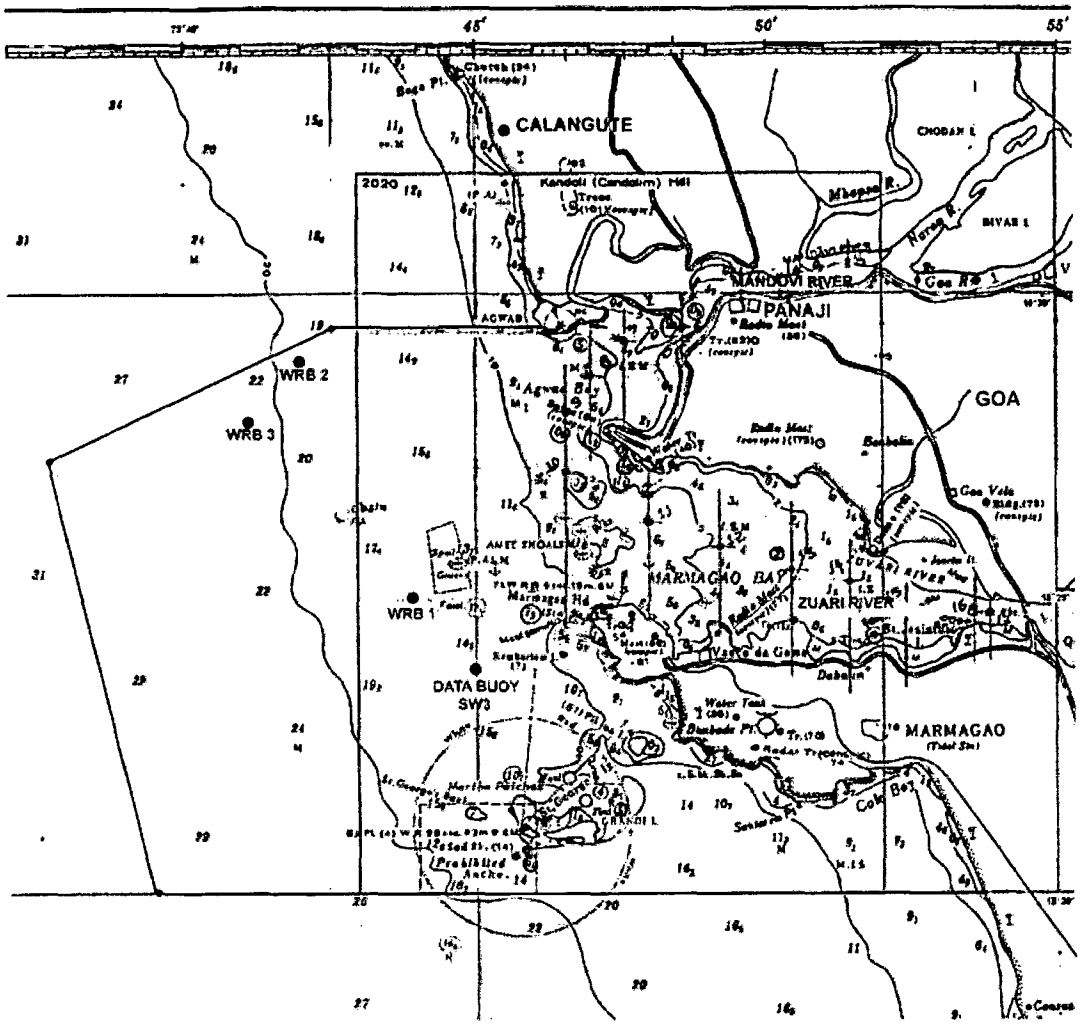

Fig. 1 Study region including the locations of wave rider buoys and moored data buoy off Goa. Mormugao port limit is marked inside. Water depths: WRB1: 15 m (6–20 May 2005); WRB2: 25 m (1–21 May 2005); WRB3: 25 m (February 96–May 97); SW3: 12 m (May–September 2001 and October–March 2005)

Winds measured using AWS located at Dona Paula coastal station during May–September 2004 and April–May 2005 were analysed to study wind characteristics off Goa during pre-monsoon and south west monsoon periods as well as to validate the forecast winds.

In order to predict deep water waves in the north Indian Ocean, the NCEP re-analysis (Kalney et al. 1996) winds (May 2004–June 2005) and NCMRWF winds (July–August 1999, May–July 2000 and May–September 2001) were utilised. The NCEP winds (U and V components) available in 2.5° × 2.5° grids were linearly interpolated to 0.75° × 0.75° grid size as the resolution of offshore model bathymetry considered was 0.75° × 0.75° grid size. NCMRWF winds (U and V components) available in 1.5° × 1.5° grid size for every six hour interval were also converted into resultant winds in 0.75° × 0.75° grids. In order to ascertain the accuracy of NCEP winds, the May–August 2000 winds were validated with buoy wind data off Goa, Kochi and Chennai, and the match was found to be good. Vethamony et al. (2003) and Sudheesh et al. (2004) further used these NCMRWF and NCEP winds to force MIKE 21 Offshore Spectral Wave model (OSW) to generate offshore waves, and the comparison with measured wave parameters also demonstrates a good match.

In the present study, offshore and nearshore wave modelling have been carried out using MIKE 21 OSW (Offshore Spectral Wave model) and MIKE 21 NSW (Nearshore Spectral Wave model), developed by Danish Hydraulic Institute (DHI), Denmark (Anonymous 2001).

MIKE 21 OSW is a discrete spectral model, which describes the wave field by the directional-frequency wave energy spectrum. The energy is calculated in discrete points of a rectangular grid for a number of discrete frequencies and directions. The model includes two different descriptions of physical processes governing the wind–wave generation and decay: state-of-the-art third generation formulation and second generation formulation. The third generation model is based on the internationally developed WAM Cycle 4 model (WAMDI Group 1988) originally developed for deep water application on global and regional scales. The model is based on the numerical integration of the spectral energy balance equation formulated in Cartesian co-ordinates.

The basic input parameters to the model are bathymetry and wind fields. The model domain was divided into different grids and input parameters were provided at each grid point. Time step corresponding to the Courant Number was chosen, keeping the minimum wave period present. MIKE 21 NSW is a stationary, directionally decoupled parametric model. The model takes into account the effects of refraction and shoaling due to varying depth, local wind generation and energy dissipation due to bottom friction and wave breaking. The model also takes into account the effect of wave–current interaction. The basic equations were solved using an Eulerian finite difference technique. The zeroth and the first moment of the action spectrum were calculated on a rectangular grid for a number of discrete directions. A once-through marching procedure was applied in the predominant direction of wave propagation.

The bathymetry for the regional model (north Indian Ocean) was generated using ETOPO5 bathymetry data obtained from NGDC (National Geophysical Data Center, Colorado, USA), representing the best available bathymetry values spaced at every five-minute latitude/longitude. The model domain covers the region 5° S to 25° N and 45° E to 100° E and the domain is divided into 0.75° × 0.75° grid size. The depth values were provided at all the grid points. The bathymetry for the local model (Goa region, 15°18′N to 15°36′N and 73°36′E to 73°55′E) was generated from the C-MAP electronic chart database of MIKE 21. The grid spacing is 200 m × 50 m. The bathymetry data are with reference to World Geodetic System 1984 (WGS 84).

Winds measured (10 min interval) at Dona Paula coastal station during May–September 2004 and April–May 2005 and the winds measured off Goa using moored buoy during October 2004–March 2005 were utilised in the nearshore wave modelling. The wave parameters for the boundary of local model are extracted from the regional model output, and applied as boundary conditions along with the AWS winds. The nearshore wave simulation using NSW was carried out for the period May 2004–May 2005. The basic output of the model is SWH, wave period, wave direction and directional spread. The wave model results were validated with measured wave parameters.

Significant wave heights derived from model results were used to draw IVL contours as follows: (i) regions where SWH < 0.6 m, (ii) regions where 0.6 m $\leq$ SWH ≤ 1.2 m and (iii) regions where 1.2 m $\leq$ SWH ≤ 2.0 m.

3 Results and discussion

The analysis of waves measured off Goa during February 1996–May 1997 shows that (Table 1) SWH varies from 0.16 to 5.85 m throughout the measurement period. The

Table 1 Monthly variations of SWH and mean wave period off Goa during February 1996–May 1997

Year	Month	SWH (m)	Mean wave period (s)
1996	February	0.33–1.50	3.0–5.0
	March	0.42–1.82	3.0–5.7
	April	–	–
	May	0.75–1.37	3.7–6.3
	June	0.93–5.85	4.6–9.1
	July	1.32–4.29	5.2–8.7
	August	1.20–3.25	4.4–7.5
	September	0.80–1.80	4.1–8.0
	October	0.47–3.31	3.6–6.9
	November	0.36–1.20	3.1–6.5
	December	0.29–0.96	2.7–6.5
1997	January	0.27–1.65	2.7–5.6
	February	0.38–1.39	3.1–5.3
	March	0.39–1.77	3.1–5.7
	April	0.16–1.50	2.8–5.7
	May	0.38–1.36	2.9–6.1

highest SWH value of 5.85 m and the maximum wave height of 10.47 m were observed in June 1996 when a monsoon depression was formed over the Arabian Sea.

An analysis of waves measured at 25 and 15 m water depths off Mormugao, Goa, during May 2005, shows that SWH varies from 0.56 to 1.26 m and from 0.54 to 1.16 m, and mean wave period from 4.4 s to 9.3 s and from 4.4 s to 8.6 s, respectively. The relative changes in wave parameters at these two locations could be attributed to wave transformation due to refraction, shoaling and bottom friction.

A few typical 3 h interval wave spectra for 13 May 2005 are shown in Fig. 2. The two major peaks present in the wave spectra at two different frequency bands can be attributed to wave trains coming from two different directions. This is a combination of short period wind seas generated due to local winds and long period swells generated far away. Vethamony and Sastry (1986); Rao and Baba (1996); Sanil Kumar et al. (2004) also observed multipeaks in wave spectra along the Indian coast.

It has been found from the analysis of AWS winds during May–September 2004 and April–May 2005 that the local winds dominate in pre-monsoon period (April and May), and there exists diurnal variations in wind speed and direction due to localised convective activity. A typical case for 12–14 May 2005 is highlighted in Fig. 3. It is evident from the analysis of local winds measured at the coastal station and wave spectra measured off Goa that the diurnal variations in the wave parameters are mainly due to the co-existence of locally generated wind seas over the pre-existing swells.

The comparison between NCEP and measured winds off Goa match closely with buoy observed winds, though at times they are marginally higher than the buoy observed winds (Vethamony et al. 2006). These winds were further used in OSW for wave modelling. Figure 4 shows the validation of modelled (using OSW) and measured SWHs at a deep water location off Goa during August 1999. Similarly, the nearshore waves simulated using NSW for May 2005 have been compared with measurements, and the match is very good (Fig. 5).

It has been observed from Tables 2, 3 that range of SWH exceeds 2.5 m during June–August 2004, whereas it is below 2.0 m in September and does not exceed 1.2 m during

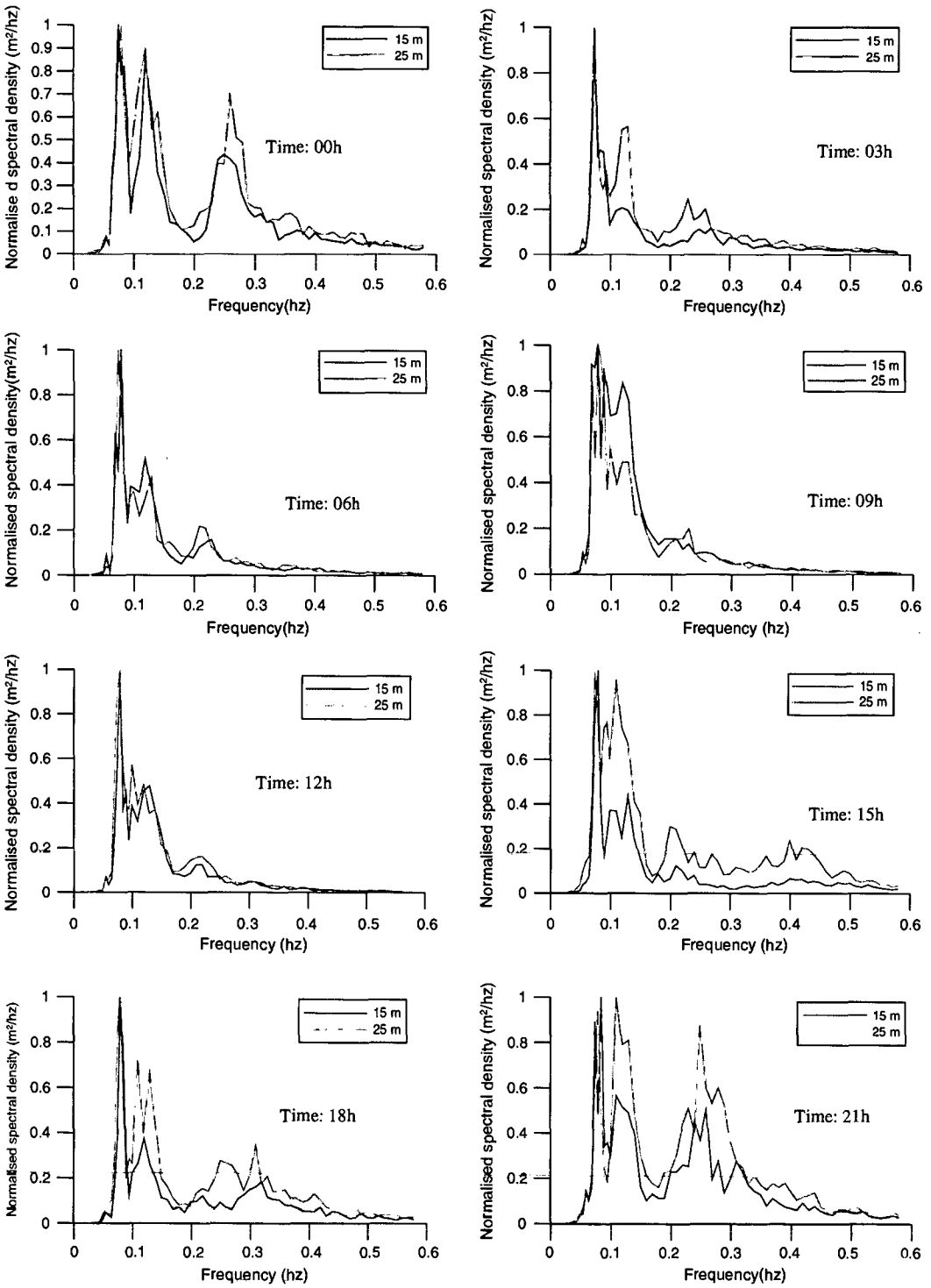

Fig. 2 Typical wave spectra at two locations on 13 May 2005 (00, 03, 06, 09, 12, 15, 18 and 21 h, respectively)

October 2004–May 2005. The highest value of 4.30 m obtained in May 2001 was due to extreme event prevailed in the region. Table 3 shows the ranges of SWHs derived from available moored buoy data off Goa. The higher values of SWH are obtained during June–August in all years. In all other months, the SWHs obtained are below 2.0 m. Hence, it is

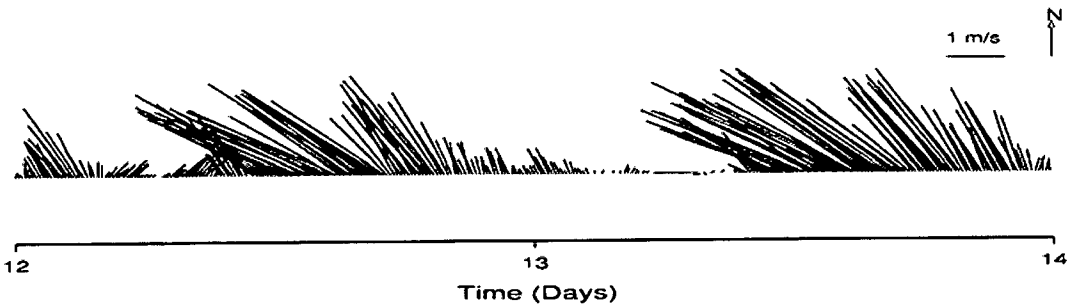

Fig. 3 Diurnal variations in wind speed and direction due to sea breeze and land breeze systems (12–14 May 2005)

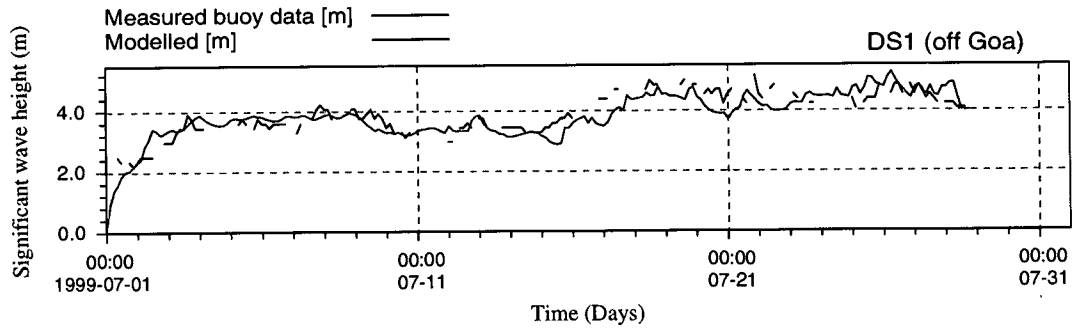

Fig. 4 Comparison of SWH between model and buoy observed at deep water locations for July 1999

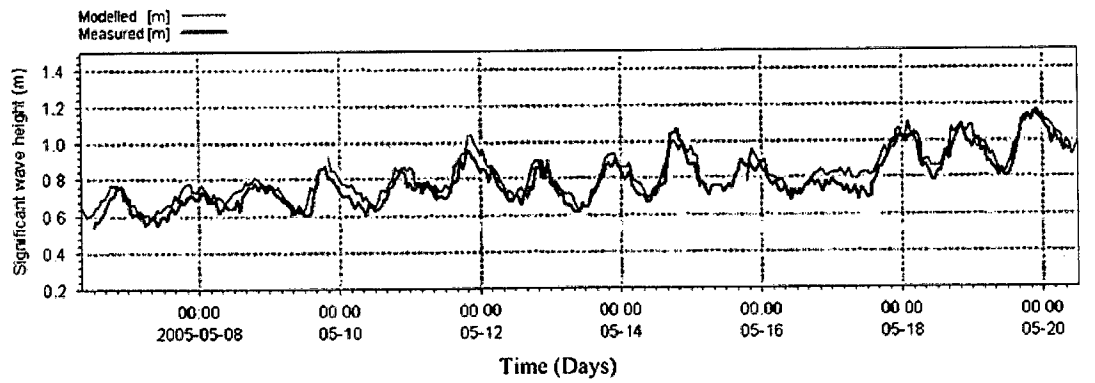

Fig. 5 Comparison between measured and modelled SWH at 15 m water depth during 01–21 May 2005

Table 2 Statistics of measured SWHs exceeding 2.0 m during southwest monsoon for different years

Month	May		June			July		August		September
	2001	2004	2001	2002	2003	2001	2003	2001	2003	2001
Total wave heights	237	247	178	124	240	145	246	218	118	230
SWH > 2.0 m	59	20	120	36	151	71	228	78	52	0
% of SWH > 2.0 m	24.9	8.1	67.4	29.0	62.9	49.0	92.7	35.8	44.1	0

Table 3 Range of SWHs (in m) derived from available moored buoy data off Goa

Months	Years				
	2001	2002	2003	2004	2005
Jan		0.23–1.41	0.33–1.15	0.23–1.25	0.33–1.8
Feb	0.31–1.41	0.31–1.41	0.38–1.50	0.39–1.02	0.35–1.45
Mar	0.31–1.56	0.47–1.09	0.30–1.87	0.16–1.17	0.41–1.21
Apr				0.55–1.17	
May	0.55–4.30	0.53–1.87	0.46–1.53	0.63–2.27	
Jun	0.80–3.91	0.96–4.41	0.78–3.80		
Jul	1.48–2.81		1.61–3.78		
Aug	1.56–2.97		1.26–2.52		
Sep	0.55–1.88				
Oct	0.39–1.48	0.42–1.42		0.31–1.31	
Nov	0.31–0.78	0.38–0.76		0.29–1.05	
Dec	0.23–0.70	0.30–1.29	0.23–1.02	0.31–0.96	

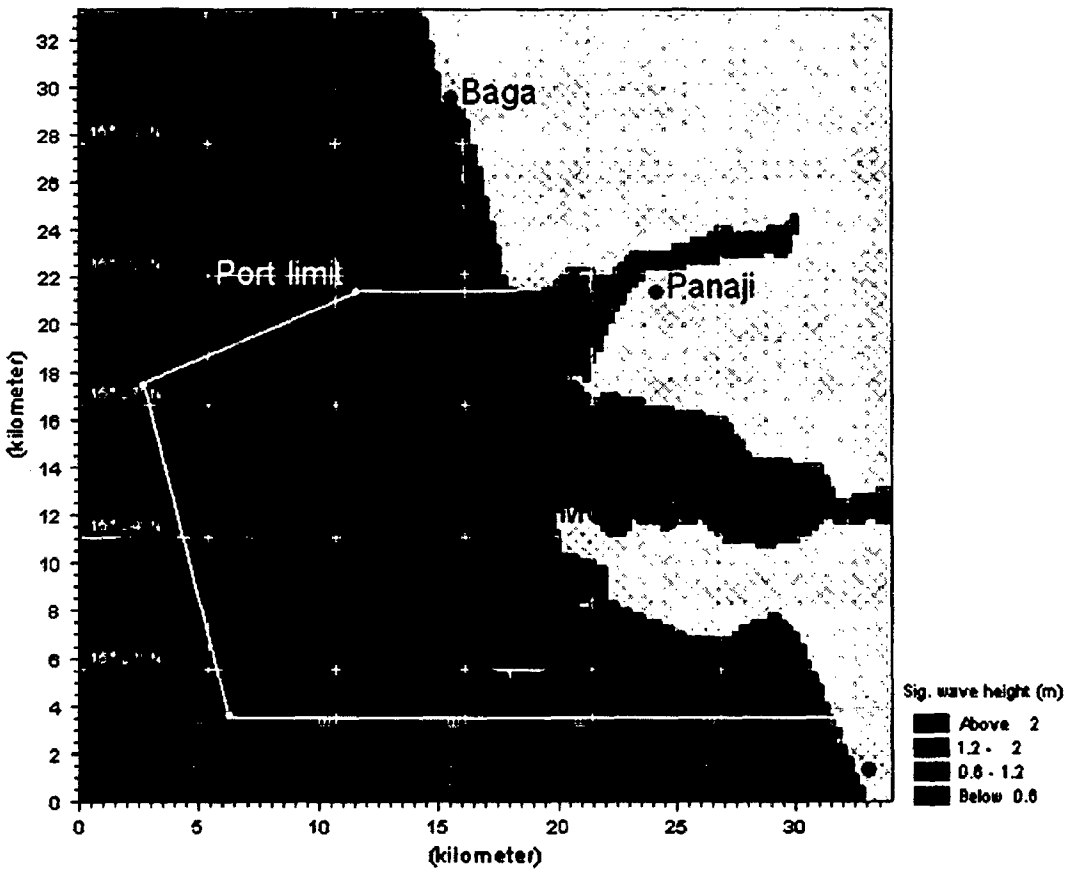

Fig. 6 Typical SWH distribution off Mormugao port during southwest monsoon (region showing the Mormugao port limit is marked)

very evident that Mormugao port and Panaji coastal region are safe from large waves, except during June–August.

Figure 6 shows a typical SWH distribution off Mormugao port during southwest monsoon. It is very clear that most of the region is influenced by large monsoon waves

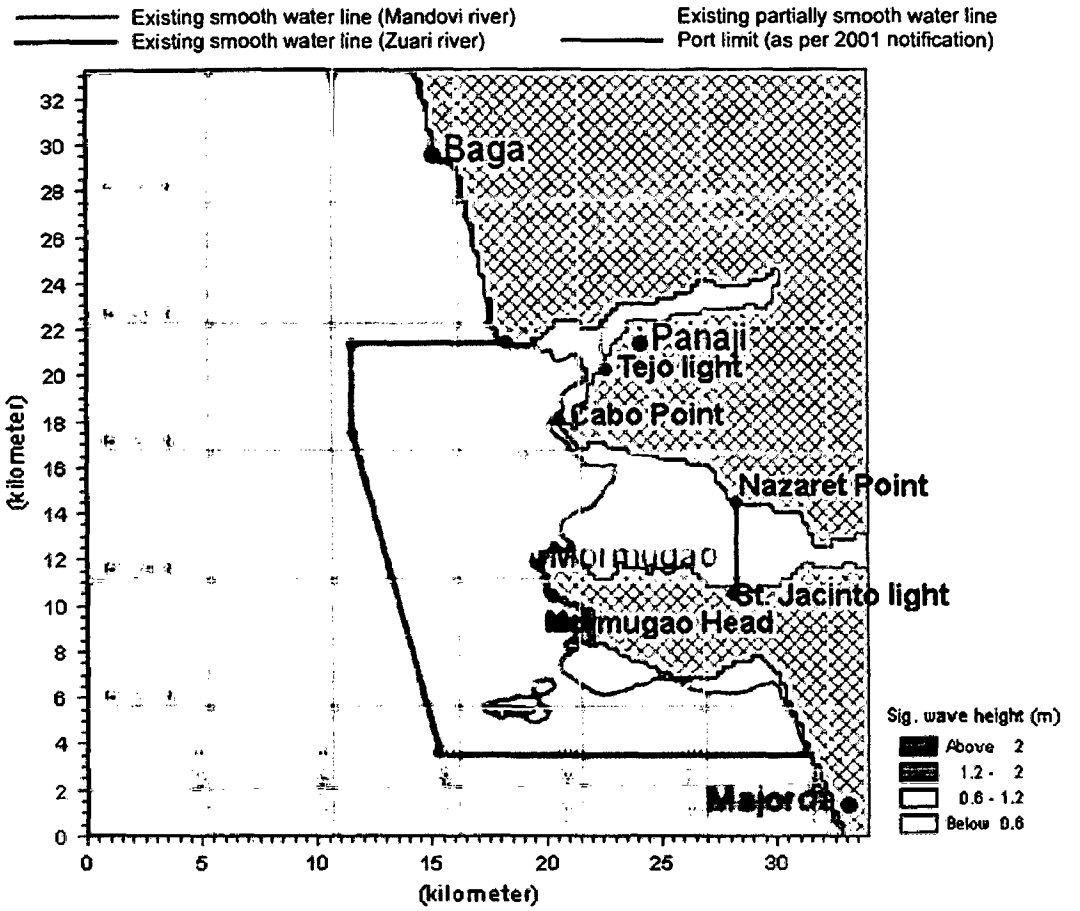

Fig. 7 IVL regions demarcated based on wave heights (April 2005) with existing smooth and partially smoothed water lines

having SWHs greater than 2.5 m. As the inland vessels are smaller in size and they are permitted to ply only during non-monsoon months, especially when SWHs are less than 2.0 m, IVL is required to be fixed for non-monsoon months. The following criteria were used to fix IVL contours: (i) regions where SWH < 0.6 m, (ii) regions where $0.6 \text{ m} \leq \text{SWH} \leq 1.2$ m and (iii) regions where $1.2 \text{ m} \leq \text{SWH} \leq 2.0$ m. The outer boundary of the 2.0 m decides the extreme IVL. Accordingly, IVL contours were fixed for all the months. These results will be used by the Ministry of Shipping (MoS) for implementing the IVL. A typical SWH distribution along with IVL contours for a non-monsoon month is shown in Fig. 7. This figure also contains the existing smooth and partially smooth water lines which are practised now by the inland vessels along with the port limit. The present study gives hope for larger area of movement for the vessels, as seen by the existing waterlines and the proposed IVL (Fig. 7).

4 Conclusions

The SWHs obtained from the nearshore wave model as well as wave measurements during different years indicate that during non-monsoon months (October–May) and in September, SWHs, in general, do not exceed 2.0 m off Mormugao port and Panaji coastal regions. During monsoon months (June - August), the SWHs exceed 2.5 m in most of the regions,

and plying of inland vessels would not be possible. For non-monsoon months, Ministry of Shipping desires to implement IVL, depending on size and other structural specifications of the inland vessels, for the safety of vessels and onboard personnel. Based on the SWH distribution around the coastal region, the IVL is demarcated.

Acknowledgements We thank Dr. S.R. Shetye, Director, National Institute of Oceanography (NIO), Goa, for his interest in this study and to our colleagues, especially Mr. P.S. Pednekar, for their involvement in data collection.

References

Anonymous (2001) MIKE 21 Wave modelling user guide. DHI Water & Environment, Denmark, p 66

Kalney E, Kanamitsu M, Kistler R, Collins W, Deaven D, Gandin L et al (1996) The NCEP/NCAR reanalysis project. Bull Am Meteorol Soc 77:437–471. doi:10.1175/1520-0477(1996)077<0437:TNYRP>2.0.CO;2

Rao CVKP, Baba M (1996) Observed wave characteristics during growth and decay: a case study. Cont Shelf Res 16(12):1509–1520. doi:10.1016/0278-4343(95)00084-4

Sanil Kumar V, Ashok Kumar K, Raju NSN (2004) Wave characteristics off Visakhapatnam coast during a cyclone. Curr Sci 86:1524–1529

Sudheesh K, Vethamony P, Babu MT, JayaKumar S (2004) Assessment of wave modeling results with buoy and altimeter deep water waves for a summer monsoon. In: Proceedings of the third Indian national conference on harbour and ocean engineering (INCHOE - 2004), NIO, Goa (India), pp 184–192

Vethamony P, Sastry JS (1986) On the characteristics of multipeaked spectra of ocean surface waves. J Inst Eng India 66:129–132

Vethamony P, Sudheesh K, Asha Rajan, Saran AK, Sujit Basu, Raj Kumar , Abhijit Sarkar (2003) Wave modelling using MSMR analysed winds, Report No. NIO/TR/10/2003, February 2003. National Institute of Oceanography, Goa, India

Vethamony P, Sudeesh K, Rupali SP, Babu MT, Jayakumar S, Saran AK et al (2006) Wave modelling for the north Indian Ocean using MSMR analysed winds. Int J Remote Sens 27(18):3767–3780. doi:10.1080/01431160600675820

WAMDI Group (1988) The WAM model: a third generation ocean wave prediction model. J Phys Oceanogr 18:1775–1810. doi:10.1175/1520-0485(1988)018<1775:TWMTGO>2.0.CO;2

Annexure II

List of papers under revision

List of papers under revision

1. **Aboobacker, V.M.**, R. Rashmi, P. Vethamony and H.B. Menon: On the dominance of pre-existing swells over wind seas off Goa, west coast of India.
2. Vethamony, P., **V.M. Aboobacker**, H.B. Menon, Ashok Kumar and Luigi Cavaleri: Superimposition of wind seas on pre-existing swells off Goa coast.
3. Rashmi, R., **V.M. Aboobacker**, P. Vethamony and M.P. John: Co-existence of wind seas and swells along the west coast of India during non-monsoon season.